Characterization of Diverse Megathrust Fault Behavior Related to Seismic Supercycles, Mentawai Islands, Sumatra

Thesis by
Belle Philibosian

In Partial Fulfillment of the Requirements for the degree
of
Doctor of Philosophy

CALIFORNIA INSTITUTE OF TECHNOLOGY
Pasadena, California
2013
(Defended May 29th, 2013)

ACKNOWLEDGEMENTS

The pronoun “we” is used throughout this thesis rather than “I” as a reflection of the contributions of many people to my results. The published papers that have come and will come from my thesis always have a long list of co-authors. First and foremost I would like to thank my two advisors Kerry Sieh and Jean-Philippe Avouac for their vital insight, inspiration, and unwavering support. The other members of my thesis committee, Paul Asimow, Joann Stock, and Mark Simons have also provided a great deal of helpful guidance along the way. Danny Hilman Natawidjaja made vital contributions by providing the raw data from his previous work as well as assisting with field work and logistics. This project would not have been possible without the excellent field and logistics support from my Indonesian colleagues Mudrik R. Daryono, Bambang W. Suwargadi, Dudi Prayudi, and Imam Suprihanto, and all the crew members of the *K.M. Andalas*.

All of the uranium-thorium dating was performed by Hong-Wei Chiang, Chung-Che Wu, and Ke (Coco) Lin under the guidance of Chuan-Chou “River” Shen at the HISPEC Laboratory at the National Taiwan University; thanks to all of them for taking time out of their own projects to process my samples and discuss the trials and tribulations of age-dating corals. Thanks are also due to Hugo Perfettini and Emma Hill for their assistance with modeling projects, as well as to Emma’s students and postdocs Louisa Tsang, Lujia Feng, Ashar M. Lubis, and Qiang Qiu for numerous helpful discussions. Fellow Caltech graduate students Marion Thomas and Thomas Ader as well as Kelly Wiseman and Andrew Kositsky also provided snippets of MATLAB code and helped with PCAIM. I particularly wish to express my heartfelt thanks to my academic “big brother” Aron

Meltzner, for continuous scientific discussions, moral support, and friendship over the years; I am so grateful for the opportunity to stand on his shoulders.

Numerous other people (too many to list) at the Earth Observatory of Singapore have helped me out in one way or another over the years, but I wish to thank Linda Chua and Suxian Bu especially for arranging the logistics of my many trips to Singapore. Financial support for this project came from many sources, including grants from the National Science Foundation, grants from the Taiwan ROC National Science Council, the Earth Observatory of Singapore, the Research Center for Geotechnology at the Indonesian Institute of Sciences (LIPI), the Caltech Tectonics Observatory, and the Gordon and Betty Moore Foundation. The Japanese documentary agency NHK also funded a special one-week field expedition in 2012 which allowed us to collect some final data that we would otherwise not have.

Last, but most certainly not least, I would like to thank my husband Adam Azarchs for tolerating my many extended absences while I traveled to Southeast Asia, for always providing a sympathetic ear and occasionally a scientific insight, and most of all for love. Thanks also to my parents Richard Philibosian and Shirley Imsand for cultivating my love of science and the outdoors, for teaching me uncountable things (but particularly writing skills), and for always encouraging me to excel at all my pursuits.

ABSTRACT

Long paleoseismic histories are necessary for understanding the full range of behavior of faults, as the most destructive events often have recurrence intervals longer than local recorded history. The Sunda megathrust, the interface along which the Australian plate subducts beneath Southeast Asia, provides an ideal natural laboratory for determining a detailed paleoseismic history over many seismic cycles. The outer-arc islands above the seismogenic portion of the megathrust cyclically rise and subside in response to processes on the underlying megathrust, providing uncommonly good illumination of megathrust behavior. Furthermore, the growth histories of coral microatolls, which record tectonic uplift and subsidence via relative sea level, can be used to investigate the detailed coseismic and interseismic deformation patterns. One particularly interesting area is the Mentawai segment of the megathrust, which has been shown to characteristically fail in a series of ruptures over decades, rather than a single end-to-end rupture. This behavior has been termed a seismic "supercycle." Prior to the current rupture sequence, which began in 2007, the segment previously ruptured during the 14th century, the late 16th to late 17th century, and most recently during historical earthquakes in 1797 and 1833. In this study, we examine each of these previous supercycles in turn.

First, we expand upon previous analysis of the 1797–1833 rupture sequence with a comprehensive review of previously published coral microatoll data and the addition of a significant amount of new data. We present detailed maps of coseismic uplift during the two great earthquakes and of interseismic deformation during the periods 1755–1833 and 1950–1997 and models of the corresponding slip and coupling on the underlying megathrust. We derive magnitudes of M_w 8.7–9.0 for the two historical earthquakes, and

determine that the 1797 earthquake fundamentally changed the state of coupling on the fault for decades afterward. We conclude that while major earthquakes generally do not involve rupture of the entire Mentawai segment, they undoubtedly influence the progression of subsequent ruptures, even beyond their own rupture area. This concept is of vital importance for monitoring and forecasting the progression of the modern rupture sequence.

Turning our attention to the 14th century, we present evidence of a shallow slip event in approximately A.D. 1314, which preceded the "conventional" megathrust rupture sequence. We calculate a suite of slip models, slightly deeper and/or larger than the 2010 Pagai Islands earthquake, that are consistent with the large amount of subsidence recorded at our study site. Sea-level records from older coral microatolls suggest that these events occur at least once every millennium, but likely far less frequently than their great downdip neighbors. The revelation that shallow slip events are important contributors to the seismic cycle of the Mentawai segment further complicates our understanding of this subduction megathrust and our assessment of the region's exposure to seismic and tsunami hazards.

Finally, we present an outline of the complex intervening rupture sequence that took place in the 16th and 17th centuries, which involved at least five distinct uplift events. We conclude that each of the supercycles had unique features, and all of the types of fault behavior we observe are consistent with highly heterogeneous frictional properties of the megathrust beneath the south-central Mentawai Islands. We conclude that the heterogeneous distribution of asperities produces terminations and overlap zones between fault ruptures, resulting in the seismic "supercycle" phenomenon.

TABLE OF CONTENTS

LIST OF FIGURES

LIST OF TABLES

CHAPTER 1

INTRODUCTION AND METHODS

1.1 Introduction

With each recent great earthquake, it has become more and more clear that long paleoseismic records are necessary to accurately anticipate the future behavior of fault systems. In the case of the 2004 Aceh-Andaman earthquake and tsunami, paleoseismic and paleotsunami studies a few years after the disaster revealed that such large events occur approximately every 500 years and that the previous event had occurred as a doublet in the late-14th and mid-15th centuries [*Jankaew et al.*, 2008; *Monecke et al.*, 2008; *Meltzner et al.*, 2010]. The consensus among scientists before the disaster had been that this long-dormant section of the Sunda megathrust did not generate great earthquakes [e.g., *McCann et al.*, 1979]. In the case of the 2011 Tohoku earthquake and tsunami, paleotsunami records had revealed just a few years before the disaster that such events had happened about once every 1000 years for the past few millennia and that the previous great tsunami had occurred in A.D. 869 [*Minoura et al.*, 2001; *Sawai et al.*, 2007]. Tragically, scientific consensus and dissemination of this information was still a few years away when the earthquake occurred. Only by obtaining long paleoseismic records may we anticipate and properly prepare for such events.

The islands above the Sunda megathrust west of Sumatra (Figure 1.1) provide an exceptional environment for studying past subduction megathrust behavior. In this region, the Australian and Indian plates subduct beneath the Sunda plate. A diffuse zone

of deformation west of Sumatra forms the boundary between the Australian and Indian plates, sometimes incorporated into the Capricorn microplate [*DeMets et al.*, 2010]; however, the subduction zone is fairly uncomplicated. As the islands are located above the part of the megathrust which is frictionally locked between great earthquakes, the buildup and release of tectonic strain at depth causes cyclic subsidence and uplift at the surface [e.g., *Thatcher*, 1984]. Furthermore, the tropical environment supports the formation of coral "microatolls," which grow in the intertidal zone tracking relative sea level [*Scoffin et al.*, 1978]. These natural geodetic instruments contain long, high-temporal-resolution records not only of fault ruptures, but also of deformation between large earthquakes. For most other fault systems around the world, this level of detail is limited to the few decades of the instrumental period.

The 700-km-long Mentawai section of the Sunda megathrust, between the Batu Islands and Enggano Island, is particularly interesting because it appears to be a distinct segment of the fault bounded by persistent barriers to major ruptures, and characterized by rupture sequences rather than single end-to-end ruptures [*Sieh et al.*, 2008]. Coral microatolls illuminate a 700-year-long paleoseismic and paleogeodetic record comprising four long periods of aseismic strain accumulation, each of which culminated in a series of large megathrust ruptures. *Sieh et al.* [2008] coined the term "supercycles" for these seismic cycles that culminate in a series of large ruptures rather than in a single event. The 2007 Mentawai earthquakes were the first large earthquakes in nearly two centuries and, judging from the past three supercycles, are the beginning of a potentially complex rupture sequence that will take place over several decades. We are motivated to study the

previous supercycles, because of the insights they are likely to yield about how the current rupture sequence may progress.

Sieh et al. [2008] determined that the three most recent rupture sequences occurred during the 14th century, during the late 16th to late 17th centuries, and during the late 18th and early 19th centuries as the historically known earthquakes of 1797 and 1833. In each of the following chapters, we examine one of these supercycles in greater detail, illuminating a varied paleoseismic history involving diverse types of fault behavior.

1.2 Methods

The upper surfaces of annually banded coral microatolls, which track relative sea level as they grow near the base of the intertidal zone, record tectonic vertical deformation. In this study, we employed now well-established techniques pioneered by *Zachariasen et al.* [1999; 2000] and *Natawidjaja et al.* [2004] to extract paleoseismic and paleogeodetic data from such microatolls. In the field, we precisely surveyed the relative elevations of microatoll surfaces before cutting radial or diametric vertical slices with a chainsaw designed for underwater cutting of concrete. Because there may be numerous specimen- or site-specific non-tectonic environmental influences on coral growth, we did not usually rely on solitary specimens. Instead, we preferentially selected corals that belonged to populations with similar morphology and at similar elevations. We also place more emphasis on data that are consistent across multiple sites.

We later prepared an x-ray image of each collected coral slice to illuminate the annual density bands, and mapped them in cross section. To constrain the dates of growth we

determined ages of one or more small samples from each slice, using uranium-thorium disequilibrium techniques developed and described by *Edwards et al.* [1988] and *Shen et al.* [2002; 2008; 2010]. We sampled predominantly *Porites lutea* and *lobata* species, as these form the longest-lived hemispherical colonies (all corals we present are of this type unless otherwise specified). However, we occasionally sampled other types of hemispherical colonies with larger corallites, as these have thicker aragonitic structures that frequently yield more precise U-Th ages. We tentatively identify those with 3–5 mm diameter corallites as *Goniastrea retiformis* and those with ~1 cm corallites as belonging to the genus *Favia*.

The results are time series of upward coral growth, with absolute ages constrained to within a few years to a few decades. Following *Meltzner et al.* [2010], we have made two improvements to earlier coral interpretation methodologies. First, we have refined the time series ages by using the dates of regional, non-tectonic, oceanographically induced die-downs in the coral records. Second, we have calculated interseismic rates of subsidence using the most reliable subset of points on the growth curves. The following two sections describe in detail the reasons for and the details of these improved methods.

1.2.1 Improved Absolute Ages of Coral Records Using Oceanographic Die-Downs

One of the problems in determining precise time series is the imprecision of U-Th disequilibrium ages. Although exceptionally clean samples yield dates with uncertainties of only a few years, samples with abundant initial ^{230}Th commonly have uncertainties of several decades. This is certainly a problem when it is important to resolve the dates of

earthquakes that are separated by only a few years or decades, as is the case for the 1797/1833 doublet. In some cases, one can use the historical dates of large earthquakes to reduce the uncertainty in the date of an event, as *Natawidjaja et al.* [2006] did. However, this typically relies on the questionable assumption that the outermost preserved band on a microatoll represents the living surface at the time of death. This is often an invalid assumption because most "fossil" microatolls are at least slightly eroded and some number of bands are missing from the outer perimeter of the sampled slice. A more reliable method of reducing age uncertainty is to correlate the coral records based on the pattern of non-tectonic die-downs, events during which the upper several centimeters of the living coral surface die due to a temporary lowering of the sea surface. Because oceanographic phenomena are typically regional in scope, they can be expected to impose an isochronous marker on most or all corals over a wide area, which allows correlation between coral records.

We tested this method on 20th-century coral records (from *Natawidjaja et al.* [2007] and our own study), which have little or no absolute age uncertainty because the outer surface was usually living when each coral was collected. Die-downs typically occur close to the beginning or ending of a calendar year, but the exact location of the year boundaries is rarely unequivocal. We adopt the policy of assigning die-downs to the later of the two possible years (e.g., the die-down which occurred in late 1997/early 1998 is assigned to 1998). By counting the number of coral records with die-downs in each year, it is easy to identify regional die-down events (Figure 1.2a). We then use these events to

resolve uncertainties in band counting by choosing the interpretations that allow the best correlation between die-down years among all the records.

As an additional confirmation, we compare the identified die-down events to independent measurements of the Indian Ocean Dipole (IOD). Instrumental records of the past few decades show that this oscillation, the primary non-tidal-harmonic variation of sea surface height in the Indian Ocean, can lower sea level in the Mentawai Islands by tens of centimeters in a strong positive mode [*Saji et al.*, 1999; *Webster et al.*, 1999; *Murtugudde et al.*, 2000]. *Abram et al.* [2008] identified positive IOD events between 1845 and 2007 based on isotope geochemistry of coral records in the Mentawai region and the Seychelles. As shown on Fig. 1.2a, almost all of the late 20th-century IOD events are associated with coral microatoll die-downs, but there are additional interspersed die-down events which are likely due to other oceanographic phenomena that did not leave an IOD-type isotopic signature.

There is also a good correspondence between Mentawai regional die-downs and robust regional die-downs hundreds of kilometers to the north, on Simeulue Island [*Meltzner et al.*, 2010; 2012]. The weaker correspondence with the less robust Simeulue events (open circles in Fig. 1.2a) is not surprising, given that some of those represent a die-down on only one microatoll, and that IOD effects are strongest in the southern Mentawais and weaker farther north.

Based on the success of this test, we applied the same technique to the 18th- and 19th-century coral records (from *Natawidjaja et al.* [2006] and this study), using the correlations between die-downs as well as the dates of the historical earthquakes to assign

a best estimate of the absolute date span of each record, within the uncertainty of the U-Th ages. As with the modern case, we were able to identify regional die-down events and adopt interpretations of band-counting uncertainties to maximize consistency among all the records. The final analysis reveals four robust regional die-downs and nine less robust events (Fig. 1.2b), suggesting that IOD events were significantly less common between 1750 and 1830 than between 1950 and 2010. This is in and of itself an interesting result for climate science, but further investigation of IOD patterns is beyond the scope of this study.

It is worth noting that one robust regional die-down that we identify occurred in the same year (1818) as a historical tsunamigenic earthquake reported in the Bengkulu area on the coast of Sumatra [*Newcomb and McCann*, 1987]. However, unless the earthquake affected a much larger area than reported, it seems unlikely that it would have caused such a widespread coral die-down (Bengkulu is 150 km southeast of the nearest coral record we have). Moreover, in every one of our coral records, the 1818 die-down has oceanographic characteristics rather than tectonic characteristics (i.e., the coral recovered completely from the die-down and returned to its original growth trend, rather than adjusting to a new, lower relative sea level). We conclude that the 1818 die-down was largely oceanographic and its correlation with the 1818 earthquake is coincidental. However, we cannot exclude the possibility that the die-down had a tectonic component, particularly at our southernmost sites which are closest to Bengkulu.

1.2.2 Interseismic Rate Fitting Procedure

Rates and patterns of interseismic subsidence and uplift place important constraints on the behavior of the underlying megathrust. Over many decades, deformation at a given location can typically be well approximated by a constant linear rate. This rate can be determined from coral growth time series, but because corals respond to oceanographic fluctuations as well as land level changes, it is inappropriate to simply fit all points in the time series to obtain a rate. To choose the points to fit in order to accurately extract the interseismic signal, we must consider certain characteristics of coral growth. Upward coral growth in any one year is limited by its growth rate and the level of that year's extreme low water (ELW) [*Taylor et al.*, 1987], with the species we dominantly sample (*Porites lutea* and *lobata*) typically surviving ~20 cm above ELW in this region [*Meltzner et al.*, 2010]. This ELW-limited elevation is termed the highest level of survival (HLS), while lower growth-limited elevations are termed highest level of growth (HLG). Because of the growth-rate limitation, coral records are not sensitive to brief rises in sea level (such as negative IOD events) as they are to brief drops in sea level (such as positive IOD events), which means most recorded HLS "hits" are in years with anomalously low ELW.

Natawidjaja et al. [2006; 2007] fit combinations of preserved HLS and HLG points to obtain interseismic rates. However, these rates are biased because all of the fit points lie below the long-term trend in HLS controlled by relative mean sea level. In particular, very large die-downs early or late in the coral record (such as the 1962 and 1998 die-downs in many records) can substantially skew the results. To avoid this problem, we

adopt the method of *Meltzner et al.* [2010], which is based on the idea that HLG points just before oceanographic die-downs represent the best estimates of the long-term trend in HLS. These HLG points are frequently somewhat eroded, but they are closer to the inter-annual average HLS than lower preserved HLG points. For our linear fits, we select the highest HLG point just before each die-down, excluding the HLG before the first die-down in a coral record if it is significantly below the trend. We calculate 2σ uncertainties on these least-squares fit rates whenever there are enough points being fit (generally 4 or more) for the uncertainty to be meaningful. Since corals subjected to high interseismic subsidence rates typically record less frequent die-downs, uncertainties on high subsidence rates tend to be larger.

References

Abram, N. J., M. K. Gagan, J. E. Cole, W. S. Hantoro, and M. Mudelsee (2008), Recent intensification of tropical climate variability in the Indian Ocean, *Nature Geoscience*, *1*, 849–853.

Briggs, R. W., et al. (2006), Deformation and slip along the Sunda megathrust in the great 2005 Nias-Simeulue earthquake, *Science*, *311*, 1897–1901.

DeMets, C., R. G. Gordon, and D. F. Argus (2010), Geologically current plate motions, *Geophys. J. Int.*, *181*, 1–80.

Edwards, R. L., F. W. Taylor, and G. J. Wasserburg (1988), Dating earthquakes with high-precision thorium-230 ages of very young corals, *Earth Planet. Sci. Lett.*, *90*(4), 371–381.

Hill, E. M., et al. (2012), The 2010 M_w 7.8 Mentawai earthquake: Very shallow source of a rare tsunami earthquake determined from tsunami field survey and near-field GPS, *J. Geophys. Res.*, *117*, B06402, doi:10.1029/2012JB009159.

Jankaew, K., B. F. Atwater, Y. Sawai, M. Choowong, T. Charoentitirat, M. E. Martin, and A. Prendergast (2008), Medieval forewarning of the 2004 Indian Ocean tsunami in Thailand, *Nature*, *455*(1228–1231).

Konca, A. O., et al. (2008), Partial rupture of a locked patch of the Sumatra megathrust during the 2007 earthquake sequence, *Nature*, *456*, 631–635.

McCann, W. R., S. P. Nishenko, L. R. Sykes, and J. Krause (1979), Seismic gaps and plate tectonics; seismic potential for major plate boundaries, *Pure and Applied Geophysics*, *117*(6), 1082–1147.

Meltzner, A. J., K. Sieh, H.-W. Chiang, C.-C. Shen, B. W. Suwargadi, D. H. Natawidjaja, B. E. Philibosian, R. W. Briggs, and J. Galetzka (2010), Coral evidence for earthquake recurrence and an A.D. 1390-1455 cluster at the south end of the 2004 Aceh-Andaman rupture, *J. Geophys. Res.*, *115*, B10402, doi:10.1029/2010JB007499.

Meltzner, A. J., K. Sieh, H.-W. Chiang, C.-C. Shen, B. W. Suwargadi, D. H. Natawidjaja, B. Philibosian, and R. W. Briggs (2012), Persistent termini of 2004- and 2005-like ruptures of the Sunda megathrust, *J. Geophys. Res.*, *117*, B04405, doi:10.1029/2011JB008888.

Minoura, K., F. Imamura, D. Sugawara, Y. Kono, and T. Iwashita (2001), The 869 Jogan tsunami deposit and recurrence interval of large-scale tsunami on the Pacific coast of Northeast Japan, *Journal of Natural Disaster Science*, *23*(2), 83–88.

Monecke, K., W. Finger, D. Klarer, W. Kongko, B. G. McAdoo, A. L. Moore, and S. U. Sudrajat (2008), A 1,000-year sediment record of tsunami recurrence in northern Sumatra, *Nature*, *455*(7217), 1232–1234.

Murtugudde, R., J. P. McCreary, and A. J. Busalacchi (2000), Oceanic processes associated with anomalous events in the Indian Ocean with relevance to 1997-1998, *J. Geophys. Res.*, *105*(C2), 3295–3306.

Natawidjaja, D. H., K. Sieh, S. N. Ward, H. Cheng, R. L. Edwards, J. Galetzka, and B. W. Suwargadi (2004), Paleogeodetic records of seismic and aseismic subduction from central Sumatran microatolls, Indonesia, *J. Geophys. Res.*, *109*(B04), 4306, doi:10.1029/2003JB002398.

Natawidjaja, D. H., K. Sieh, M. Chlieh, J. Galetzka, B. W. Suwargadi, H. Cheng, R. L. Edwards, J.-P. Avouac, and S. N. Ward (2006), Source parameters of the great Sumatran megathrust earthquakes of 1797 and 1833 inferred from coral microatolls, *J. Geophys. Res.*, *111*(B6), 6403, doi:10.1029/2005JB004025.

Natawidjaja, D. H., K. Sieh, J. Galetzka, B. W. Suwargadi, H. Cheng, R. L. Edwards, and M. Chlieh (2007), Interseismic deformation above the Sunda Megathrust recorded in coral microatolls of the Mentawai islands, West Sumatra, *J. Geophys. Res.*, *112*(B02), 2404, doi:10.1029/2006JB004450.

Newcomb, K. R., and W. R. McCann (1987), Seismic history and seismotectonics of the Sunda Arc, *J. Geophys. Res.*, *92*(B1), 421–439.

Saji, N. H., B. N. Goswami, P. N. Vinayachandran, and T. Yamagata (1999), A dipole mode in the tropical Indian Ocean, *Nature*, *401*, 360–363.

Sawai, Y., M. Shishikura, Y. Okamura, T. Matsu'ura, J. Komatsubara, and T. T. Aung (2007), Tsunami inundation history in Sendai Plain, inferred from tsunami deposits, *Abstracts With Programs - Geological Society of America*, *39*(6), 158.

Scoffin, T. P., D. R. Stoddart, and B. R. Rosen (1978), The nature and significance of microatolls, *Philos. Trans. R. Soc. London Ser. B*, *284*(999), 99–122.

Shearer, P., and R. Bürgmann (2010), Lessons learned from the 2004 Sumatra–Andaman megathrust rupture, *Annu. Rev. Earth Planet. Sci.*, *38*, 103–131.

Shen, C.-C., R. L. Edwards, H. Cheng, J. A. Dorale, R. B. Thomas, S. B. Moran, S. E. Weinstein, and H. N. Edmonds (2002), Uranium and thorium isotopic and concentration measurements by magnetic sector inductively coupled plasma mass spectrometry, *Chem. Geol.*, *185*, 165–178.

Shen, C.-C., et al. (2008), Variation of initial $^{230}Th/^{232}Th$ and limits of high precision U-Th dating of shallow-water corals, *Geochim. Cosmochim. Acta*, *72*(17), 4201–4223.

Shen, C.-C., A. Kano, M. Hori, K. Lin, T.-C. Chiu, and G. S. Burr (2010), East Asian monsoon evolution and reconciliation of climate records from Japan and Greenland during the last deglaciation, *Quat. Sci. Rev.*, *29*, 3327–3335.

Sieh, K., D. H. Natawidjaja, A. J. Meltzner, C.-C. Shen, H. Cheng, K.-S. Li, B. W. Suwargadi, J. Galetzka, B. Philibosian, and R. L. Edwards (2008), Earthquake supercycles inferred from sea-level changes recorded in the corals of west Sumatra, *Science*, *322*, 1674–1678.

Taylor, F. W., C. Frohlich, J. Lecolle, and M. R. Strecker (1987), Analysis of partially emerged corals and reef terraces in the central Vanuatu Arc; comparison of contemporary coseismic and nonseismic with Quaternary vertical movements, *J. Geophys. Res.*, *92*(B6), 4905–4933.

Thatcher, W. (1984), The earthquake deformation cycle, recurrence, and the time-predictable model, *J. Geophys. Res.*, *89*(B7), 5674–5680.

Webster, P. J., A. M. Moore, J. P. Loschnigg, and R. R. Leben (1999), Coupled ocean-atmosphere dynamics in the Indian Ocean during 1997-98, *Nature*, *401*(6751), 356–360.

Zachariasen, J., K. Sieh, F. W. Taylor, R. L. Edwards, and W. S. Hantoro (1999), Submergence and uplift associated with the giant 1833 Sumatran subduction earthquake: Evidence from coral microatolls, *J. Geophys. Res.*, *104*(B1), 895–919.

Zachariasen, J., K. Sieh, F. W. Taylor, and W. S. Hantoro (2000), Modern vertical deformation above the Sumatran subduction zone: Paleogeodetic insights from coral microatolls, *Bull. Seismol. Soc. Am.*, *90*(4), 897–913.

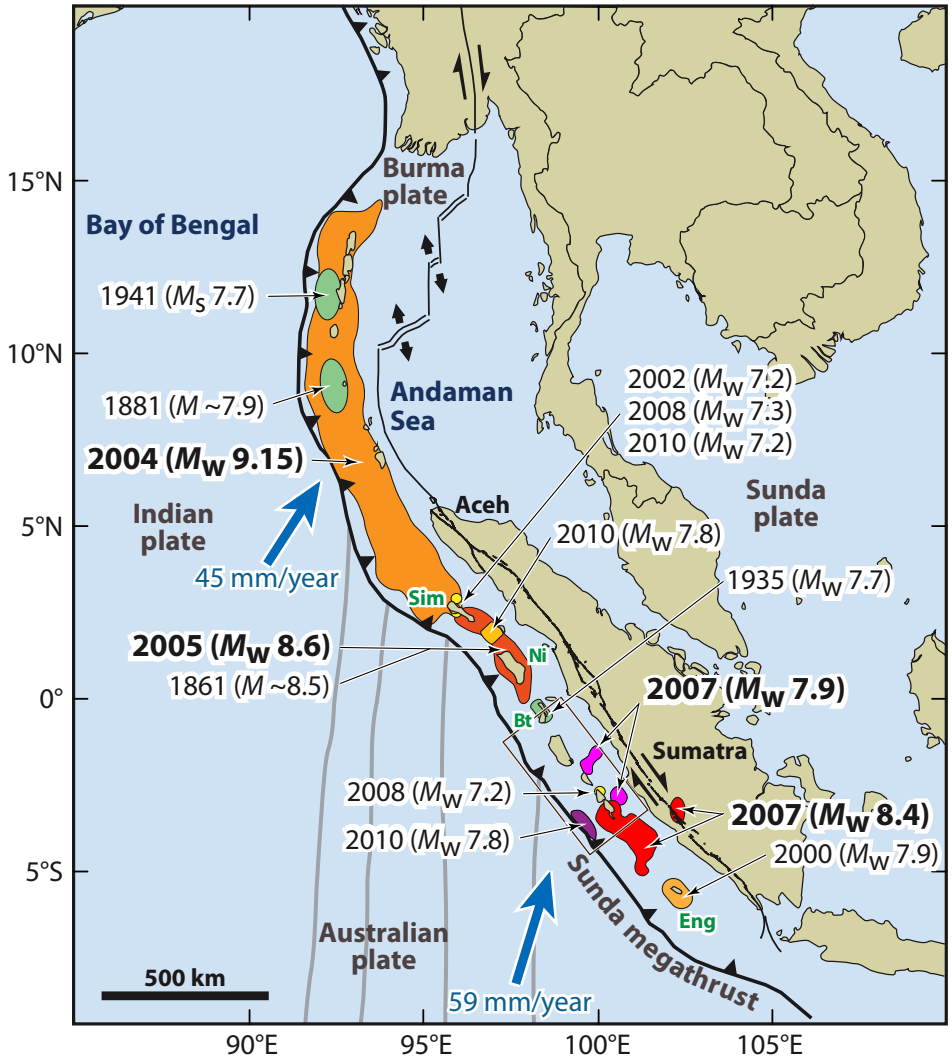

Figure 1.1. Map of southeast Asia showing recent and selected historical ruptures of the Sunda megathrust. Black lines with sense of motion are major plate-bounding faults and gray lines are seafloor fracture zones. Sim = Simeulue, Ni = Nias, Bt = Batu Islands, and Eng = Enggano. Brown box centered at 2°S, 99°E delineates the Mentawai Islands. Figure adapted from *Meltzner et al.* [2012] with rupture areas and magnitudes from *Briggs et al.* [2006], *Konca et al.* [2008], *Meltzner et al.* [2010], *Hill et al.* [2012], and references therein; relative plate motions from *Shearer and Bürgmann* [2010].

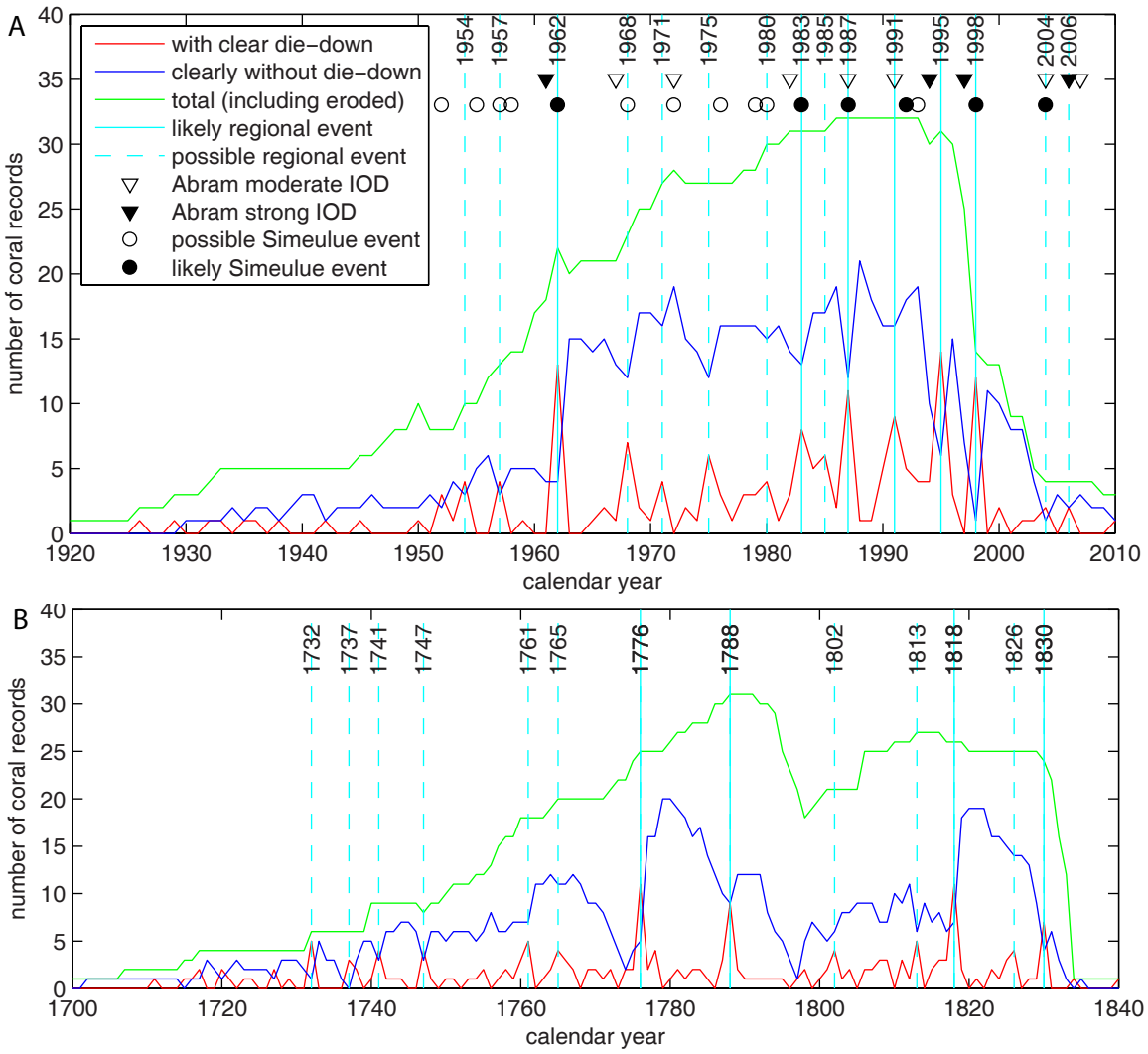

Figure 1.2. Oceanographic effects on coral growth expressed as widespread die-downs in certain years, likely related to positive IOD conditions. These events generally do not cause die-downs on every coral, but stand out on these graphs as red spikes correlated with blue troughs. A) Records covering the 20th and early 21st centuries, with comparison to positive IOD events identified by *Abram et al.* [2008] based on coral geochemistry. Some IOD events appear the year before the die-down occurs due to the way die-down years are assigned, but every IOD event except possibly 1972 corresponds to a die-down. About a third of the die-downs (generally the less robust ones) do not correspond to IOD events. There is also a strong correspondence with likely regional die-downs on Simeulue Island [*Meltzner et al.* 2010; 2012]. B) Records covering the 18th and early 19th centuries show four particularly widespread die-downs and nine less robust events. It appears that IOD events were less common during this period than in the mid-late 20th century.

CHAPTER 2

EXPANDED ANALYSIS OF THE HISTORICAL 1797–1833 SEISMIC SUPERCYCLE

2.1 Introduction

As is common for geologic data, the paleogeodetic record from coral microatolls becomes less and less complete as one searches farther and farther back in time. Thus, the record of the penultimate rupture sequence (comprising the historical great earthquakes of 1797 and 1833) is the most complete. *Natawidjaja et al.* [2006] presented uplift maps and some basic forward models of megathrust slip during these events. Here, we present a revised analysis of this historical supercycle, including a substantial amount of new coral data as well as a comprehensive review of previously published data. We synthesize all these data, first, to refine the megathrust ruptures of the 1797 and 1833 earthquakes, and second, to investigate megathrust behavior during the intervening decades. Since the first rupture in the current sequence has already occurred, the behavior of the megathrust between earlier great earthquakes is of particular interest. This analysis offers evidence of how great earthquakes change the state of coupling on faults and influence subsequent ruptures, vital concepts both for scientific understanding of the seismic cycle and for earthquake forecasting.

2.2 Coral Data and Interpreted Vertical Deformation

We now analyze coral microatolls relevant to understanding the 1797 and 1833 megathrust ruptures and interseismic behavior during adjacent time periods. In addition to consistently synthesizing all coral records from the Mentawai Islands covering the 18th and 19th centuries, we also compile the records covering the 20th and early 21st centuries. This has two purposes: first, we wish to compare recent interseismic behavior to past behavior, and second, we obtain first-order estimates of total coseismic uplift by projecting recent interseismic subsidence rates back to the time of past earthquakes. This estimation is necessary if tectonic uplift killed the corals completely, as was the case everywhere for the 1833 earthquake and in the northern Mentawais for the 1797 earthquake. We supplement coral records from *Natawidjaja et al.* [2006; 2007] and *Sieh et al.*[2008] with new data from 2 old sites (Siruamata and Badgugu), 10 complete new sites, and some data from 7 other new sites that are discussed in Chapter 4 (Figure 2.1). In this section, we first summarize our re-analysis of previously published data, then present new data, and finally synthesize all these coral records to show the spatial patterns of coseismic and interseismic deformation. In the interests of brevity, we highlight data from only a few exemplary new sites in this text; the remainder can be found in the supplementary figures. Figures 2.S1–2.S2 show compilations of all coral time series used in this study, and all interseismic rates and coseismic uplifts derived from these records are compiled in Tables 2.1–2.2 (coordinates are relative to WGS-84 datum).

2.2.1 Synthesis of Previously Published Data

We re-interpret all coral records of the relevant ages from the previous papers using the improved correlation and rate-fitting techniques described in section 1.2. By and large our re-analysis yields interseismic rates and coseismic uplifts that differ only slightly from those previously published and are within previously estimated uncertainties. However, a handful of our revisions are more significant and warrant more specific explanation here.

At Sikici site B on Sipora, the coral SKC03-B3 was interpreted by *Natawidjaja et al.*[2006] and *Sieh et al.* [2008] to have died in 1833, despite an age uncertainty that was large enough to encompass death in either 1797 or 1833. Based on the correlation techniques described above and new data from the nearby Sikici site D that records uplift and death of a large population of precisely dated corals in 1797 (see Figs. 2.S6–2.S7), we now interpret SKC03-B3 as having died in 1797. Uplift in 1833 is not recorded at Sikici since the reefs apparently died completely in 1797.

In the coral record SMY03-C4 from Simanganya on North Pagai, *Natawidjaja et al.*[2006] and *Sieh et al.* [2008] attribute the final death of the colony to 1833 uplift and a tiny 5-cm die-down (indistinguishable from small non-tectonic die-downs) to 1797 uplift. However, there is a larger >10-cm die-down about 8 years earlier which clearly offsets the interseismic trend. The earlier studies presumably did not assign this more obviously tectonic uplift to 1797 because there appeared to be more than 35 years of growth between it and the death of the colony. In actuality the banding in the outer part of the coral head is quite unclear. We assign the >10-cm uplift to 1797 and count a smaller

number of bands in the outer half of the head based on correlations of oceanographic die-downs.

Zachariasen et al. [1999] and *Natawidjaja et al.*[2006] presented a total of five coral records covering the 18th and 19th centuries from Silabu on North Pagai: SLB00-A2, which died for non-tectonic reasons in the mid-1700s; SLB00-A4, which died in 1797; SLB00-A3, which had a large die-down in 1797 and died completely in 1833; and NP94-A8 and A9, which hit HLS after 1797 and died in 1833. However, the scenario for this site presented by *Natawidjaja et al.*[2006] has unexplained internal inconsistencies. We favor a different interpretation of the site history which is detailed in Fig. 2.S3. Our new interpretation does not change the coseismic uplift estimates, but informs our calculation of interseismic subsidence rates.

At Saomang off the coast of South Pagai, *Natawidjaja et al.*[2006] and *Sieh et al.* [2008] presented the very poorly dated coral record SMG02-A2. It was unclear how this record fit into the site's history. We obtained a much more precise age, which suggests that it died due to uplift in the 1797 earthquake. In combination with the younger P96F-1 record from a microatoll which died due to 1833 uplift, these new data allowed us to determine that the 1797 uplift at Saomang was 28 ± 4 cm, much less than the 80–100 cm previously estimated based on less-certain extrapolations.

2.2.2 New Data

2.2.2.1 Betumonga

The Betumonga site lies in a bay on the southwest corner of North Pagai Island. A large population of long-lived, mostly hat-shaped fossil microatolls (Figure 2.2) provides an exemplary record of interseismic deformation before and between the 1797 and 1833 earthquakes, as well as large coseismic uplift during both of those earthquakes. The hat shape of the microatolls reflects partial uplift in 1797 (which left the crown of the hat), followed by radial outward growth at a lower level (which created the hat's brim), culminating in the death of the coral colony by uplift in 1833. We sampled two of the best-preserved microatolls. One of these is hat-shaped, recording the total 1797 uplift and the interseismic period between the two earthquakes. The other died completely in 1797 and thus did not record sea level following that earthquake (Figure 2.3.)

These corals recorded a 90 ± 5 cm uplift in 1797 and at least 40 cm of uplift in 1833, in addition to fairly well-constrained interseismic subsidence rates between 1730 and 1797 and between 1797 and 1833. The pre-1797 rate derived from A1 is somewhat higher than that derived from A2 (though the uncertainties do overlap). It is possible that the A1 record has an uncorrected tilt, as the central overgrowth obscured the concentric rings which we would normally use to measure tilt. Head A1 sits 10–20 cm lower in elevation than A2, indicating that A1 settled into the substrate and might well have tilted as it settled. We calculate the pre-1797 interseismic subsidence rate based on A2 alone, since the longer record provides a more precise rate estimate and the many exposed concentric rings make it clear that A2 is untilted. The rates both before and after 1797

are ~1 cm/yr and are identical within uncertainty, illustrating that the interseismic behavior at this site did not change appreciably following the 1797 earthquake.

2.2.2.2 Siruamata and Bangkaulu

Siruamata is an islet off the southwest coast of Sipora Island. *Zachariasen et al.* [1999] originally presented a record from the particularly well-preserved hat-shaped microatoll Si94A-6 from a site on Siruamata's northern shore. *Natawidjaja et al.* [2006] reinterpreted this record and presented a record from a nearby modern microatoll. Si94A-6 recorded subsidence for a few decades before 1797 and a 70-cm coseismic uplift in 1797, but the outer ring that grew after 1797 was quite eroded and apparently stopped growing for non-tectonic reasons prior to 1833 (perhaps due to the postulated strong IOD event in ~1818). In order to secure a reliable sea-level history for the period between 1797 and 1833, we returned to this site in 2010 to collect a new slab (SRM10-A6) from a better-preserved radius of the same microatoll. Along this radius, the outer ring of coral continued to live and grow until 1833 (Figure 2.4A). The combination of the previous and the new slabs illustrates that the interseismic subsidence rate changed markedly after the 1797 earthquake, dropping almost in half from 6.9 to 3.9 mm/yr (Figure 2.4B).

This change in rate is intriguingly similar to the behavior at Bangkaulu, near the southeast end of South Pagai, about 150 km distant. The microatoll BKL03-A1 was uplifted and died in 1833 [*Natawidjaja et al.*, 2006]. The site is near the southern terminus of the 1797 rupture and BKL03-A1 records little or no uplift in 1797, but the interseismic subsidence rate does appear to decrease from 7.6 to 3.8 mm/yr around that

time (Figure 2.4C). Betumonga, with no apparent rate change, lies about halfway between Siruamata and Bangkaulu.

2.2.2.3 Badgugu

One other coral record of particular interest comes from Badgugu A (West Badgugu), at the southeastern end of the Batu Islands. The site, microatoll cross sections, and U-Th dates were fully described by *Natawidjaja* [2003], and parts of the microatoll growth histories were included by *Natawidjaja et al.* [2006]. BDG00-A1 is an exceptionally long-lived coral head that reached a diameter over 8 meters after more than 200 years of growth (Figure 2.5). It emerged and died during the 1935 Batu Islands earthquake [*Natawidjaja et al.*, 2004].

Located at the northern end of both the Mentawai segment and the 1797 rupture, this coral subsided at low rates of 0–2 mm/yr throughout its life, supporting previous claims of weak coupling beneath the Batu Islands [*Rivera et al.*, 2002; *Natawidjaja et al.*, 2004; *Chlieh et al.*, 2008]. The record is punctuated by a 20-cm uplift in the late 1700s (presumably due to the 1797 earthquake) and a 5–10-cm uplift in 1833, however, the latter uplift was recovered (presumably due to postseismic fault slip or lithospheric relaxation) within 5 years of the earthquake. It is uncertain whether interseismic deformation rates changed following either of the great Mentawai earthquakes, but any change was clearly not large. This record demonstrates the long-term stability of the megathrust beneath the Batu Islands over an entire Mentawai supercycle as well as a Nias-Simeulue segment rupture in 1861 [*Newcomb and McCann*, 1987]. Interestingly,

interseismic subsidence at Badgugu increased markedly following the 1935 earthquake [*Natawidjaja et al.*, 2004], averaging 6.7 mm/yr over the period 1935–1997.

2.2.2.4 Additional New Sites

In addition to those discussed in the previous sections, we collected coral slabs at 7 other sites in the Mentawais where the primary populations of fossil corals date to the 18^{th}–19^{th} centuries: Trait and Sikici D on Sipora, North North Pagai (an uninhabited, nameless bay), Silabusabeu (a small islet near Silabu village on North Pagai), and the small islands of Pecah Belah, Simaturugogo, and Simungguk in the archipelago southeast of South Pagai (Fig. 2.1). We also collected slabs from living microatolls at two other sites: Pulau Karangmadjat in the archipelago south of Siberut, and Pulau Simasin off the north coast of Siberut. The Karangmadjat modern subsidence rate is only 3.9 mm/yr, considerably lower than other sites at the southwest end of Siberut. The Simasin record is flat with essentially zero interseismic deformation, suggesting that it lies on the hinge line of interseismic deformation. Complete descriptions of all of these sites and slabs are in the supplementary Figures 2.S4–2.S18.

We complete our dataset with slabs from 7 additional new sites: Pulau Panjang C and North Pukarayat on Sipora, Pasapuat and Cimpungan on North Pagai, Basua on South Pagai, a second site on the Pecah Belah islet, and a new site on Sanding, a small island 30 km southeast of South Pagai (Fig. 2.1). All of these sites have significant populations of microatolls which date to the 17^{th} century or earlier, so they are discussed in Chapter 4.

Cross sections and growth histories of the relevant 18th- and 19th-century microatolls from these sites appear in the supplementary figures 2.S19–2.S24).

2.2.3 Patterns of Coseismic and Interseismic Deformation

Having produced these datasets with consistent methods, we are now in a position to compare patterns of interseismic and coseismic deformation in different time periods. At this juncture, however, it is necessary to consider the possible impacts of sea-level change over decades or centuries, so that we do not mistakenly ascribe climatic changes to tectonic processes.

2.2.3.1 Effects of Sea-Level Change

It is reasonable to assume that any climate-related changes in sea level would be regional in extent, affecting all Mentawai corals equally. This assumption is supported by satellite altimetry data covering the last few decades that indicates that sea level across the Mentawai region has been rising uniformly by about 3.5 mm/yr [*Beckley et al.*, 2007]. If the modern period is representative of earlier periods, then, spatial variations in rate within a given time period can only be explained tectonically. However, variations in rate from one time period to another may be due in part to differing rates of sea-level change.

It is known from tide gauge records that during the 20th century, the globally averaged rate of sea-level rise was ~1.7 mm/yr [*Church and White*, 2006]. Due to changing wind and ocean circulation patterns, sea-level trends in individual ocean basins differed

significantly from this average, ranging from 0 to 5 mm/yr [*Church et al.*, 2004]. Unfortunately, there is little data constraining 20th-century sea-level change in the Indian Ocean. A reconstruction by *Church et al.* [2006] based on long-term tide gauge records and recent satellite altimetry suggests a very high rate of sea-level rise (4 mm/yr) southwest of Sumatra. However, the accuracy of this result is questionable since their model includes only one long-term tide gauge in the Indian Ocean, located on the opposite side of the ocean from Sumatra. *Jevrejeva et al.* [2006] used a different tide gauge dataset and methodology to estimate basin-wide trends. Their results suggest that the average rate of sea-level rise over the 20th century in the Indian Ocean has been similar to the global average, but fluctuated significantly: increasing from 2 mm/yr in 1910 to 4 mm/yr in 1940, then steadily decreasing to less than 1 mm/yr in 2000. However, their tide gauge dataset also does not include any records from Sumatra [*Woodworth and Player*, 2003].

Rates and patterns of sea-level change in the 18th and 19th centuries are of course even less well known. Few if any tide gauge records extend so far back. While the effects of anthropogenic climate change were presumably smaller than in the 20th century, other natural climate fluctuations (such as the Little Ice Age) undoubtedly contributed. It is likely that net global sea-level change was negligible over the past 2000 years, as postulated by *Lambeck et al.* [2004], but this does not mean that sea level did not fluctuate on the scale of centuries. A rise of 1 mm/yr sustained over a century would change sea level by only 10 cm, which could easily go unnoticed if sea level then fell during the next century.

Given the generally poor constraints on decade- and century-scale sea-level change in the Mentawai region, we elect to present our interpretations of interseismic deformation rates without correction for sea-level change. We note that we must be cautious in comparing the magnitudes of interseismic rates between different time periods, but we can be fairly confident that changes in deformation patterns within the spatial extent of our study area reflect tectonic processes rather than climatic processes. The most significant potential effect on our results is in the estimation of coseismic uplift in 1833, since this depends on the extrapolation of modern interseismic rates over ~160 years. For instance, correcting for the global average rate of sea-level rise would essentially uniformly reduce our calculated 1833 coseismic uplifts by 27 cm, and the hinge line would be shifted southwest toward the islands. However, as with the interseismic measurements, the spatial patterns of coseismic uplift would be unaffected.

2.2.3.2 Changing Interseismic Deformation Patterns

Figure 2.6 shows contour maps of interseismic deformation rates for the decades prior to 1797, the decades between 1797 and 1833, and for the latter half or the 20th century. The measurements of rates for each of these periods are independent of the measurements for the other two periods, as they are derived from relative elevations of growth bands on individual microatolls and do not depend on absolute elevation measurements. The first and last periods show generally similar patterns: a decreasing gradient of subsidence rate from southwest to northeast across the islands, roughly perpendicular to the trench. The hinge line between uplift and subsidence is constrained by data only near the northern

end of the maps, but by extrapolation is likely located 30–50 km northeast of Sipora and the Pagai Islands.

One significant deviation from this unidirectional decrease in subsidence rates is apparent in the 20th-century records: lower subsidence rates nearer to the trench south of Siberut and on the north end of Sipora define a peak in subsidence rates about 100 km from the trench. Unfortunately our data do not constrain whether this was also the case in the pre-1797 period. However, both patterns are consistent with the updip limit of locking on the megathrust being beneath the southwest coasts of the islands. It is not surprising that deformation patterns in these two periods are similar, as they both cover the five decades or so leading up to the initiation of a supercycle rupture sequence.

In contrast, the deformation pattern during the period between the two great earthquakes is markedly different from the others. The data for this period are more limited in spatial extent, but there were clearly steeply decreasing gradients in subsidence rate along strike from the southeast end and likely also the northwest end of the Pagai Islands. This suggests that the 1797 rupture reduced the degree of coupling on at least two separated patches of the megathrust. However, the magnitude and pattern of subsidence throughout most of the Pagai Islands remained similar to what it had been prior to the 1797 rupture. It is not known how coupling patterns might have changed following the 1833 earthquake, as the reefs died completely due to uplift during that event and no corals from the later 19th century appear to have been preserved in the intertidal zone. We can conclude only that by 1950, interseismic coupling patterns had returned to a more “normal” state.

The notable change in deformation pattern after the 1797 earthquake, which was the beginning of a Mentawai rupture sequence, is intriguingly analogous to recent changes measured by the Sumatran GPS Array (SuGAr) following the 2007 Mentawai earthquakes. Despite being beyond the typical postseismic period, interseismic deformation rates have still not returned to pre-2007 conditions and appear to have stabilized at lower rates, suggesting reduced coupling [*Qiu et al.*, 2012]. Based on the historical rupture sequence, we expect that this new coupling state will persist, perhaps for decades, until the next major rupture in the sequence occurs. This inter-earthquake coupling pattern will no doubt influence the slip distributions of future ruptures. Additional potential modern analogues may be found in the comparison of GPS velocity datasets before and after 2001, which suggest that coupling decreased in the Batu Islands and Enggano regions around that time [*Prawirodirdjo et al.*, 2010]. The sparse temporal sampling of campaign GPS datasets makes it unclear exactly when the changes occurred, but the 2000 Enggano earthquake and 2005 Nias-Simeulue earthquake are obvious candidates for the triggering of these coupling changes.

2.2.3.3 Coseismic Uplift Distributions

At many of our sites, the coseismic uplift in 1797 can be directly measured on microatolls which survived that event. However, no microatolls that we have found (except for the Badgugu specimen) survived the 1833 uplift. As previously noted, all uplifts for 1833 are calculated by projecting the modern subsidence rates (with uncertainty) back to the time of the earthquake, and subtracting this assumed post-

earthquake elevation from the known pre-earthquake HLS. Figure 2.7 schematically illustrates how this is done, and Figure 2.8 shows the resultant uplift distributions for the great earthquakes of 1797 and 1833. For fossil coral sites where no modern coral was collected, we use rates from nearby sites or interpolated modern rates based on the 20th-century contour map in Fig. 2.6.

At some sites (particularly on Siberut and Sipora), the fringing reefs died completely in 1797 and had apparently not re-established by 1833. At these sites, we add the additional subsidence between 1797 and 1833 to estimate the total coseismic uplift due to both earthquakes (black numbers on Fig. 2.8). For sites on the Pagai Islands we use the known rates for 1797–1833 period (Fig. 2.7C), but for those on Siberut and Sipora we assume the rates between 1797 and 1833 were the same as the modern rates (Fig. 2.7B), because our data do not constrain the inter-earthquake behavior there. If the subsidence between 1797 and 1833 was indeed slower than the modern subsidence at any of those sites, the total coseismic uplift we calculate is an overestimate. Finally, we partition the uplift between the two earthquakes (parenthetical numbers on Fig. 2.8) based on the trends of more certain contours and likely uplift gradients. The uplift gradients we derive are similar to those observed for the 2005 and 2007 earthquakes [*Briggs et al.*, 2006; *Sieh et al.*, 2008].

It should be noted that none of our methods can distinguish between coseismic and postseismic uplift, as fossil microatolls are inevitably too eroded to distinguish uplift that occurred within a few years of the initial event from the sudden coseismic uplift. (Postseismic uplift can sometimes be discerned in modern coral records such as PJG12-

C5; see Fig. 2.S20). Thus, our "coseismic" uplifts are more accurately summations of coseismic and postseismic uplift. However, in contrast to afterslip on the same patch which ruptured coseismically, postseismic slip surrounding the coseismic rupture area would produce postseismic vertical deformation opposite the coseismic deformation. Indeed, afterslip following the recent ruptures of the Sunda megathrust has generally followed this pattern [e.g., *Hsu et al.*, 2006; *Paul et al.*, 2007; *Lubis et al.*, 2013], so it is likely that the ancient ruptures behaved similarly. Therefore, our coral records more likely include postseismic subsidence rather than postseismic uplift. Unfortunately, postseismic subsidence is also difficult to discern in coral records because it is superimposed on interseismic subsidence and oceanographic fluctuations. We make the case that it occurred at Badgugu following the 1833 earthquake (see section 2.2.2.3), but it is apparent in that record only because the interseismic subsidence rate is so low. Most of our coral records potentially include a few centimeters of postseismic subsidence; however, in most cases this subsidence is constrained to be a small percentage of the uplift, at most.

Our data clearly resolve the southeastward lessening and termination of the 1797 uplift across the Pagai Islands. The northwestern terminus is constrained by the Badgugu record, though less well. Though our one site on Siberut cannot constrain much of the uplift pattern, it is likely that 1797 uplift peaked on central or southwestern Siberut, as the uplift gradients trend toward that area from both ends.

For 1833, the trench-parallel pattern of contours over the Pagai Islands is largely derived from that same pattern in the modern interseismic rates, since the uplifts are

estimated by projecting those rates. The southern terminus of the rupture was apparently well southeast of Sanding Island, as there is no hint of a southeastward-decreasing uplift gradient between South Pagai and Sanding. However, northwestward-decreasing uplifts between North Pagai and Sipora (and plausibly across Sipora) imply that the magnitude of slip on the underlying megathrust tapered off beneath those islands. Due to the death of fringing reefs in 1797, the precise northwestern extent of the 1833 uplift is not constrained, but extrapolating the established uplift gradient to the northwest yields a point of zero uplift south of Siberut. The growth of the Badgugu coral much farther north was apparently perturbed in 1833 (10 cm uplift), but this was a transient effect that disappeared within 5 years. We infer that the Badgugu uplift was a relatively small, isolated patch (perhaps due to a large aftershock of the primary 1833 earthquake, or purely postseismic), unconnected to the primary 1833 uplift farther south.

In summary, these coseismic uplift patterns are consistent with primary rupture patches down-dip of the islands, though we cannot exclude the possibility that some parts of the shallow megathrust slipped as well (updip of Siberut for 1797 and updip of the Pagai Islands for 1833). The broad zone of overlap between the two uplift patches indicates almost certain re-rupture in 1833 of the southeastern and central portions of the 1797 rupture patch.

2.3 Modeling Megathrust Behavior

To more quantitatively estimate the underlying slip on the megathrust that is presumably the source of the surface deformation patterns we observe, we employ

inverse modeling techniques. We assume that the medium surrounding the megathrust can be considered to be linear elastic, as is customary in modeling studies of coseismic and interseismic deformation [e.g., *Cohen*, 1999]. It is well established that this elastic dislocation theory typically works well for modeling coseismic deformation. Its application to interseismic deformation is more questionable because of possible deformation within the hanging wall or footwall of the megathrust, such as secondary faulting in the forearc or bending of the subducting plate. However, in the case of the Sumatran Sunda megathrust the assumption of negligible long term deformation of the hanging wall is supported by observations of low long-term deformation rates [*Briggs et al.*, 2008; Section 3.4 of this dissertation]. To relate surface displacement to fault slip at depth, we use the semi-analytical solutions of *Okada* [1985] which assume a homogenous linear elastic half-space. Because surface strain carries very little information about fault geometry at depth [e.g., *Vergne et al.*, 2001], the geometry of the megathrust must be described *a priori*. We model the megathrust as a curved fault plane made up of 15 x 15 km rectangular patches, starting at 1.2 km depth and 7.5° dip below the trench axis and ending at 100 km depth and 29° dip below the Sumatran coastline, a two-dimensional approximation of the Slab 1.0 model [*Hayes et al.*, 2012].

The oblique convergence between the Indian/Australian and Sunda plates is a classic example of strain partitioning, with the convergence concentrated on the subduction zone and the lateral motion on the right-slip Sumatran fault [e.g., *Fitch*, 1972; *McCaffrey et al.*, 2000]. In reality, the subduction beneath the fore-arc sliver between the two fault traces is still slightly oblique. However, for the purposes of our modeling, we ignore this small

oblique component and restrict the megathrust to dip-slip motion because the measurement of vertical displacements alone cannot constrain the strike-parallel component of slip. This component is known to have been small for the coseismic slip during the recent large earthquakes in the area [*Konca et al.,* 2007; *Konca et al.,* 2008] and for the recent period of interseismic strain [*Chlieh et al.,* 2008]. For our interseismic coupling models, we adopt the backslip modeling approach pioneered by *Savage* [1983], representing megathrust coupling as the mathematically equivalent backwards slip on the fault interface. 100% coupling is defined as backslip equal to the convergence rate across the subduction zone, 4.5 cm/yr [*Chlieh et al.,* 2008].

To relate slip on the megathrust to the seismic moment classically used to quantify earthquake sources, we follow *Chlieh et al.* [2008] by using a shear modulus of 65 GPa, based on the average (down to 100 km depth) of the one-dimensional CRUST 2.0 layered structure model for this region [*Bassin et al.,* 2000]. While the regional layered structural model does not take subduction zones into account, increasing rigidity with depth is consistent with observed earthquake parameters, and 65 GPa is a likely average value for megathrust ruptures at depths of 40–60 km [*Bilek and Lay*, 1999; *Lay et al.*, 2012]. Similarly high rigidities may be required to reconcile geodetic and seismic moment estimates for the 2004 Aceh-Andaman earthquake [*Kreemer et al.,* 2006].

As is typically the case for buried elastic dislocation models, inverting the observed surface deformation for slip at depth is a highly under-constrained problem. We regularize our solutions by penalizing rough slip distributions. In effect we minimize a

cost function CF that is the sum of the reduced chi-squared error (the first term in the equation below) and the Laplacian of the slip distribution ($\nabla^2 S$):

$$CF = \frac{1}{N-P}\sum_{i=1}^{N}\frac{(o_i - p_i)^2}{\sigma_i^2} + \lambda\,\nabla^2 S \quad (1)$$

Here, N is the number of observations, P is the number of parameters being fit, σ_i is the uncertainty assigned to each observation o_i, and p_i is the corresponding model prediction. The Laplacian penalty λ, which quantifies the degree of smoothing from each patch to its neighboring patches, is weighted locally based on how precisely the data can resolve slip on that patch. Our implementation of this method, originally developed by *Lohman* [2004], is modified following *Ader et al.* [2012]. In essence, it applies a strong smoothing to poorly resolved areas of the fault plane far from our observations while permitting a rougher distribution of slip in areas directly beneath our observation sites. Resolution distributions for each of the models appear in the supplementary materials (Figs. 2.S26–2.S27; 2.S29). For each model, we apply the maximum weight to the Laplacian penalty (scale factor of λ) that provides misfits to the data of the order of the average data uncertainties (reduced chi-squared of ~1; see Fig. 2.S25). For each model presented below we report the value of the reduced chi-squared in Tables 2.3 and 2.4.

2.3.1 Coseismic Slip Models

Figure 2.9 shows possible coseismic slip models for the two great earthquakes. All models are forced to zero slip at the base of the fault (100 km depth) as this is likely the base of the seismogenic zone and no significant slip at this depth has been observed

during the modern large megathrust earthquakes in Sumatra and elsewhere. Models for 1797 are not permitted to slip along the northwest or southeast edges of the fault, as our data suggests the slip terminated within the bounds of our fault patch. Models for 1833 are permitted to slip along the southeast edge, as there is no reason to believe the rupture did not extend in that direction. For each earthquake, we present two slip distributions: one for which slip is forced to zero at the trench, and one for which slip is not constrained below the trench. In the latter case, the penalty on the Laplacian favors large slip updip of the Mentawai Islands because the data themselves do not express any significant updip tapering of slip, so the slip gradient below the islands is extrapolated updip. As deformation measurements on the Mentawai Islands are not sensitive to slip near the trench, both classes of models can fit our coral uplift data equally well, and the differences in residuals are nearly imperceptible (residuals are shown in Fig. 2.S26). These models can be considered as end members, bracketing the 1797 earthquake between moment magnitudes 8.7–8.9 and the 1833 earthquake between 8.8–9.0. Misfits, moments, and moment magnitudes are summarized in Table 2.3.

The higher-slip end members could be considered "Tohoku 2011-type" events, with large areas of slip concentrated on the shallow part of the megathrust, and could produce similarly devastating tsunamis. The end members with slip limited to intermediate depths would produce minor tsunamis similar to the 2007 events [*Borrero et al.*, 2009]. Given the major tsunamis reported at Padang in 1797 and Bengkulu in 1833 (from historical records summarized by *Natawidjaja et al.* [2006]), some slip likely extended to the shallow megathrust during both events, though not necessarily as much as in our end-

member models. Based on the plate tectonic convergence rate of 4.5 cm/yr, the ~9 m of modeled shallow slip in 1797 would build up within 200 years (assuming a complete locking of the plate interface during the interseismic period), comparable to the Mentawai supercycle recurrence interval estimated by *Sieh et al.* [2008]. The larger ~16 m of shallow slip in our 1833 model would require a longer ~350-year recurrence interval, so it is unlikely that slip is so large in every megathrust rupture (though it could be on occasion.)

Our models confirm that the 2007 Mentawai ruptures, which collectively released a moment of about 7.5 x 10^{21} Nm (equivalent to a M_w 8.5 earthquake), were in total significantly smaller than the 1833 rupture, as noted by *Konca et al.* [2008] and *Sieh et al.* [2008]. Slip in 2007 (contours on Fig. 2.9) approximately equaled our lower end member model of 1833 slip in the area between Sanding and Mega islands, but was significantly lesser beneath South Pagai and nonexistent beneath North Pagai and southern Sipora.

2.3.2 18th–19th-Century Interseismic Coupling Models

To model interseismic coupling, we employ the Principal Component Analysis Inversion Method (PCAIM) developed by *Kositsky and Avouac* [2010]. PCAIM performs a singular value decomposition of the time series data matrix, d = USV, where S is a diagonal matrix and the vectors U and V represent the spatial distributions and time functions associated with each component. The particular technique implemented in PCAIM allows weighting the data matrix according to the uncertainties and tolerates

temporal gaps in the time series. Components are ordered according to their respective contribution to explaining the data variance. The data are then filtered by discarding the lower-order components, since the primary features of the data can be reproduced by the first few components. PCAIM then inverts the spatial deformation components to obtain fault slip components (L), and re-combines V with L to produce a complete time series of slip on the fault plane. This method greatly reduces the otherwise very large number of computations necessary to model a deformation time series, and allows the combination of time series with different observation epochs and variable uncertainties. Table 2.4 summarizes decomposition misfit, model misfits, and moment deficit rates for all our interseismic models.

To prepare the coral time series for modeling, we assign uncertainties of ±2.6 cm to die-down and HLG points, ±5–10 cm to moderately eroded points, and remove severely eroded points. The uncertainty for un-eroded points is based on the natural variability in coral HLS [*Natawidjaja et al.*, 2004], and increased based on the estimated amount of erosion for eroded points. We do not include any HLG points before a coral first reached HLS, since such points were not limited by relative sea level. We use a single time series for each site (either from the single longest, best-preserved sampled coral or a concatenation of coral records covering different time periods) and remove the 1797 coseismic uplift. Oceanographic die-downs remain in the data and are modeled as megathrust slip, but since these are relatively small deviations which are typically recovered within a few years, this non-tectonic contamination has little effect on the long-term average coupling we derive.

When the entire 1755–1832 time period is considered, the time series are reconstructed within uncertainties from the principal component analysis using only 2 components. We therefore invert for time history of slip on the megathrust using only these two components. The model produces an approximately linear first component V and a second component V with an abrupt change in rate at the time of the 1797 earthquake, confirming that a fundamental change in behavior occurred at that time (Figure 2.S28A). However, this decomposition is unstable, due in part to the large number of time series that end in 1797 (death of the reef due to uplift). Therefore, we model the pre- and post-earthquake time periods separately to obtain more robust models. For each period the first component accounts for most of the data variance and we therefore use a single component decomposition. The time functions (V) for both time periods are approximately linear, except for deviations related to widespread oceanographic die-downs (Fig. 2.S28B).

Figure 2.10 illustrates that before the 1797 earthquake, there was a strongly coupled patch beneath the Pagai Islands and moderately coupled patches extending northwest and southeast. After 1797, the Pagai patch remained strongly coupled but the patches below Sipora and Sanding became very weakly coupled. Coupling beneath Siberut is unconstrained after 1797. As with the coseismic cases, models where shallow coupling is permitted can fit the data equally well. Shallow coupling would of course be necessary to build up strain for coseismic events involving shallow slip.

2.3.3 20th-Century Interseismic Coupling Models

The previous inversions are based on vertical displacement data only. For the modern period we have the opportunity to add horizontal displacement data measured by the Global Positioning System (GPS). It is therefore possible, for the modern time period, to compare models obtained from both the GPS and coral and from the coral data alone, unlike those presented for the 1755–1832 time period. We supplement the purely vertical coral data covering the 1950–1997 time period with horizontal campaign GPS data collected over 1991–2001 [*Bock et al.*, 2003]. We calculate the motion of these stations relative to the fore-arc sliver using the Euler poles derived by *Chlieh et al.* [2008], and extract the trench-perpendicular component. While a small part of the trench-parallel motion of these stations is due to the slightly oblique subduction, most of the lateral motion can be attributed to strain accumulation across the locked Sumatran fault, and for our fixed-rake slip models it is more consistent to assume purely trench-perpendicular subduction.

Unlike *Chlieh et al.* [2008], we do not use any continuous data from the SuGAr network, as these stations were installed after the end of most of our coral time series. Furthermore, the SuGAr time series include many coseismic and postseismic events which make it difficult to discern the interseismic signal, and the post-earthquake coupling state is likely fundamentally different from the pre-earthquake state represented by the 20th-century coral time series (as we discovered was the case for the pre- and post-1797 periods).

We use only the first principal component of the decomposition, as including further components does not significantly improve the fit to the data. The time component V is approximately linear, except for a few deviations related to large oceanographic die-downs, and there is no evidence of a significant change in behavior over the 1950–1997 period (Fig. 2.S31A). The GPS data are added as a constraint on the inversion (but are not involved in the principal component analysis because they are too sparse in time to help constrain the time evolution). Figure 2.11A shows the resulting model, which fits the coral data reasonably well, except for the very low subsidence rates at the north end of Siberut which clash with the high horizontal GPS rate. The inclusion of the GPS data requires the majority of the fault to be locked, and even in this case the GPS motions are under-predicted (Fig. 2.S30). The under-prediction is partially due to the GPS measurement period encompassing the significant, widespread oceanographic die-down in 1995, which manifests as slower net subsidence in the last decade of the coral time series. It is likely that this apparent slowing in subsidence rates is not tectonic, especially given the horizontal GPS rates measured over the same time period. A simple linear time function (Fig. 2.11B) provides a much better fit to the GPS data while averaging out the non-tectonic deviations in the coral records. However, this model (unsurprisingly similar to the models of *Chlieh et al.* [2008], since most of the data and assumptions are the same) still requires large areas of 100% coupling.

In contrast, inverting the coral data alone produces a strongly coupled patch beneath the Pagai Islands and moderate coupling extending northward, quite similar to the pre-1797 coupling pattern. Coupling is greater in the Batu Islands in the 20th century (as

evidenced by the dramatically increased subsidence at Badgugu after the 1935 earthquake). However, the coupling pattern in the Batu Islands is generally not well constrained in our models, since we do not include most of the coral time series from that region which were presented by *Natawidjaja et al.* [2004] and included by *Chlieh et al.* [2008]. Removing the top and bottom zero-slip boundary constraints for the models including GPS would have little effect since strong coupling already spans nearly the whole fault width, but for the coral-only model the effect is more significant (Fig. 2.11D). However, in all the models, the zone of low coupling between Siberut and Sipora is robust.

2.4 Discussion & Conclusions

Comparisons between the modeled distributions of coseismic slip and interseismic coupling illustrate a number of interesting relationships. Of the two patches with decreased coupling after 1797, the northwestern one had ruptured in 1797 but the southeastern one was adjacent to the southern terminus of the rupture. The 1833 event then re-ruptured the southeastern half of the 1797 rupture, including both patches with reduced coupling. It is somewhat surprising that the 1833 rupture was able to propagate through both reduced-coupling patches, but perhaps the asperity beneath the Pagai Islands, which apparently returned to a locked state after 1797, facilitated the 1833 rupture propagation. The Pagai Islands asperity is a common feature of all our models, as the area with largest slip in 1833 and as a zone of strong coupling during all three

interseismic periods, suggesting velocity-weakening friction with rapid healing of the fault interface after a rupture.

The behavior of other areas is more variable, but it is clear that there must be multiple individual asperities on the megathrust. The patches beneath Sipora and Sanding have similar features in that both were moderately coupled prior to 1797, both became almost completely uncoupled afterward, and each formed a terminus of one of the two great earthquakes. Perhaps these areas of the megathrust exhibit velocity-strengthening friction and do not heal quickly after a rupture. In the 20th century the Sipora patch was also moderately coupled, though the Sanding patch was apparently more strongly coupled. The paucity of data from Siberut prior to the 20th century unfortunately leaves us unable to characterize the longer-term behavior of the megathrust beneath Siberut, but we can conclude that spatial variations in frictional properties on the megathrust beneath the Pagai Islands and Sipora potentially explain its unusual characteristics: forming termini and major overlap of large megathrust ruptures and changing coupling after a large rupture.

We can gain additional insight by comparing the moments of the great earthquakes with the moment deficit rates from the various interseismic models (Figure 2.12). We use the moment deficit rate derived from the modern linear model, as it provides the best fit to both the GPS and coral datasets. We apply this rate over 210 years, the interval between 1797 and 2007, and plot the variation along strike. The accrued moment deficit is still less than the moment of the 1833 end member with updip slip, so (as previously mentioned) such an earthquake would require a longer recurrence interval. However, the

accumulated moment deficit equals or exceeds the 1797 moment. Therefore, if that rate truly persisted over the entire interseismic period, sufficient moment potential for a repeat of the 1797 rupture has certainly accrued. This is the likely explanation for the difficulty of finding fossil microatolls from the 18th–19th centuries on Siberut: the interseismic subsidence has so far exceeded the 1797 uplift that microatolls from that period now lie below the intertidal zone. Indeed, the lone 1797 microatoll field that we have found, at Silogui, lay ~15 cm below modern HLS when it was sampled in 2002 [*Natawidjaja et al.*, 2006], by far the lowest of all 18th–19th century microatolls we have found, and has undoubtedly sunk even further in the decade since.

A comparison of all the interseismic moment deficit rates (Fig. 2.12B) illustrates that those derived from coral data alone are systematically lesser than those derived from a combination of coral and GPS data. While some of the differences between models may be explained by the slightly different degrees of smoothing we applied, the comparison suggests that the coral records are insensitive to an important area of megathrust coupling (either shallow, deep, or both). If that is true, the moment deficit rates we derive for the 1755–1832 period, necessarily based on coral data alone, are underestimated.

Our detailed analysis of the 18th–19th century supercycle and comparison to the modern supercycle illustrate that major Mentawai megathrust ruptures are capable of altering the fault coupling and likely influence how the rupture sequence proceeds, though the fault eventually returns to a “normal” interseismic coupling state before the next rupture sequence occurs. Spatially and even temporally varying frictional properties of the megathrust beneath the southern Mentawai Islands likely prevent end-to-end

ruptures of the Mentawai segment, producing the characteristic supercycle behavior. There are no indications that the accumulated seismic moment deficit is lesser now than it was prior to 1797. Therefore, the modern rupture sequence will probably include a rupture similar to the 1797 rupture, though perhaps including more slip beneath the Pagai Islands to make up for the difference between the 2007 and 1833 earthquakes.

References

Abram, N. J., M. K. Gagan, J. E. Cole, W. S. Hantoro, and M. Mudelsee (2008), Recent intensification of tropical climate variability in the Indian Ocean, *Nature Geoscience*, *1*, 849–853.

Ader, T., et al. (2012), Convergence rate across the Nepal Himalaya and interseismic coupling on the Main Himalayan Thrust: Implications for seismic hazard, *J. Geophys. Res.*, *117*, B04403, doi:10.1029/2011JB009071.

Bassin, C., G. Laske, and G. Masters (2000), The current limits of resolution for surface wave tomography in North America, *Eos Trans. AGU*, *81*(48), Fall Meet. Suppl., Abstract S12A-03.

Beckley, B. D., F. G. Lemoine, S. B. Luthcke, R. D. Ray, and N. P. Zelensky (2007), A reassessment of global and regional mean sea level trends from TOPEX and Jason-1 altimetry based on revised reference frame and orbits, *Geophys. Res. Lett.*, *34*, L14608, doi:10.1029/2007GL030002.

Bilek, S. L., and T. Lay (1999), Rigidity variations with depth along interplate megathrust faults in subduction zones, *Nature*, *400*, 443–446.

Bock, Y., L. Prawirodirdjo, J. F. Genrich, C. W. Stevens, R. McCaffrey, C. Subarya, S. S. O. Puntodewo, and E. Calais (2003), Crustal motion in Indonesia from Global Positioning System measurements, *J. Geophys. Res.*, *108*(B8), 2367, doi:10.1029/2001JB000324.

Borrero, J. C., R. Weiss, E. Okal, R. Hidayat, Suranto, D. Arcas, and V. V. Titov (2009), The tsunami of September 12, 2007, Bengkulu Province, Sumatra, Indonesia: post-tsunami field survey and numerical modeling, *Geophys. J. Int.*, *178*, 180–194.

Briggs, R. W., et al. (2006), Deformation and slip along the Sunda megathrust in the great 2005 Nias-Simeulue earthquake, *Science*, *311*, 1897–1901.

Briggs, R. W., K. Sieh, W. H. Amidon, J. Galetzka, D. Prayudi, I. Suprihanto, N. Sastra, B. Suwargadi, D. Natawidjaja, and T. G. Farr (2008), Persistent elastic behavior above a megathrust rupture patch: Nias island, West Sumatra, *J. Geophys. Res.*, *113*, B12406, doi:10.1029/2008JB005684.

Chlieh, M., J.-P. Avouac, K. Sieh, D. Natawidjaja, and J. Galetzka (2008), Heterogeneous coupling of the Sumatran megathrust constrained by geodetic and paleogeodetic measurements, *J. Geophys. Res.*, *113*(B05305), doi:10.1029/2007JB004981.

Church, J. A., N. J. White, R. Coleman, K. Lambeck, and J. X. Mitrovica (2004), Estimates of the regional distribution of sea level rise over the 1950–2000 period, *Journal of Climate*, *17*(13), 2609–2625.

Church, J. A., and N. J. White (2006), A 20th century acceleration in global sea-level rise, *Geophys. Res. Lett.*, *33*(L01602), doi:10.1029/2005GL024826.

Church, J. A., N. J. White, and J. R. Hunter (2006), Sea-level rise at tropical Pacific and Indian Ocean islands, *Global and Planetary Change*, *53*(3), 155–168.

Cohen, S. C. (1999), Numerical models of crustal deformation in seismic zones, *Advances in Geophysics*, *41*, 133–231.

Fitch, T. J. (1972), Plate convergence, transcurrent faults, and internal deformation adjacent to Southeast Asia and the Western Pacific, *J. Geophys. Res.*, *77*(23), 4432–4460.

Hayes, G. P., D. J. Wald, and R. L. Johnson (2012), Slab1.0: A three-dimensional model of global subduction zone geometries, *J. Geophys. Res.*, *117*, B01302, doi:10.1029/2011JB008524.

Hsu, Y., M. Simons, J.-P. Avouac, J. Galetzka, K. Sieh, M. Chlieh, D. Natawidjaja, L. Prawirodirdjo, and Y. Bock (2006), Frictional afterslip following the 2005 Nias-Simeulue earthquake, Sumatra, *Science*, *312*, 1921–1926.

Jevrejeva, S., A. Grinsted, J. C. Moore, and S. Holgate (2006), Nonlinear trends and multiyear cycles in sea level records, *J. Geophys. Res.*, *111*(C09012), doi:10.1029/2005JC003229.

Konca, A. O., V. Hjorleifsdottir, T.-R. A. Song, J.-P. Avouac, D. V. Helmberger, C. Ji, K. Sieh, R. W. Briggs, and A. J. Meltzner (2007), Rupture kinematics of the 2005 M (sub w) 8.6 Nias-Simeulue earthquake from the joint inversion of seismic and geodetic data, *Bull. Seismol. Soc. Am.*, *97*(1A), S307–S322.

Konca, A. O., et al. (2008), Partial rupture of a locked patch of the Sumatra megathrust during the 2007 earthquake sequence, *Nature*, *456*, 631–635.

Kositsky, A. P., and J.-P. Avouac (2010), Inverting geodetic time series with a principal component analysis-based inversion method, *J. Geophys. Res.*, *115*, B03401, doi:10.1029/2009JB006535.

Kreemer, C., G. Blewitt, W. C. Hammond, and H.-P. Plag (2006), Global deformation from the great 2004 Sumatra-Andaman earthquake observed by GPS: Implications for rupture process and global reference frame, *Earth Planets Space*, *58*, 141–148.

Lambeck, K., M. Anzidei, F. Antonioli, A. Benini, and A. Esposito (2004), Sea level in Roman time in the central Mediterranean and implications for recent change, *Earth Planet. Sci. Lett.*, *224*, 563–575.

Lay, T., H. Kanamori, C. J. Ammon, K. D. Koper, A. R. Hutko, L. Ye, H. Yue, and T. M. Rushing (2012), Depth-varying rupture properties of subduction zone megathrust faults, *J. Geophys. Res.*, *117*, B04311, doi:10.1029/2011JB009133.

Lohman, R. (2004), The inversion of geodetic data for earthquake parameters, Ph.D. thesis, Calif. Inst. of Technol., Pasadena, CA.

Lubis, A. M., A. Hashima, and T. Sato (2013), Analysis of afterslip distribution following the 2007 September 12 southern Sumatra earthquake using poroelastic and viscoelastic media, *Geophys. J. Int.*, *192*(1), 18–37.

McCaffrey, R., P. C. Zwick, Y. Bock, L. Prawirodirdjo, J. F. Genrich, C. W. Stevens, S. S. O. Puntodewo, and C. Subarya (2000), Strain partitioning during oblique plate convergence in northern Sumatra; geodetic and seismologic constraints and numerical modeling, *J. Geophys. Res.*, *105*(B12), 28,363–28,376.

Natawidjaja, D. H. (2003), Neotectonics of the Sumatran fault and paleogeodesy of the Sumatran subduction zone, Ph.D. thesis, Calif. Inst. of Technol., Pasadena, CA.

Natawidjaja, D. H., K. Sieh, S. N. Ward, H. Cheng, R. L. Edwards, J. Galetzka, and B. W. Suwargadi (2004), Paleogeodetic records of seismic and aseismic subduction from central Sumatran microatolls, Indonesia, *J. Geophys. Res.*, *109*(B04), 4306, doi:10.1029/2003JB002398.

Natawidjaja, D. H., K. Sieh, M. Chlieh, J. Galetzka, B. W. Suwargadi, H. Cheng, R. L. Edwards, J.-P. Avouac, and S. N. Ward (2006), Source parameters of the great Sumatran megathrust earthquakes of 1797 and 1833 inferred from coral microatolls, *J. Geophys. Res.*, *111*(B6), 6403, doi:10.1029/2005JB004025.

Natawidjaja, D. H., K. Sieh, J. Galetzka, B. W. Suwargadi, H. Cheng, R. L. Edwards, and M. Chlieh (2007), Interseismic deformation above the Sunda Megathrust recorded in coral microatolls of the Mentawai islands, West Sumatra, *J. Geophys. Res.*, *112*(B02), 2404, doi:10.1029/2006JB004450.

Newcomb, K. R., and W. R. McCann (1987), Seismic history and seismotectonics of the Sunda Arc, *J. Geophys. Res.*, *92*(B1), 421–439.

Okada, Y. (1985), Surface deformation due to shear and tensile faults in a half-space, *Bull. Seismol. Soc. Am.*, *75*(4), 1135–1154.

Paul, J., A. R. Lowry, R. Bilham, S. Sen, and R. Smalley (2007), Postseismic deformation of the Andaman Islands following the 26 December, 2004 Great Sumatra-Andaman earthquake, *Geophys. Res. Lett.*, *34*, L19309, doi 10.1029/2007GL031024.

Prawirodirdjo, L., R. McCaffrey, C. D. Chadwell, Y. Bock, and C. Subarya (2010), Geodetic observations of an earthquake cycle at the Sumatra subduction zone; role of interseismic strain segmentation, *J. Geophys. Res.*, *115*(B3), B03414, doi:10.1029/2008JB006139.

Qiu, Q., E. M. Hill, L. Feng, A. M. Lubis, P. Banerjee, J. L. Davis, and K. E. Sieh (2012), "Long-term" post-seismic rate changes detected by the Sumatran GPS Array, western Sumatra, using a Kalman filter, paper presented at 2012 Fall Meeting, AGU, San Francisco, Calif., 3-7 Dec.

Rivera, L., K. Sieh, D. Helmberger, and D. Natawidjaja (2002), A comparative study of the Sumatran subduction-zone earthquakes of 1935 and 1984, *Bull. Seismol. Soc. Am.*, *92*(5), 1721–1736.

Savage, J. C. (1983), A dislocation model of strain accumulation and release at a subduction zone, *J. Geophys. Res.*, *88*, 4983–4996.

Sieh, K., D. H. Natawidjaja, A. J. Meltzner, C.-C. Shen, H. Cheng, K.-S. Li, B. W. Suwargadi, J. Galetzka, B. Philibosian, and R. L. Edwards (2008), Earthquake supercycles inferred from sea-level changes recorded in the corals of west Sumatra, *Science*, *322*, 1674–1678.

Vergne, J., R. Cattin, and J.-P. Avouac (2001), On the use of dislocations to model interseismic strain and stress build-up at intracontinental thrust faults, *Geophys. J. Int.*, *147*(1), 155–162.

Woodworth, P. L., and R. Player (2003), The Permanent Service for Mean Sea Level: An update to the 21st century, *Journal of Coastal Research*, *19*(2), 287–295.

Zachariasen, J., K. Sieh, F. W. Taylor, R. L. Edwards, and W. S. Hantoro (1999), Submergence and uplift associated with the giant 1833 Sumatran subduction earthquake: Evidence from coral microatolls, *J. Geophys. Res.*, *104*(B1), 895–919.

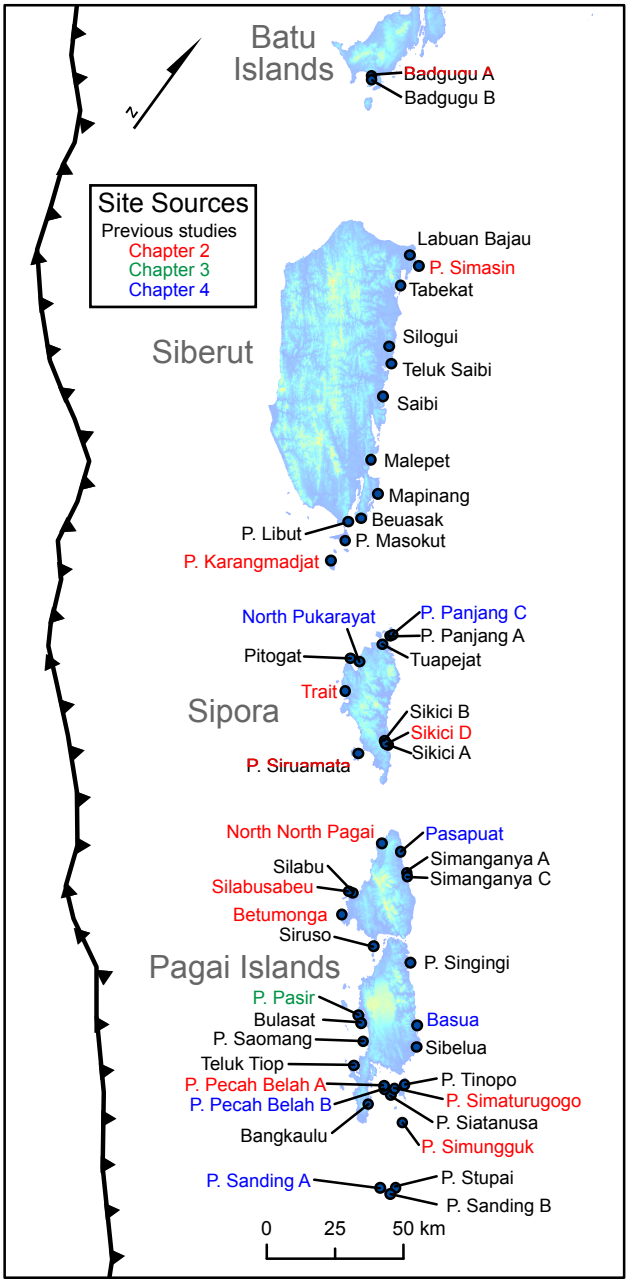

Figure 2.1. Index map of the Mentawai Islands showing sites used in this chapter. Data from previous studies (black labels) are from *Natawidjaja et al.* [2006; 2007] and *Sieh et al.* [2008]. Sites in red are fully presented in this chapter. Microatoll cross sections from sites in blue are presented in this chapter, but the maps of the sites and further discussion can be found in Chapter 4. The Pulau Pasir site is fully presented in Chapter 3.

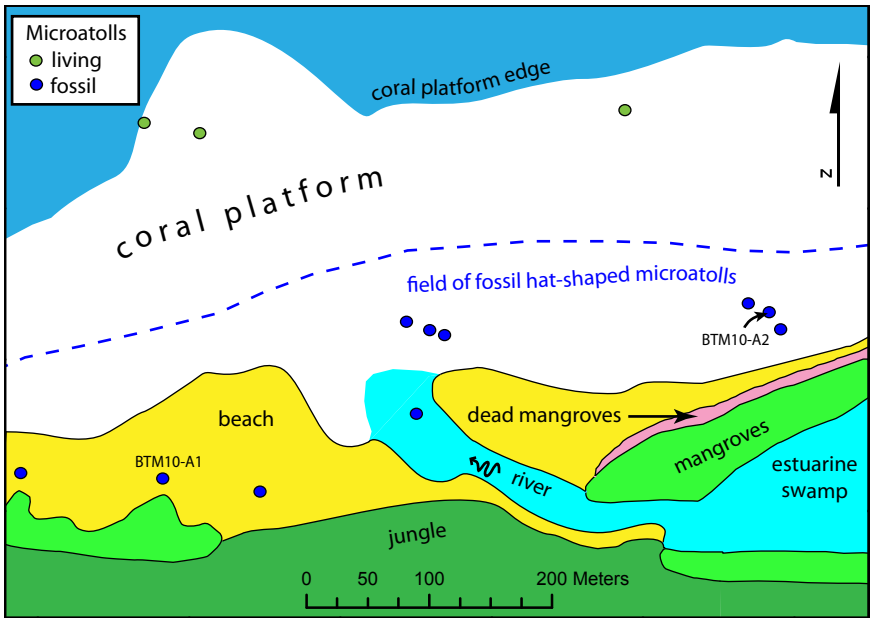

Figure 2.2. Map of the Betumonga site. Outflow of fresh water from the river hampers modern coral growth; only a few living colonies could be found at the far edge of the coral platform. The large field of huge microatolls that grew during the mid-1700s to early 1800s suggests that the river outlet was elsewhere (probably farther east) during that period. A perimeter of dead mangroves suggests ongoing modern subsidence at this site.

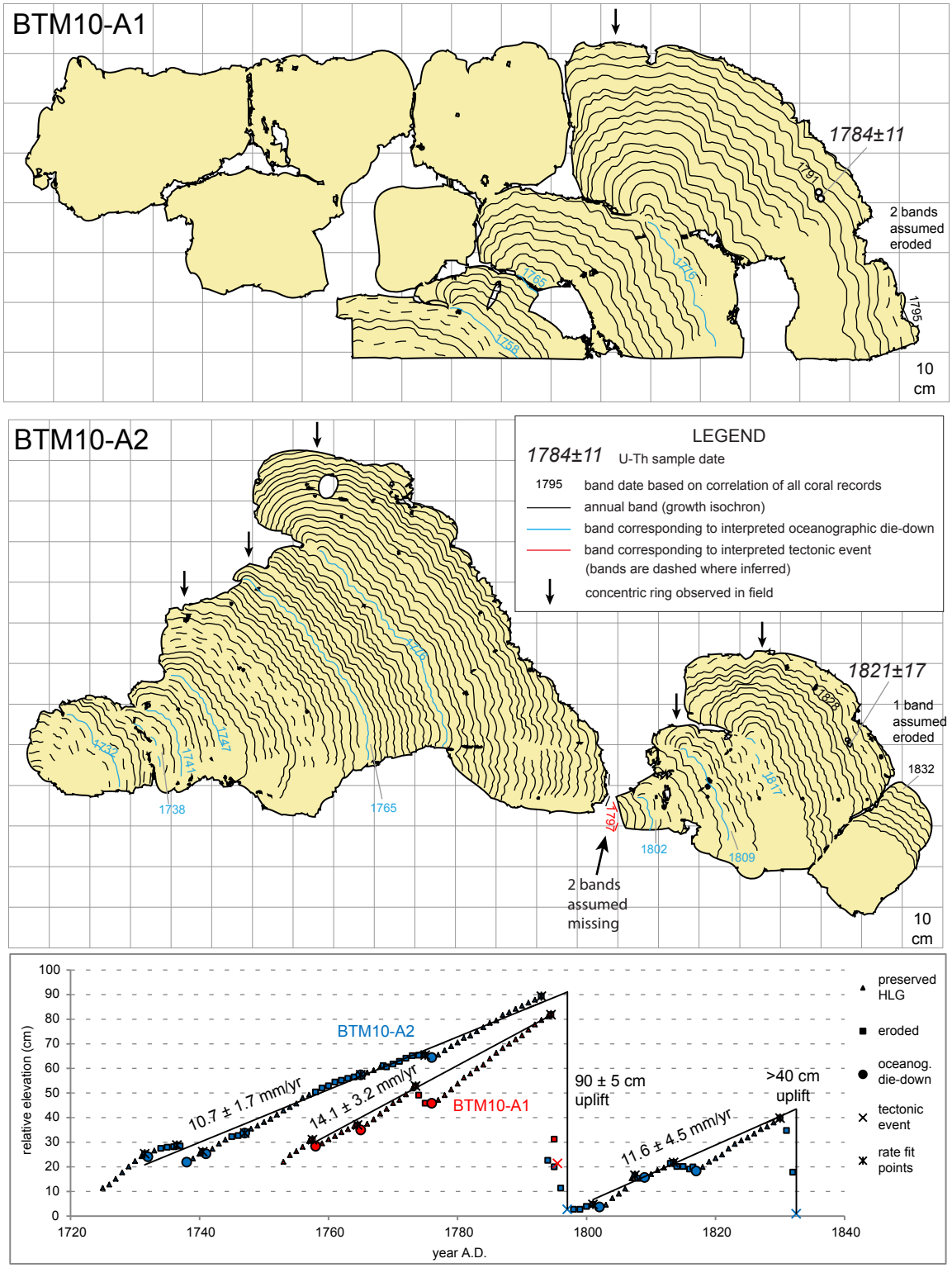

Figure 2.3. Slab cross sections and growth histories from Betumonga.

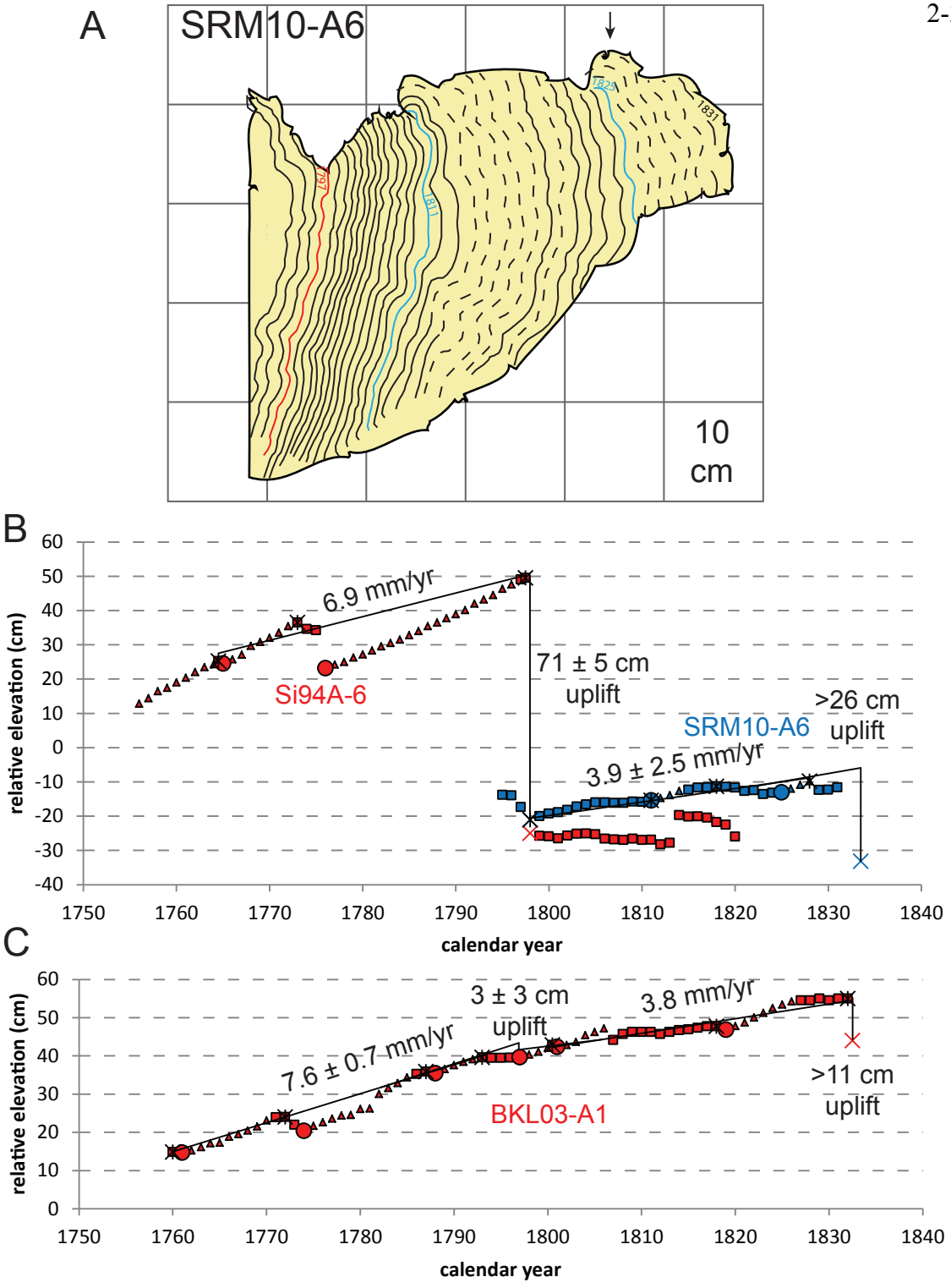

Figure 2.4. Coral records showing changes in subsidence rate after the 1797 earthquake. All symbology as in Fig. 2.3. A) Cross section of SRM10-A6 (complete outer rim of Si94A-6). B) Growth history of two slabs from the same Siruamata microatoll. C) Growth history of BKL03-A1 from Bangkaulu, showing a similar rate change but little to no uplift in 1797.

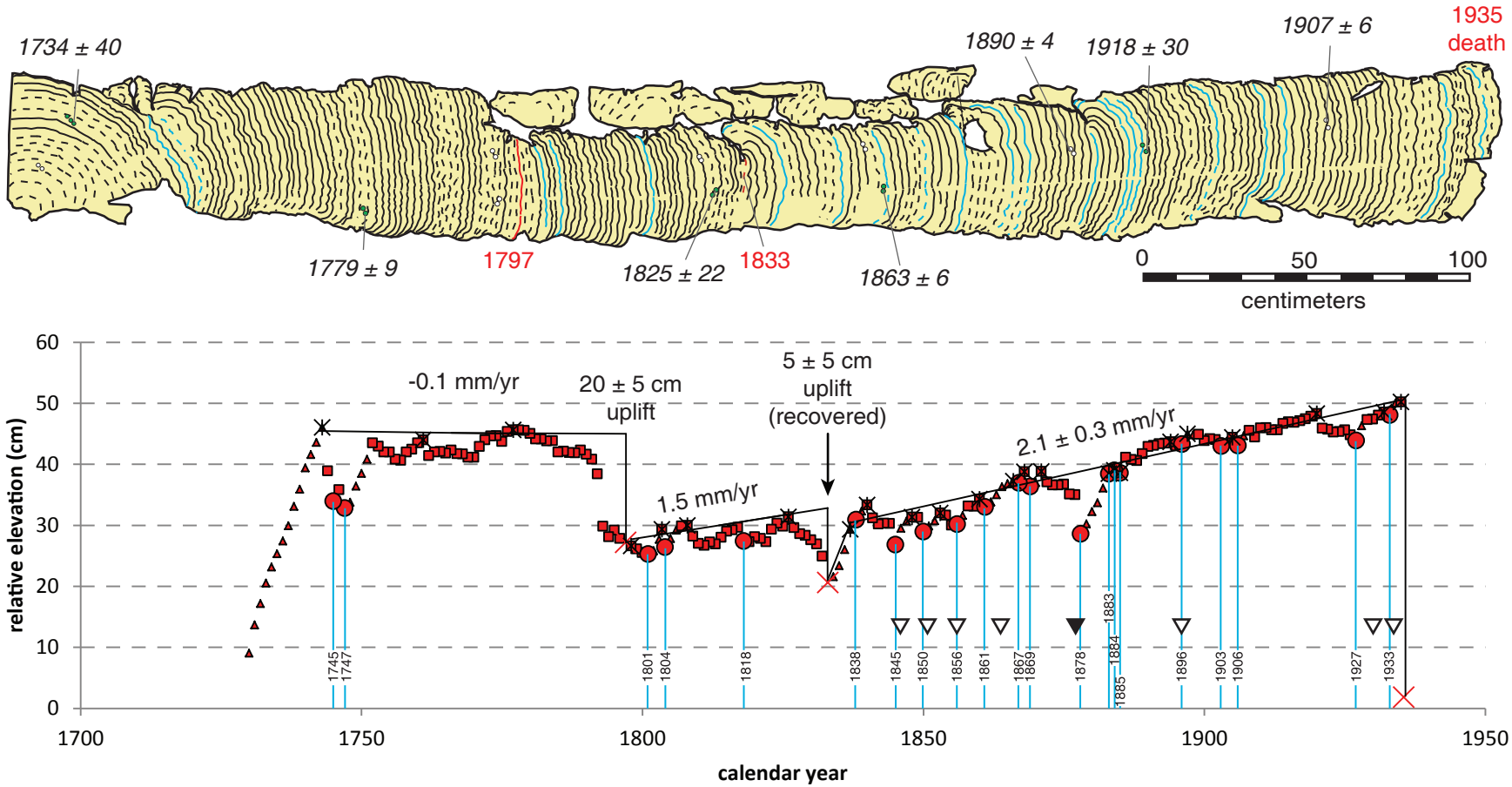
1734 ± 40
1779 ± 9
1797
1825 ± 22
1833
1863 ± 6
1890 ± 4
1918 ± 30
1907 ± 6
1935
death
0
50
100
centimeters
relative elevation (cm)
calendar year
-0.1 mm/yr
20 ± 5 cm
uplift
5 ± 5 cm
uplift
(recovered)
1.5 mm/yr
2.1 ± 0.3 mm/yr
1745
1747
1801
1804
1818
1838
1845
1850
1856
1861
1867
1869
1878
1883
1884
1885
1896
1903
1906
1927
1933

Figure 2.5

Figure 2.5. Cross section and growth history of BDG00-A1 from West Badgugu, which lived for more than 200 years. Symbology as in Fig. 2.3. Blue lines mark die-down years; triangles mark moderate (empty) and strong (filled) IOD events between 1845 and 1935 from *Abram et al.* [2008]. Most IOD events are potentially correlated with die-downs and the strong 1877 IOD is correlated with a particularly large die-down. The 1861 die-down may be an effect of the Nias-Simeulue megathrust earthquake in that year rather than an oceanographic event. This coral records a 20-cm coseismic uplift in 1797 and a 5–10 cm uplift in 1833; however, the 1833 uplift was clearly recovered in the 5 years following the earthquake. Interseismic deformation rates were low throughout the lifetime of this coral colony. Subsidence rates appear to have increased following the 1797 earthquake and possibly increased further after the 1833 earthquake, but due to uncertainties we cannot exclude the possibility of constant ~2 mm/yr subsidence for the full 200 years.

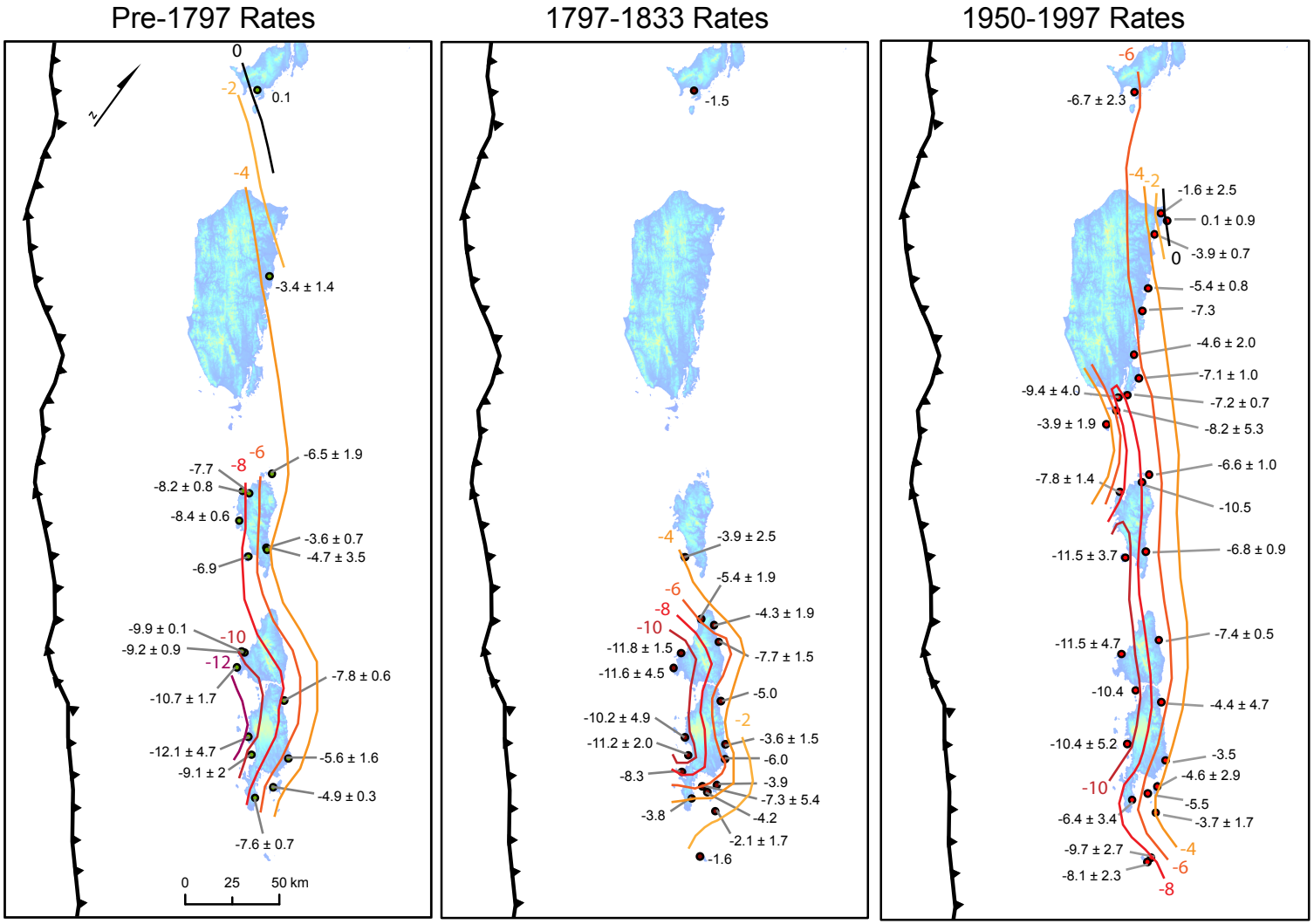
Pre-1797 Rates
1797-1833 Rates
1950-1997 Rates
N
0
-2
0.1
-4
-3.4 ± 1.4
-6
-8
-6.5 ± 1.9
-7.7
-8.2 ± 0.8
-8.4 ± 0.6
-3.6 ± 0.7
-4.7 ± 3.5
-6.9
-9.9 ± 0.1
-9.2 ± 0.9
-10
-12
-7.8 ± 0.6
-10.7 ± 1.7
-12.1 ± 4.7
-9.1 ± 2
-5.6 ± 1.6
-4.9 ± 0.3
-7.6 ± 0.7
0
25
50 km
-1.5
-4
-3.9 ± 2.5
-5.4 ± 1.9
-6
-8
-10
-4.3 ± 1.9
-11.8 ± 1.5
-7.7 ± 1.5
-11.6 ± 4.5
-5.0
-10.2 ± 4.9
-2
-11.2 ± 2.0
-3.6 ± 1.5
-6.0
-8.3
-3.9
-7.3 ± 5.4
-3.8
-4.2
-2.1 ± 1.7
-1.6
-6
-6.7 ± 2.3
-4
-2
-1.6 ± 2.5
0.1 ± 0.9
-3.9 ± 0.7
0
-5.4 ± 0.8
-7.3
-4.6 ± 2.0
-7.1 ± 1.0
-9.4 ± 4.0
-7.2 ± 0.7
-3.9 ± 1.9
-8.2 ± 5.3
-6.6 ± 1.0
-7.8 ± 1.4
-10.5
-11.5 ± 3.7
-6.8 ± 0.9
-11.5 ± 4.7
-7.4 ± 0.5
-10.4
-4.4 ± 4.7
-10.4 ± 5.2
-3.5
-4.6 ± 2.9
-10
-5.5
-6.4 ± 3.4
-3.7 ± 1.7
-9.7 ± 2.7
-4
-8.1 ± 2.3
-6
-8

Figure 2.6

Figure 2.6. Patterns of interseismic subsidence during three temporal periods. All measurements are in mm/yr, contoured at 2 mm/yr intervals. Positive and negative numbers indicate uplift and subsidence, respectively. Uncertainties shown are 95% confidence intervals; measurements without uncertainties have too few fit points to calculate a meaningful uncertainty. The pre-1797 pattern is similar to the 20th-century pattern, both of which cover time periods leading up to the beginning of a rupture sequence. However, the period between the two great earthquakes is marked by lower subsidence rates on Sipora and the southern end of South Pagai. It is not known how these patterns might have changed following the 1833 earthquake, as the reefs died completely due to uplift in that event and no corals from the later 19th century appear to have been preserved in the intertidal zone.

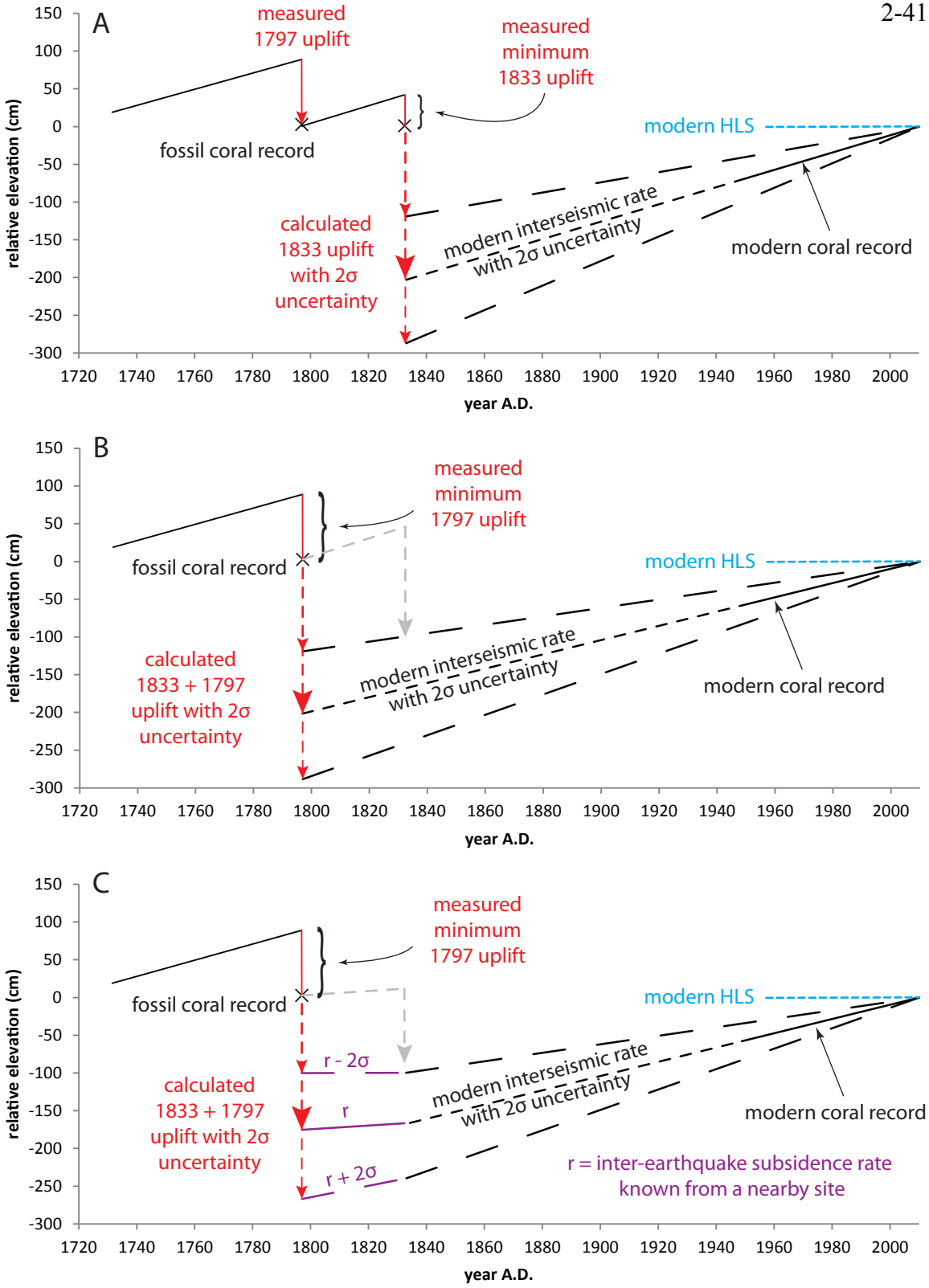

Figure 2.7. Calculations of total coseismic uplift in cases where A) 1797 uplift can be measured directly; B) all nearby reefs died completely in 1797; and C) inter-earthquake subsidence rate (different from the modern rate) is known from a nearby site.

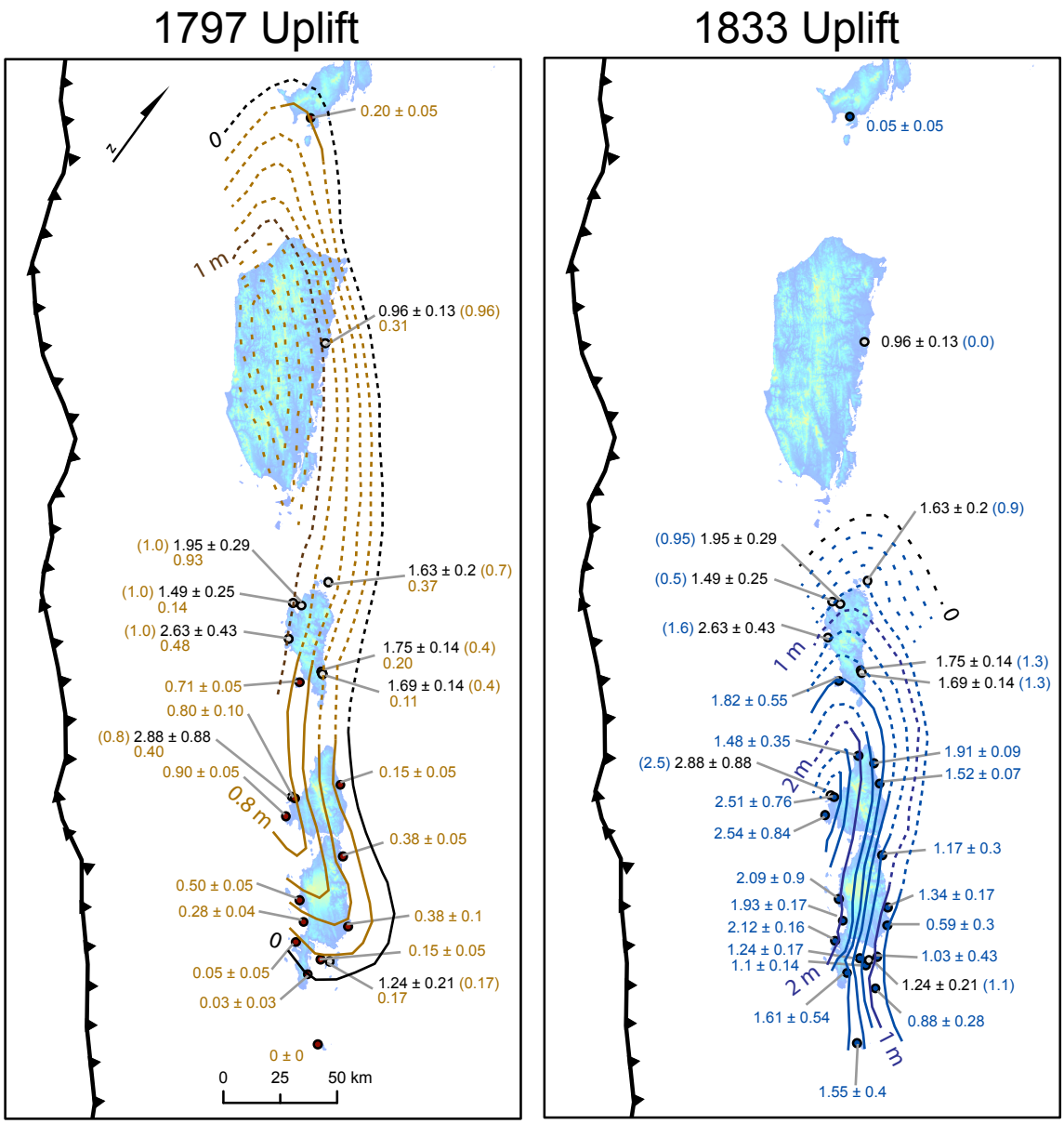

Figure 2.8. Coseismic uplift patterns of the great 1797 and 1833 earthquakes. Measurements are in cm and are contoured at 20 cm intervals. All uncertainties are 95% confidence intervals. Gray circles indicate sites where reefs died completely in 1797, so the partitioning of uplift between the two earthquakes is uncertain. At these sites, black numbers show totals and parenthetical colored numbers show inferred uplift for each earthquake. Minimum 1797 uplift at these sites is shown below black numbers on 1797 map. Dashed contours show inferred uplift at these sites based on likely uplift gradient and trends of more certain contours. Dotted contours are conjectural.

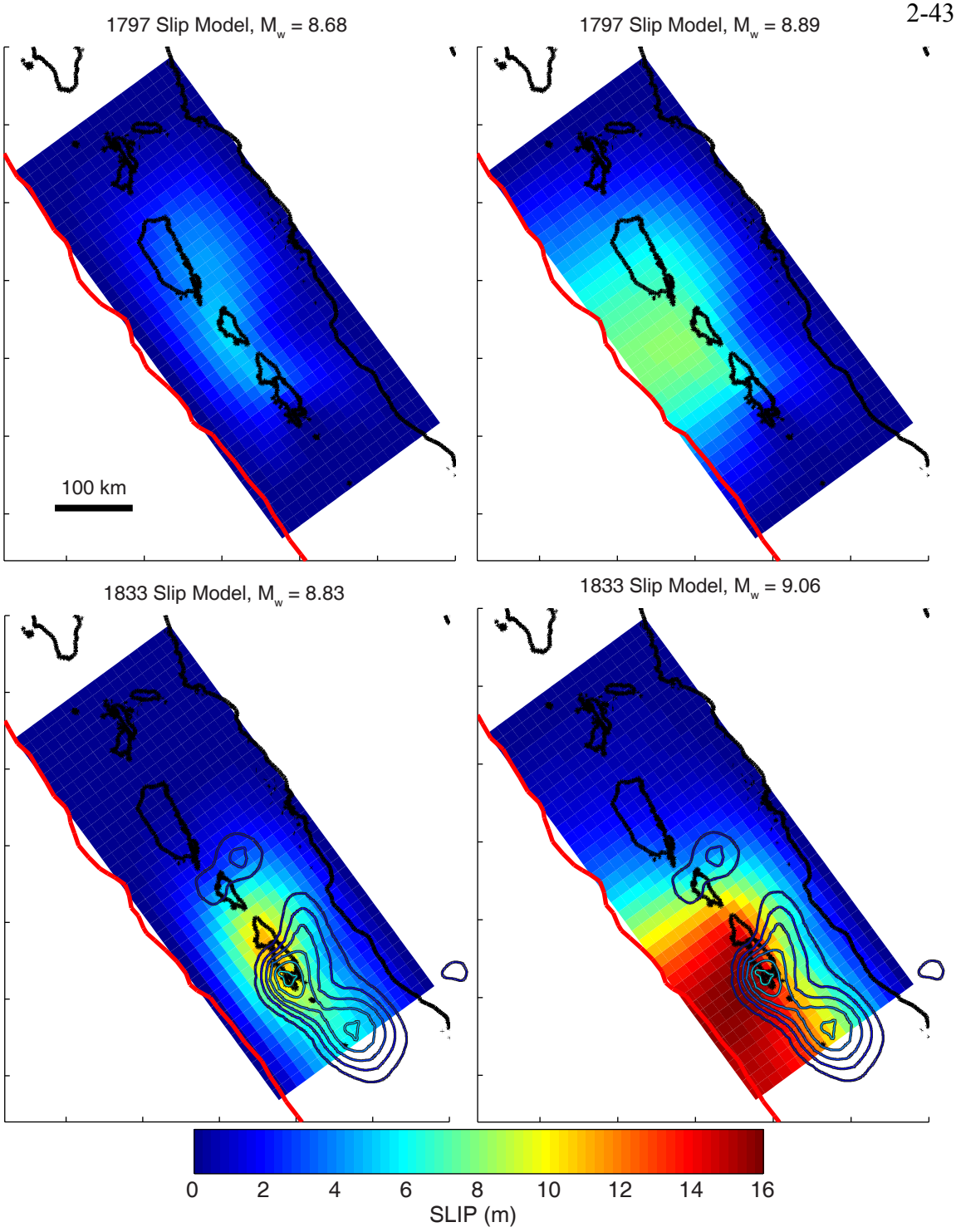

Figure 2.9. Slip models of the 1797 and 1833 earthquakes based on coral uplift data. Left column shows end members with no slip permitted at the trench, while models in the right column are permitted to slip at the trench. Due to the lack of resolution far from the islands, both types of models can fit the data equally well. Colored contours show total 2007 coseismic slip at 1-meter intervals (starting at 1 m), from *Konca et al.* [2008].

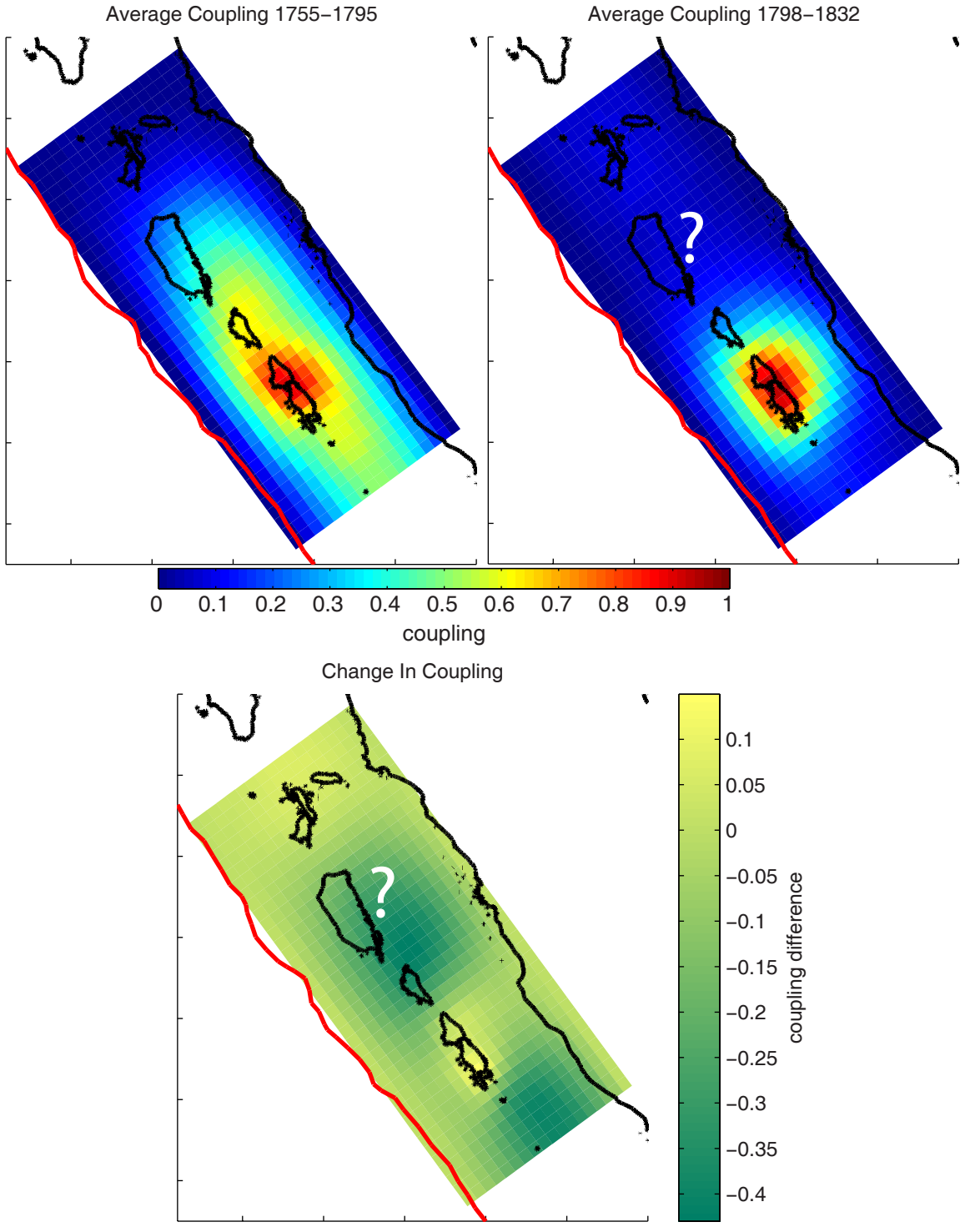

Figure 2.10. Megathrust coupling before and after the 1797 earthquake. Coupling beneath Siberut is not resolved after 1797, but substantially decreased coupling beneath Sipora and southeast of South Pagai can be seen clearly.

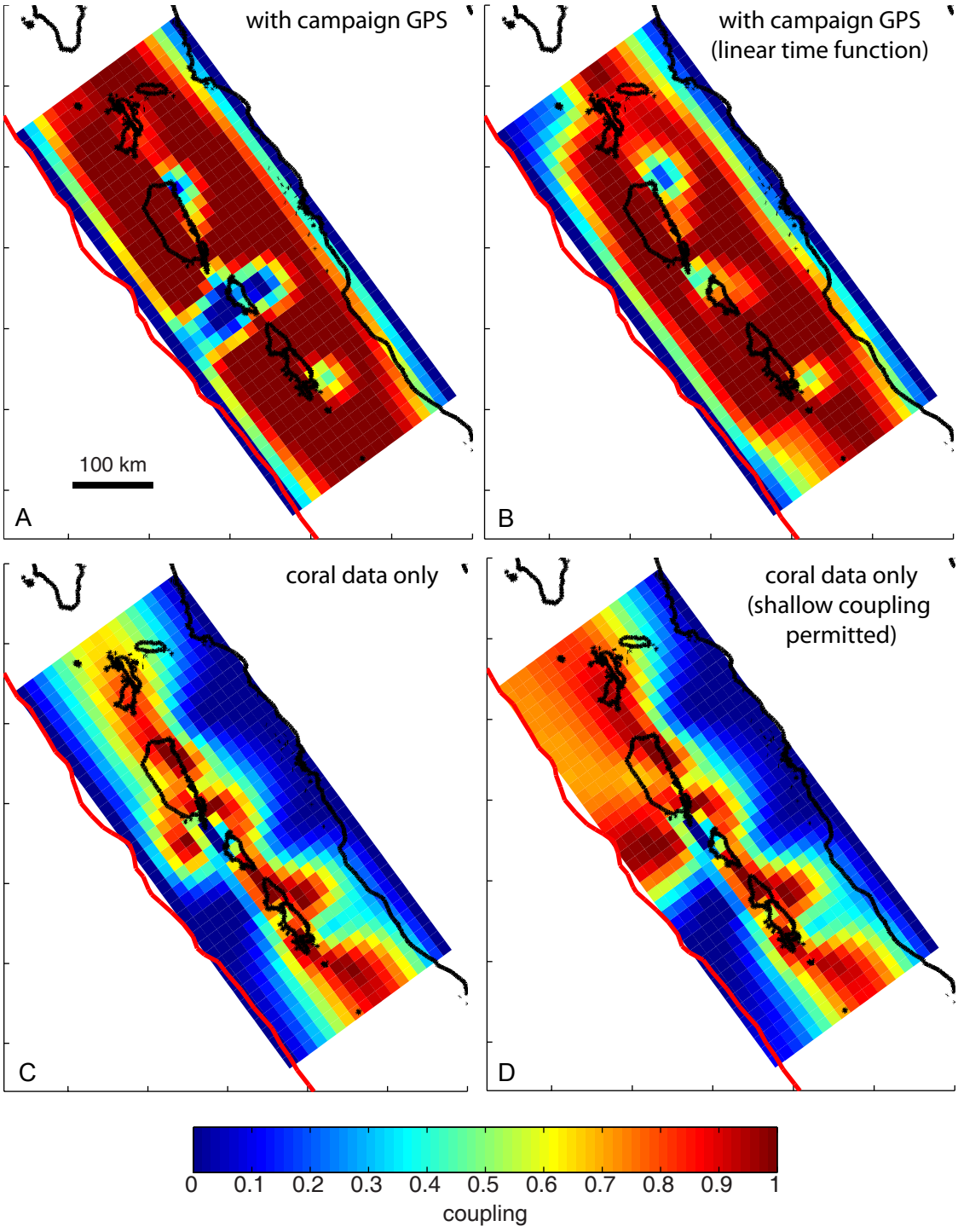

Figure 2.11. Models of late 20th-century megathrust coupling, based on coral and campaign GPS data. The GPS data require a much larger percentage of the fault plane to be fully locked than the coral dataset alone does.

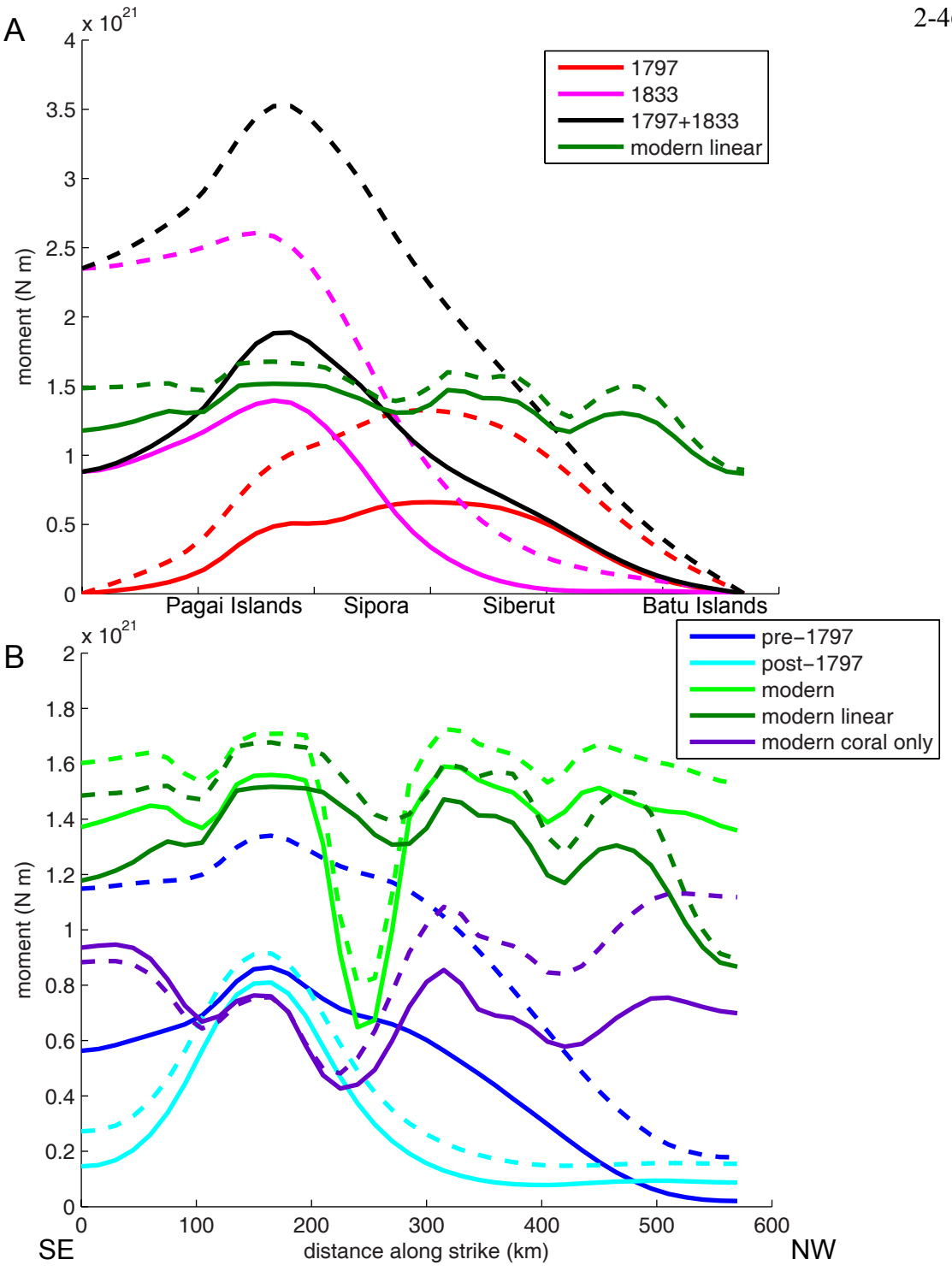

Figure 2.12. Comparison of seismic moment and moment rate deficits for our models, integrated over the 15-km model patch width. Solid and dashed lines indicate end members with constrained and free updip edge of the fault, respectively. All interseismic rate deficits are for 210 years, the interval between 1797 and 2007. A) Comparison of coseismic moments with the modern linear model, which provides the best fit to all the modern data. B) Comparison of all interseismic models.

Table 2.1 20th-Century Interseismic Vertical Deformation Rates

Latitude	Longitude	Full Name	Site Code	Rate (mm/yr)	Date Span
-0.549	98.471	Badgugu B	BDG-B	-6.7 ± 2.3	1935–1998
-0.942	98.912	Labuan Bajau	Lb	-1.6 ± 2.5	1954–1997
-0.953	98.956	P. Simasin	SMS	0.1 ± 0.9	1957–2010
-1.040	98.947	Tabekat	TBK	-3.9 ± 0.7	1953–1997
-1.269	99.073	Teluk Saibi	TSA	-5.4 ± 0.8	1926–1997
-1.371	99.113	Saibi	Sa	-7.3	1958–1997
-1.562	99.205	Malepet	MLP	-4.6 ± 2.0	1978–1997
-1.639	99.289	Mapinang	MPN	-7.1 ± 1.0	1958–1997
-1.737	99.292	Beuasak	Bs	-7.2 ± 0.7	1945–1998
-1.772	99.265	P. Libut	Li	-9.4 ± 4.0	1964–1997
-1.827	99.294	Masokut	MSK	-8.2 ± 5.3	1960–1997
-1.909	99.292	P. Karangmadjat	KMJ	-3.9 ± 1.9	1980–2010
-1.982	99.600	P. Panjang C	PJG-C	-6.6 ± 1.0	1971–2007
-2.033	99.592	Tuapejat	Tp	-10.5	1968–1995
-2.132	99.536	Pitogat	PTG	-7.8 ± 1.4	1970–1990
-2.289	99.802	Sikici A	SKC-A	-6.8 ± 0.9	1928–1997
-2.370	99.741	P. Siruamata	SRM	-11.5 ± 3.7	1962–1997
-2.594	100.101	Simanganya A	SMY-A	-7.4 ± 0.5	1961–1997
-2.752	99.995	Silabu	SLB	-11.5 ± 4.7	1986–2000
-2.853	100.152	P. Siruso	SRS	-10.4	1962–1994
-2.826	100.283	P. Singingi	SGG	-4.4 ± 4.7	1960–2003
-3.083	100.268	Bulasat	BLS	-10.4 ± 5.2	1961–1997
-3.039	100.463	Sibelua	SBL	-3.5	1955–1996
-3.163	100.505	P. Tinopo	TNP	-4.6 ± 2.9	1973–1993
-3.216	100.487	P. Siatanusa	STN	-5.5	1950–1994
-3.285	100.446	Bangkaulu	BKL	-6.4 ± 3.4	1980–2003
-3.268	100.572	P. Simungguk	SGK	-3.7 ± 1.7	1981–2007
-3.455	100.679	P. Stupai	STP	-9.7 ± 2.7	1950–1994
-3.481	100.677	P. Sanding B	SDG-B	-8.1 ± 2.3	1951–1994

Table 2.2 Coseismic Uplifts and Interseismic Vertical Deformation Rates Between 1750 and 1833

Latitude	Longitude	Full Name	Site Code	Pre-1797 Rate (mm/yr)	1797 Coseismic (cm)	1797 Min	Total Coseismic (cm)	1797-1833 Rate (mm/yr)	1833 Coseismic (cm)	1833 Min	Modern Rate (mm/yr)	Modern Rate Source
-0.539	98.464	Badgugu A	BDG-A	0.1	20 ± 5			-1.5	5 ± 5		-6.7 ± 2.3	near BDG-B
-1.226	99.034	Silogui A	SLG-A	-3.4 ± 1.4	96	31	96 ± 13		0		-5.4 ± 0.8	near TSA
-1.982	99.600	P. Panjang C	PJG-C	-6.5 ± 1.9	70	37	163 ± 20		90		-6.6 ± 1.0	same site
-2.123	99.565	North Pukarayat[a]	NPK	-7.7	100	93	195 ± 29		95		-7.8 ± 1.4	near PTG
-2.132	99.536	Pitogat	PTG	-8.2 ± 0.8	100	14	149 ± 25		50		-7.8 ± 1.4	same site
-2.256	99.604	Trait	TRT	-8.4 ± 0.6	100	38	263 ± 43		160		-10.0 ± 2.0	interpolation
-2.286	99.785	Sikici B	SKC-B	-3.6 ± 0.7	40	11	169 ± 14		130		-6.8 ± 0.9	near SKC-A
-2.290	99.794	Sikici D	SKC-D	-4.7 ± 3.5	40	20	175 ± 14		130		-6.8 ± 0.9	near SKC-A
-2.370	99.741	P. Siruamata	SRM	-6.9	71 ± 5			-3.9 ± 2.5	182 ± 55	26	-11.5 ± 3.7	same site
-2.564	99.976	North North Pagai	NNP					-5.4 ± 1.9	148 ± 35	35	-8.0 ± 2.0	interpolation
-2.550	100.044	Pasapuat	PSP					-4.3 ± 1.9	191 ± 9	7	-7.4 ± 0.5	near SMY-A
-2.603	100.110	Simanganya C	SMY-C		15 ± 5			-7.7 ± 1.5	152 ± 7	20	-7.4 ± 0.5	near SMY-A
-2.755	99.981	Silabusabeu[a]	SSB	-9.2 ± 0.9	80	40	288 ± 88[c]		250		-11.5 ± 4.7	near SLB
-2.752	99.995	Silabu	SLB	-9.9 ± 0.1	80 ± 10			-11.8 ± 1.5	251 ± 76	55	-11.5 ± 4.7	same site
-2.831	100.008	Betumonga	BTM	-10.7 ± 1.7	90 ± 5			-11.6 ± 4.5	254 ± 84	40	-11.5 ± 4.7	near SLB
-2.826	100.283	P. Singingi	SGG	-7.8 ± 0.6	38 ± 5			-5.0	117 ± 30	32	-4.4 ± 2.0	same site[b]
-3.067	100.246	P. Pasir	PSR	-12.1 ± 4.7	50 ± 5			-10.2 ± 4.9	209 ± 90	28	-10.4 ± 5.2	near BLS
-2.981	100.423	Basua	BSA					-3.6 ± 1.5	134 ± 17	30	-5.0 ± 1.0	interpolation
-3.128	100.312	P. Saomang	SMG	-9.1 ± 2.0	28 ± 4			-11.2 ± 2.0	193 ± 17	29	-9.0 ± 1.0	interpolation
-3.039	100.463	Sibelua	SBL	-5.6 ± 1.6	38 ± 10			-6.0	59 ± 30	27	-3.5 ± 2.0	same site[b]
-3.211	100.332	Teluk Tiop	TTP		5 ± 5			-8.3	212 ± 16	54	-9.0 ± 1.0	interpolation
-3.163	100.505	P. Tinopo	TNP					-3.9	103 ± 43	27	-4.6 ± 2.9	same site
-3.207	100.451	P. Pecah Belah A	PCB-A		15 ± 5			-7.3 ± 5.4	124 ± 17	30	-6.0 ± 1.0	interpolation
-3.213	100.460	P. Pecah Belah B	PCB-B							70	-6.0 ± 1.0	interpolation
-3.192	100.486	P. Simaturugogo	STG	-4.9 ± 0.3	17	17	124 ± 21[c]		107		-5.0 ± 1.0	interpolation
-3.216	100.487	P. Siatanusa	STN					-4.2	110 ± 14	23	-5.5 ± 1.0	same site[b]
-3.285	100.446	Bangkaulu	BKL	-7.6 ± 0.7	3 ± 3			-3.8	161 ± 54	11	-6.4 ± 3.4	same site
-3.268	100.572	P. Simungguk	SGK					-2.1 ± 1.7	88 ± 28	55	-3.7 ± 1.7	same site
-3.486	100.638	P. Sanding A	SDG-A		0			-1.6	155 ± 40	50	-8.1 ± 2.3	near SDG-B

[a]Sites excluded from modeling because our interpretation is inconsistent or barely consistent with the U-Th dates.

[b]Uncertainty in rate was reduced based on interpolation.

Total uplift divided between the two great earthquakes based on projection of contour patterns (corals died completely in 1797, providing a minimum.)

[c]Adjusted for inter-earthquake rate different from modern rate.

Table 2.3 Reduced Chi-Squared, Moment, and Moment Magnitude for Coseismic Models

	pinned below trench			free below trench		
Model	χ^2_r	M_0 (N m)	M_w	χ^2_r	M_0 (N m)	M_w
1797	0.75	1.3×10^{22}	8.68	0.66	2.8×10^{22}	8.89
1833	1.08	2.2×10^{22}	8.83	1.12	5.0×10^{22}	9.06

Table 2.4 Reduced Chi-Squared and Moment Deficit Rate for Interseismic Models

	decomp	uncoupled below trench		free below trench	
Model	χ^2_r	χ^2_r	M_0/yr	χ^2_r	M_0/yr
1755-1795	0.35	0.74	8.9×10^{19}	0.76	1.7×10^{20}
1798-1832	0.20	0.40	5.1×10^{19}	0.42	6.9×10^{19}
Modern with GPS	0.92	1.75	2.6×10^{20}	1.70	2.9×10^{20}
Modern with GPS (linear)	1.20	1.72	2.4×10^{20}	1.70	2.7×10^{20}
Modern coral only	0.92	1.14	1.3×10^{20}	1.14	1.6×10^{20}

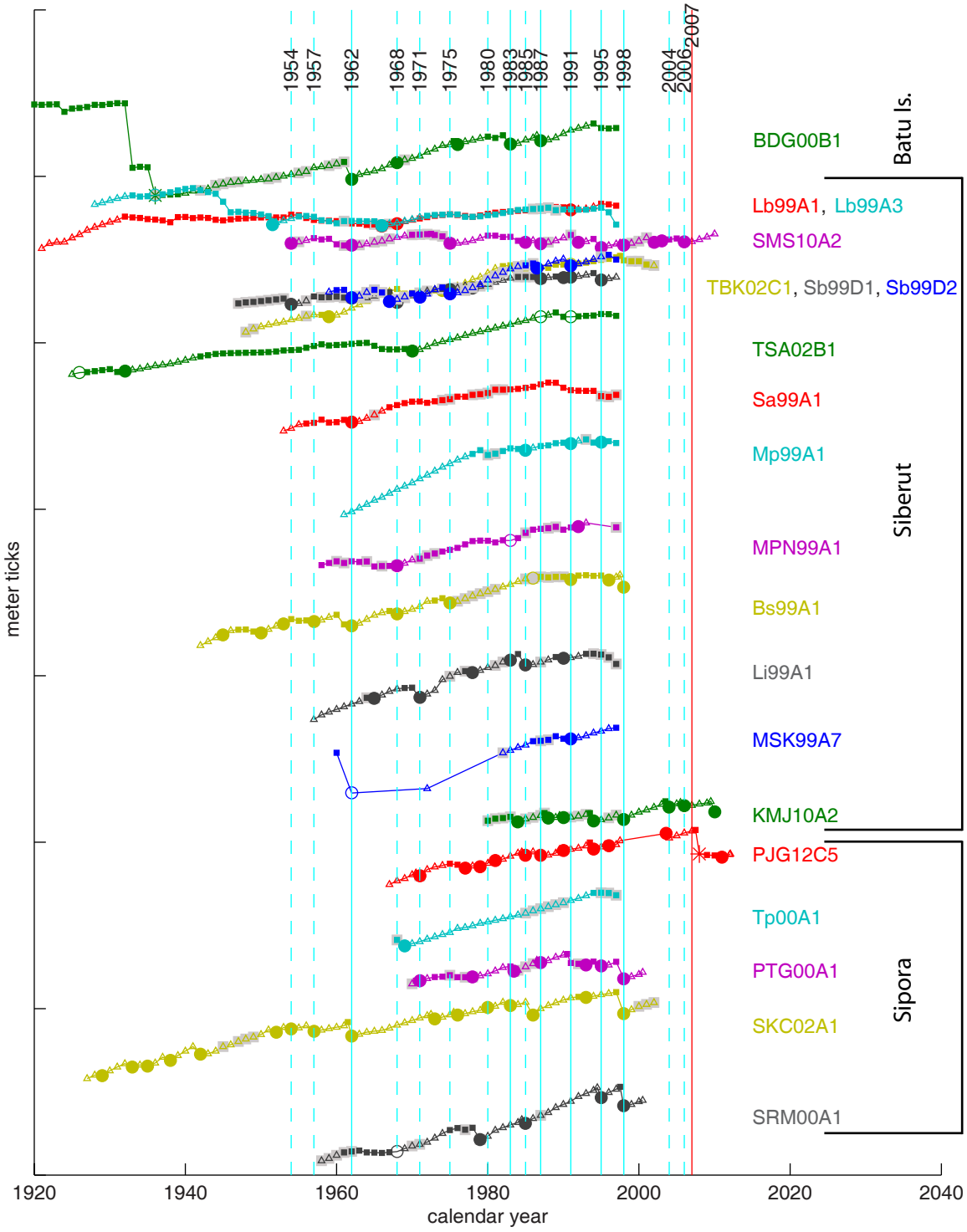

Figure 2.S1. All modern coral records arranged from northwest to southeast with records from each site offset vertically from the last. Vertical blue lines mark likely (solid) and possible (dashed) regional oceanographic die-downs. Red line marks the 2007 earthquake.

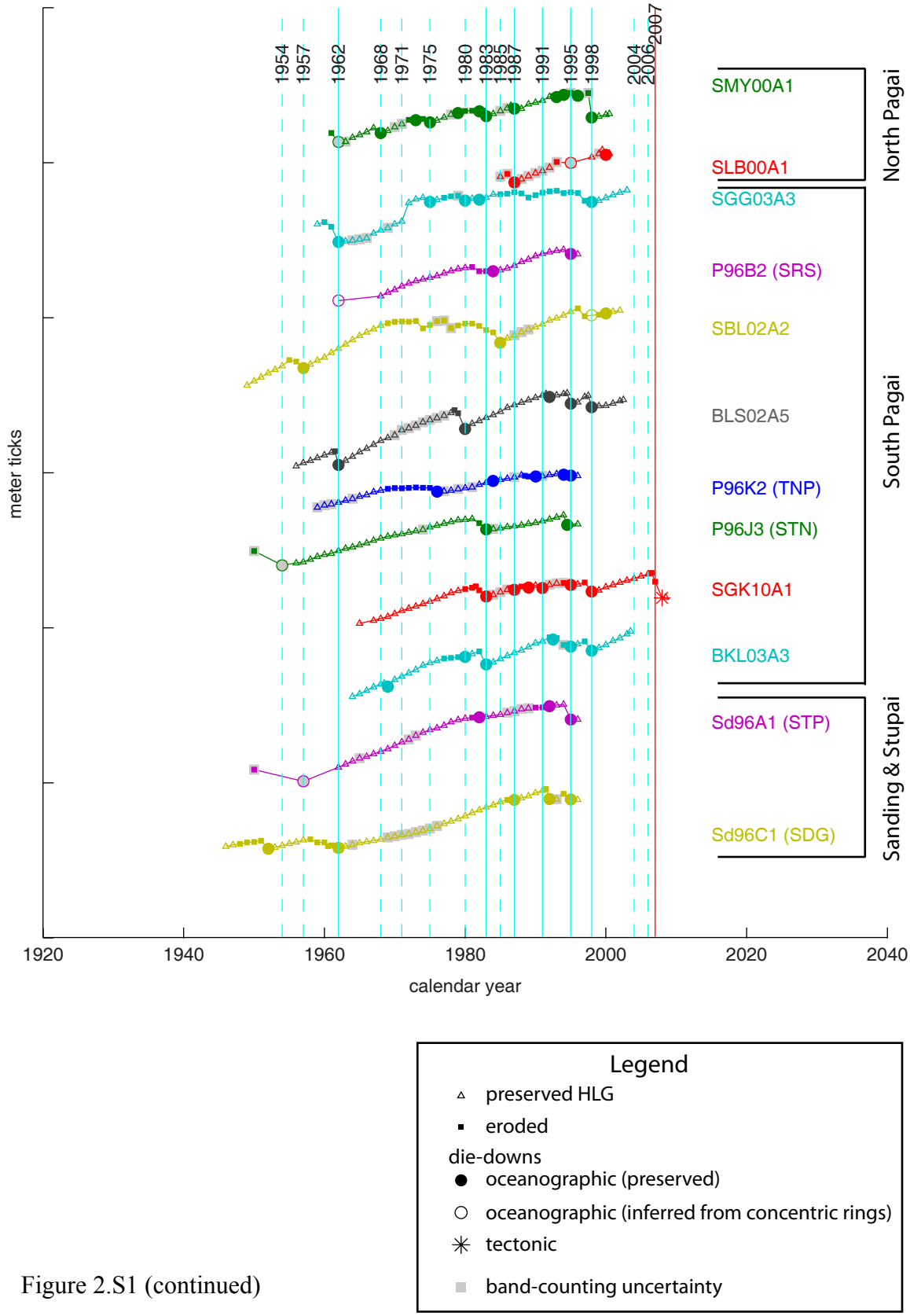

Figure 2.S1 (continued)

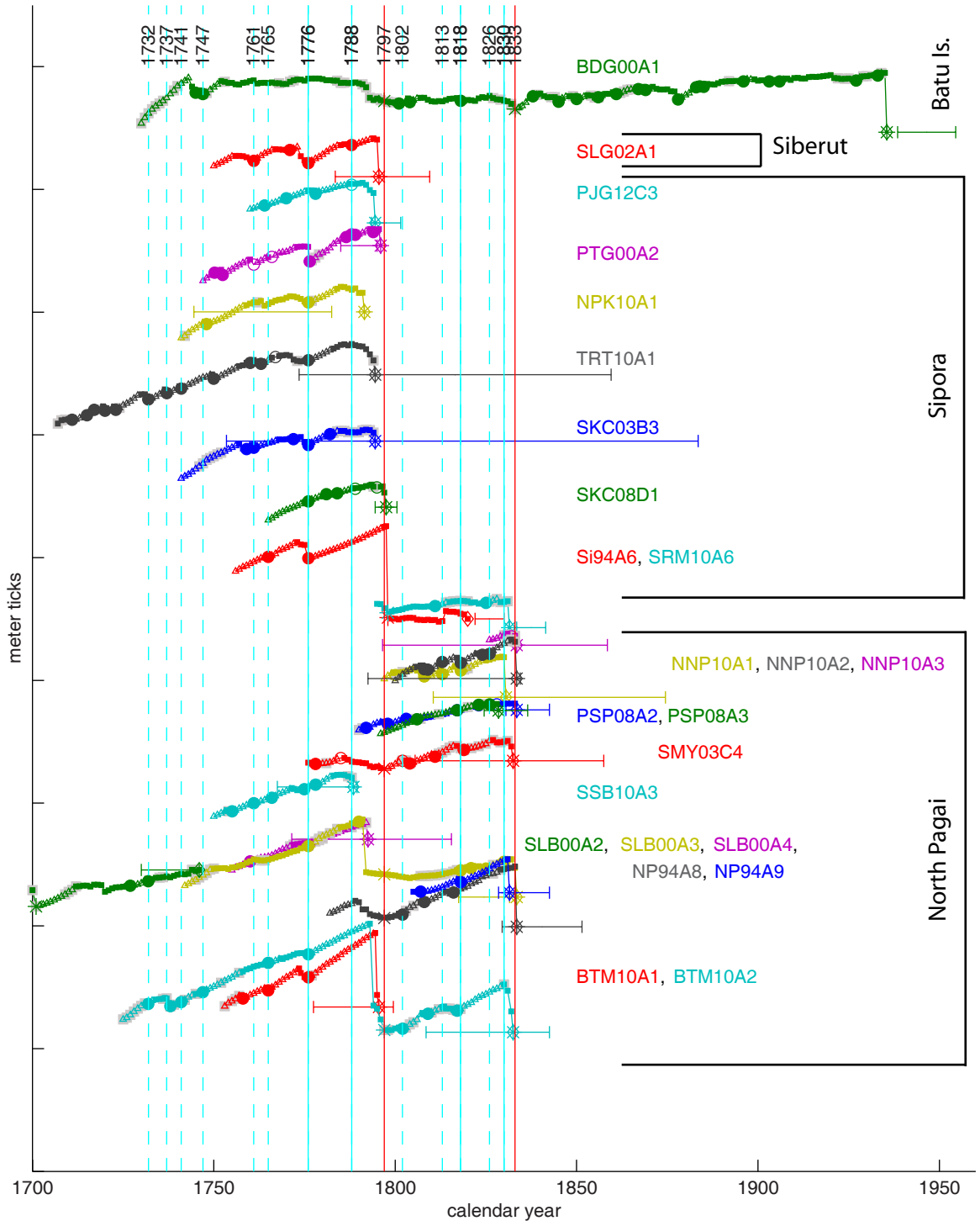

Figure 2.S2. All 18th- and 19th-century coral records arranged from northwest to south-east with records from each site offset vertically from the last. All symbology as in Fig. 2.S1 with the addition of a diamond symbol at the end of each record with error bars showing radiometric age uncertainty. Historical earthquakes are marked by red vertical lines.

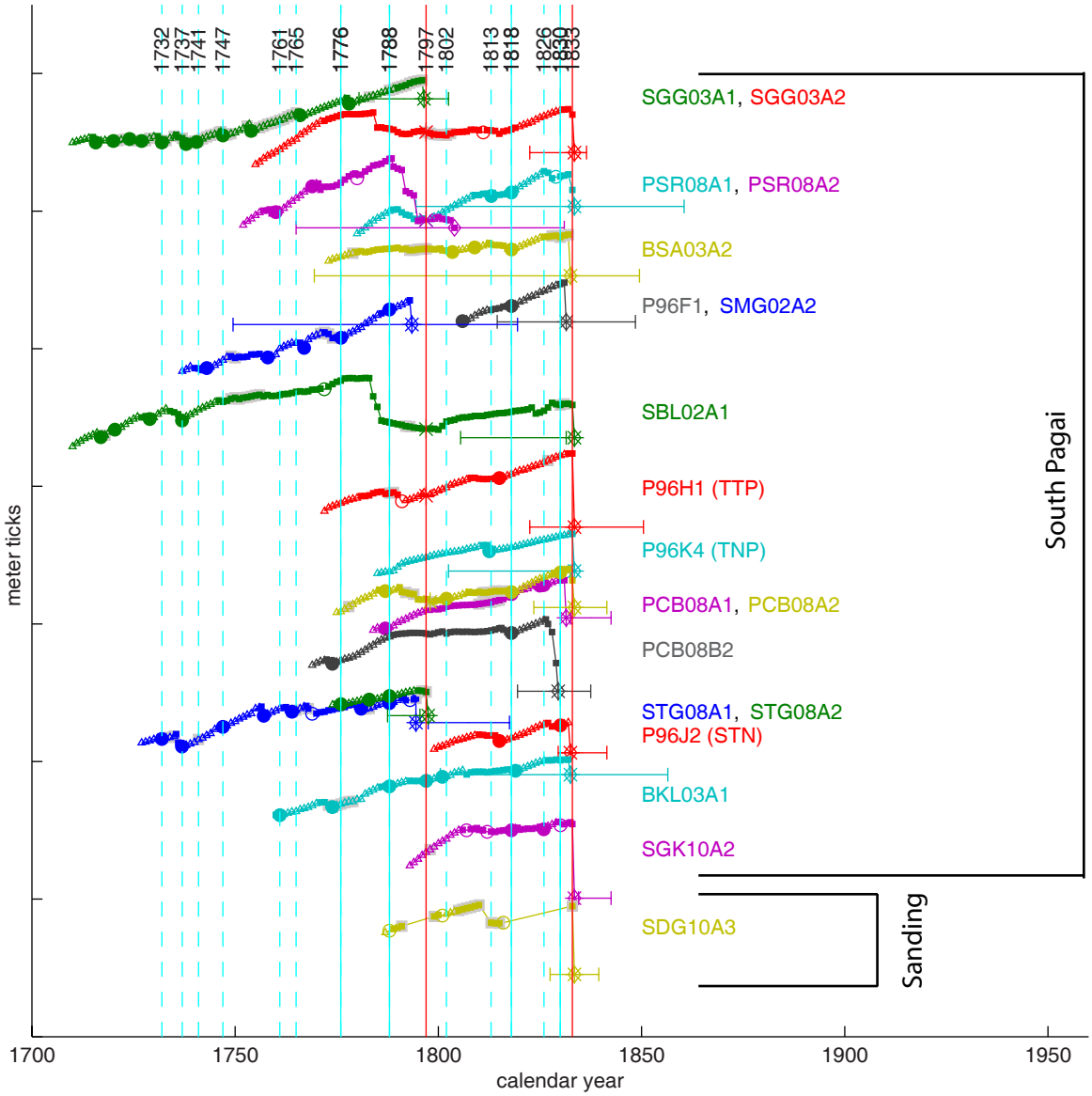

Figure 2.S2 (continued)

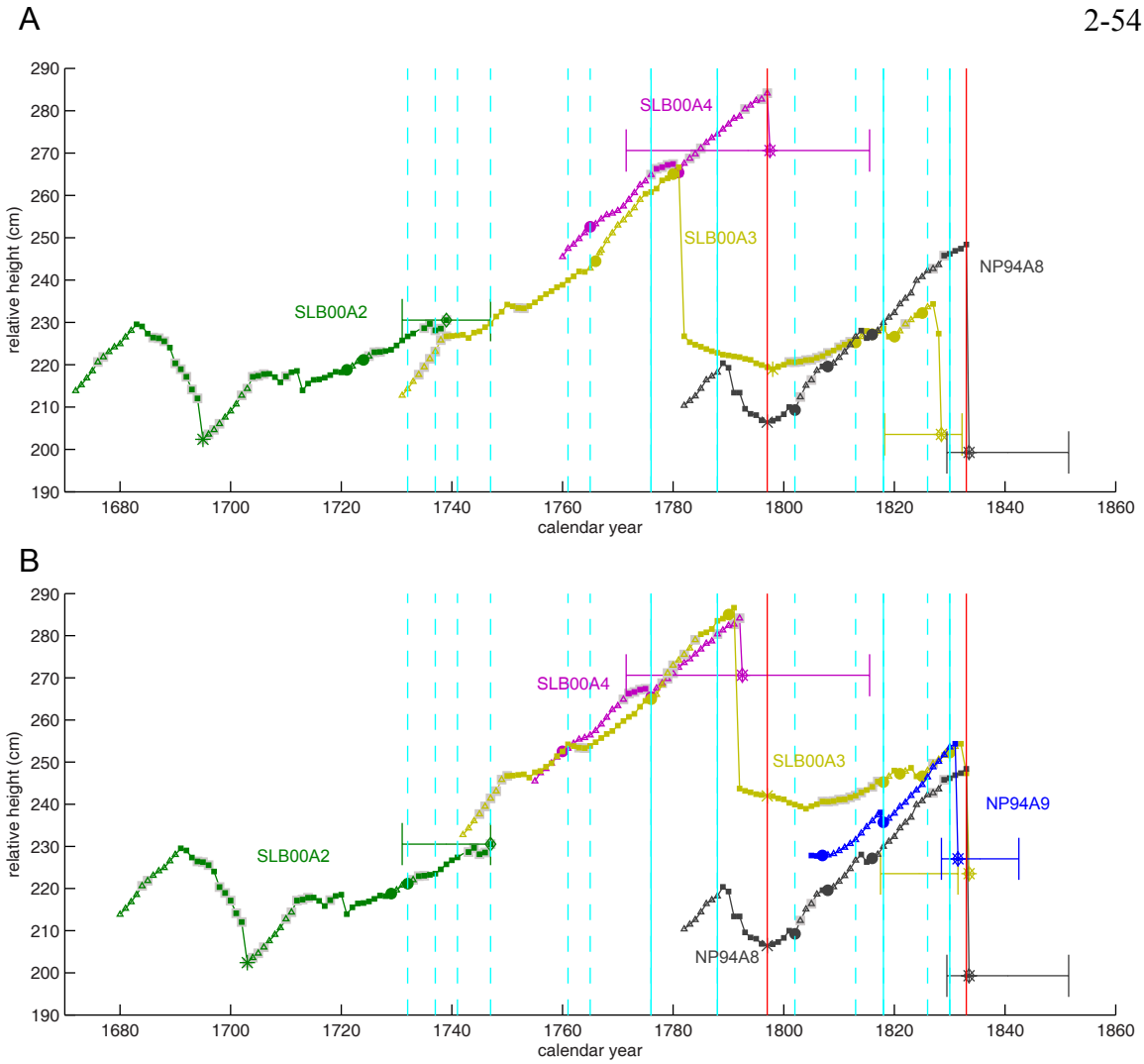

Figure 2.S3. Modifications to interpretation of Silabu history.

A) Original interpretation from *Natawidjaja et al.* [2006]. There are conflicting growth histories after 1797: SLB00-A3 had moderate upward growth (~5 mm/yr) after 1797, whereas NP94-A8 (and A9, which they omitted) shows very rapid upward growth (~12 mm/yr) during the same time period. It also seems unlikely that the surface that died in 1797 is completely un-eroded on A4 but eroded by 15 annual bands on A3, the interpretation by *Natawidjaja et al.* explaining why the top of A3 was 20 cm lower than the top of A4.

B) New interpretation. We interpret that A3 and A4 both have about 5 bands eroded off the 1797 death surface, and that the top of A3 was originally the same elevation as the top of A4 but the head has since settled into the substrate. Restoring the A3 record 20 cm upward places it higher than A8 and A9. We hypothesize that A3 was preserved in a lagoon pool some 40 cm above the open ocean ELW in 1797, a plausible idea since A3 was much nearer to the beach than most of the other sampled corals. This explains why its upward growth was not tracking the 12 mm/yr of relative sea-level rise recorded by A8 and A9. We use A3 and A4 to calculate the interseismic subsidence rate before 1797, but we use only A8 and A9 to calculate the rate between 1797 and 1833, since we have reason to believe A3 is not representative after 1797. We also use the elevation difference between A4 and A8 to calculate the 1797 coseismic uplift and ignore the smaller uplift suggested by the step in the A3 record, as did *Natawidjaja et al.* [2006]. We also shift the SLB00A2 record forward based on correlations with other corals that died in the 17th century (see Chapter 4).

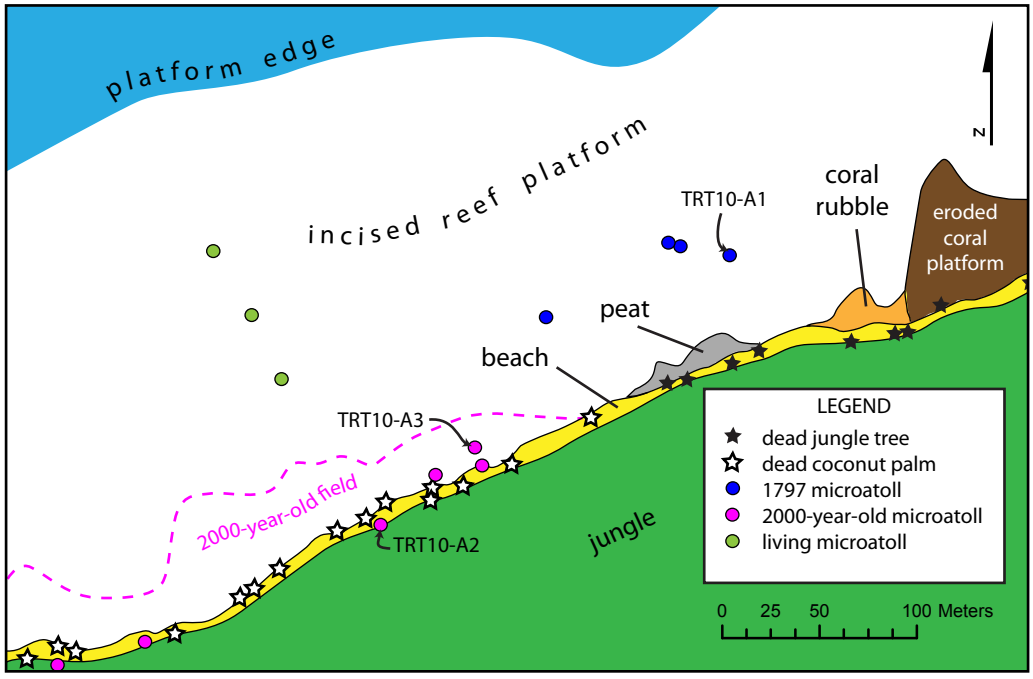

Figure 2.S4. Map of the Trait site. Dead trees that line the beach are evidence of recent interseismic subsidence. In addition to a population of corals that died due to uplift in 1797, there is a large population of ~2000-year-old microatolls in and near the beach. Dates from TRT10-A2 and A3 are discussed in Chapter 3.

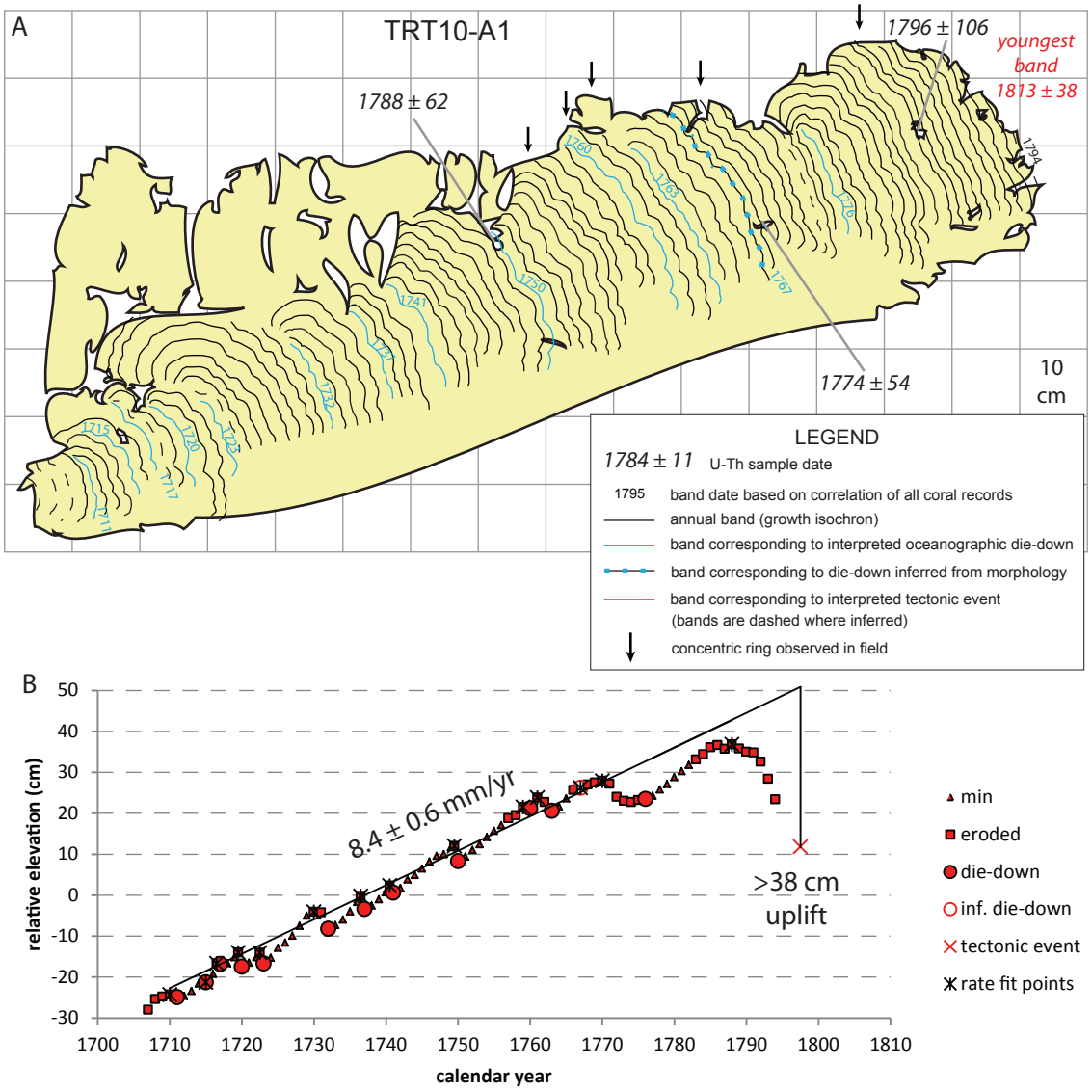

Figure 2.S5. A) Cross section and B) growth history of TRT10-A1 from Trait. Youngest preserved band date in red is based on band counting and a weighted average of the U-Th dates. Some die-downs are not clearly preserved but can be inferred from the concentric ring morphology of the microatoll.

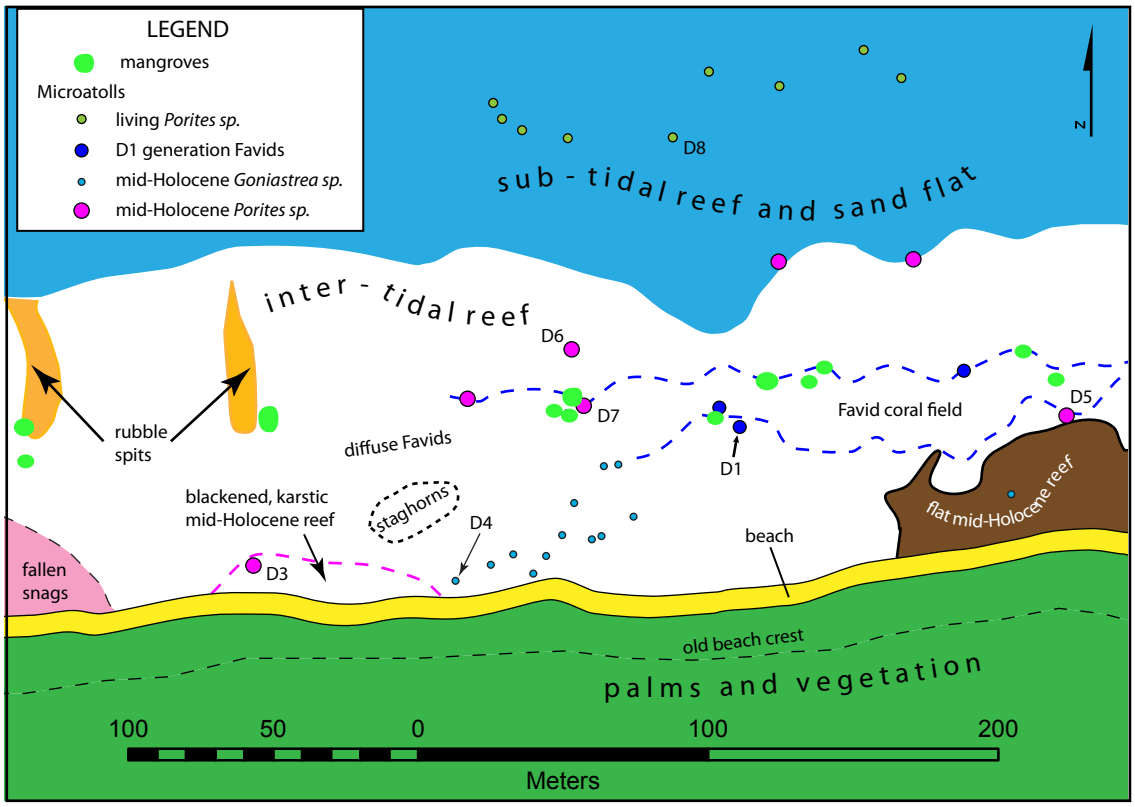

Figure 2.S6. Map of Sikici site D. A large field of ~1-meter diameter Favid corals died due to uplift in the 1797 earthquake, based on analysis of the sampled slab SKC08-D1. Chiseled samples of heads D3–D7 date to the mid-Holocene and are discussed in Chapter 3.

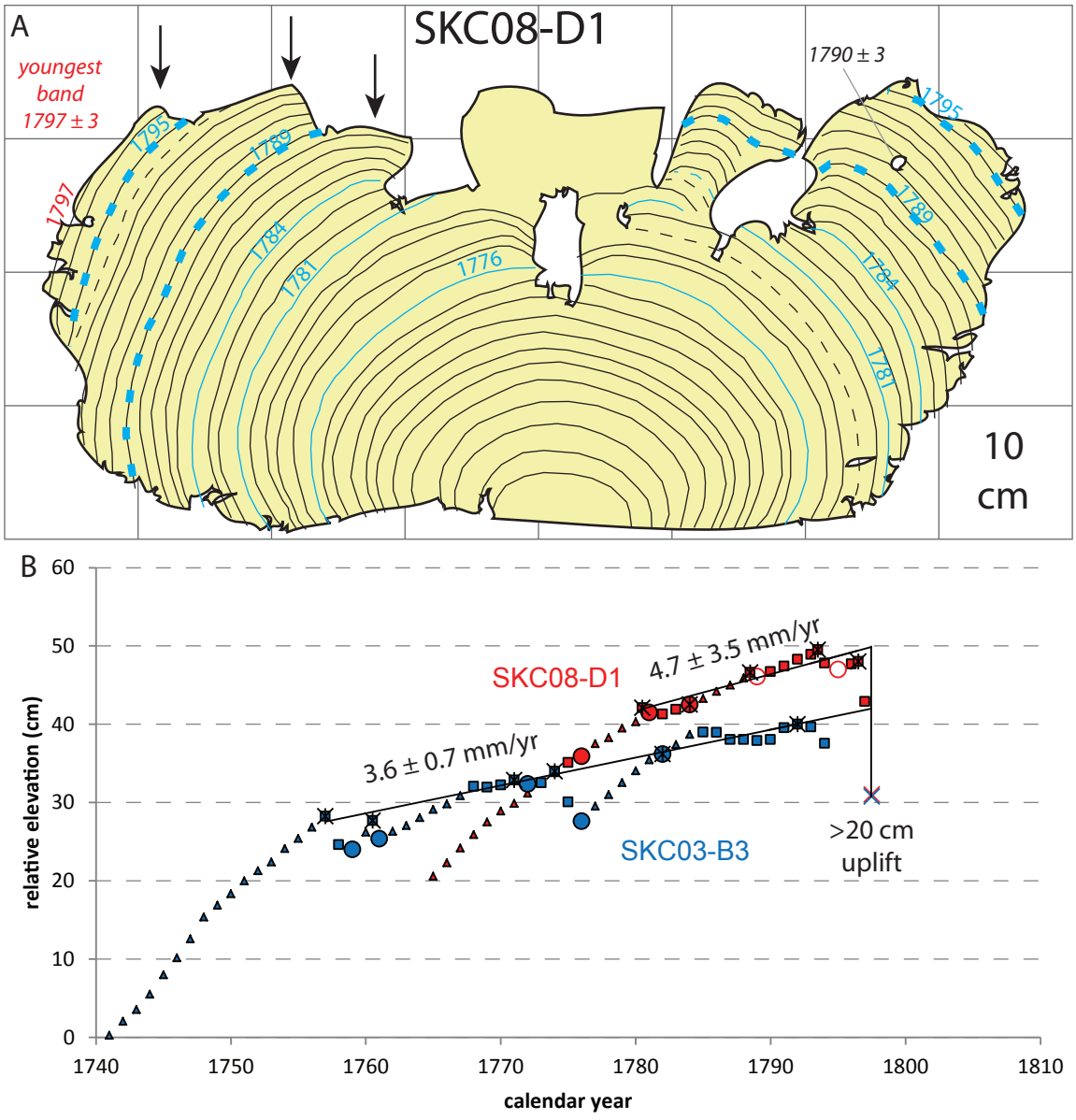

Figure 2.S7. A) Cross section of the Favid microatoll SKC08-D1 from Sikici D. Symbology as in Fig. 2S5. Large-corallite species tend to yield more precise U-Th dates, and this is no exception: it clearly died due to uplift in the 1797 earthquake. B) Growth history of SKC08-D1 and reinterpreted SKC03-B3. Interseismic subsidence rates are identical within uncertainty, but the longer B3 record provides a more tightly constrained estimate. As is common, the HLS for the Favid D1 was about 10 cm higher than for the *Porites sp.* B3.

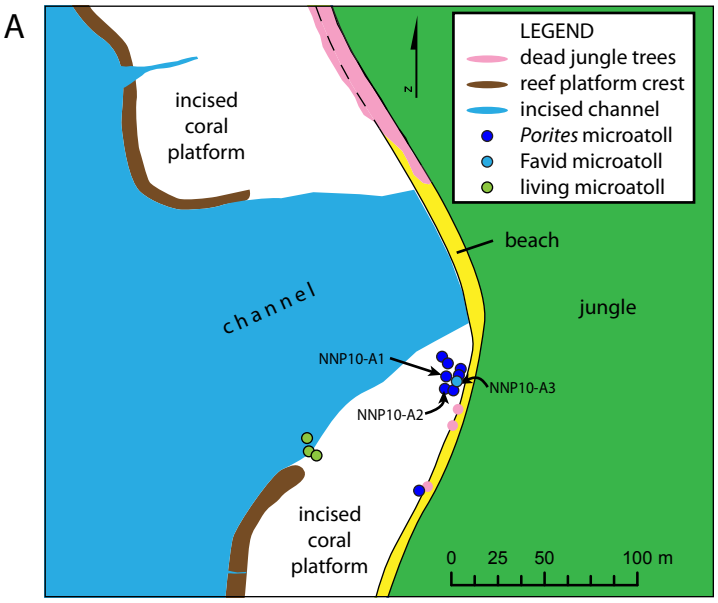

Figure 2.S8. Data from the North North Pagai site.

A) Map of the site on the northwest coast of North Pagai Island. The wide channel through the ancient coral platform suggests that there was formerly a freshwater stream outflow in this area. A band of dead trees along the beach is evidence of ongoing inter-seismic subsidence. There is a single population of fossil microatolls at this site, mostly *Porites sp.* but with a few Favids.

B) Cross sections of slabs NNP10-A1, A2, and A3 (symbology as in Fig. 2.S5A). Dates are consistent with uplift and death of all corals during the 1833 earthquake. A subset of the *Porites* coral population have a high satellite ring around the middle, as illustrated by sample A2. The satellite growth apparently grew contemporaneously with the outer perimeter, though it is considerably higher (inner satellite growths frequently have higher HLS than the coral's outer perimeter, perhaps due to water pooling inside the microatoll). The number of bands in the satellite indicate that about three bands must have been eroded off the perimeter.

C) Growth histories of A1 and A2 (symbology as in Fig. 2.S5B). A2 records a faster subsidence rate than A1, though there is considerable overlap between the confidence intervals. We adopt an average rate of 5.4 mm/yr for this site, which is consistent with both records. One other possible scenario is that the population of corals with morphology similar to A2 (i.e., with inner satellite heads) were uplifted and died in 1797, while the A1 population grew later and died in 1833. This scenario would explain the differing morphologies and subsidence rates and would also be consistent with the U-Th dates. However, due to the strong correspondence in the pattern of oceanographic die-downs on the two heads, contemporaneous growth of A1 and A2 is the more likely scenario. Most importantly, adopting the non-contemporaneous scenario would not significantly alter our final results: a 40-cm 1797 uplift preceded by 6.8 mm/yr of subsidence is consistent with the regional pattern.

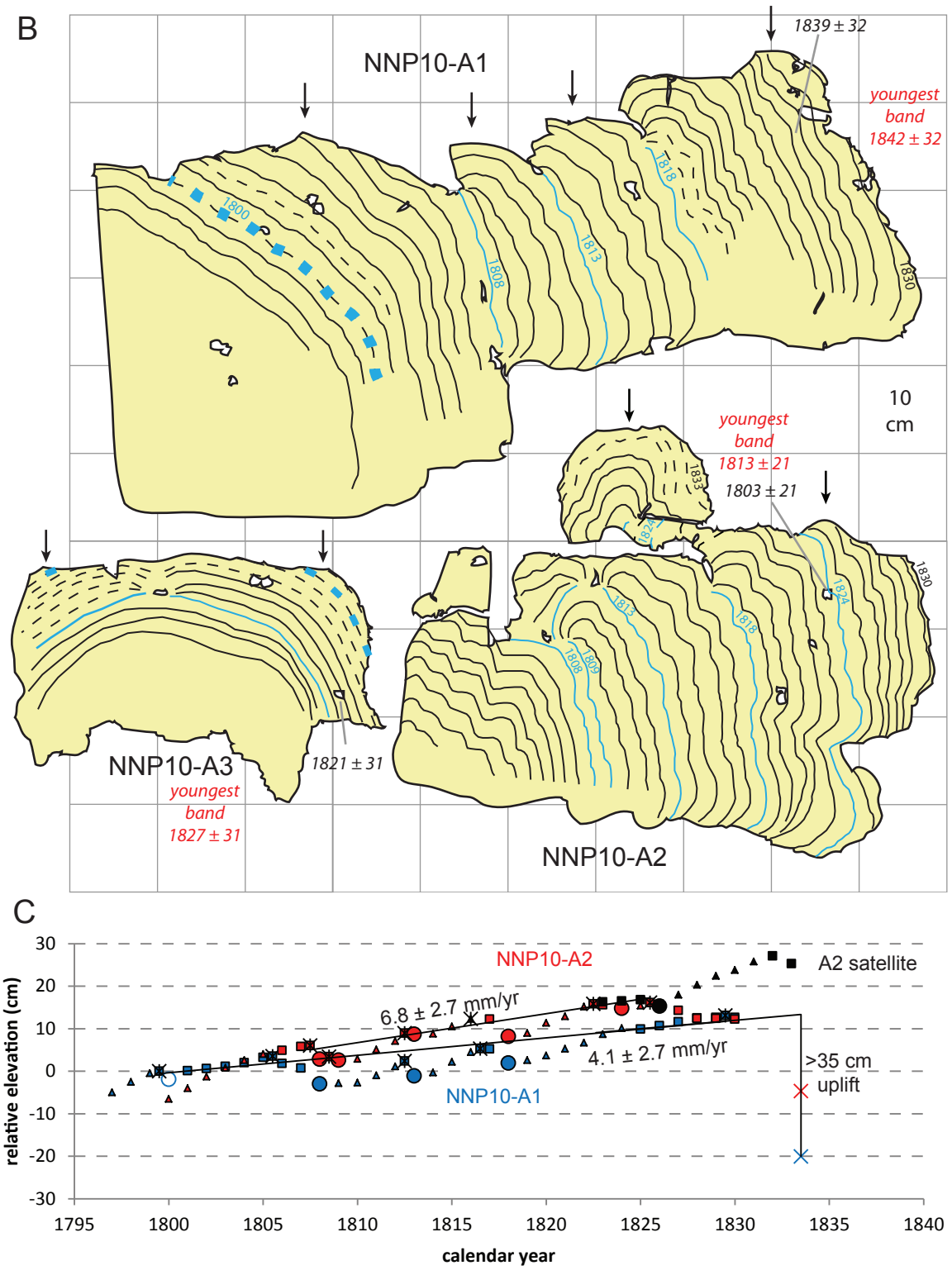

Figure 2.S8 (continued)

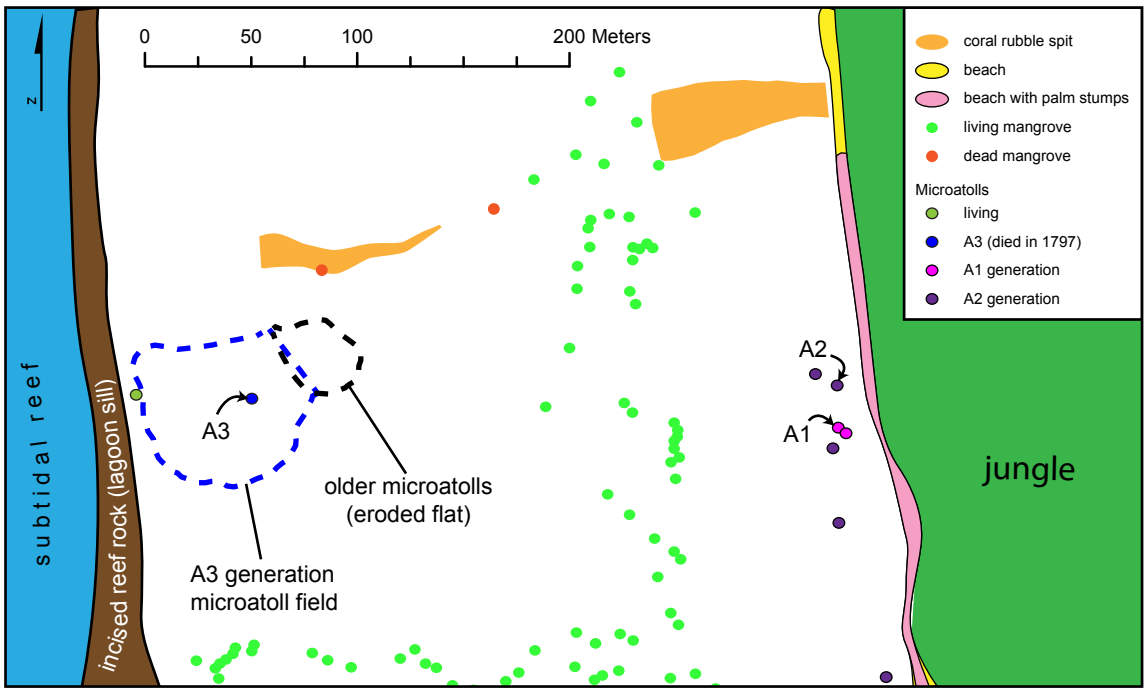

Figure 2.S9. Map of the site on Pulau Silabusabeu, an islet near Silabu village on the west coast of North Pagai. Palm stumps lining the beach and dead mangroves on the coral platform are evidence of recent interseismic subsidence. We sampled three populations of fossil microatolls. The A1 and A2 groups died in the 6th century A.D., while the A3 group died due to uplift in the 1797 earthquake.

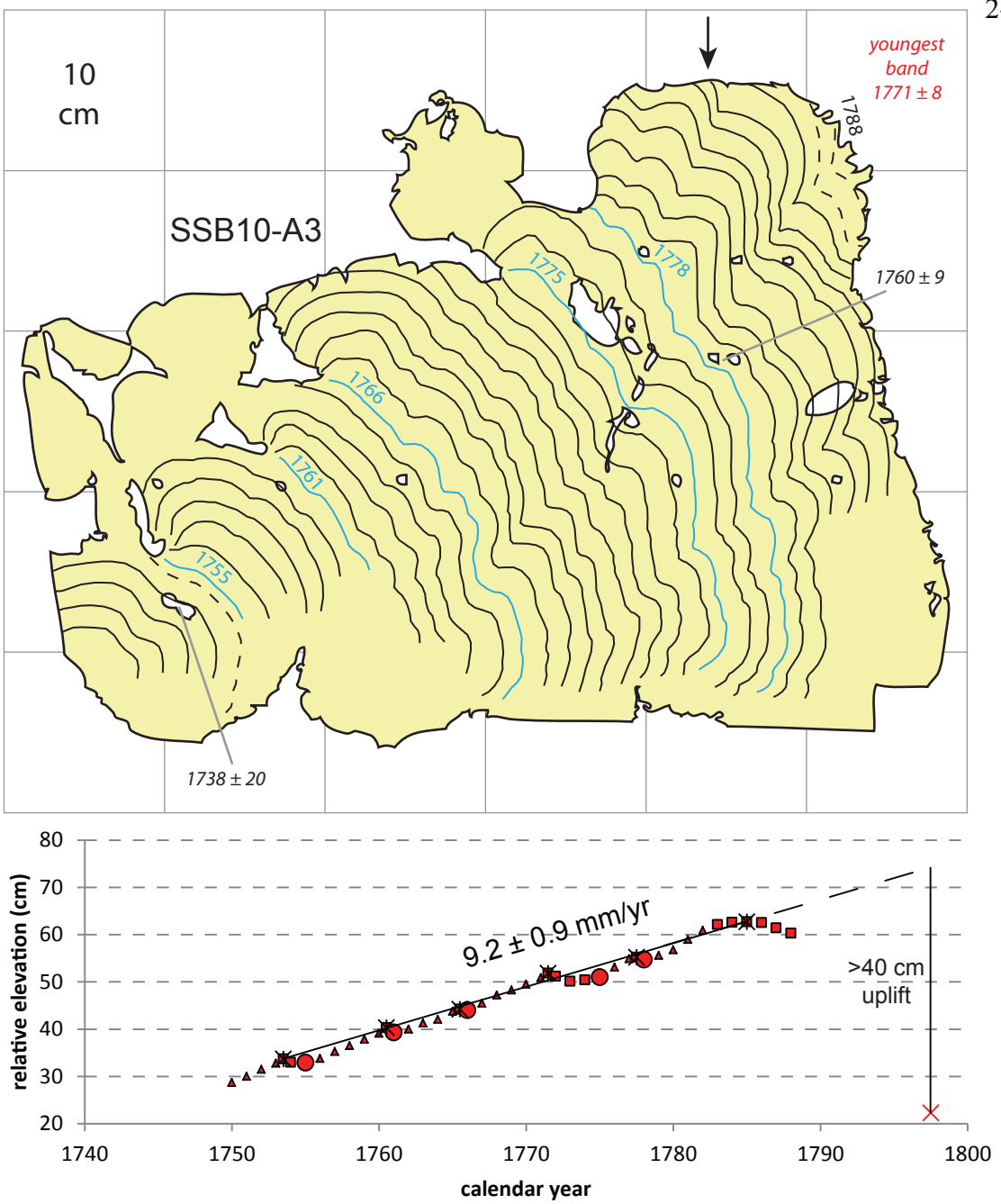

Figure 2.S10. Cross section and growth history of a microatoll from the south coast of Silabusabeu, a small island west of Silabu Village on North Pagai. Symbology as in Fig. 2.S5. The U-Th ages suggest death in ~1770, but the large population that this specimen came from indicates death due to tectonic uplift, most likely in 1797. Assuming the age uncertainty is underestimated, die-down matching suggests that the youngest preserved band grew in 1788. This interpretation requires that 9 annual bands have been eroded from the outer perimeter of this microatoll, a large but not impossible number. The high pre-1797 interseismic subsidence rate is well constrained and very similar to the contemporaneous rate at the nearby Silabu site.

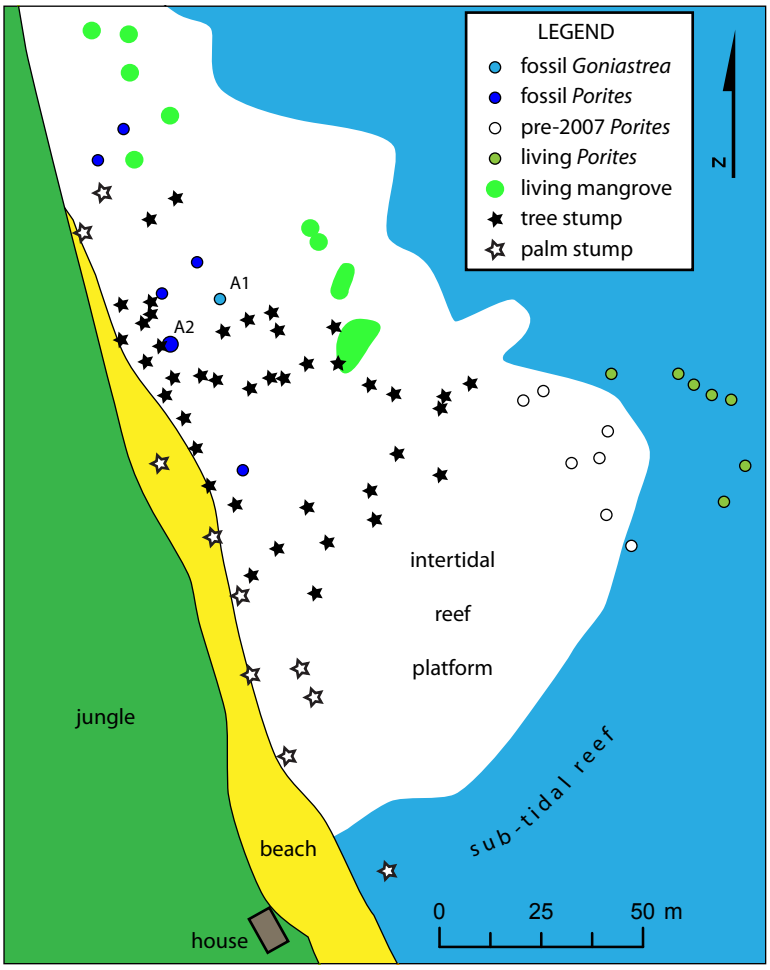

Figure 2.S11. Map of Pecah Belah site A, on the northern coast of the islet Pecah Belah in the South Pagai archipelago. Two sampled microatolls represent a population that died due to uplift in the 1833 earthquake. White circles indicate microatolls which died due to uplift in the 2007 earthquake; green circles indicate those which were growing at lower elevation and survived. A broad swath of jungle trees grew on the reef platform (likely following the 1833 uplift) but have since died due to interseismic submergence. The 68-cm 2007 uplift [*Sieh et al.* 2008] was insufficient to raise the platform above high tide, as would be required to support jungle trees. In contrast, we estimate that the uplift in 1833 was about 1.2 meters.

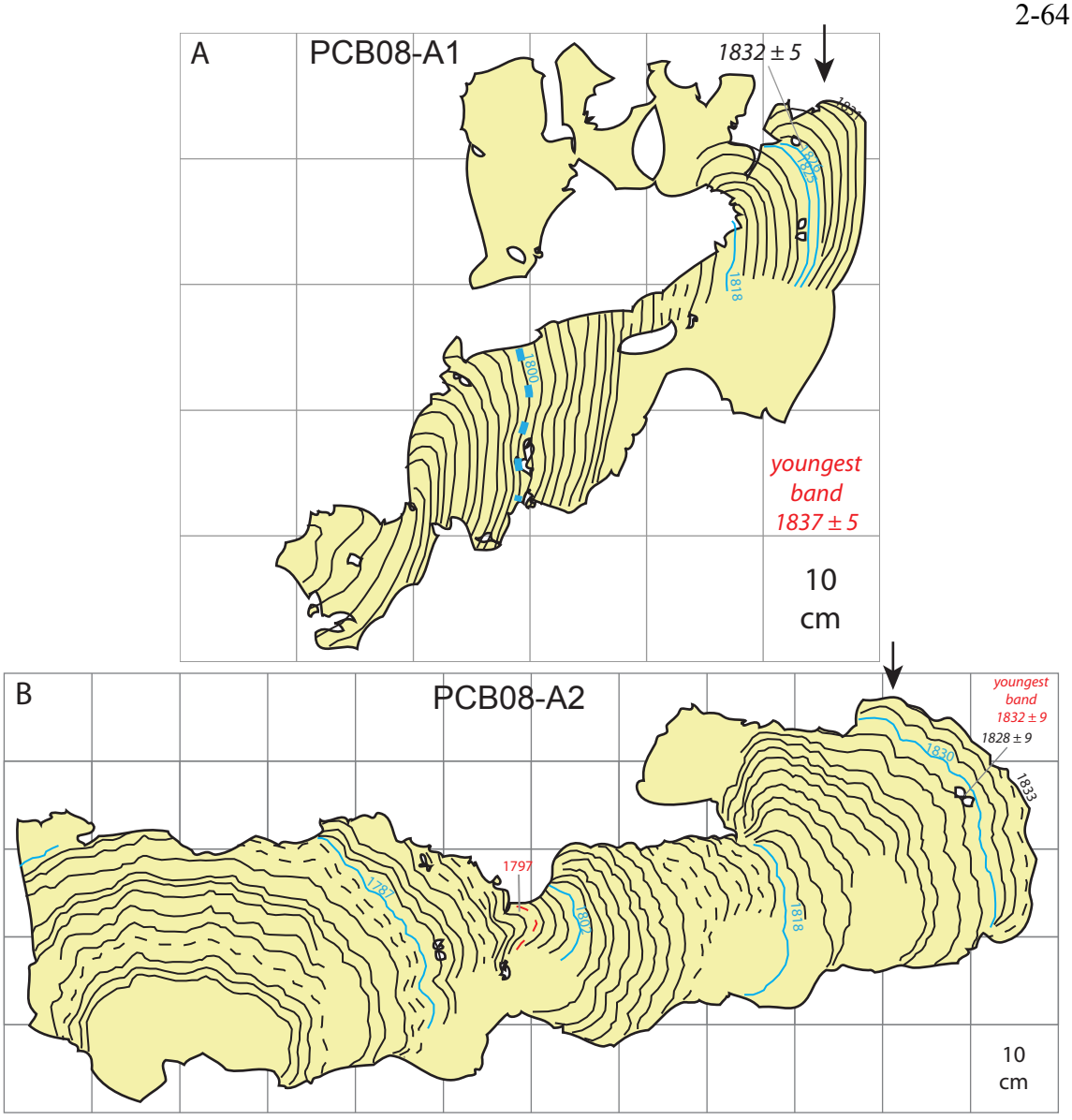

Figure 2.S12. Cross sections and growth histories from Pecah Belah (symbology as in Fig. 2.S5). A) PCB08-A1 is a *Goniastrea sp.* which first hit HLS shortly after the 1797 earthquake, and died due to uplift in the 1833 earthquake. B) PCB08-A2 is a *Porites sp.* which experienced a 15-cm die-down in 1797 and died completely in 1833. C) Cross section of PCB08-B2 from Pecah Belah B, a nearby site that appears in Chapter 4. The surface of this microatoll has been significantly eroded, but it suggests a low subsidence rate before it was killed by a large uplift in 1833. D) Comparative growth history of all three PCB coral samples. B2 almost certainly settled ~20 cm into the muddy substrate (other microatolls of this generation were at somewhat higher elevations.) A1 may have settled as well, since *Goniastrea sp.* frequently can survive higher than *Porites sp.* The 20 years of unhindered upward growth of B2 after it first hit HLS in 1774 suggests that the interseismic subsidence rate before 1797 was relatively high, but this is an uncertain result.

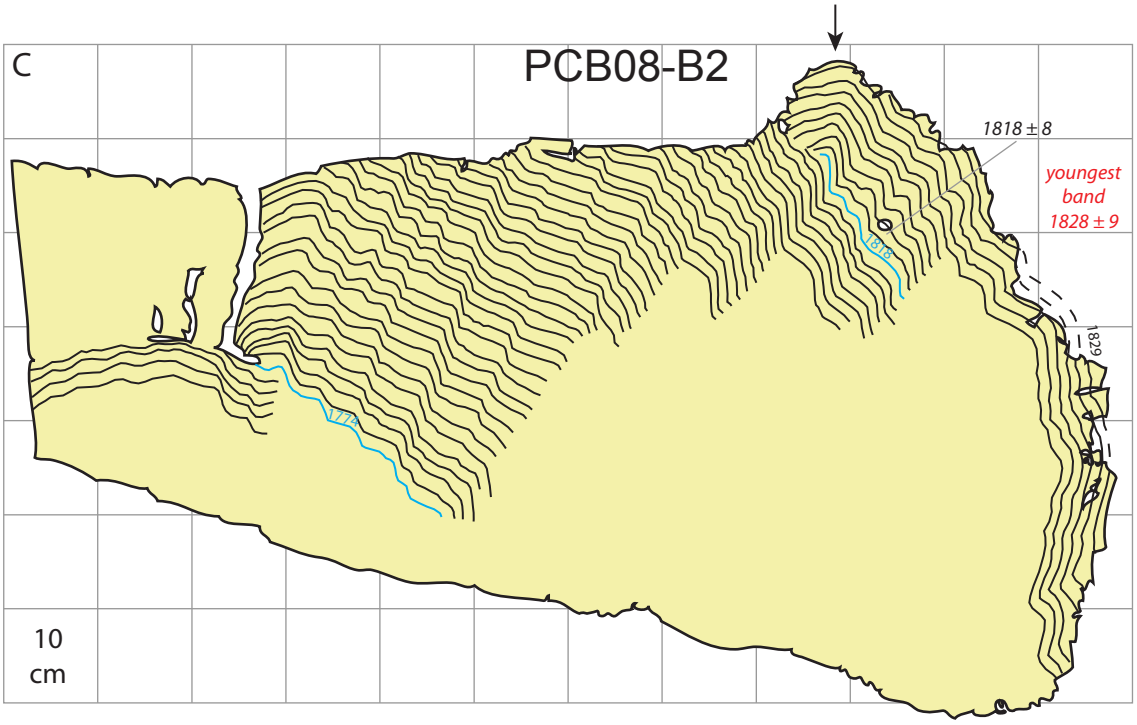

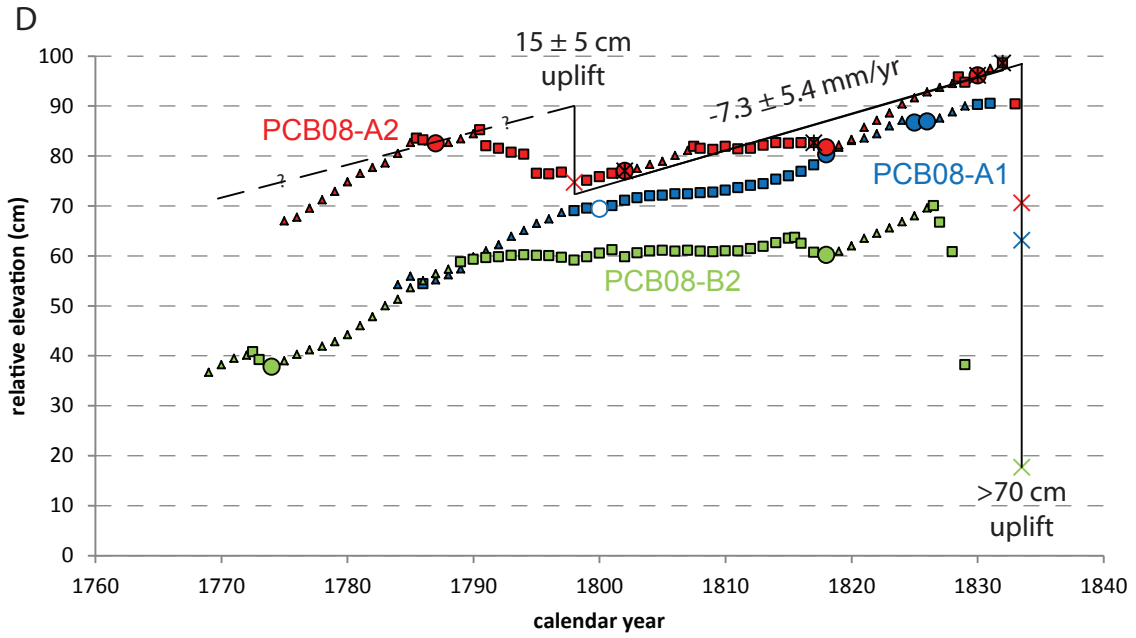

Figure 2.S12 (continued)

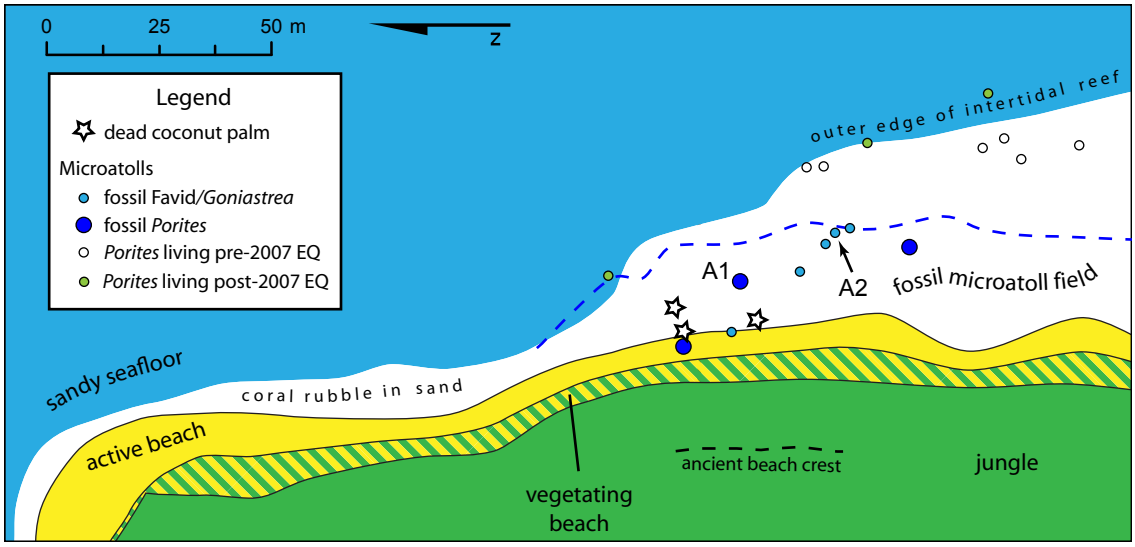

Figure 2.S13. Data from Pulau Simaturugogo, an islet in the South Pagai archipelago.

A) Map of the site on the west side of the islet. During the 2007 earthquake the site was uplifted 45 cm, killing many living corals. Between that time and our visit in 2008, the old beach began to vegetate and a new beach formed at a lower elevation. We sampled two microatolls from a population near the beach which died due to uplift in the 1797 earthquake. An ancient beach crest (now covered by jungle) probably corresponds to the fossil coral population.

B) Cross sections of *Porites* A1 and *Goniastrea* A2 from Simaturugogo (symbology as in Fig. 2.S5A). The innermost part of A1 appears to be tilted, so we do not include the growth history before 1742 in our analysis (the head tilted and possibly rolled into deeper water in about 1742).

C) Growth histories of the two microatolls (symbology as in Fig. 2.S5B). The very low average subsidence rate of A1 after 1757 seems inconsistent with the preceding much faster subsidence (1747–1757) and the moderate subsidence rate recorded by A2 (1776–1797). We infer that the HLS of A1 was controlled by a very local pool above the open ocean HLS between 1747 and 1776. By excluding the fit points within that period (orange stars) and including the fit point before 1747 (pink star), we obtain a subsidence rate for A1 which is consistent with A2. We use the rate derived from A2 as the pre-1797 rate for this site, since the interpretation of A1 is questionable.

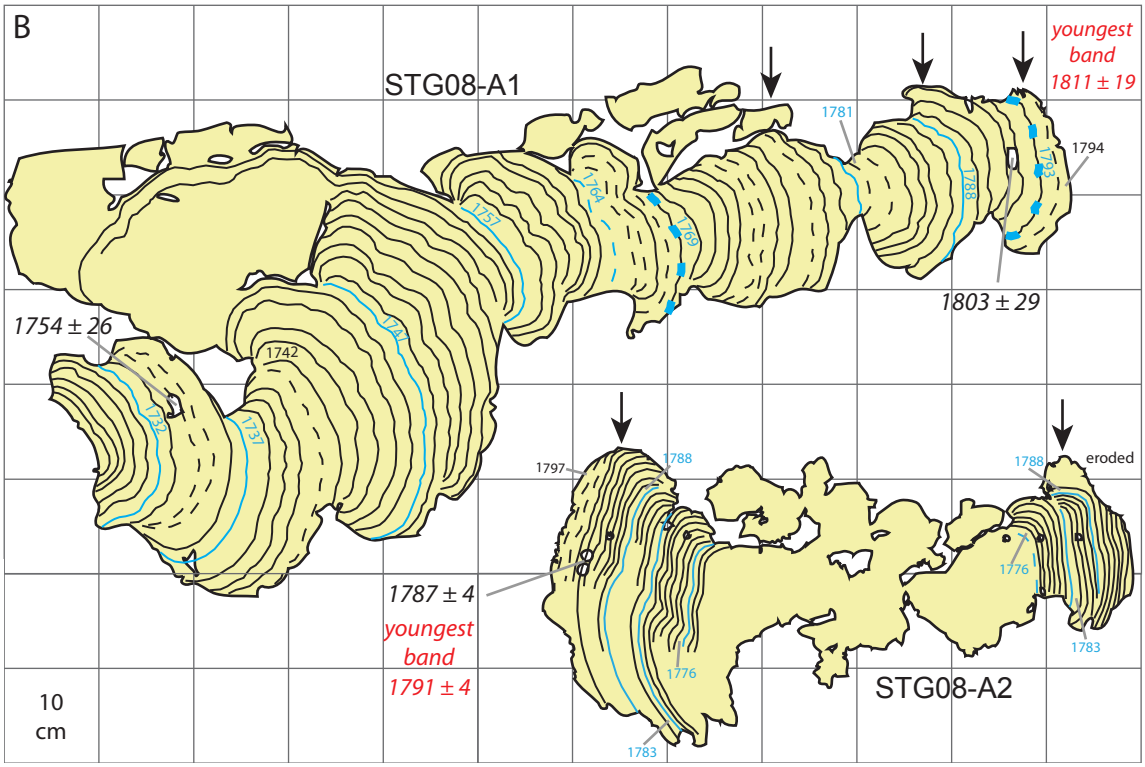

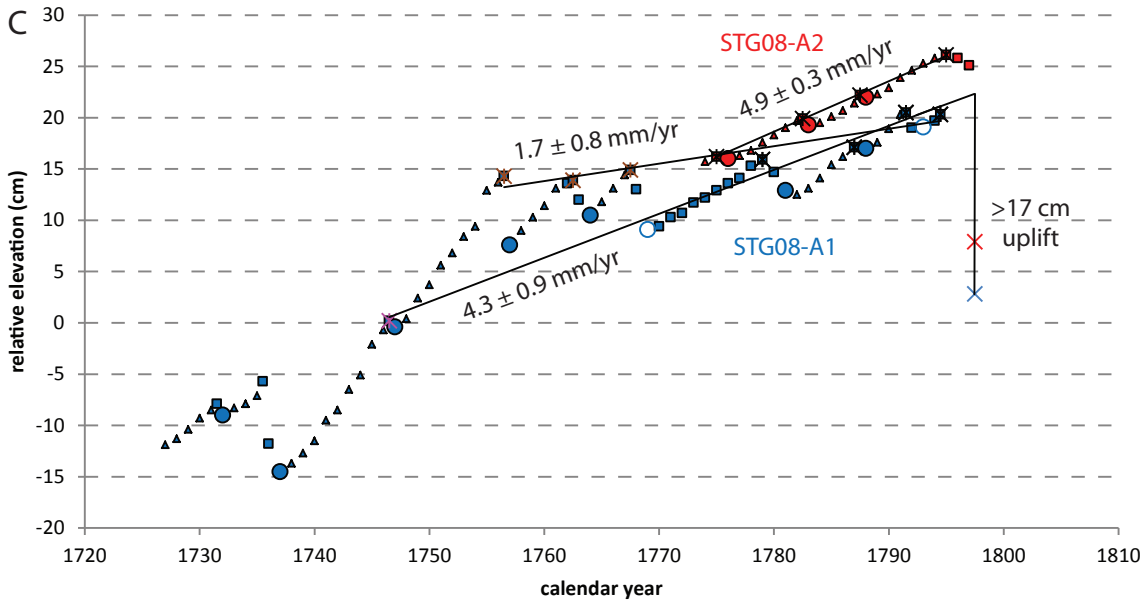

Figure 2.S13 (continued)

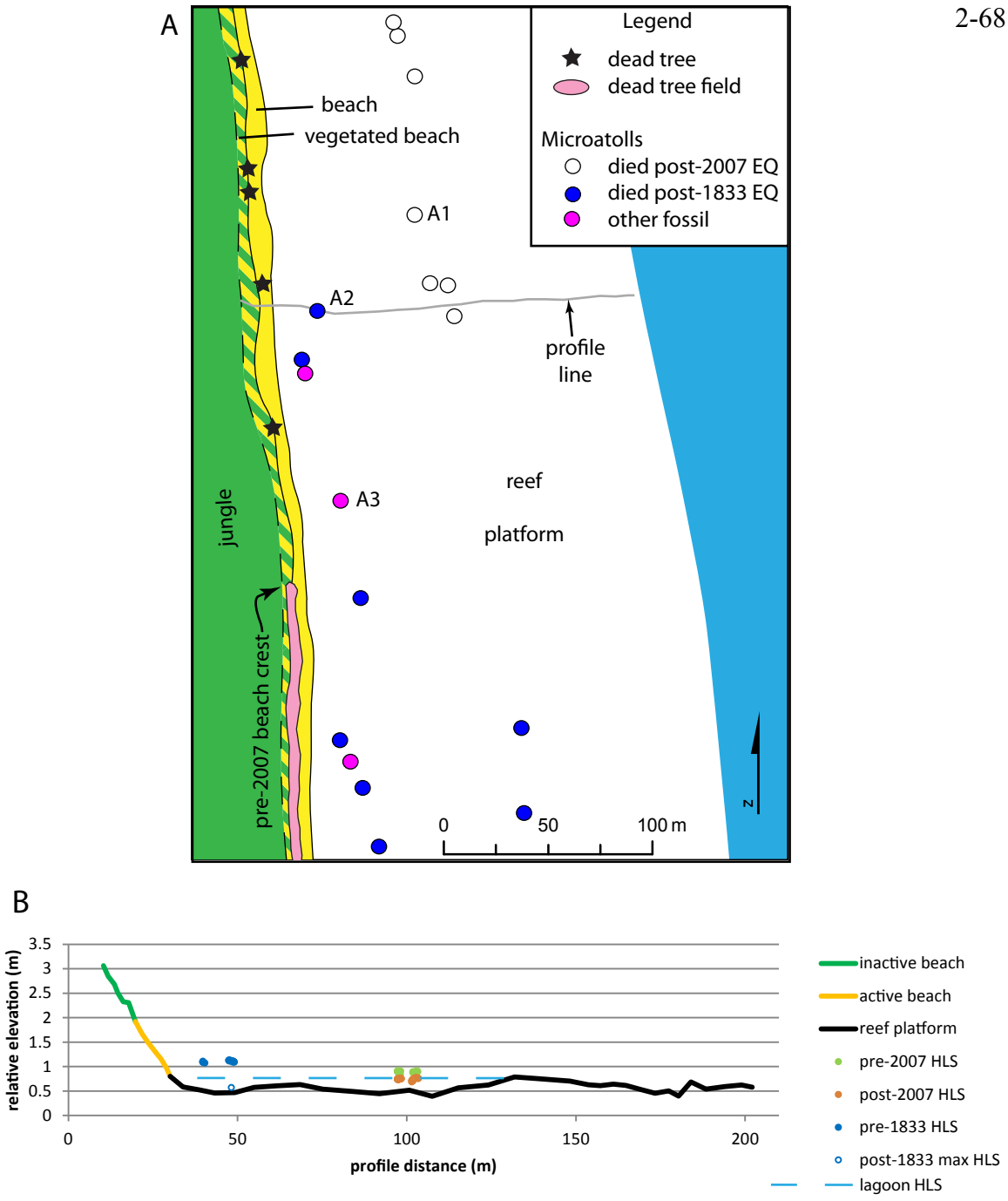

Figure 2.S14. A) Map of the Simungguk site, on the east side of the southernmost islet in the South Pagai archipelago. B) Elevation profile illustrating that corals survived in a lagoon pool after the 2007 uplift. The corals since died for other reasons (likely bleaching due to the hot, shallow lagoon environment). The abandoned beach crest about 1 meter higher than the active crest implies that the 2007 uplift was significantly larger than the 15-cm die-down on the modern corals suggests. The base of coral head A2 could have similarly survived in the lagoon pool for a short time after the 1833 uplift (uncertain due to erosion of the coral surface).

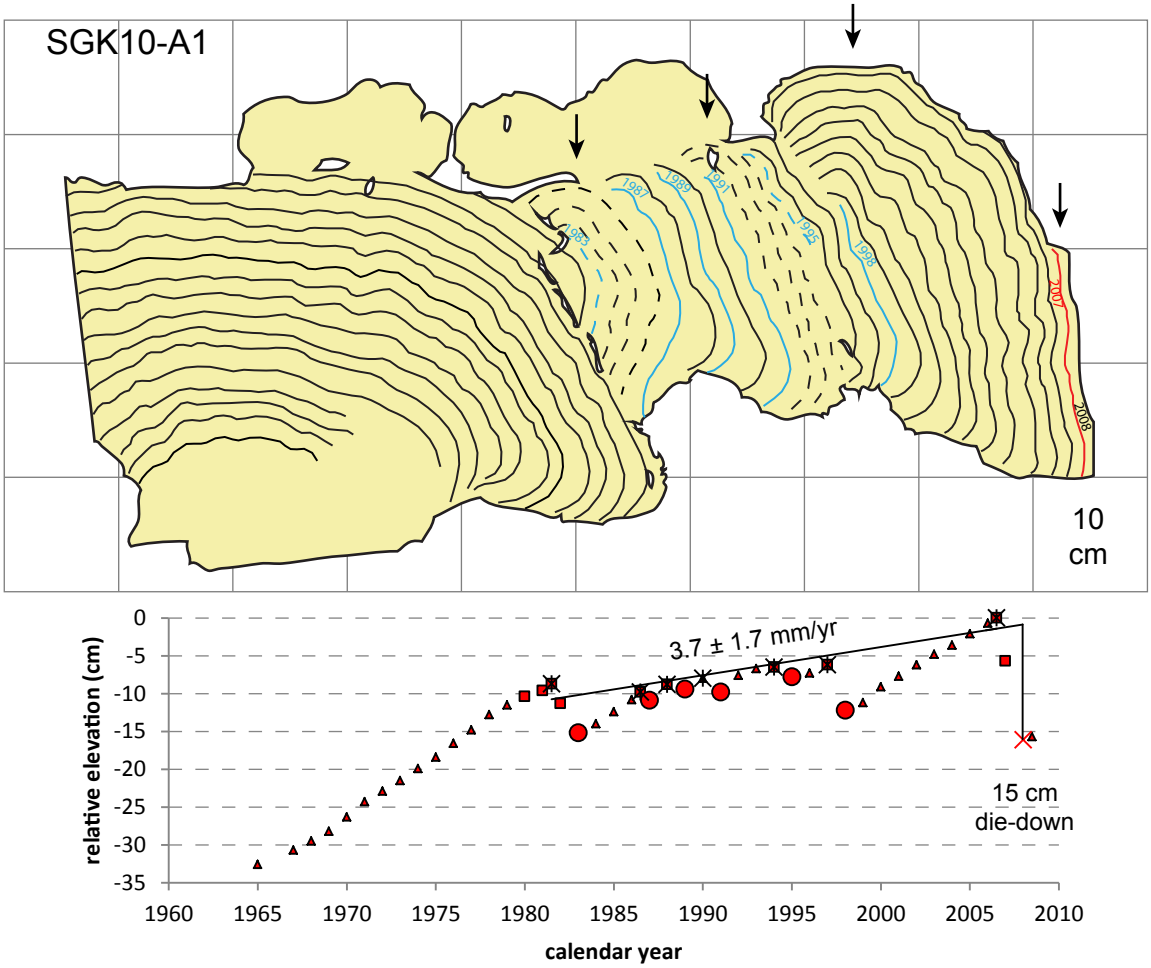

Figure 2.S15. Cross section and growth history of modern slab SGK10-A1 from Simungguk (symbology as in Fig. 2.S5). After 25 years of moderate interseismic subsidence, the 2007 earthquake caused a 15-cm die-down. Though the actual uplift was likely greater than the height of the living coral perimeter, the lagoon pool held water substantially higher than the ocean level and permitted the lower 20 cm of coral surface to continue growing. After about 1 year of post-earthquake growth, this coral died completely.

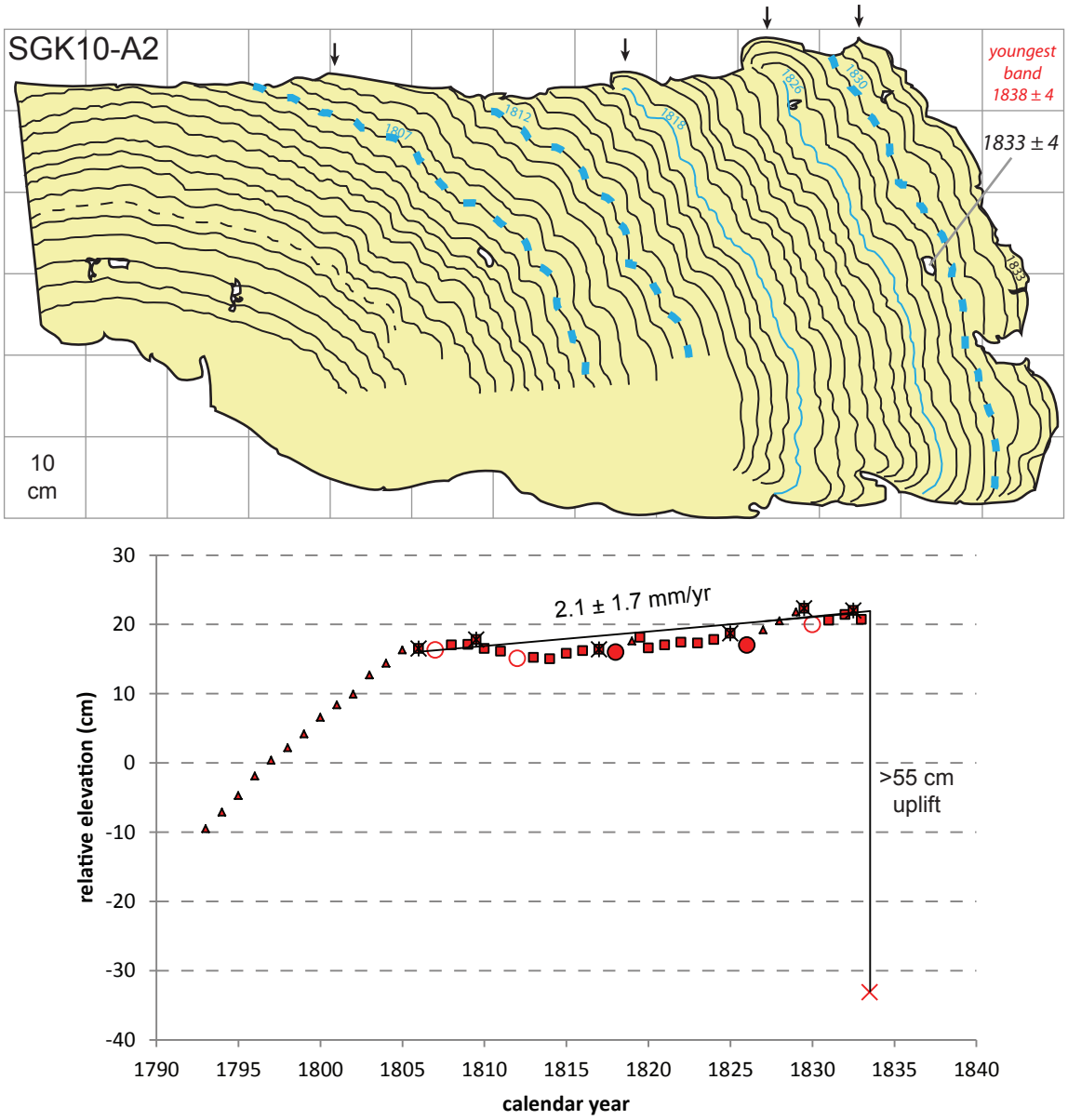

Figure 2.S16. Cross section and growth history of "fossil" slab SGK10-A2 from Simungguk (symbology as in Fig. 2.S5). The subsidence rate leading up to the uplift and death in 1833 appears to have been lower than the rate before the 2007 earthquake. The lowest 15–20 cm of the outer perimeter is below the lagoon-controlled HLS and could have survived after 1833, though there is no positive evidence that it did.

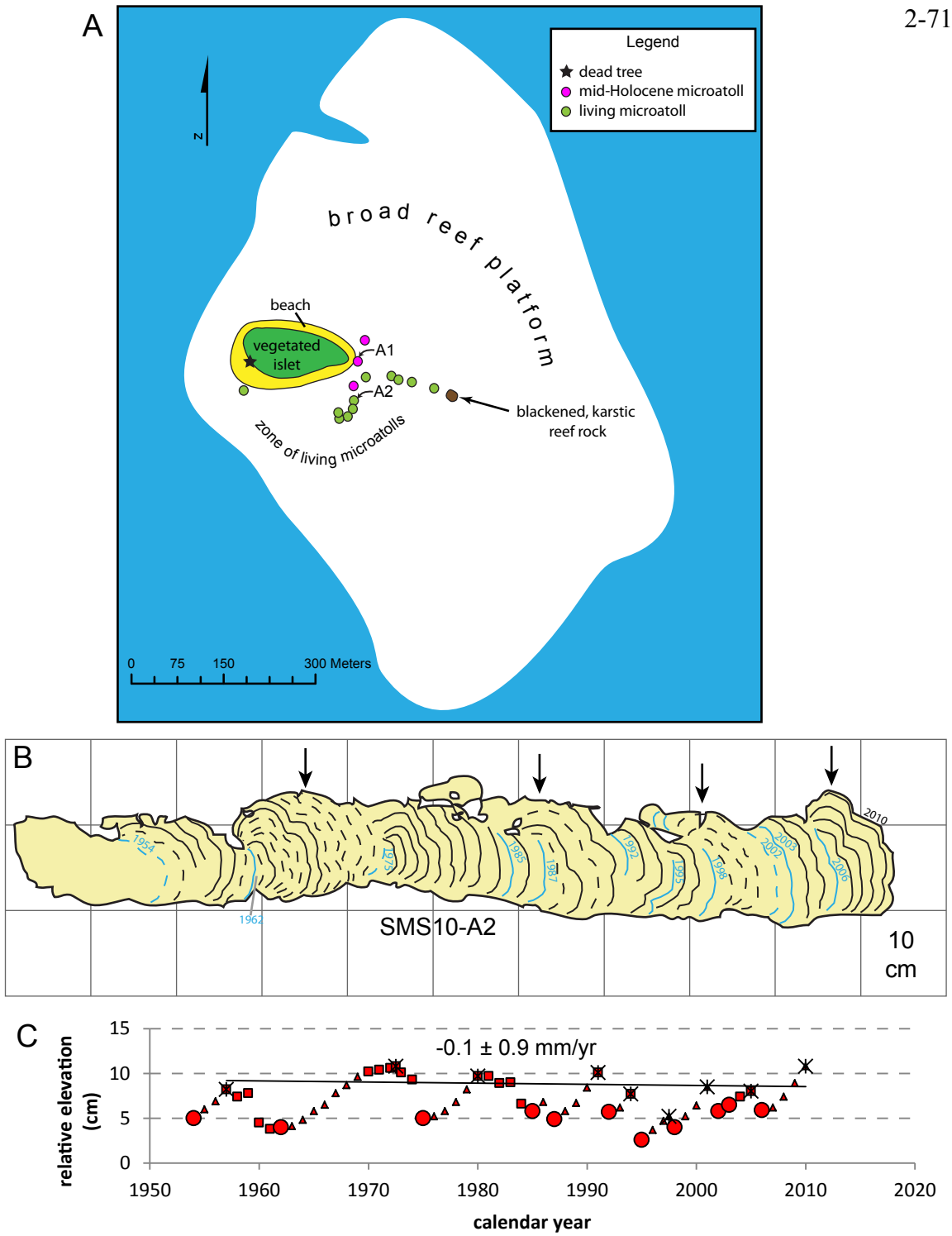

Figure 2.S17. Data from Pulau Simasin, a small islet off the north coast of Siberut. A) Map of the site. Much of the broad reef platform is covered with living microatolls. A small group of "fossil" microatolls dates to the mid-Holocene (date from SMS10-A1 discussed in Chapter 3). B) Cross section and C) growth history of modern microatoll SMS10-A2, showing essentially stable relative sea level for the past 55 years (symbology as in Fig. 2.S5).

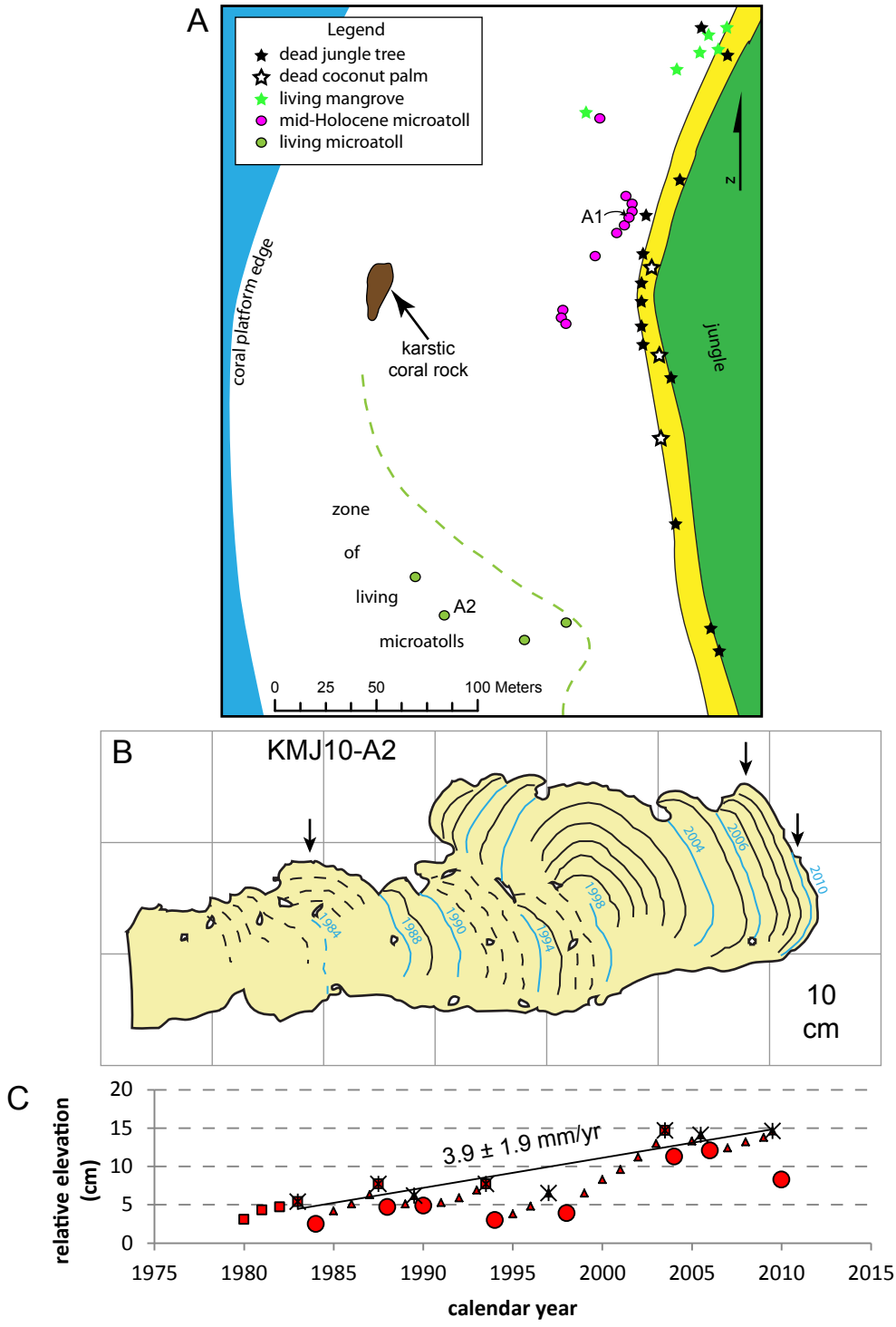

Figure 2.S18. Data from Pulau Karangmadjat, a small island in the archipelago south of Siberut. A) Map of the site on the northwest side of Pulau Karangmadjat. A population of "fossil" microatolls dates to the mid-Holocene (date from KMJ10-A1 discussed in Chapter 3). B) Cross section and C) growth history of the living microatoll KMJ10-A2, which records a moderate rate of interseismic subsidence. Symbology as in Fig. 2.S5.

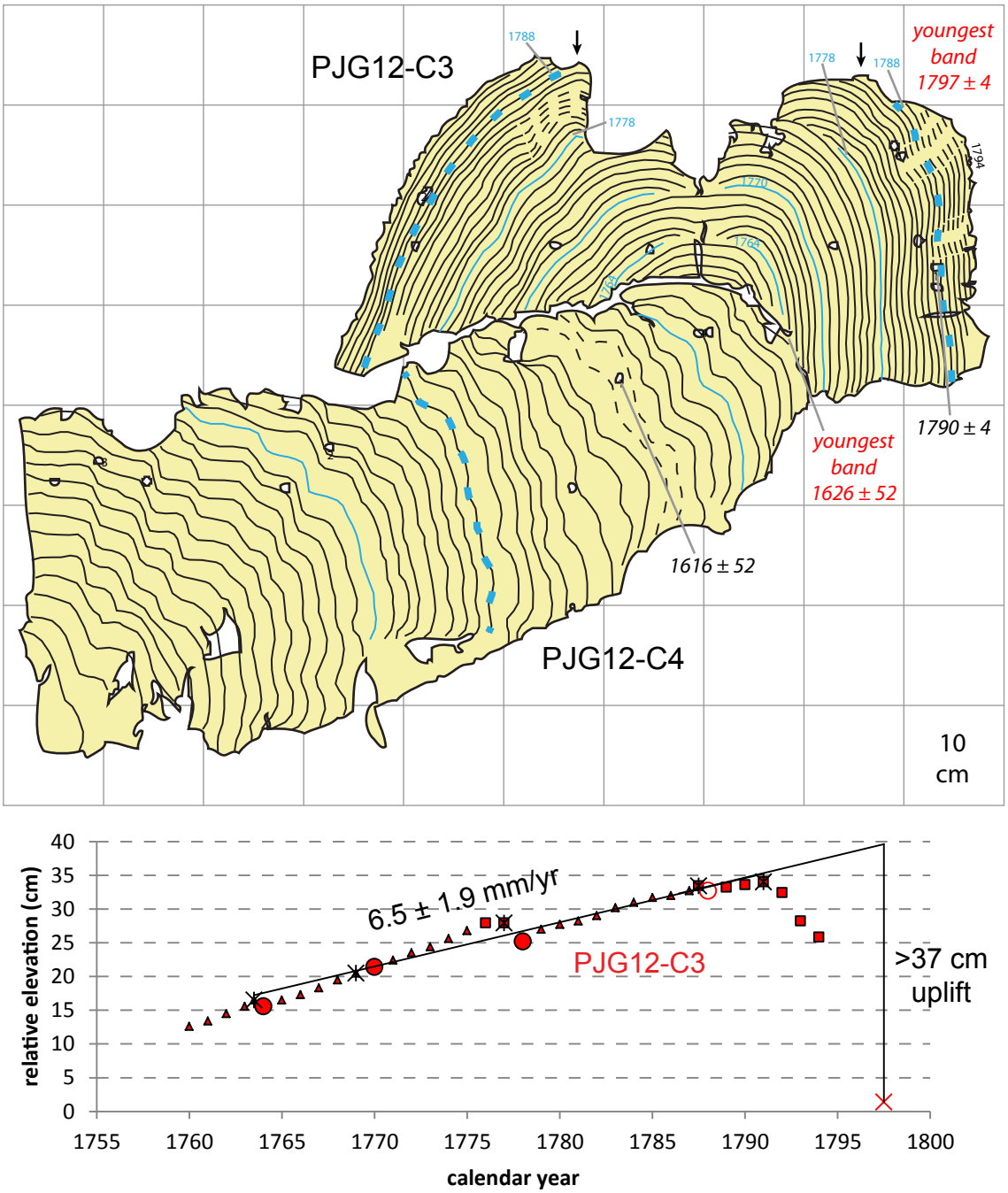

Figure 2.S19. Fossil microatolls from Pulau Panjang, an island north of Sipora (symbology as in Fig. 2.S5). A) At site PJG-C, a large population of fossil Favid microatolls sits at a higher elevation than a population of *Porites* microatolls. This cross section shows a Favid of the higher population (C3) which actually grew on the rim of a *Porites* of the lower population (C4). C4 died in the 17th century (uplifted during an earlier megathrust rupture sequence), and C3 began growing about 1760 after interseismic subsidence had lowered the dead C4 below HLS once more. C3 was uplifted and died during the 1797 earthquake. B) Growth history of C3.

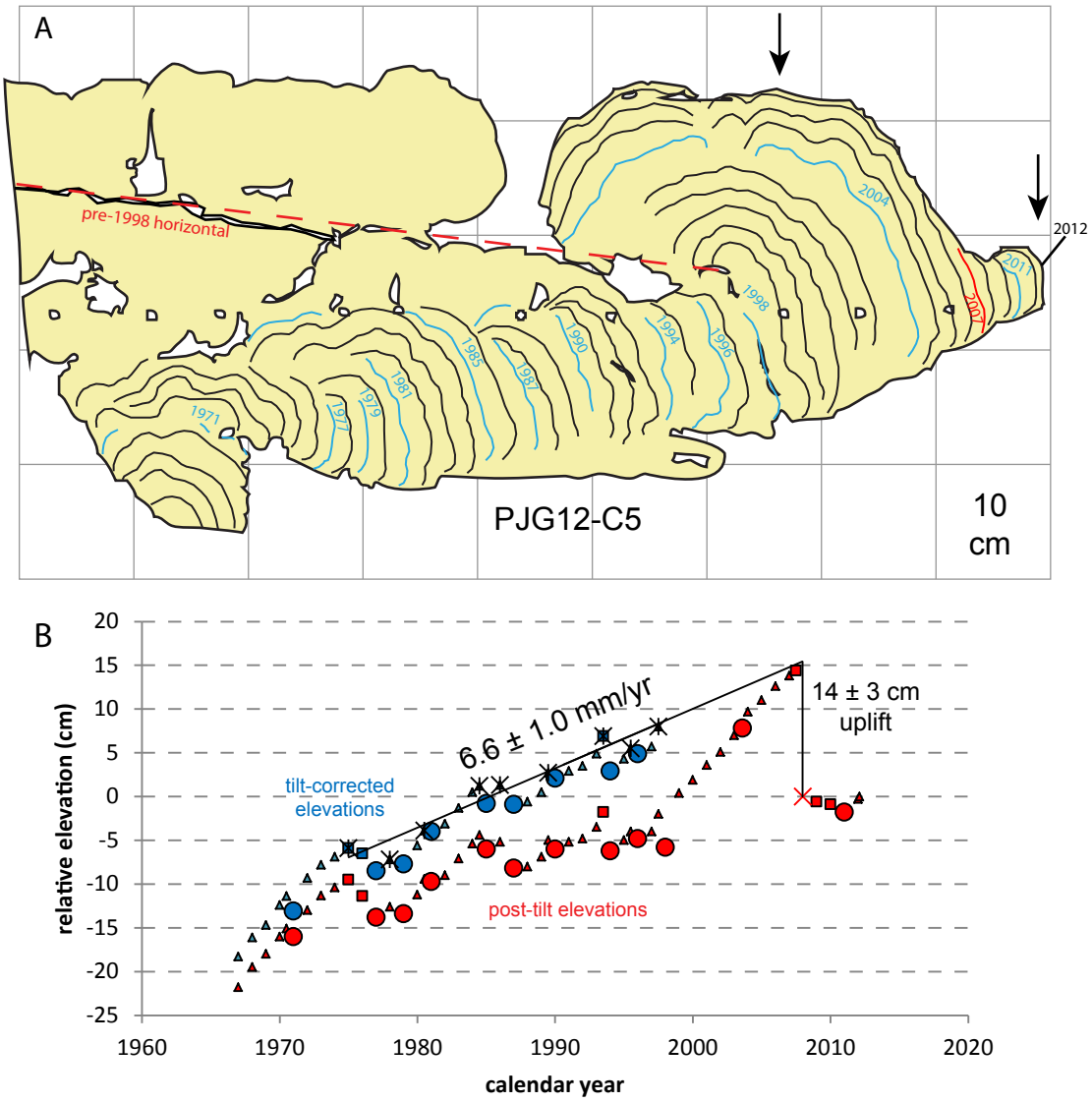

Figure 2.S20. Modern coral data from Pulau Panjang (symbology as in Fig. 2.S5). A) Cross section of the living microatoll PJG12-C5. About 14 cm of uplift occurred during the 2007 M_w 7.9 earthquake, which uplifted an area on northern Sipora disconnected from the more extensive uplift on South Pagai during the M_w 8.4 earthquake 12 hours earlier [*Konca et al.* 2008]. The PPNJ cGPS station less than 2 km south recorded 23 cm uplift, suggesting that the uplift dropped off extremely steeply. This and several other modern microatolls at the site record about 2 cm of postseismic uplift since 2007, which is consistent with the PPNJ record. As indicated by a preserved formerly horizontal surface, this microatoll clearly tilted sometime after 1998, lowering this side so that growth did not catch up to HLS again until 2004. B) Growth history of PJG12-C5. Correcting the pre-1998 record for the tilt yields an accurate interseismic subsidence rate. As the annual bands are far clearer and the tracking of HLS is more certain on this sample than on Pj03-A1 [*Natawidjaja et al.* 2007], we use this record alone to calculate the modern interseismic subsidence rate on Pulau Panjang.

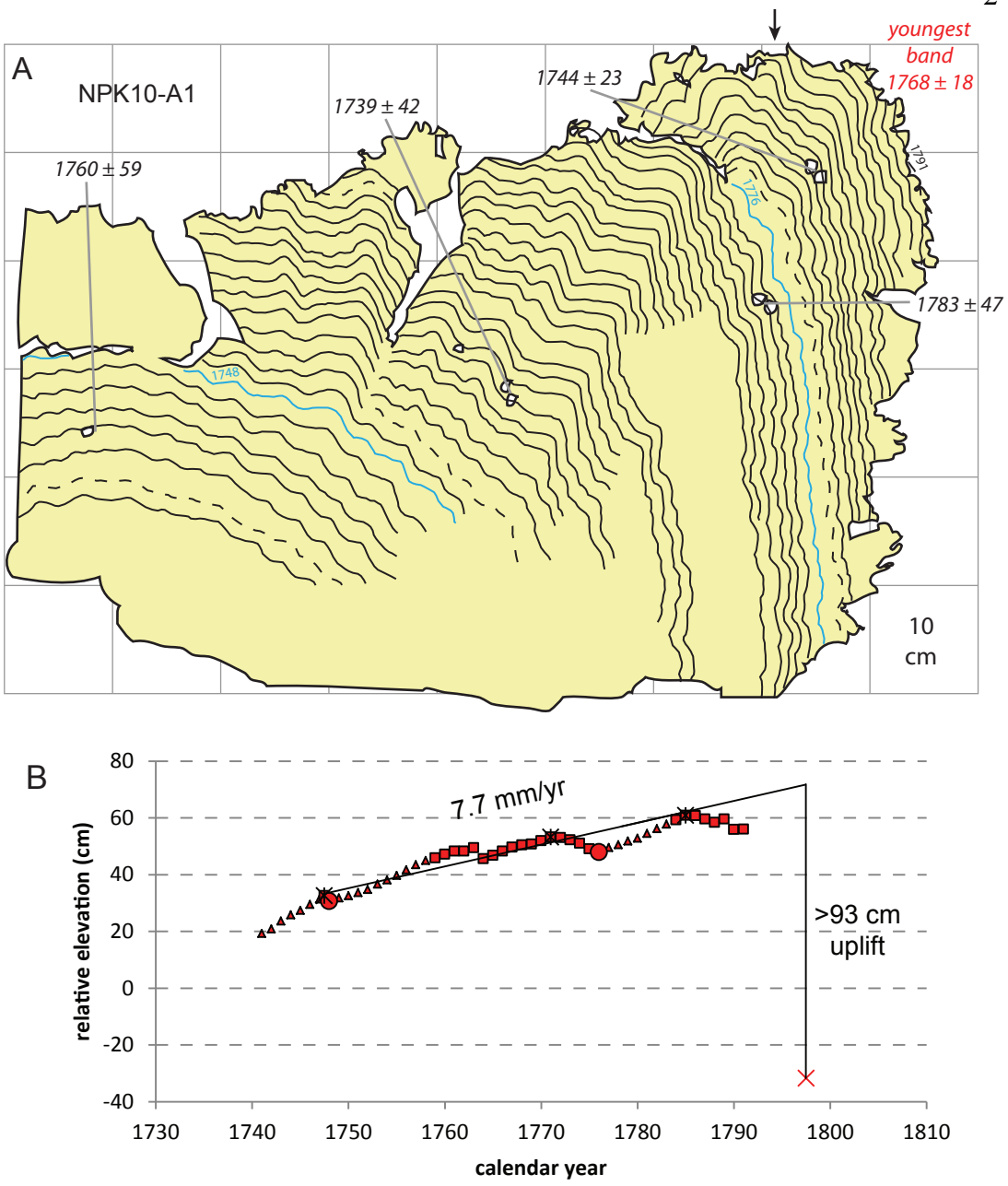

Figure 2.S21. Data from North Pukarayat, on the south coast of Sipora (symbology as in Fig. 2.S5). A) Cross section of a large microatoll which was part of a population with similar morphology. A weighted average of four U-Th dates suggests that the head died in the mid-1700s. Our coral dataset does not support the occurrence of a large tectonic uplift in that period (at many sites, the possibility is specifically excluded.) We infer that this population of corals probably died due to uplift in 1797 (which is inconsistent with only one of the four U-Th dates). Matching the large die-down preserved in this record with the robust regional 1776 die-down requires 6 bands to be eroded from the outer surface. B) Growth history of NPK10-A1. Regardless of precisely when the coral died, it records a high interseismic subsidence rate during the 1700s.

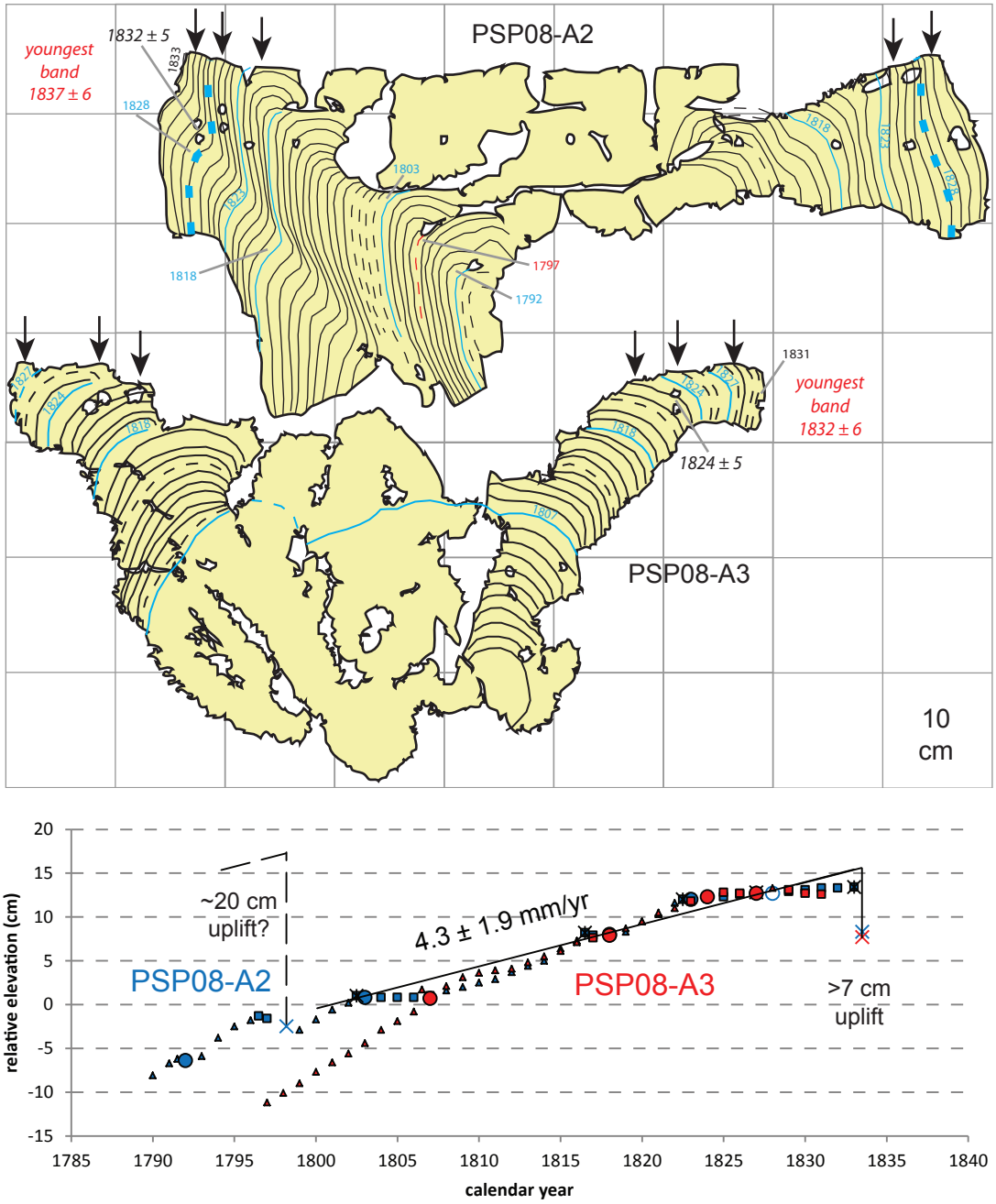

Figure 2.S22. Data from Pasapuat on the north coast of North Pagai (symbology as in Fig. 2.S5). A) Cross sections of *Goniastrea* (A2) and Favid (A3) microatolls which clearly died due to uplift in 1833. A2 also had a small die-down at the time of the 1797 earthquake. However, since other sites in the region suggest that uplift in 1797 was tens of centimeters in this area, we infer that A2 had not actually hit HLS before the 1797 earthquake. The 1792 die-down is so minor that it is quite plausible that it represents a growth irregularity rather than a sea-level-controlled die-down. B) Growth histories of the two microatolls are highly consistent. We derive the interseismic rate from A2 since its record is slightly longer, but we exclude the points before 1797.

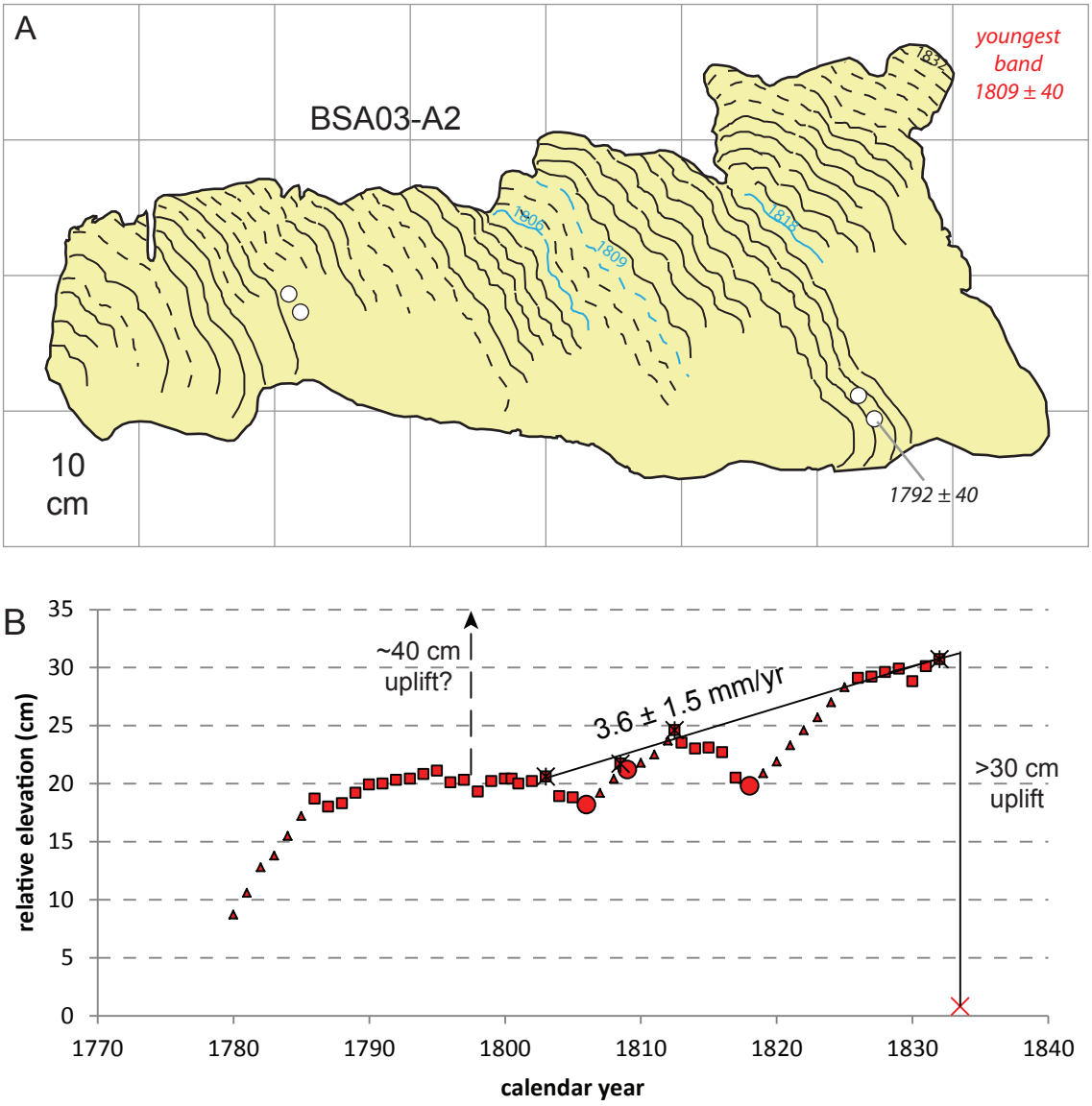

Figure 2.S23. A) Cross section of a microatoll from Basua on the north coast of South Pagai (symbology as in Fig. 2.S5A). This slab was collected in 2003 but not included in previous papers due to the high uncertainty of its date of death, which encompasses both 1797 and 1833. We infer that this microatoll died in 1833, as this interpretation matches its large die-down with the robust regional 1818 die-down. B) Growth history of BSA03-A2 (symbology as in Fig. 2.S5B). Nearby sites uplifted ~40 cm in 1797, but this coral would not yet have reached HLS before the earthquake, so it recorded a smaller die-down (the inner hemisphere has since been significantly eroded).

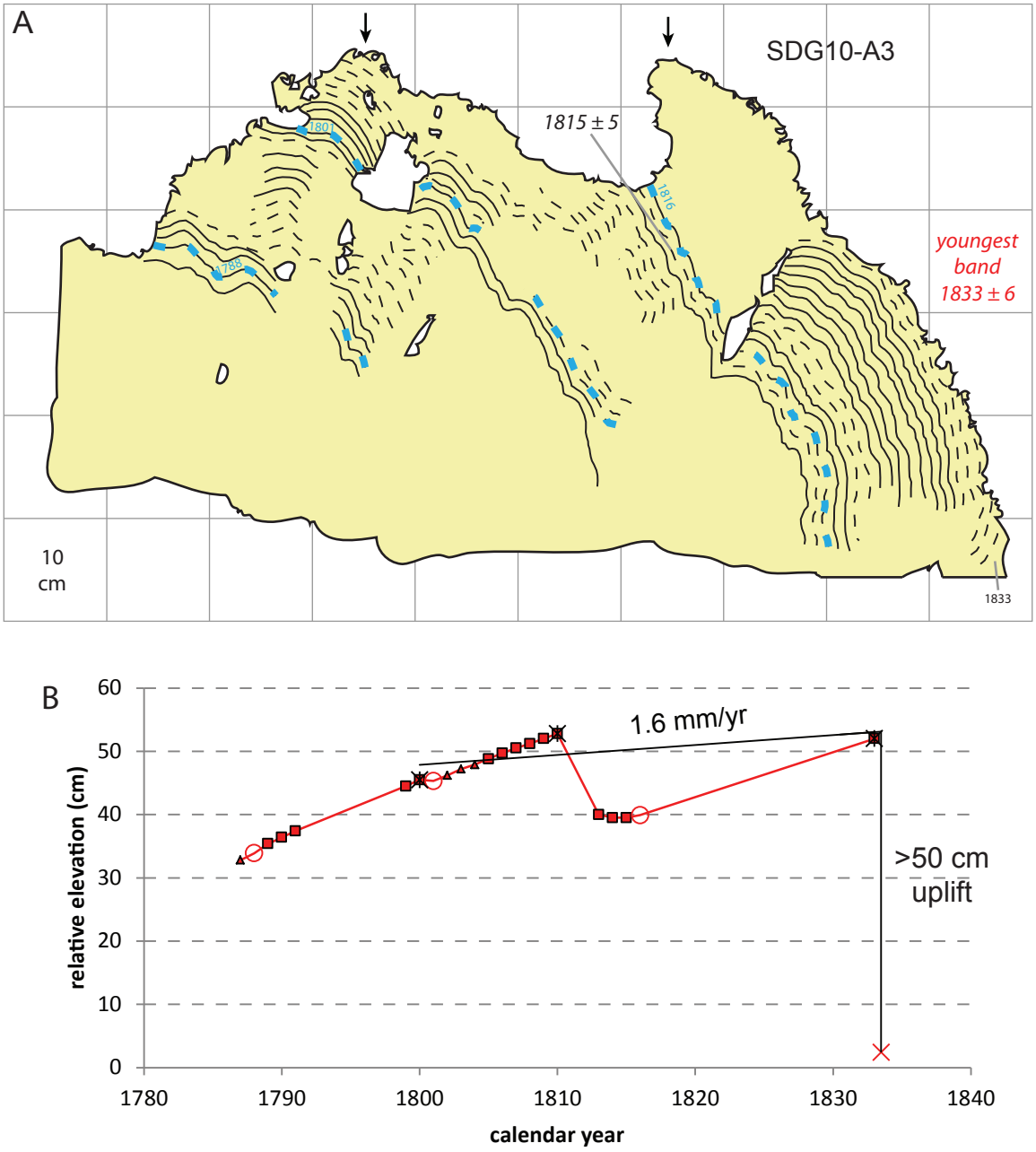

Figure 2.S24. Data from a site on the south side of Sanding Island (symbology as in Fig. 2.S5). A) Cross section of a microatoll with a precise date demonstrating the final uplift and death was in 1833. However, the annual bands are extremely unclear and are largely inferred based on an average growth rate. B) Growth history of SDG10-A3 suggests a low rate of interseismic subsidence. It is clear that there was no significant uplift in 1797. The unimpeded upward growth between the 1788 and 1801 die-downs suggests that the subsidence rate may have been higher before the 1797 earthquake, but this is an uncertain result.

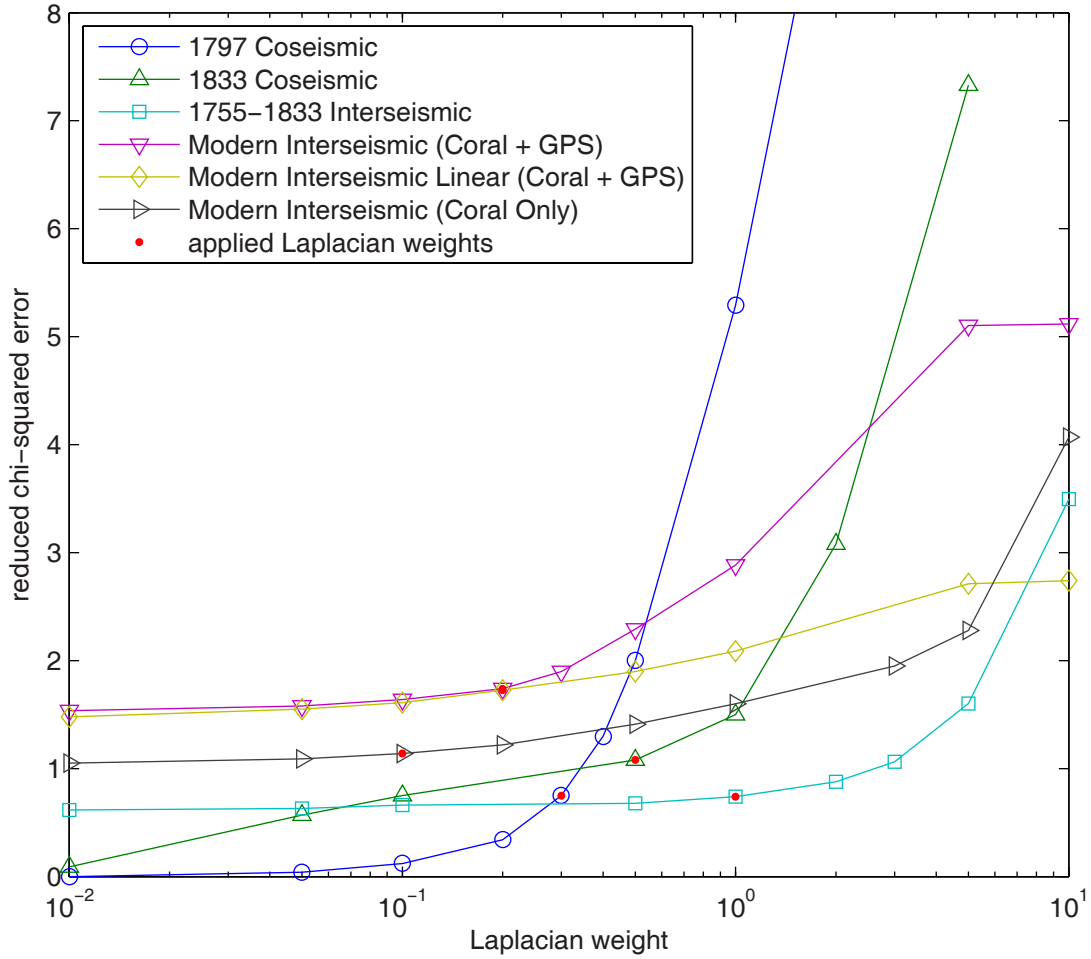

Figure 2.S25. Reduced chi-squared error as a function of the strength of spatial smoothing (overall weight of the Laplacian regularization term). For our final models we applied the weights marked by red dots, which correspond to the strongest smoothing that produces a good fit to the data. These points are generally found near the point of maximum curvature of each curve, in the vicinity of chi-squared values of 1. Note that the misfits of some of the interseismic models level off at high smoothing values, because the fault slip becomes essentially homogeneous.

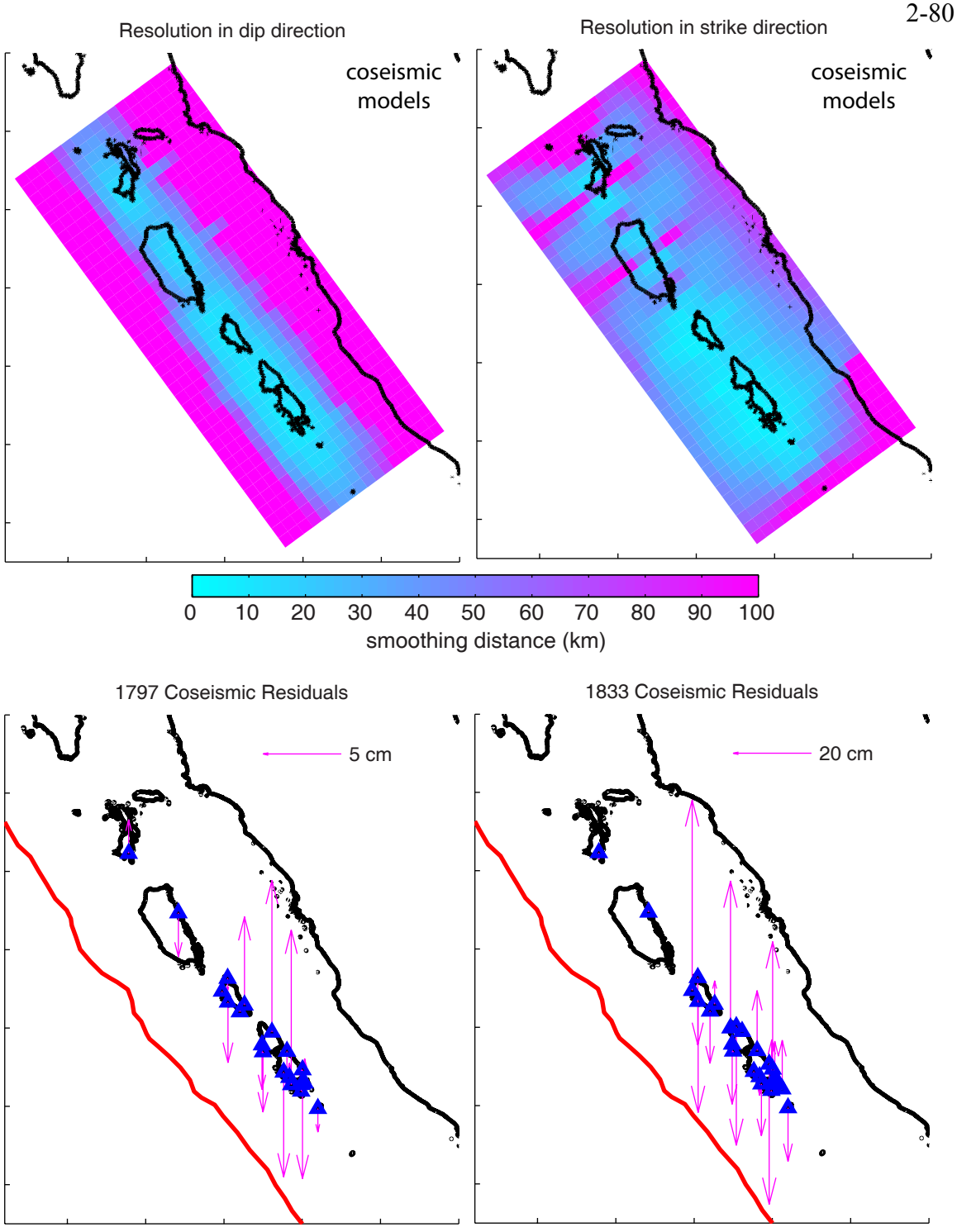

Figure 2.S26. Resolution of the fault plane (in terms of smoothing distance) and residuals for the coseismic models. As we would expect, the shallow and deep parts of the megathrust are very poorly resolved. The fit to the 1797 uplift data is very good, within the data uncertainty virtually everywhere. The residuals for 1833 are much larger, but the fit is still acceptable since the uncertainties for 1833 uplift data are much larger than for 1797 (uncertainties are listed in Table 2.2).

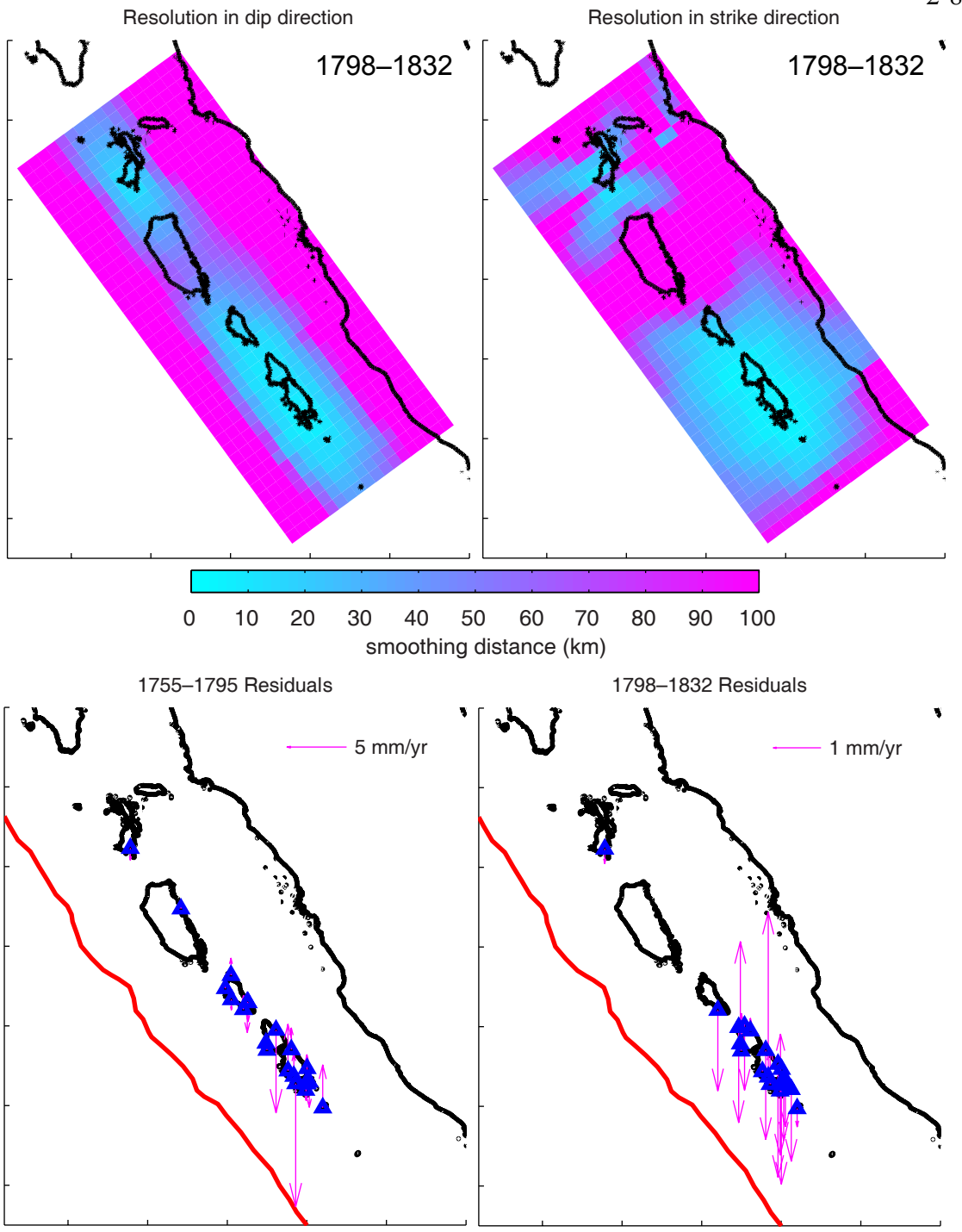

Figure 2.S27. Resolution during the 1798–1832 period and residuals for the pre- and post-1797 interseismic models. Resolution for the 1755–1795 period is virtually indistinguishable from the distribution for the coseismic models in Fig. 2.S26, so we do not show it separately. However, for the 1798–1832 period the Siberut region is very poorly resolved. The fits to the data for both models are quite good, as uncertainties of 1–2 mm/yr are typical. The two sites with large residuals in the 1755–1795 model have only a few data points within that time period, so it is not surprising that they are anomalous.

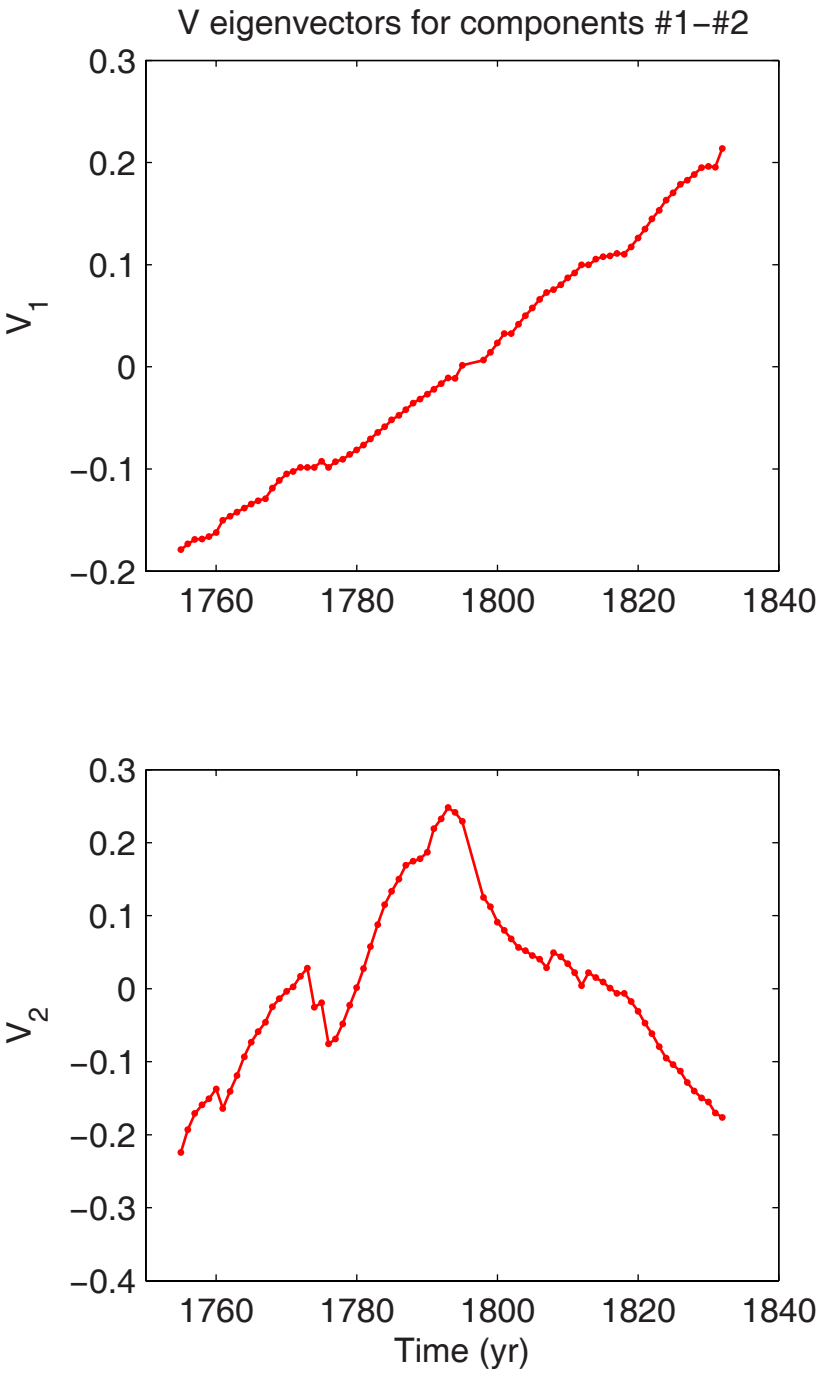

Figure 2.S28A. Time functions for a two-component decomposition of the complete 1755–1832 time period, showing the abrupt change in the second component at the time of the 1797 earthquake. Ultimately, we did not use this model because the decomposition was unstable.

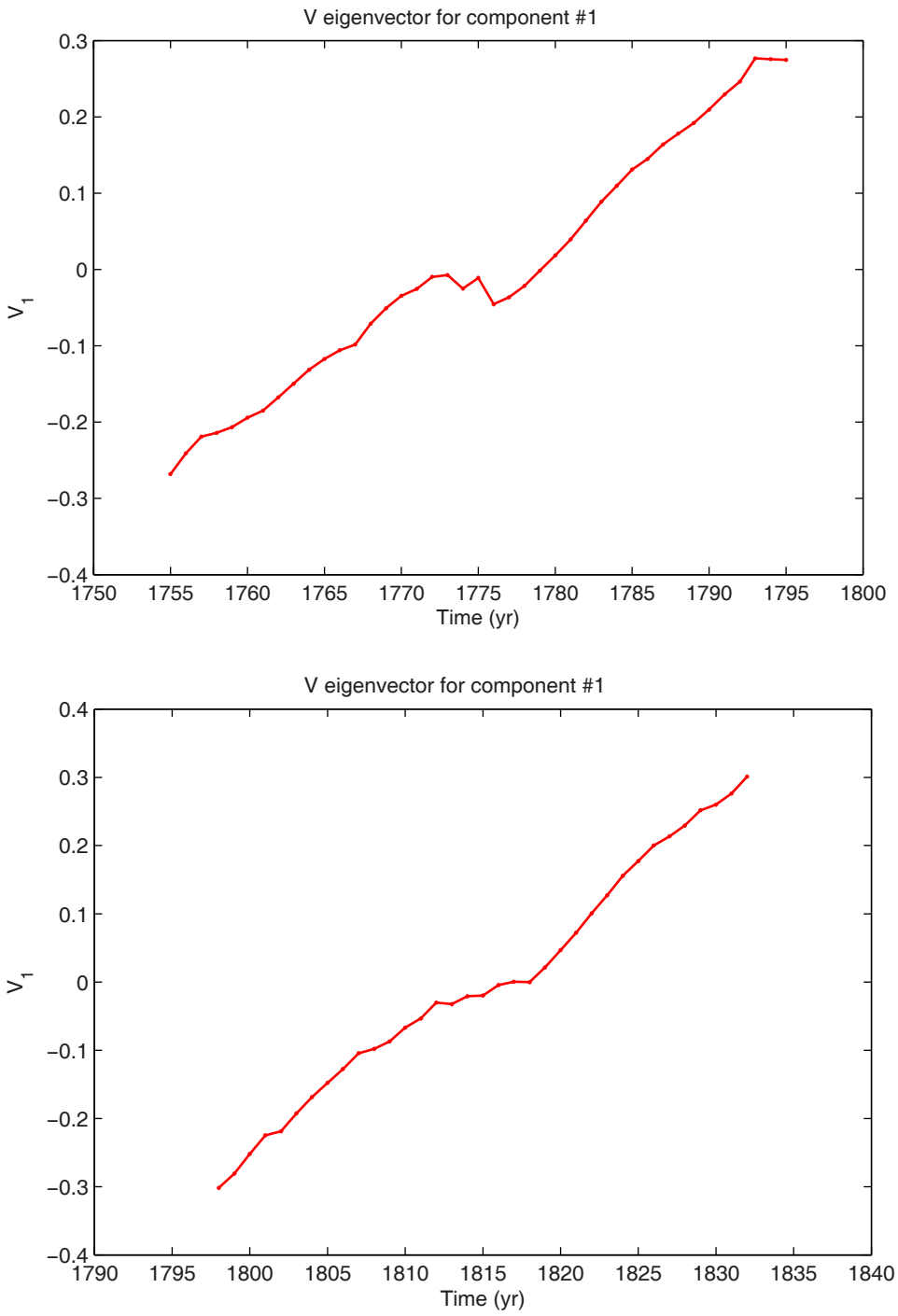

Figure 2.S28B. Normalized time functions for the 1755–1795 and 1798–1832 interseismic models. Both are close to linear. The deviations midway through each time period are expressions of the two largest and most widespread oceanographic die-downs (in 1776 and 1818). There is no evidence of a significant tectonic deviation from a linear function.

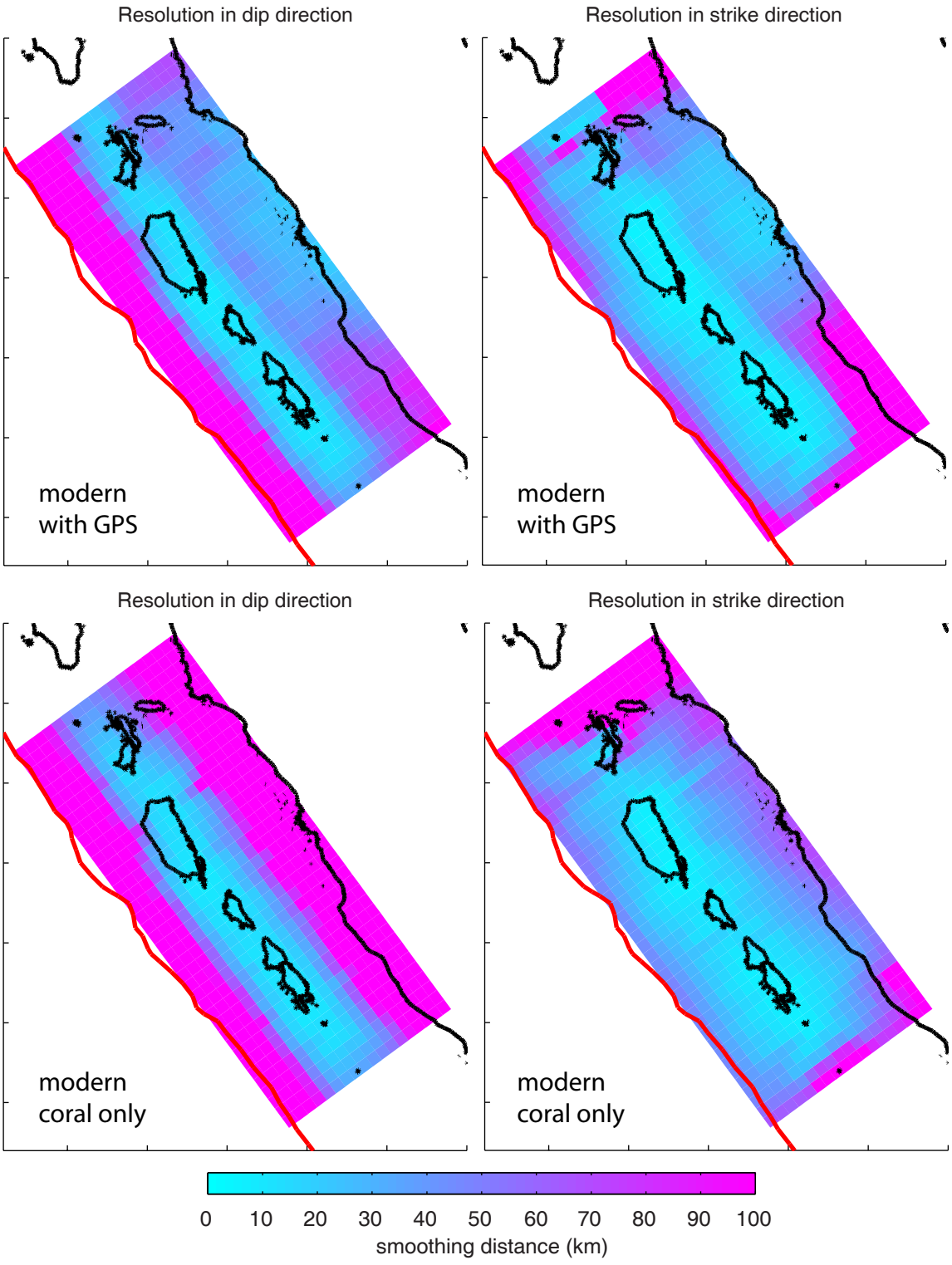

Figure 2.S29. Resolution maps for the 1950–1997 period.

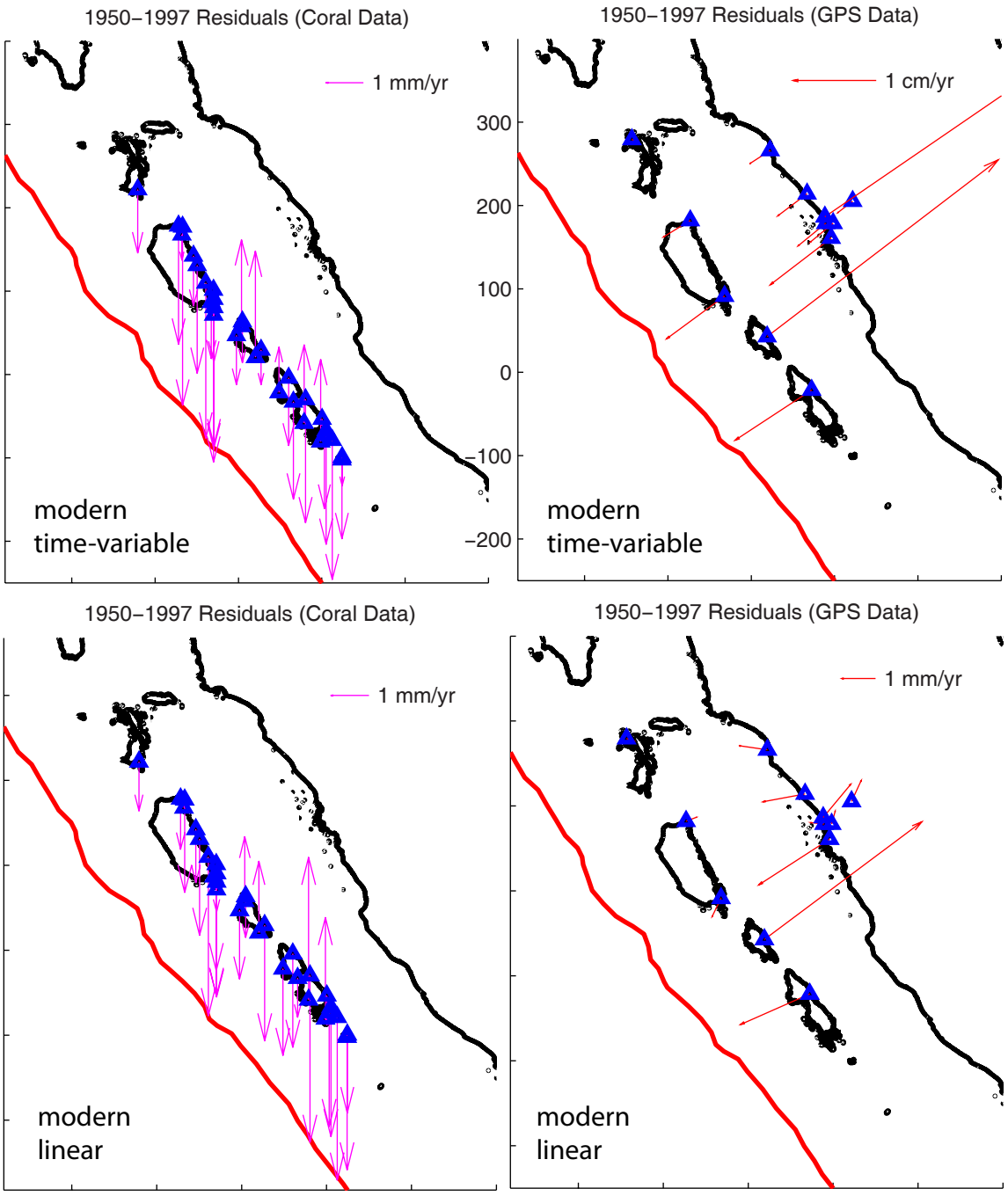

Figure 2.S30. Residuals for the combined coral + GPS models covering 1950–1997. For the time-variable model, the fit to the coral data is fair but the fit to the GPS data is poor, because the GPS measurement interval happens to coincide with a deviation in the time function that is largely or entirely a reflection of oceanographic processes. The two stations with ~4 cm/yr residuals have only one year of measurement in the modeled time interval (first occupied in 1996), so the fit is even more sensitive to short-term fluctuations. The linear model provides a vastly improved fit to the GPS data and is only slightly worse at fitting the long-term trends in the coral data.

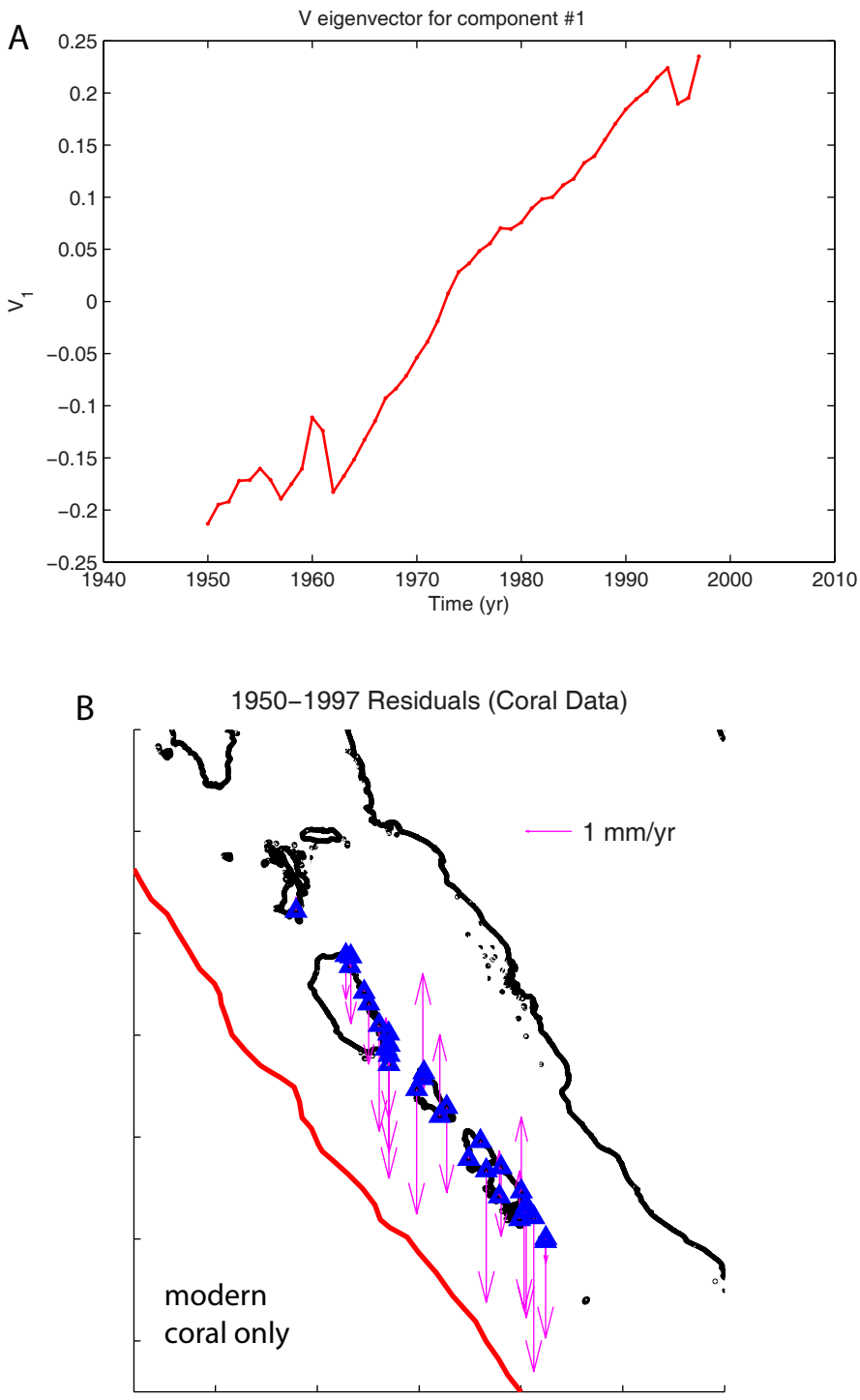

Figure 2.S31. A) Time function for modern coral data, which is quite close to linear. The major deviations are expressions of the widespread, large oceanographic die-downs in 1957, 1962, and 1995. The 1995 die-down interferes with properly fitting the GPS data. B) Residuals for the model using only the modern coral data, which are smaller than for any of the models including GPS data.

Table 2.S1 Uranium and thorium isotopic compositions and ^{230}Th ages of coral subsamples by MC-ICPMS with dates A.D.

Subsample	Weight g	^{238}U ppb	^{232}Th ppt	δ^{234}U measured[a]	[^{230}Th/^{238}U] activity[c]	[^{230}Th/^{232}Th] ppm[d]	Age uncorrected	Age corrected [c,e]	$\delta^{234}U_{initial}$ corrected[b]	$^{230}Th/^{232}Th_{initial}$ ppm[f]	Calendar Year A.D.[h]
PJG12-C3-1	0.0776	1776.7 ± 1.6	129.8 ± 9.0	146.6 ± 1.6	0.002357 ± 0.000026	533 ± 37	224.7 ± 2.5	221.9 ± 3.7	146.7 ± 1.6		1790 ± 4
PJG12-C4-1	0.0672	1711.0 ± 1.3	2345 ± 11	144.9 ± 1.7	0.004684 ± 0.000056	56.43 ± 0.73	447.6 ± 5.4	396 ± 52	145.0 ± 1.7		1616 ± 52
NPK10-A1-1-1		2191 ± 6	3816 ± 14	148.6 ± 3.1	0.00285 ± 0.00007	27 ± 1	271 ± 6				
NPK10-A1-1-2	M10	2207 ± 2	5087 ± 12	147.0 ± 1.6	0.0028 ± 0.0001	20 ± 1	271 ± 7				
NPK10-A1-1-3	M11	2184 ± 2	3647 ± 11	146.6 ± 1.5	0.00285 ± 0.00007	28 ± 1	272 ± 7				
NPK10-A1-1-4	M12	2233 ± 4	3649 ± 10	146.4 ± 2.5	0.0028 ± 0.0001	28 ± 1	269 ± 6	267 ± 23	146.0 ± 6	0.3 ± 2.1	1744 ± 23
NPK10-A1-2	0.06665	2033.9 ± 5.2	2250 ± 15	149.1 ± 3.6	0.003299 ± 0.000089	49.2 ± 1.4	313.9 ± 8.5	273 ± 42	149.2 ± 3.6		1739 ± 42
NPK10-A1-3	0.0671	1447.2 ± 1.3	2274 ± 11	149.5 ± 1.6	0.003263 ± 0.000060	34.28 ± 0.65	310.4 ± 5.7	252 ± 59	149.7 ± 1.6		1760 ± 59
NPK10-A1-4	0.06721	2255.4 ± 2.3	2811 ± 12	145.6 ± 1.6	0.002902 ± 0.000038	38.44 ± 0.53	276.9 ± 3.7	230 ± 47	145.7 ± 1.6		1783 ± 47
TRT10-A1-1	0.1057	2351 ± 6	6636 ± 23.8	147.6 ± 2.9	0.0034 ± 0.0001	20 ± 0.5	320 ± 7.6	214 ± 106	147.7 ± 2.9		1796 ± 106
TRT10-A1-2	0.08588	2258.9 ± 4.1	10587 ± 27	144.9 ± 2.4	0.00441 ± 0.00010	15.53 ± 0.35	421 ± 10				
TRT10-A1-2	0.08284	2301.7 ± 3.3	8673 ± 21	147.0 ± 2.1	0.00398 ± 0.00011	17.43 ± 0.46	379 ± 10				
TRT10-A1-2	0.08960	2333.5 ± 1.8	7458 ± 35	145.1 ± 1.6	0.003811 ± 0.000079	19.69 ± 0.42	364.0 ± 7.6				
TRT10-A1-2	0.12819	2303.8 ± 2.1	7816 ± 20	145.3 ± 1.5	0.003754 ± 0.000075	18.27 ± 0.37	358.5 ± 7.2	224 ± 62	145.0 ± 15	7.2 ± 2.9	1788 ± 62
TRT10-A1-4	0.0580	2172.4 ± 1.8	3106 ± 13	146.1 ± 1.8	0.003062 ± 0.000050	35.36 ± 0.60	292.1 ± 4.8	238 ± 54	146.2 ± 1.8		1774 ± 54
SKC08-D1	0.1718	2239 ± 2	72 ± 4.1	146.1 ± 2.1	0.0023 ± 0.0000	1177 ± 68.5	219 ± 3.3	218 ± 3	146.2 ± 2.1		1790 ± 3
NNP10-A1-1-1		2460 ± 9	5275 ± 22	147.0 ± 4.4	0.00308 ± 0.00008	24 ± 1	293 ± 7				
NNP10-A1-1-2	M4	2359 ± 4	4380 ± 13	149.0 ± 2.4	0.0029 ± 0.0001	26 ± 1	274 ± 6				
NNP10-A1-1-3	M5	2452 ± 4	5712 ± 15	146.6 ± 2.4	0.00314 ± 0.00007	22 ± 0	299 ± 7				
NNP10-A1-1-4	M6	2420 ± 5	4517 ± 14	149.4 ± 2.6	0.0029 ± 0.0001	26 ± 1	274 ± 6	172 ± 32	160.0 ± 13	9.4 ± 2.7	1839 ± 32
NNP10-A2-1-1		2367 ± 3	3965 ± 16	145.0 ± 1.6	0.00282 ± 0.00007	28 ± 1	269 ± 7				
NNP10-A2-1-2	M7	2240 ± 2	5270 ± 13	143.2 ± 1.7	0.00303 ± 0.00007	21 ± 1	290 ± 7				
NNP10-A2-1-3	M8	2272 ± 2	6062 ± 14	144.8 ± 1.6	0.0032 ± 0.0001	20 ± 0	307 ± 8				
NNP10-A2-1-4	M9	2136 ± 2	5406 ± 13	145.9 ± 1.9	0.00312 ± 0.00008	20 ± 1	298 ± 8	208 ± 21	145.0 ± 6	6.2 ± 3.0	1803 ± 21
NNP10-A3-1	0.1384	2133 ± 5	1765 ± 7.1	145.5 ± 2.4	0.0023 ± 0.0001	46 ± 1.1	220 ± 5.0	189 ± 31	145.6 ± 2.4		1821 ± 31
PSP08-A2-2	0.1125	2020 ± 2	60 ± 6.2	147.6 ± 1.5	0.0019 ± 0.0001	1036 ± 110.1	178 ± 5.0	177 ± 5	147.7 ± 1.5		1832 ± 5
PSP08-A3-2	0.1104	2180 ± 2	30 ± 6.3	148.9 ± 1.6	0.0019 ± 0.0000	2370 ± 508.6	185 ± 4.8	185 ± 5	149.0 ± 1.6		1824 ± 5
SSB10-A3-1	0.0978	2447 ± 3	516 ± 7.2	142.7 ± 1.9	0.0027 ± 0.0000	211 ± 4.9	258 ± 4.8	250 ± 9	142.8 ± 1.9		1760 ± 9
SSB10-A3-2	0.09639	2531.7 ± 2.0	1351.1 ± 7.4	146.9 ± 1.3	0.003080 ± 0.000031	95.3 ± 1.1	293.6 ± 2.9	274 ± 20	147.0 ± 1.3		1738 ± 20
BTM10-A1-1	0.1017	2199 ± 4	505 ± 7.5	146.4 ± 2.0	0.0025 ± 0.0001	177 ± 5.8	235 ± 6.9	226 ± 11	146.5 ± 2.0		1784 ± 11
BTM10-A2-1	0.114	2008 ± 4	874 ± 6.6	147.1 ± 2.3	0.0022 ± 0.0001	82 ± 2.3	205 ± 5.6	189 ± 17	147.2 ± 2.3		1821 ± 17
CMP08-A2-2	0.12412	2706.2 ± 3.8	48721 ± 310	145.8 ± 2.2	0.00515 ± 0.00027	4.72 ± 0.25	492 ± 26				
CMP08-A2-2	0.10651	2827.1 ± 3.0	33997 ± 167	144.3 ± 1.7	0.00446 ± 0.00022	6.13 ± 0.30	427 ± 21				
CMP08-A2-2	0.05934	2656.1 ± 1.9	23073 ± 89	146.3 ± 1.5	0.00391 ± 0.00018	7.44 ± 0.34	373 ± 17				
CMP08-A2-2	0.14231	2745.6 ± 2.2	25967 ± 115	146.1 ± 1.7	0.00435 ± 0.00015	7.59 ± 0.27	415 ± 14	294 ± 77	149.2 ± 8.1	1.8 ± 1.2	1718 ± 77
CMP08-A2-3	0.0964	2348 ± 5	4951 ± 12.0	148.6 ± 2.2	0.0038 ± 0.0001	29 ± 0.7	357 ± 9.1	279 ± 79	148.7 ± 2.2		1730 ± 79
CMP08-A2-4	0.08463	2462.2 ± 6.7	4005 ± 22	140.9 ± 3.6	0.003877 ± 0.000085	39.35 ± 0.88	371.7 ± 8.2	310 ± 62	141.1 ± 3.6		1702 ± 62
BSA03A2-1b	0.3515	2371 ± 3	2490 ± 8	148.5 ± 1.4	0.00264 ± 0.00003	41.5 ± 0.5	251 ± 3	212 ± 40	148.6 ± 1.4		1792 ± 40

Table 2.S1 (continued)

Subsample	Weight g	^{238}U ppb	^{232}Th ppt	δ^{234}U measured[a]	[^{230}Th/^{238}U] activity[c]	[^{230}Th/^{232}Th] ppm[d]	Age uncorrected	Age corrected [c,e]	$\delta^{234}U_{initial}$ corrected[b]	^{230}Th/$^{232}Th_{initial}$ ppm[f]	Calendar Year A.D.[h]
SMG02-A2-1b	0.08052	2131.8 ± 2.2	7129 ± 20	145.5 ± 1.8	0.003856 ± 0.000087	19.04 ± 0.43	368.2 ± 8.3				
SMG02-A2-1b	0.09799	2239.7 ± 2.7	6242 ± 16	145.0 ± 1.8	0.003729 ± 0.000079	22.09 ± 0.47	356.2 ± 7.6				
SMG02-A2-1b	0.05976	2358.6 ± 2.8	7737 ± 23	144.0 ± 1.9	0.003868 ± 0.000080	19.47 ± 0.40	369.8 ± 7.7				
SMG02-A2-1b	0.11169	2107.5 ± 2.9	5342 ± 18	144.0 ± 2.1	0.003503 ± 0.000088	22.82 ± 0.58	334.9 ± 8.5	242 ± 35	142.2 ± 8.4	6.7 ± 2.1	1770 ± 35
PCB08-A1	0.1061	1961 ± 1	57 ± 6.6	149.3 ± 1.3	0.0019 ± 0.0001	1082 ± 129.2	180 ± 5.2	179 ± 5	149.4 ± 1.3		1832 ± 5
PCB08-A2-1	0.0937	2463 ± 2	462 ± 7.4	145.0 ± 1.3	0.0020 ± 0.0000	172 ± 5.2	187 ± 4.8	180 ± 9	145.0 ± 1.3		1828 ± 9
PCB08-B2-1	0.0985	2320 ± 2	414 ± 7.1	145.6 ± 1.6	0.0021 ± 0.0001	191 ± 5.7	197 ± 4.8	190 ± 8	145.7 ± 1.6		1818 ± 8
STG08-A1-1-1	0.1027	2439 ± 2	31238 ± 114.0	144.5 ± 1.5	0.0046 ± 0.0002	6 ± 0.2	444 ± 18.2		144.6 ± 1.5		
STG08-A1-1-2	0.1007	2452 ± 2	1797 ± 7.3	145.8 ± 1.6	0.0023 ± 0.0001	53 ± 1.2	224 ± 5.1		145.9 ± 1.6		
STG08-A1-1-3	0.098	2264 ± 2	2543 ± 7.8	148.3 ± 1.5	0.0024 ± 0.0001	35 ± 0.9	228 ± 5.9	205 ± 11	148.4 ± 1.5	3.2 ± 0.8	
STG08-A1-1-4	0.0947	2356 ± 2	1371 ± 7.8	146.3 ± 1.5	0.0022 ± 0.0001	62 ± 1.6	208 ± 5.3	205 ± 29[g]	146.4 ± 1.5	3.2 ± 2.1[g]	1803 ± 29[g]
STG08-A1-2	0.1227	2020.8 ± 1.6	1408.2 ± 5.9	145.4 ± 1.4	0.002972 ± 0.000028	70.43 ± 0.72	283.7 ± 2.7	258 ± 26	145.5 ± 1.4		1754 ± 26
STG08-A2	0.1940	2016 ± 2	32 ± 3.6	147.6 ± 1.9	0.0023 ± 0.0000	2449 ± 280.8	222 ± 3.8	221 ± 4	147.7 ± 1.9		1787 ± 4
SGK10-A2-1	0.1115	2417 ± 4	31 ± 6.2	147.7 ± 1.9	0.0019 ± 0.0000	2397 ± 487.5	177 ± 4.5	177 ± 4	147.7 ± 1.9		1833 ± 4
SDG10-A3-1	0.1208	2477 ± 8	88 ± 5.8	148.9 ± 4.1	0.0021 ± 0.0000	956 ± 66.5	196 ± 4.7	195 ± 5	149.0 ± 4.1		1815 ± 5

Analytical errors are 2σ of the mean. Alternating gray and white shading groups analyses of single annual band samples.

[a] $\delta^{234}U = ([^{234}U/^{238}U]_{activity} - 1) \times 1000$.

[b] $\delta^{234}U_{initial}$ corrected was calculated based on ^{230}Th age (T), i.e., $\delta^{234}U_{initial} = \delta^{234}U_{measured} \, X \, e^{\lambda_{234} * T}$, and T is corrected age.

[c] $[^{230}Th/^{238}U]_{activity} = 1 - e^{-\lambda_{230} T} + (\delta^{234}U_{measured}/1000)[\lambda_{230}/(\lambda_{230} - \lambda_{234})](1 - e^{-(\lambda_{230} - \lambda_{234}) T})$, where T is the age.

Decay constants are 9.1577 x 10^{-6} yr^{-1} for ^{230}Th, 2.8263 x 10^{-6} yr^{-1} for ^{234}U [*Cheng et al.*, 2000], and 1.55125 x 10^{-10} yr^{-1} for ^{238}U [*Jaffey et al.*, 1971] .

[d] The degree of detrital ^{230}Th contamination is indicated by the [^{230}Th/^{232}Th] atomic ratio instead of the activity ratio.

[e] Age corrections were calculated using an estimated atomic ^{230}Th/^{232}Th ratio of 6.5 ± 6.5 ppm [*Zachariasen et al.*, 1999].

[f] For certain samples, more precise ages, $\delta^{234}U_{initial}$, and ^{230}Th/$^{232}Th_{initial}$ values were derived from isochron techniques using an Excel macro, *Isoplot* 3.00 [*Ludwig and Titterington*, 1994; *Ludwig*, 2003].

[g] For isochron regressions with a p-value < 0.05, we increase the uncertainty of both the ^{230}Th/$^{232}Th_{initial}$ and the age by a factor of the square root of the mean square of weighted deviates (MSWD), as suggested by *Ludwig* [2003].

[h] Calculated by subtracting the corrected sample age from the year of chemical analysis.

References

Cheng, H., R. L. Edwards, J. Hoff, C. D. Gallup, D. A. Richards, and Y. Asmerom (2000), The half-lives of uranium-234 and thorium-230, *Chemical Geology*, *169*, 17-33.

Jaffey, A. H., K. F. Flynn, L. E. Glendenin, W. C. Bentley, and A. M. Essling (1971), Precision measurements of half-lives and specific activities of ^{235}U and ^{238}U, *Physical Review C*, *4*, 1889-1906.

Ludwig, K. R. (2003), Mathematical–statistical treatment of data and errors for ^{230}Th/U geochronology, *Reviews in Mineralogy and Geochemistry*, *52* (1), 631-656.

Ludwig, K. R., and D. M. Titterington (1994), Calculation of ^{230}Th/U isochrons, ages, and errors, *Geochim. Cosmochim. Acta*, *58* (22), 5031-5042.

Zachariasen, J., K. Sieh, F. W. Taylor, R. L. Edwards, and W. S. Hantoro (1999), Submergence and uplift associated with the giant 1833 Sumatran subduction earthquake: Evidence from coral microatolls, *J. Geophys. Res.*, *104* (B1), 895-919.

CHAPTER 3

AN ANCIENT SHALLOW SLIP EVENT PRIOR TO THE 14TH-CENTURY SUPERCYCLE RUPTURE SEQUENCE

Note: This chapter was published as a stand-alone paper in the Journal of Geophysical Research [*Philibosian et al.*, 2012].

3.1 Introduction

The identification of historical seismic gaps along subduction megathrusts has long been the principal basis for anticipating which section of these great faults are most likely to rupture next [e.g., *Imamura*, 1928; *Kelleher et al.*, 1973]. Nonetheless, it has been known for several decades that this method sometimes fails to identify significant seismic sources. For example, great fault ruptures sometimes overlap patches that have already ruptured during other recent large earthquakes, such as the 2004 Aceh-Andaman earthquake [*Bilham et al.*, 2005] and the 2011 Tohoku-Oki earthquake [*Simons et al.*, 2011]. Moreover, great ruptures do not always involve failure of the entire seismic width of a megathrust. Models for coseismic slip during the great Nias-Simeulue earthquake of 2005, for example, do not infer rupture of a wide band of the megathrust between the outer-arc islands and the trench [*Briggs et al.*, 2006] and afterslip on that updip section does not appear to be accumulating fast enough to recoup potential slip accumulating at the rate of plate convergence [*Hsu et al.*, 2006]. The tsunamigenic 1907 Nias-Simeulue earthquake may have been produced by a major shallow megathrust rupture that filled in this gap [*Kanamori et al.*, 2010].

It used to be thought that such shallow, near-trench sections of subduction megathrusts failed only aseismically and thus posed no seismic or tsunami threat [e.g., *Byrne et al.*, 1988; *Scholz*, 1998]. The insensitivity of land-based geodetic measurements to strain accumulation near the trench falsely reinforced this notion [*Avouac*, 2011]. Several recent large, near-trench earthquakes have shown that shallow sections of megathrusts may commonly slip seismically. Modeling of surface deformation and seismic data suggests that the 2004 Aceh-Andaman rupture extended all the way up to the trench along much of its length [e.g., *Subarya et al.*, 2006], the tsunamigenic 2006 Java earthquake was caused by failure of a section of the Sunda megathrust very close to the trench [*Ammon et al.*, 2006; *Fuji and Satake*, 2006], and much of the moment of the 2011 Tohoku-Oki earthquake resulted from failure updip from previous magnitude 7–8 earthquakes, possibly within a few tens of kilometers of the trench [e.g., *Lay et al.*, 2011]. As such shallow ruptures often produce disproportionately devastating tsunamis [*Polet and Kanamori*, 2000], it is of significant humanitarian (as well as scientific) interest to investigate the recurrence of shallow megathrust ruptures.

An example of particular importance to this study is the M_w 7.8 Pagai Islands earthquake of October 2010 (Figure 3.1). It and its lethal tsunami were caused by rupture of a section of the megathrust within just a few tens of kilometers of the trench and updip from the ruptures of the M_w 8.4 and 7.9 earthquakes of 2007 [*Hill et al.*, 2012]. In this chapter we present and analyze data from one coral microatoll that implies a large seismic rupture of the megathrust (at intermediate depths between the 2007 and 2010 earthquake source regions) occurred about 700 years ago.

The tops of annually banded coral microatolls, which track relative sea level as they grow near the base of the intertidal zone, record tectonic vertical deformation [*Zachariasen et al.*, 1999; *Zachariasen et al.*, 2000; *Natawidjaja et al.*, 2004] and can be dated precisely using uranium-thorium disequilibrium techniques [*Edwards et al.*, 1988; *Shen et al.*, 2002; *Shen et al.*, 2008; *Shen et al.*, 2010]. Almost without exception plots of vertical growth history of microatolls from the Sumatran outer-arc islands display a sawtooth pattern of gradual interseismic subsidence that is interrupted and restored by sudden coseismic uplifts. This is evidence of interseismic strain accumulation across the megathrust and subsequent rupture. A coral record from Pulau Pasir, an islet off the west coast of South Pagai Island (Fig. 3.1), provides the first evidence of an ancient coseismic subsidence in this region, potentially linked to rupture of the megathrust updip of the "conventional" seismogenic zone.

3.2 Pulau Pasir Coral Record

The ancient microatoll that displays a striking exception to the sawtooth pattern sits on the fringing reef of Pulau Pasir ("Sand Island," alternatively called Pulau Kasi on some charts), a small island at 100.25°E, 3.07°S, off the southwest coast of South Pagai Island (Figure 3.2). Like numerous other sites on South Pagai [*Natawidjaja et al.*, 2006], this locality contains a population of coral microatolls that are known, from U-Th disequilibrium dating, to have died due to uplifts during great earthquakes in 1797 and 1833 (Figure 3.S1). Pulau Pasir also contains a population of microatolls that died c. A.D. 1350. Microatoll populations of similar age at several neighboring sites on South

Pagai suggest that these corals were also killed by uplift due to megathrust rupture [*Sieh et al.*, 2008].

One of the 14th-century coral microatolls at Pulau Pasir is unusual in that it contains a record of sea level that spans 150 years prior to its death (most coral colonies live less than 100 years). This specimen is particularly accessible to sampling, because its raised outer rim has fallen radially outward in pieces, exposing its interior and making it amenable to sampling by chainsaw (Figure 3.3). We determined its growth history by reconstructing the original morphology from three different slices, each representing a partial radius that overlaps with its neighbor. Figure 3.4 displays the reconstructed cross section and the derived sea-level time series. The cross section is a cartoon of the perimeter of the radial slice and the form of its annual growth bands. The reconstruction is apparent in the overlap of the three slabs, each represented on the sea-level graph by a different color of symbol.

3.2.1 Interseismic Subsidence and Climatic Die-Downs

The cross section shows that the overall trend of growth of the microatoll was upward and outward through its two-hundred year history. Hence, during most of the life of the coral, the island was dropping relative to the sea surface. The brief primer that follows on the interaction of coral with sea level is necessary to understand how one can read this from the cross section.

Coral growth in any one year is limited by its growth rate and the level of that year's extreme low water (ELW) [*Taylor et al.*, 1987]. Initially, a coral head grows radially

upward and outward, limited only by its growth rate; its elevation in each year can be termed its highest level of growth (HLG). When an upward-growing hemispherical coral colony first reaches the upward limit at which it can survive, termed its highest level of survival (HLS), the top surface dies while its outer perimeter continues to grow radially outward below the HLS. The HLS for *Porites lutea* and *lobata* in this region is ~20 cm above ELW [*Meltzner et al.*, 2010], so HLS is a proxy for ELW plus about 20 cm. After first reaching HLS, due to short-term oceanographic sea-level fluctuations, corals are typically growth-limited for periods of several years between subsequent HLS "hits" which again kill the uppermost surface.

Figure 3.4 shows that the coral head was growing radially upward and outward through the latter decades of the 12th century. (Note: all calendar years mentioned in the following discussion are based on the weighted average of U-Th subsample ages and band counting, which for this coral record produce an absolute age uncertainty of ±19 years. The relative timing of events recorded by coral morphology is dependent only on band counting and is therefore far more precisely known, generally within a few years.) About A.D. 1208 the upper part of the colony died, due to a relative drop of sea level. Until about 1220 the remaining, living perimeter of the head experienced another period of unfettered upward growth. Erosion obscures the details of sea level between 1220 and about 1235, but it appears that sea level did not change much during that period. A ~50-cm drop in the coral's HLS occurred in about 1237. Because the outer annulus of the coral head later broke away from the central disc at this growth discontinuity (after the death of the colony), there is some uncertainty in the original elevation of the outer annulus. The reconstruction shows the minimum original elevation; the true elevation

may have been higher. However, regardless of its original elevation, for the next 80 years after ~1237, the coral records a more-or-less steady rise in HLS of about 1 cm/yr, broken by only a few small drops in HLS. This 80-year subsidence rate is similar to long-term interseismic subsidence rates recorded over the past 7 centuries in corals at the nearby Bulasat site [*Sieh et al.*, 2008], as well as to the pre-2007 rate recorded in the past decade by the continuous Global Positioning System (cGPS) station there [*Natawidjaja et al.*, 2007]. It is most reasonable to attribute this long-term, interseismic strain accumulation to locking of the subjacent megathrust [*Chlieh et al.*, 2008].

The "die-downs" recorded in the coral bands, during which the HLS dropped below its long-term trend, have several plausible causes. Although tidal harmonic ELW in a given location varies only a few centimeters from year to year, non-harmonic oceanographic phenomena such as the Indian Ocean Dipole (IOD) can temporarily change local sea level by tens of centimeters [*Webster et al.*, 1999]. Consequently, the coral die-down events in this record may be either climatic (due to a temporary ocean lowering) or tectonic (due to uplift of the ground). Examination of coral morphology may allow discrimination between these causes: after a climatic temporary lowering in sea level, the coral will grow back upward until reaching an HLS that is in line with its previous trend. In contrast, after a tectonically induced die-down, the coral will resume growing radially outward and upward, but the trend after it reaches HLS will not align with the previous trend due to the ground level change. The morphology of this microatoll suggests that the first two die-downs (about 1208 and 1237) were tectonic, involving uplift of the island, whereas the other, smaller die-downs were climatic.

3.2.2 Sudden Subsidence Event

About 35 years prior to the final death of the microatoll in about A.D. 1350, an abrupt, major change in the morphology of the microatoll records a sudden submergence of at least 35 cm. The large subsidence event is most obvious in the middle slab, where one can clearly see that the growth morphology of the microatoll abruptly changed about A.D. 1314 from occasional small HLS impingements to unfettered, columnar upward growth, completely devoid of die-downs (Fig. 3.3). The columnar growth has broken or eroded off the outer slab, but it can be seen adjacent to the slab's location in Fig. 3.3. This style of growth continued for the remainder of the lifetime of the coral colony, a span of at least 31 years (a few annual bands have likely been eroded off the outer surface). The upper surface of this columnar growth has been eroded, with its highest preserved point 70 cm above the c. 1314 HLS. This indicates that a minimum of 70 cm of subsidence occurred in the last ~35 years of the colony's lifetime, equivalent to an average rate ≥2 cm/yr, double the rate observed during the first ~115 years of growth. While this could have been accomplished simply by a change in interseismic subsidence rate, the death of some sections of the colony's outer surface (such as that shown the middle slab, Fig. 3.4) coincident with the change in morphology suggests that at least some of the subsidence occurred suddenly rather than gradually. The outer surface along the portion of the perimeter cut by the middle slab must have died due to some very local disturbance to the microatoll in ~1314, since the outer perimeter cut by the outer slab continued to grow without incident until ~1346 (Fig. 3.4). Sedimentation caused by seismic shaking or a tsunami could be responsible for killing part of the outer surface. Assuming that the site

continued to subside at only 1 cm/yr for 35 years, at least 35 cm of subsidence must have occurred suddenly. We can obtain some idea of the post-1314 interseismic subsidence rate from BLS02-A3, a microatoll that died c. 1350 at the nearby Bulasat site [*Sieh et al.*, 2008]. Its short history suggests a subsidence rate of ~1.5 cm/yr during ~1335–1350. If the subsidence rate at P. Pasir was truly that high, a greater proportion of the 70 cm total subsidence would be allocated to interseismic rather than coseismic deformation. However, due to the sporadic nature and varying magnitude of climatic die-downs, a 15-year coral HLS record is insufficient to constrain the rate precisely, and a rate of only 1 cm/yr is still plausible given the data.

3.3 Forward Modeling of Possible Rupture Models

A seismic rupture of the megathrust (or a splay fault in the accretionary prism) trenchward of Pulau Pasir is the most plausible explanation for the sudden subsidence, since the down-dip limit of slip must have been below or southwest of the islands in order to produce such subsidence. Unfortunately, other data that might constrain the size and extent of the rupture are scarce. We have not found any other coral microatolls in the region that were living and recording HLS through the early decades of the 14th century. The microatoll BLS02-A3 at Bulasat began growing after 1314 [*Sieh et al.*, 2008] and thus cannot directly constrain the subsidence event. Microatolls at Simanganya and Sikici [*Sieh et al.*, 2008] and Pasapuat (Figure 3.S2) started growing before 1314 and hit HLS shortly thereafter, suggesting that any coseismic subsidence that occurred there cannot have been large. However, dating uncertainties of the coral samples at these sites

preclude precise constraints. With so few constraints, it is not reasonable to attempt to invert for or otherwise speculate about a single "best-fit" earthquake rupture model. However, it is instructive to identify the range of possible models that fit the data.

To characterize the range of fault ruptures that could have produced the observed subsidence at Pulau Pasir, we employed a grid-search technique to select plausible models from a suite of forward models. Our models are based on the analytical solution of *Okada* [1985] for surface displacement due to slip on a dislocation embedded in an elastic half-space. Each model imposed uniform dip slip (between 1 and 50 m) on a single rectangular fault plane with a strike corresponding to the trench orientation (325°), centered southwest of Pulau Pasir. The parameter space comprised fault planes 20 to 100 km long, 10 to 60 km wide, dipping between 5° and 15°, with updip edges located between 0 and 50 km from the trench and 1.5–15 km burial depth. Note that our model does not account for the ~6 km of topography between the trench and the islands, instead placing our "zero datum" flat free surface at the level of the seafloor at the trench. This simplification means that we may slightly underestimate the fault slip required to reproduce the observed deformation. However, the effects of topography on vertical elastic deformation are likely no more than a few percent [*Hsu et al.*, 2011].

While the precise geometry of the shallow megathrust trenchward of the Mentawai Islands is not well constrained, seismic reflection studies [*Singh et al.*, 2011] and Wadati-Benioff zone earthquake distributions [*Engdahl et al.*, 2007] suggest that the megathrust dip between the trench and the outer-arc high falls within our 5°–15° range, and that the megathrust interface is buried below ~1.5 km of sediment at the trench [*Singh et al.*, 2011]. The dip of each model fault plane is required to be consistent with a

concave-down fault geometry (e.g., if the position of the model fault plane would require an average 10° dip to crop out at the trench, the model fault plane cannot have a dip shallower than 10°).

Figure 3.5 shows pairwise parameter plots of the minimum fault slip required to produce 35 cm of subsidence at Pulau Pasir. We excluded models that produced more than 10 cm of subsidence at Simanganya, Pasapuat, or Sikici. Our results indicate that at least 2 m of slip is required to produce 35 cm of subsidence at the Pulau Pasir site, regardless of the other model parameters. With that limitation, a wide variety of megathrust rupture scenarios fit the data, ranging in moment magnitude between 7.4 and 8.6 (based on a constant rigidity of 33 GPa).

Two representative megathrust slip models selected to match the fault geometry revealed by a nearby seismic reflection study [*Singh et al.*, 2011] are shown in Figure 3.6. The c. 1314 subsidence data can be reproduced by large slip on the shallowest part of the megathrust, or by smaller slip on a deeper patch. Fig. 3.6 also shows one model with slip on a splay fault. This hypothetical fault crops out on the ocean floor a few kilometers southwest of the islands. Although this is not specifically known to be the location of a splay fault, nearby seismic reflection data show faults in the accretionary prism at a similar distance from the trench [*Singh et al.*, 2011].

3.4 Recurrence Constraints from Bulasat Record and Mid-Holocene Age Corals

The sudden subsidence event of about A.D. 1314 recorded at Pulau Pasir is the only known direct evidence of an ancient shallow megathrust rupture along the Mentawai

island chain. However, there are clear, indirect indications of at least two earlier subsidence events. Figure 3.7 displays a combined record of coral HLS levels from Pulau Pasir and the nearby Bulasat site (see Fig. 3.2 inset for location). The younger records from corals BLS02-A1, 3, and 5 were presented in detail by *Sieh et al.* [2008], whereas the older Bulasat coral records appear in Figs. 3.S3–3.S6. Ages for the Bulasat corals are from *Shen et al.* [2008]. Our reconstruction places the pre-1350 elevation of PSR10-A3 only about 10 cm higher than the contemporaneous BLS02-A3 (Fig. 3.7A), suggesting that the minimum-elevation restoration of the outer annulus is correct (restoring the outer annulus higher would require excessively disparate tectonic behavior for sites only 3 km apart).

As noted by *Sieh et al.* [2008], a long-term uplift rate of about 1.8 mm/yr appears to be superimposed on the seismic cycle sawtooth curve for the past 700 years (Fig. 3.7C), resulting in the elevation of PSR10-A3 and BLS02-A3 about 1 m above their modern (pre-2007 earthquake) counterparts. However, this long-term uplift cannot be extrapolated farther into the past, since microatolls dating to the first millennia A.D. and B.C. are no higher in elevation than the 14th-century microatolls. Thus, the 1.8 mm/yr uplift over the past 700 years cannot represent permanent inelastic deformation, but must be balanced by subsidence. The relative elevations of older corals are consistent with similar long-term uplift rates in the past, provided that large subsidence events occurred to recover this uplift. The ~35 cm of subsidence that occurred c. 1314 is actually insufficient to recover the ~150 cm of uplift that we infer to have accumulated during the previous thousand years. Therefore, if our interpretation is correct, a second, larger subsidence event occurred prior to the one recorded in 1314. Similarly, one or more

subsidence events must have occurred between ~430 B.C. and ~A.D. 350 (Fig. 3.7D). The most plausible explanation for this cycle, opposite in sign to the deformation cycle produced by strain accumulation and release on that portion of the megathrust below the island chain, is a similar seismic cycle on the shallow megathrust updip and seaward of the island chain. (The lack of appreciable permanent deformation is evidence against the splay fault model.) These coral records suggest that shallow megathrust ruptures have a much longer recurrence interval than conventional megathrust ruptures, about 1000 years. The magnitude of residual strain accumulated at ~1.8 mm/yr since the most recent such event, ~A.D. 1314, is about 1.25 m. An equivalent amount of subsidence would require fault slip of at least 5.5 m on a patch immediately updip of the islands, comparable to the average slip magnitude during the 2010 event [*Hill et al.*, 2012]; such a rupture seems entirely plausible.

A direct calculation of potential slip on the trenchward section of the megathrust would be 32 m (4.6 cm/yr times 700 years), three times the maximum slip in 2010. The recent Tohoku earthquake has illustrated that even larger near-trench slip is possible [e.g., *Lay et al.*, 2011]. However, it is unlikely that a narrow-width rupture could produce slip so large, and a Tohoku-type earthquake would involve rupture of the 2007 patch as well as the 2010 patch, likely producing uplift rather than subsidence of the islands. While not impossible, there is no evidence that Tohoku-type (full width) ruptures have occurred on the Mentawai segment, and it is not unlikely that a significant portion of the interplate motion on the shallow megathrust is accommodated aseismically.

An obvious remaining question is whether the shallow megathrust ruptures seismically along its entire length, or whether such events only occur in a limited area

southwest of the Pagai Islands. While the Simanganya and Sikici sites do not seem to have experienced significant subsidence during the 1314 event, both sites exhibit long-term uplift trends over the past 700 years similar to Bulasat [*Sieh et al.*, 2008]. The presence of mid-Holocene age microatolls in the modern intertidal zone throughout the Mentawai Islands (Figure 3.8) indicates that, similarly to Bulasat, this uplift cannot reflect inelastic, permanent deformation. Sea levels between 7000 and 2000 yr B.P. (before A.D. 1950) are not well constrained in this region, but probably were no lower than present levels [e.g., *Horton et al.*, 2005]. Thus, if the observed 1–2 mm/yr uplift rate had been sustained over thousands of years, corals of that age would be expected to be meters higher than their modern counterparts. These data rule out permanent uplift rates greater than about 0.2 mm/yr, suggesting even lower inelastic deformation rates than those observed on Nias Island [*Briggs et al.*, 2008]. While we have no direct evidence for subsidence events at sites other than Pulau Pasir, the data from other sites are generally consistent with strain buildup and release on the shallow megathrust along the entire Mentawai segment (though it will not necessarily all rupture in a single earthquake).

3.5 Conclusions

The coral record at Pulau Pasir implies that a large rupture of the megathrust between the trench and the islands occurred c. A.D. 1314. This rupture must have been larger and/or deeper than the 25 October 2010 rupture. The elevations of four older microatolls at Bulasat suggest that at least two other shallow megathrust ruptures occurred during the

1500 years before the A.D. 1314 event. The existence of numerous mid-Holocene microatolls in the intertidal zone throughout the Mentawai island chain precludes any large permanent uplift for the last ~7000 years, and implies that the long-term trend of emergence observed at Bulasat and other sites (1–2 mm/yr) is due to tectonic strain accumulation across the megathrust between the trench and the islands.

The amount of uplift accumulated at Bulasat since 1314 is about 1.3 m, whereas only ~4 cm of subsidence occurred coseismically in 2010 [*Hill et al.*, 2012]. It is important to note that post-seismic subsidence recorded by the Bulasat cGPS station is already more than double the October 2010 coseismic subsidence [*Feng et al.*, 2011], but nevertheless the total subsidence is still only ~10% of the accumulated uplift. Therefore, it is possible that an additional shallow megathrust event larger than the October 2010 rupture will occur in the near future. (The recent post-seismic behavior also suggests that a significant portion of the c. 1314 subsidence may have been post-seismic as well, but there is no way to determine this from the coral record). Regardless of the exact characteristics of the ancient and modern shallow megathrust slip events, it is clear that such ruptures play an important part in the seismic cycle of the Sumatran subduction zone. Geoscientists and policymakers alike should be aware that shallow tsunamigenic earthquakes similar to (or perhaps larger than) the 25 October 2010 event may occur in the future on adjacent parts of the Sunda megathrust, and should be included in scenario-based forecasts for the region.

References

Ammon, C. J., H. Kanamori, T. Lay, and A. A. Velasco (2006), The 17 July 2006 Java tsunami earthquake, *Geophys. Res. Lett.*, *33*, L24308, doi:10.1029/2006GL028005.

Avouac, J.-P. (2011), Earthquakes: The lessons of Tohoku-Oki, *Nature*, *475*(7356), 300–301.

Bilham, R., R. Engdahl, N. Feldl, and S. P. Satyabala (2005), Partial and complete rupture of the Indo-Andaman Plate boundary 1847-2004, *Seismo. Res. Lett.*, *76*(3), 299–311.

Briggs, R. W., et al. (2006), Deformation and slip along the Sunda megathrust in the great 2005 Nias-Simeulue earthquake, *Science*, *311*, 1897–1901.

Briggs, R. W., K. Sieh, W. H. Amidon, J. Galetzka, D. Prayudi, I. Suprihanto, N. Sastra, B. Suwargadi, D. Natawidjaja, and T. G. Farr (2008), Persistent elastic behavior above a megathrust rupture patch: Nias island, West Sumatra, *J. Geophys. Res.*, *113*, B12406, doi:10.1029/2008JB005684.

Byrne, D. E., D. M. Davis, and L. R. Sykes (1988), Loci and maximum size of thrust earthquakes and the mechanics of the shallow region of subduction zones, *Tectonics*, *7*(4), 833–857.

Chlieh, M., J.-P. Avouac, K. Sieh, D. Natawidjaja, and J. Galetzka (2008), Heterogeneous coupling of the Sumatran megathrust constrained by geodetic and paleogeodetic measurements, *J. Geophys. Res.*, *113*(B05305), doi:10.1029/2007JB004981.

Edwards, R. L., F. W. Taylor, and G. J. Wasserburg (1988), Dating earthquakes with high-precision thorium-230 ages of very young corals, *Earth Planet. Sci. Lett.*, *90*(4), 371–381.

Engdahl, E. R., A. Villaseñor, H. R. DeShon, and C. H. Thurber (2007), Teleseismic relocation and assessment of seismicity (1918–2005) in the region of the 2004 Mw 9.0 Sumatra–Andaman and 2005 Mw 8.6 Nias Island great earthquakes, *Bull. Seismol. Soc. Am.*, *97*(1A), S43–S61.

Feng, L., E. M. Hill, P. Banerjee, A. M. Lubis, Q. Qiu, and K. E. Sieh (2011), Very rapid afterslip following the shallow 2010 M_w 7.8 Mentawai tsunami earthquake, Abstract T23C-2405, paper presented at 2011 Fall Meeting, AGU, San Francisco, CA.

Fuji, Y., and K. Satake (2006), Source of the July 2006 West Java tsunami estimated from tide gauge records, *Geophys. Res. Lett.*, *33*, L24317, doi:10.1029/2006GL028049.

Hill, E. M., et al. (2012), The 2010 M_w 7.8 Mentawai earthquake: Very shallow source of a rare tsunami earthquake determined from tsunami field survey and near-field GPS, *J. Geophys. Res.*, *117*, B06402, doi:10.1029/2012JB009159.

Horton, B. P., P. L. Gibbard, G. M. Milne, R. J. Morley, C. Purintavaragul, and J. M. Stargardt (2005), Holocene sea levels and palaeoenvironments, Malay-Thai Peninsula, southeast Asia, *The Holocene*, *15*(8), 1199–1213.

Hsu, Y.-J., M. Simons, C. Williams, and E. Casarotti (2011), Three-dimensional FEM derived elastic Green's functions for the coseismic deformation of the 2005 M_w 8.7 Nias-Simeulue, Sumatra earthquake, *Geochem. Geophys. Geosyst.*, *12*, Q07013, doi:10.1029/2011GC003553.

Hsu, Y., M. Simons, J.-P. Avouac, J. Galetzka, K. Sieh, M. Chlieh, D. Natawidjaja, L. Prawirodirdjo, and Y. Bock (2006), Frictional afterslip following the 2005 Nias-Simeulue earthquake, Sumatra, *Science*, *312*, 1921–1926.

Imamura, A. (1928), On the seismic activity of central Japan, *Japanese Journal of Astronomy and Geophysics*, *6*, 119–137.

Kanamori, H., L. Rivera, and W. H. K. Lee (2010), Historical seismograms for unraveling a mysterious earthquake: The 1907 Sumatra earthquake, *Geophys. J. Int.*, *183*(1), 358–374.

Kelleher, J., L. R. Sykes, and J. Oliver (1973), Possible criteria for predicting earthquake locations and their application to major plate boundaries of the Pacific and the Caribbean, *J. Geophys. Res.*, *78*(14), 2547–2585.

Konca, A. O., et al. (2008), Partial rupture of a locked patch of the Sumatra megathrust during the 2007 earthquake sequence, *Nature*, *456*, 631–635.

Lay, T., C. J. Ammon, H. Kanamori, L. Xue, and M. J. Kim (2011), Possible large near-trench slip during the 2011 M_w 9.0 off the Pacific coast of Tohoku earthquake, *Earth, Planets, and Space*, *63*(7), 687–692.

Lin, J., and R. S. Stein (2004), Stress triggering in thrust and subduction earthquakes, and stress interaction between the southern San Andreas and nearby thrust and strike-slip faults, *J. Geophys. Res.*, *109*, B02303, doi:10.1029/2003JB002607.

Meltzner, A. J., K. Sieh, H.-W. Chiang, C.-C. Shen, B. W. Suwargadi, D. H. Natawidjaja, B. E. Philibosian, R. W. Briggs, and J. Galetzka (2010), Coral evidence for earthquake recurrence and an A.D. 1390–1455 cluster at the south end of the 2004 Aceh-Andaman rupture, *J. Geophys. Res.*, *115*, B10402, doi:10.1029/2010JB007499.

Natawidjaja, D. H., K. Sieh, S. N. Ward, H. Cheng, R. L. Edwards, J. Galetzka, and B. W. Suwargadi (2004), Paleogeodetic records of seismic and aseismic subduction from central Sumatran microatolls, Indonesia, *J. Geophys. Res.*, *109*(B04), 4306, doi:10.1029/2003JB002398.

Natawidjaja, D. H., K. Sieh, M. Chlieh, J. Galetzka, B. W. Suwargadi, H. Cheng, R. L. Edwards, J.-P. Avouac, and S. N. Ward (2006), Source parameters of the great Sumatran megathrust earthquakes of 1797 and 1833 inferred from coral microatolls, *J. Geophys. Res.*, *111*(B6), 6403, doi:10.1029/2005JB004025.

Natawidjaja, D. H., K. Sieh, J. Galetzka, B. W. Suwargadi, H. Cheng, R. L. Edwards, and M. Chlieh (2007), Interseismic deformation above the Sunda Megathrust recorded in coral microatolls of the Mentawai islands, West Sumatra, *J. Geophys. Res.*, *112*(B02), 2404, doi:10.1029/2006JB004450.

Okada, Y. (1985), Surface deformation due to shear and tensile faults in a half-space, *Bull. Seismol. Soc. Am.*, *75*(4), 1135–1154.

Philibosian, B., K. Sieh, D. H. Natawidjaja, H.-W. Chiang, C.-C. Shen, B. W. Suwargadi, E. M. Hill, and R. L. Edwards (2012), An ancient shallow slip event on the Mentawai segment of the Sunda megathrust, Sumatra, *J. Geophys. Res.*, *117*, B05401, doi:10.1029/2011JB009075.

Polet, J., and H. Kanamori (2000), Shallow subduction zone earthquakes and their tsunamigenic potential, *Geophys. J. Int.*, *142*, 684–702.

Scholz, C. H. (1998), Earthquakes and friction laws, *Nature*, *391*(6662), 37–42.

Shen, C.-C., R. L. Edwards, H. Cheng, J. A. Dorale, R. B. Thomas, S. B. Moran, S. E. Weinstein, and H. N. Edmonds (2002), Uranium and thorium isotopic and concentration measurements by magnetic sector inductively coupled plasma mass spectrometry, *Chem. Geol.*, *185*, 165–178.

Shen, C.-C., et al. (2008), Variation of initial $^{230}Th/^{232}Th$ and limits of high precision U-Th dating of shallow-water corals, *Geochim. Cosmochim. Acta*, *72*(17), 4201–4223.

Shen, C.-C., A. Kano, M. Hori, K. Lin, T.-C. Chiu, and G. S. Burr (2010), East Asian monsoon evolution and reconciliation of climate records from Japan and Greenland during the last deglaciation, *Quat. Sci. Rev.*, *29*, 3327–3335.

Sieh, K., D. H. Natawidjaja, A. J. Meltzner, C.-C. Shen, H. Cheng, K.-S. Li, B. W. Suwargadi, J. Galetzka, B. Philibosian, and R. L. Edwards (2008), Earthquake supercycles inferred from sea-level changes recorded in the corals of west Sumatra, *Science*, *322*, 1674–1678.

Simons, M., et al. (2011), The 2011 magnitude 9.0 Tohoku-oki earthquake: Mosaicking the megathrust from seconds to centuries, *Science*, *332*(6036), 1421–1425.

Singh, S., N. Hananto, M. Mukti, H. Permana, Y. Djajadihardja, and H. Harjono (2011), Seismic images of the megathrust rupture during the 25th October 2010 Pagai earthquake, SW Sumatra: Frontal rupture and large tsunami, *Geophys. Res. Lett.*, *38*, L16313, doi:10.1029/2011GL048935.

Subarya, C., M. Chlieh, L. Prawirodirdjo, J.-P. Avouac, Y. Bock, K. Sieh, A. J. Meltzner, D. Natawidjaja, and R. McCaffrey (2006), Plate-boundary deformation associated with the great Sumatra-Andaman earthquake, *Nature*, *440*(7080), 46–51.

Taylor, F. W., C. Frohlich, J. Lecolle, and M. R. Strecker (1987), Analysis of partially emerged corals and reef terraces in the central Vanuatu Arc; comparison of contemporary coseismic and nonseismic with Quaternary vertical movements, *J. Geophys. Res.*, *92*(B6), 4905–4933.

Toda, S., R. S. Stein, K. Richards-Dinger, and S. Bozkurt (2005), Forecasting the evolution of seismicity in southern California: Animations built on earthquake stress transfer, *J. Geophys. Res.*, *110*, B05S16, doi:10.1029/2004JB003415.

Webster, P. J., A. M. Moore, J. P. Loschnigg, and R. R. Leben (1999), Coupled ocean-atmosphere dynamics in the Indian Ocean during 1997–98, *Nature*, *401*(6751), 356–360.

Zachariasen, J. (1998), Paleoseismology and paleogeodesy of the Sumatran subduction zone: A study of vertical deformation using coral microatolls, Ph.D. thesis, 418 pp., Calif. Inst. of Technol., Pasadena, CA.

Zachariasen, J., K. Sieh, F. W. Taylor, R. L. Edwards, and W. S. Hantoro (1999), Submergence and uplift associated with the giant 1833 Sumatran subduction earthquake: Evidence from coral microatolls, *J. Geophys. Res.*, *104*(B1), 895–919.

Zachariasen, J., K. Sieh, F. W. Taylor, and W. S. Hantoro (2000), Modern vertical deformation above the Sumatran subduction zone: Paleogeodetic insights from coral microatolls, *Bull. Seismol. Soc. Am.*, *90*(4), 897–913.

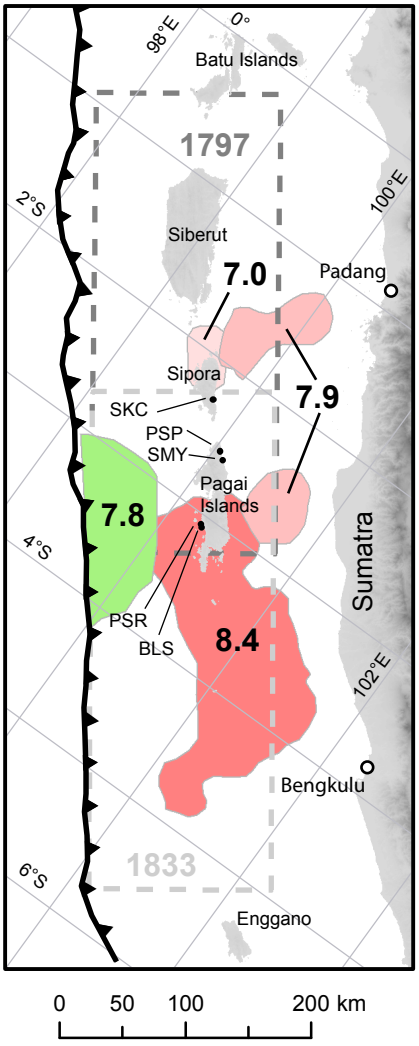

Figure 3.1. Recent and ancient ruptures along the Mentawai section of the Sunda megathrust. Colored patches are surface projections of 1-meter slip contours of the deep megathrust ruptures on 12–13 September 2007 (pink to red) and the shallow rupture on 25 October 2010 (green). Dashed rectangles indicate roughly the sections that ruptured in 1797 and 1833. Ancient ruptures are adapted from *Natawidjaja et al.* [2006] and recent ones come from *Konca et al.* [2008] and *Hill et al.* [2012]. Labeled points indicate coral study sites Sikici (SKC), Pasapuat (PSP), Simanganya (SMY), Pulau Pasir (PSR), and Bulasat (BLS).

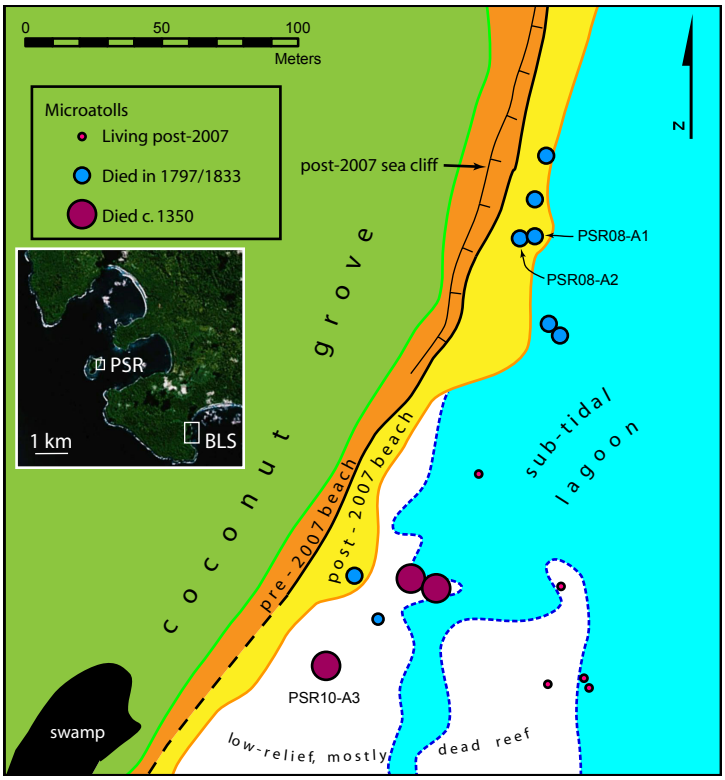

Figure 3.2. Map of living and fossil microatolls at the Pulau Pasir site. One family of microatolls died in the historical great earthquakes of 1797 and 1833 and another died in about A.D. 1350. The site rose tectonically ~50 cm during the 2007 Mw 8.4 earthquake, causing many of the modern coral microatolls to die and the beach to re-establish itself farther seaward. Microatoll PSR10-A3 contains a very long record of interseismic subsidence and a sudden subsidence of ≥35 cm in ~A.D. 1314.
(inset) Satellite image of the southwest coast of South Pagai Island showing locations of Pulau Pasir (PSR) and Bulasat (BLS) sites.

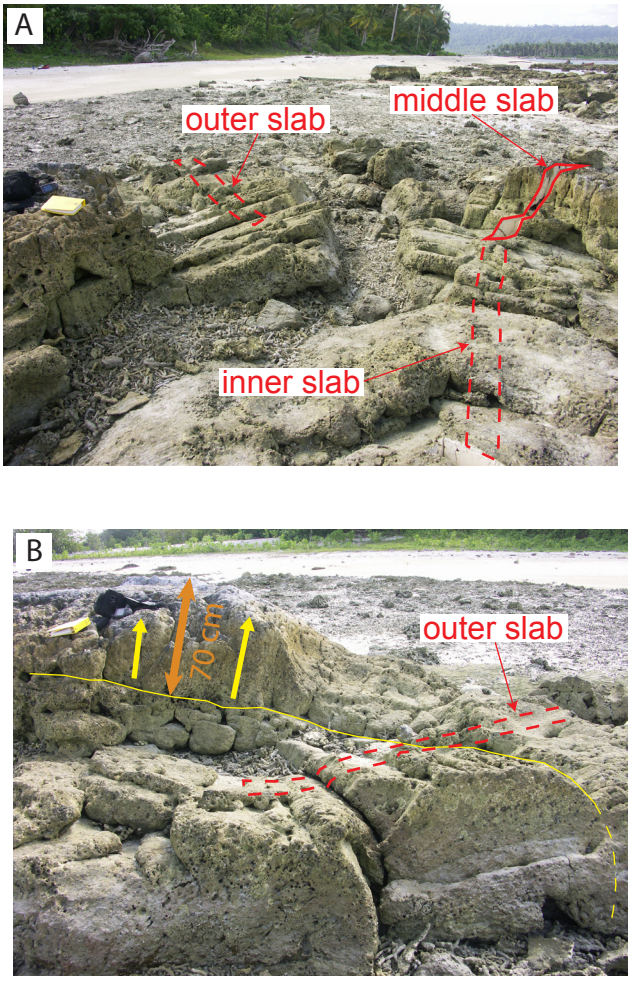

Figure 3.3. Field photographs of coral microatoll PSR10-A3 show that its raised outer annulus has fallen away in sections, revealing the older core of the colony. Yellow notebook is 16 x 20 cm in dimension, and lies in the same place in both photographs. (A) View from the center of the head shows fallen and broken sections of outer rim and locations of collected slabs. (B) Cross-sectional view of a piece of the outer rim shows unfettered columnar overgrowth (yellow arrows) above the c. A.D. 1314 isochron surface (yellow line). Vertical overgrowth has eroded or broken from the part of the head from which the slab was taken, but is clearly contemporaneous with the post-1314 eroded section of the outer slab. The highest preserved point on the columnar overgrowth extends 70 cm above the 1314 surface (orange arrow).

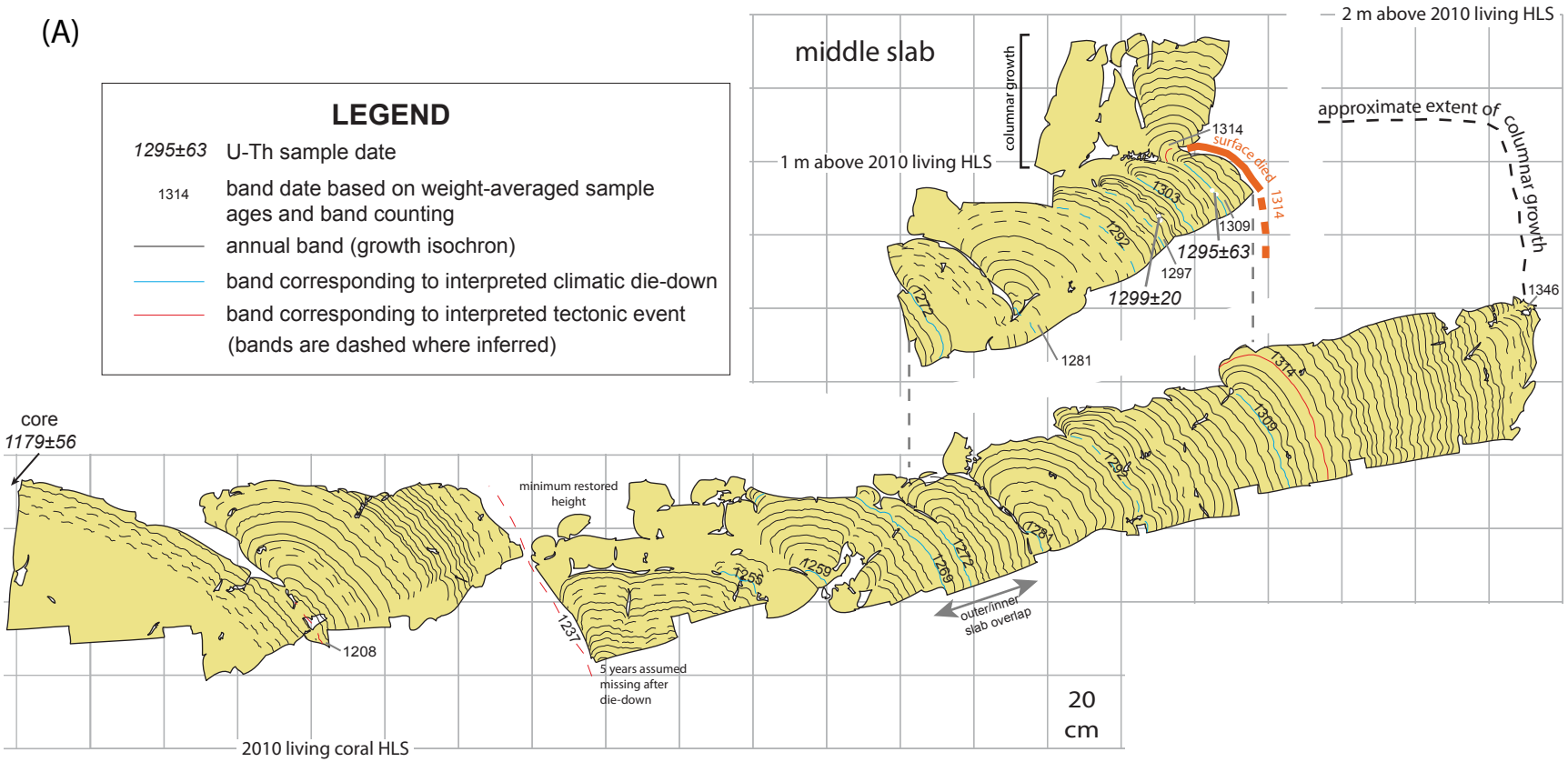
(A)
LEGEND
1295±63 U-Th sample date
1314 band date based on weight-averaged sample ages and band counting
annual band (growth isochron)
band corresponding to interpreted climatic die-down
band corresponding to interpreted tectonic event
(bands are dashed where inferred)
middle slab
columnar growth
2 m above 2010 living HLS
approximate extent of columnar growth
1 m above 2010 living HLS
1314
surface died 1314
1303
1309
1292
1295±63
1297
1299±20
1272
1281
1346
core
1179±56
minimum restored height
1314
1309
1292
1289
1272
1259
1256
1237
1208
outer/inner slab overlap
5 years assumed missing after die-down
20 cm
2010 living coral HLS

Figure 3.4A

(B)

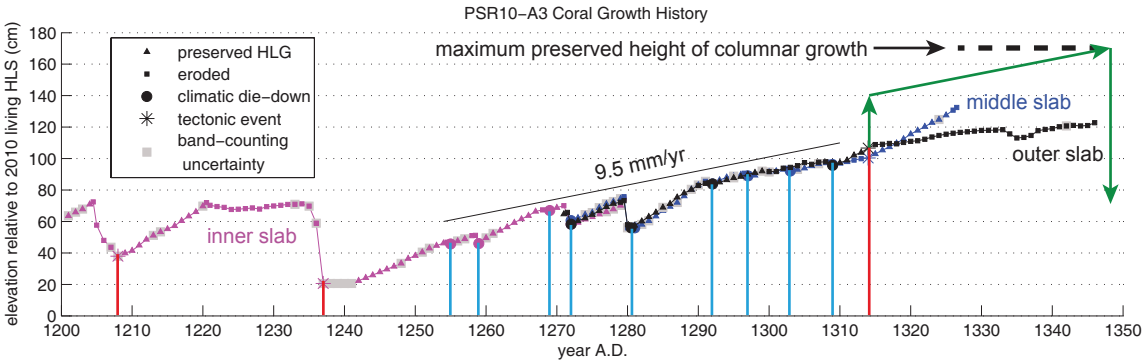

Figure 3.4. A sea-level record spanning ~A.D. 1200 to 1350 reveals two small uplifts in about 1208 and 1237, followed by a sustained interseismic subsidence at about 9.5 mm/yr. Sudden subsidence occurred in about 1314, and death due to uplift occurred in about 1350.

(A) Cross section of PSR10-A3 reconstructed from three slabs and corrected for post-mortem tilting. Some preserved columnar growth can be seen on the middle slab. The outer slab originally had similar growth but this has been eroded away in the immediate vicinity of the slab cut. The approximate original extent of the columnar growth is shown based on the less eroded area adjacent to the outer slab (see Fig. 3.3). Heavy orange line shows the outer surface of middle slab which died at the same time columnar growth initiated on the top surface.

(B) HLS/HLG history of PSR10-A3. Vertical lines highlight timing of climatic and tectonic morphology changes. Green arrows show inferred post-1314 relative sea-level history: 35 cm coseismic subsidence, followed by 35 cm interseismic subsidence (at the same rate as before), and finally >1 m of uplift which killed the coral colony. The continued upward growth of the coral during this period is evidenced by the thick section of columnar growth shown in Fig. 3.3B, which our slabs do not transect but clearly grew at the same time as the post-1314 section of the outer slab.

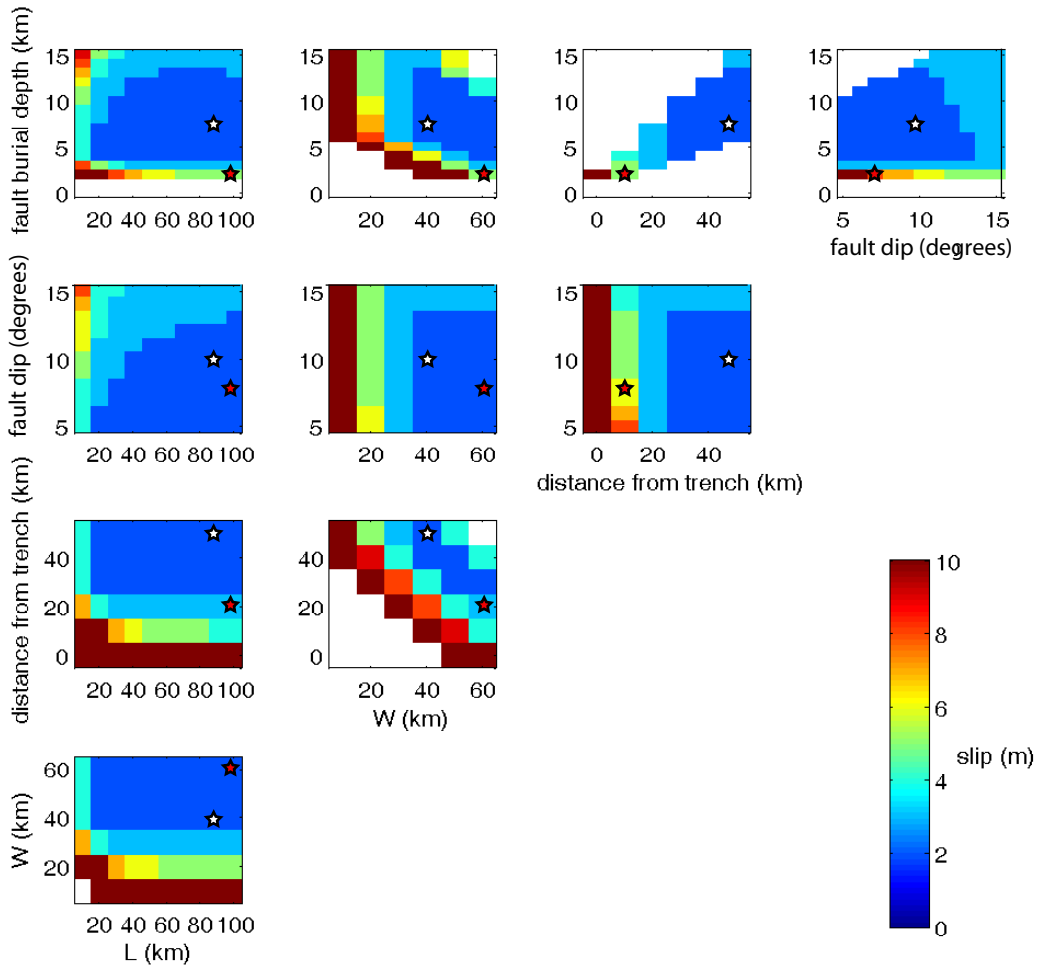

Figure 3.5. A grid search for fault parameters that would reproduce a sudden subsidence c. 1314. Each plot displays two model parameters on the x and y axes, whereas color indicates the minimum amount of fault slip required to produce 35 cm of subsidence at the Pulau Pasir site for each parameter pairing. Areas colored brown require very large slip (between 10 and 50 m). White parameter space either requires unreasonably large (>50 m) slip or was eliminated by other constraints such as the deformation limits at PSP and SMY. All scenarios require at least 2 m of slip. White and red stars show parameters for deep and shallow example models, respectively, in Fig. 3.6. Note that the 9-m slip for the shallow model is required by the combination of fault burial depth and dip. The splay fault model does not fall within this parameter space.

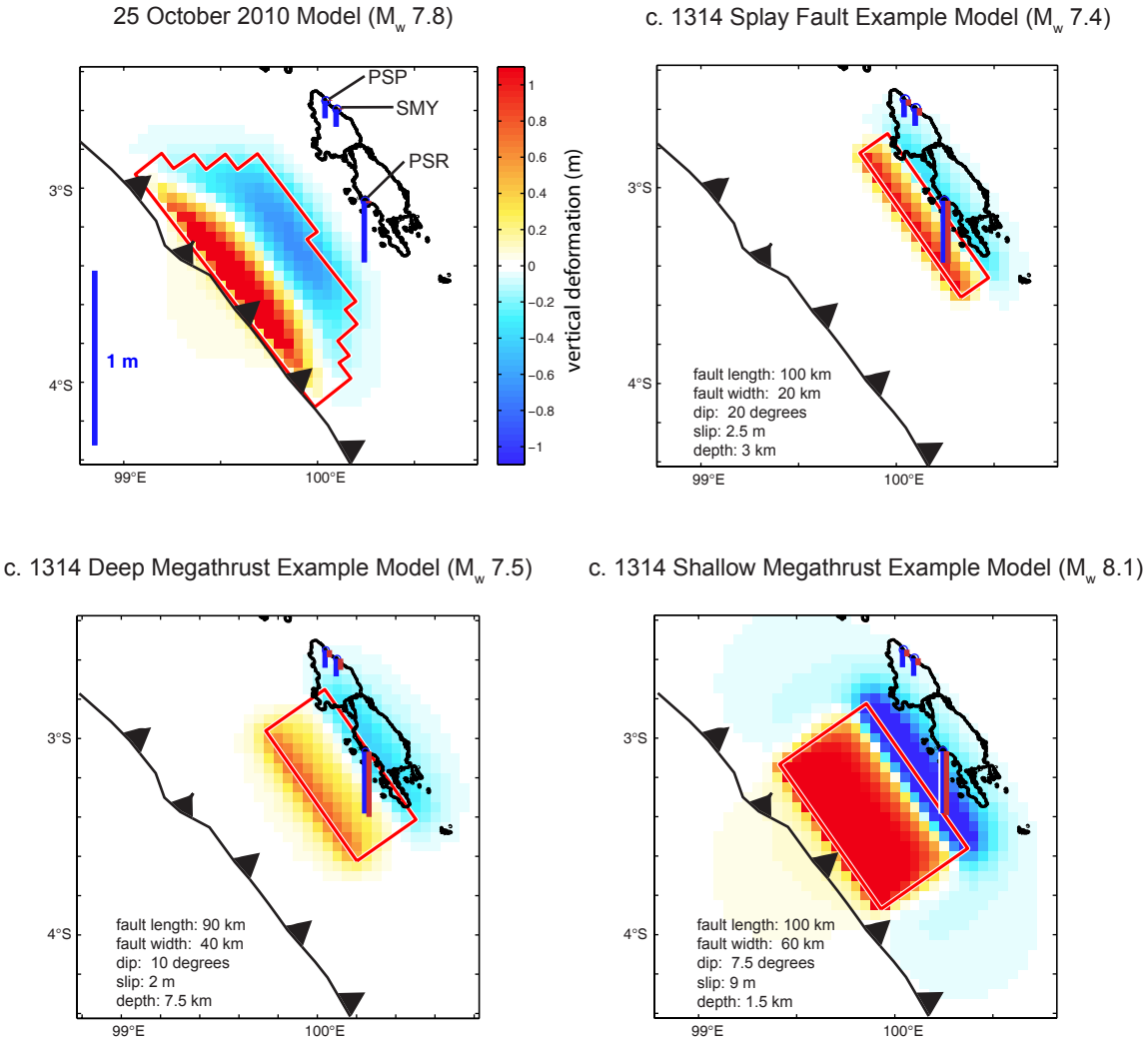

Figure 3.6. Comparison of the modeled 25 October 2010 fault rupture [*Hill et al.*, 2012] with selected fault slip models for the c. 1314 event. Slip in 1314 must have been either larger than in 2010 or closer to the islands. Red outlines indicate areas of fault slip. Colored areas show uplift and subsidence generated by each model fault, saturated at 1 meter to more clearly show areas of lesser displacement. Vertical blue bars at Pasapuat (PSP) and Simanganya (SMY) represent the maximum permitted subsidence of 10 cm, whereas the blue bar at Pulau Pasir (PSR) represents the minimum required subsidence of 35 cm. Red bars show subsidence produced by each model rupture at each site. Models generated using the Coulomb 3.2 software [*Lin and Stein*, 2004; *Toda et al.*, 2005].

Figure 3.7

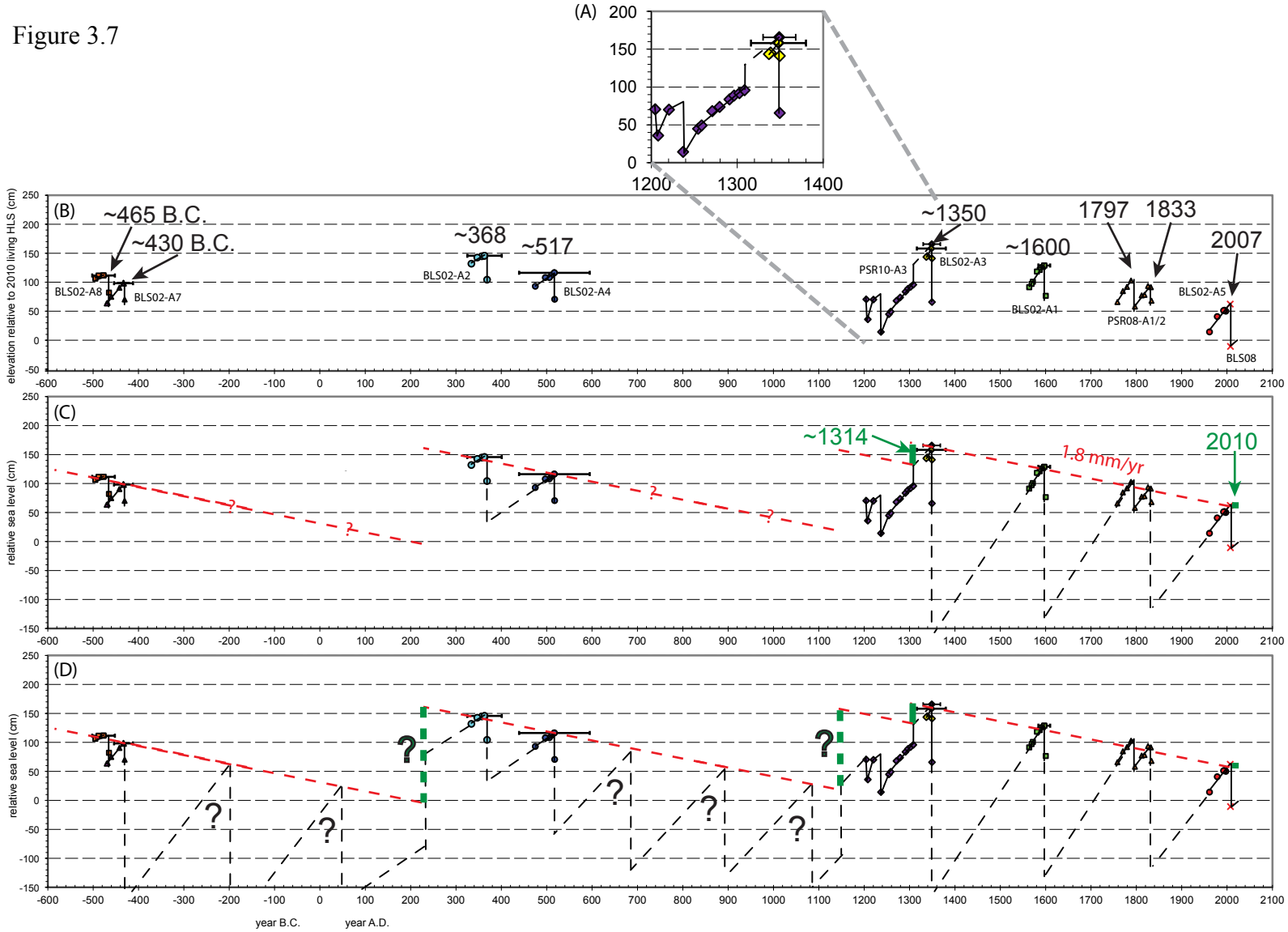
(A)
(B)
(C)
(D)
~465 B.C.
~430 B.C.
~368
~517
~1350
~1600
1797
1833
2007
~1314
2010
1.8 mm/yr
BLS02-A8
BLS02-A7
BLS02-A2
BLS02-A4
PSR10-A3
BLS02-A3
BLS02-A1
PSR08-A1/2
BLS02-A5
BLS08
elevation relative to 2010 living HLS (cm)
relative sea level (cm)
year B.C.
year A.D.

Figure 3.7. The combined relative sea-level record from Pulau Pasir (PSR) and nearby Bulasat (BLS) site implies that sudden subsidence events relieve residual uplifts accumulated over the centuries at a rate of about 1.8 mm/yr.

(A) Relative sea-level history of PSR10-A3 (purple symbols), simplified from Fig. 4B. Yellow symbols show the much shorter BLS02-A3 record, which is at a comparable elevation.

(B) Compilation of coral microatoll records that constrain relative sea level over the past 2500 years, with dates (A.D.) of uplifts interpreted as down-dip ("conventional") megathrust ruptures. Horizontal error bars indicate uncertainty in U-Th age for each microatoll.

(C) The relative sea-level sawtooth curve is interpolated between down-dip ruptures by extending the measured late-cycle interseismic rates over entire interseismic periods (dashed black line). A longer-term uplift rate of 1.8 mm/yr appears to be superimposed on the last 700 years of cycles (red dashed line), but projecting this trend farther into the past is inconsistent with the height of older microatolls unless the uplift is periodically balanced by subsidence. The c. 1314 subsidence helps to complete the cycle, but is not large enough to span the vertical offset between the projected 1.8 mm/yr trends. The 2010 subsidence has barely any effect.

(D) Dashed green bars show hypothetical sudden subsidence events that could have balanced the accumulated uplift. We assume that there are many "conventional" seismic cycles missing from our record (black question marks); this may be because the corals growing during these times were at lower elevations and thus subject to greater wave erosion after the land level dropped. In our interpretation, the red/green sawtooth curve represents strain accumulation and release on the shallow megathrust updip of the islands, a cycle which is superimposed on the higher-frequency down-dip seismic cycle to form the complete relative sea-level history (black sawtooth curve). If uplift accumulated since 1314 were relieved soon, about 1.25 m of subsidence would occur. This would reflect far larger slip on the megathrust than in either 1314 or 2010.

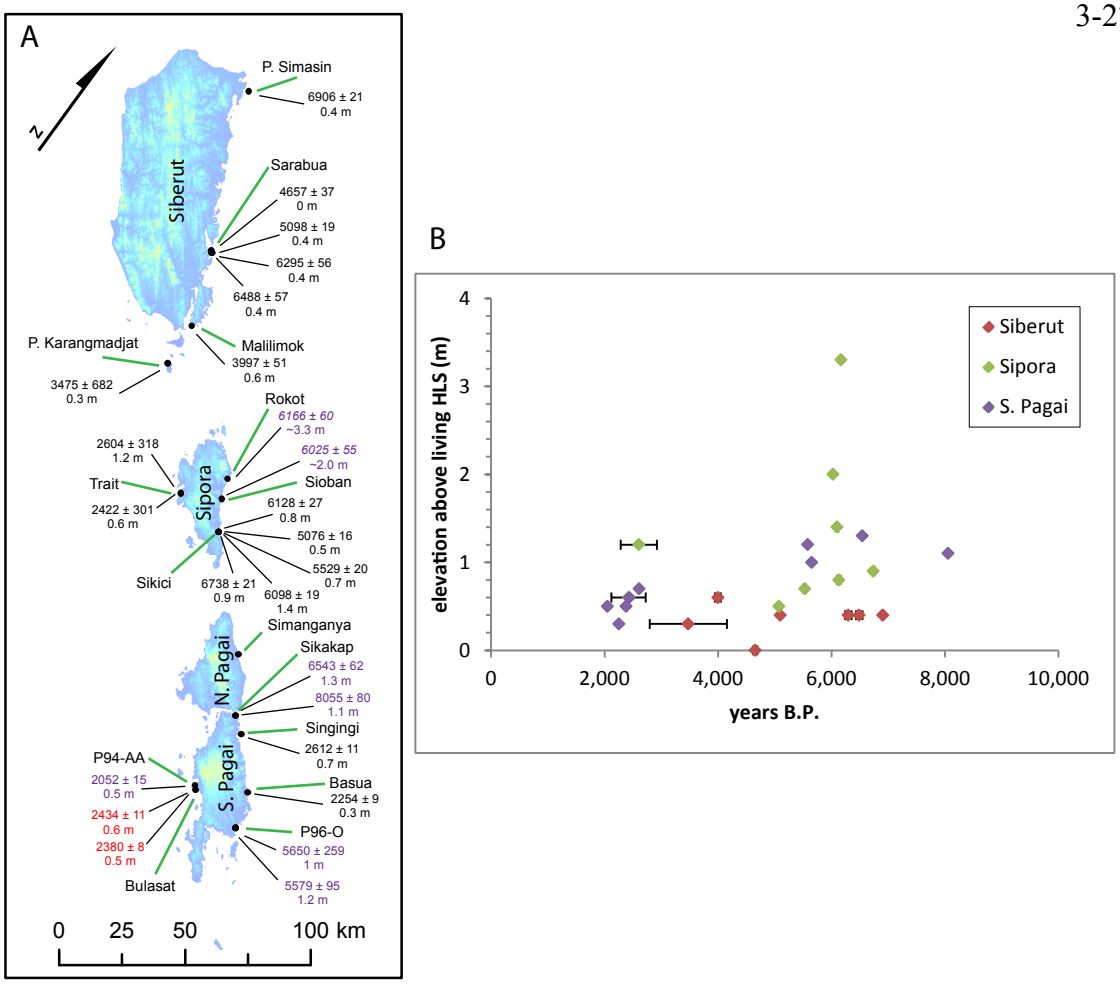

Figure 3.8. Many fossil microatolls more than 2,000 years old still lie within the modern intertidal zone throughout the Mentawai Islands, which indicates that little or no permanent uplift has occurred since these corals were alive. This implies that very long-term residual rates of emergence seen throughout the islands are due to tectonic strain accumulation that is relieved by slip on the megathrust between the islands and the trench. (A) Map of microatoll locations with dates in years B.P. (before 1950) and heights in meters above modern living coral HLS. Ages in purple are from *Zachariasen* [1998], in red from *Shen et al.* [2008], and black from this study (see Table 3.S2). Radiocarbon ages appear in italics; all others are U-Th ages. (B) Plot of elevation versus age reveals no obvious trend, suggesting that seismic cycle deformation swamps any long-term vertical deformation. Permanent uplift rates greater than ~0.2 mm/yr are unlikely given these data. (Note: age error bars on most data points are smaller than the symbols).

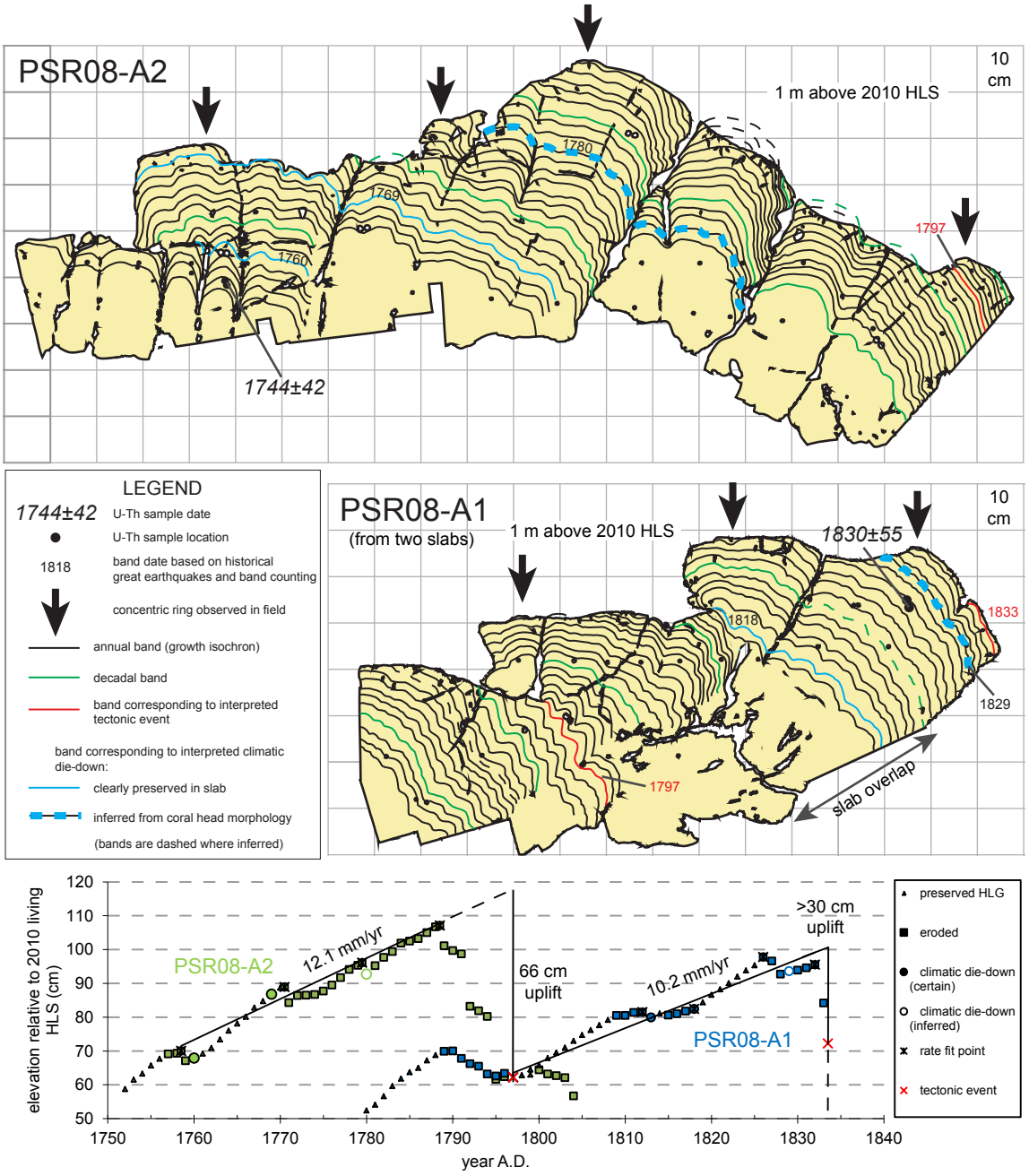

Figure 3.S1. Cross sections and growth plot of PSR08-A2 and PSR08-A1.

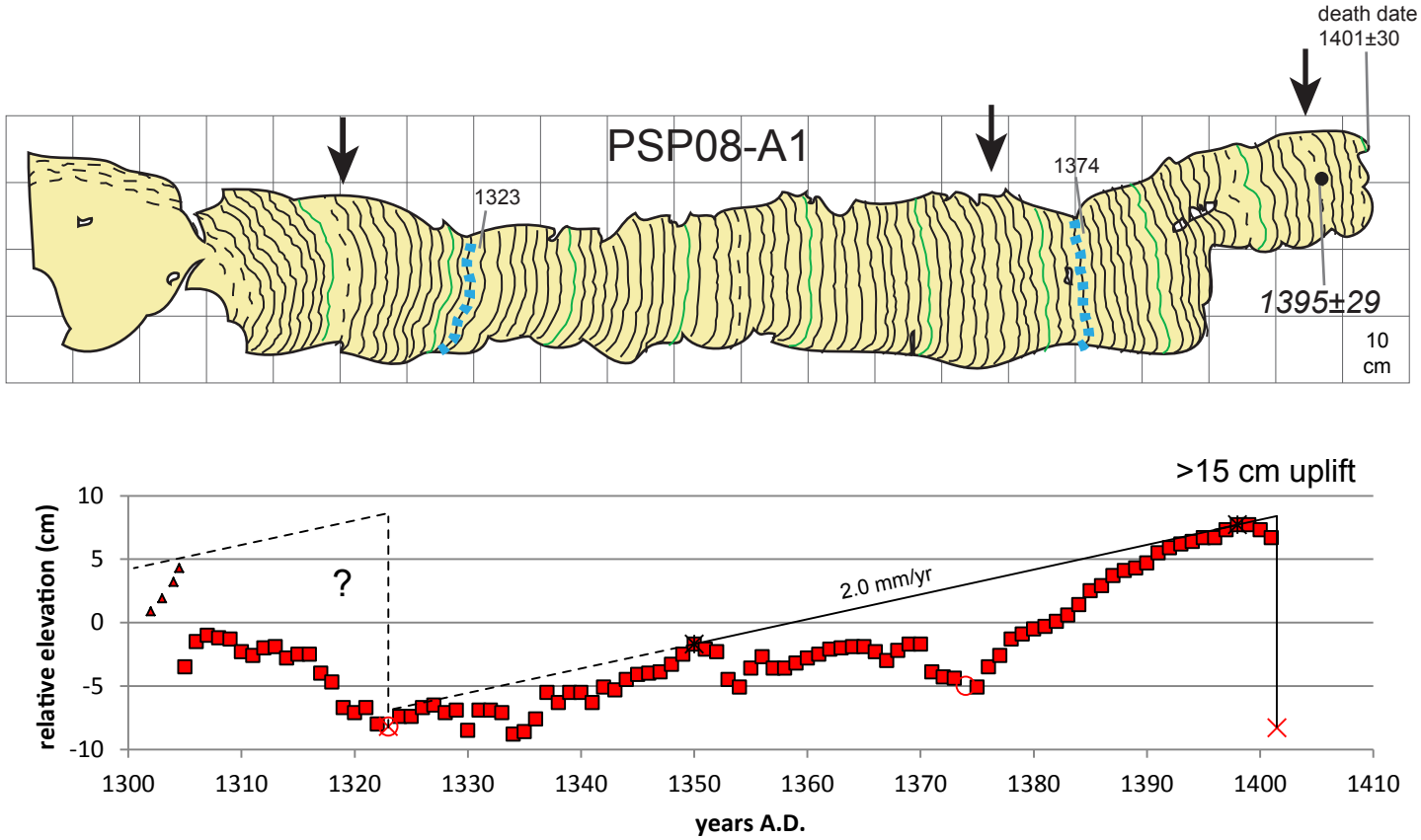

Figure 3.S2. Cross section and growth plot of PSP08-A1, a microatoll from Pasapuat. Symbology as in Fig. 3.S1. Since this microatoll was substantially eroded and no die-downs were clearly preserved, the interseismic subsidence rate cannot be estimated very precisely, but was clearly low (around 2 mm/yr). The first of the two inferred die-downs may have resulted from a tectonic uplift of ~15 cm in the early 1300s, since there appears to be an offset in the trend of the coral's growth. This record precludes a significant subsidence event at this site during the 1300s. This microatoll was probably uplifted and killed in the same tectonic event that killed corals at several other sites around A.D. 1390 [*Sieh et al.* 2008].

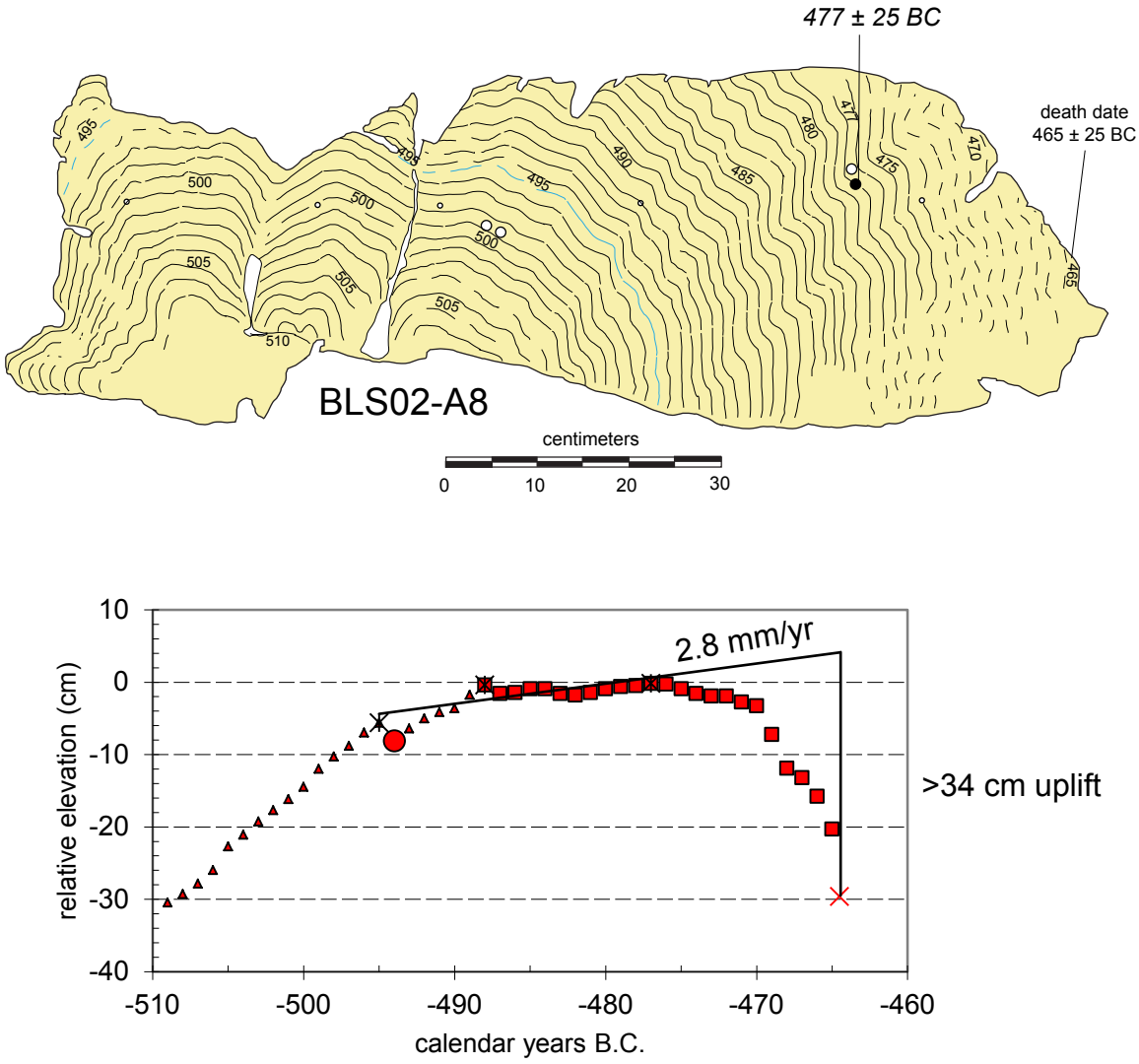

Figure 3.S3. Cross section and growth plot of BLS02-A8. Symbology as in Fig. 3.S1. Derived interseismic subsidence rate may be inaccurately low since only one climatic die-down is preserved in this record.

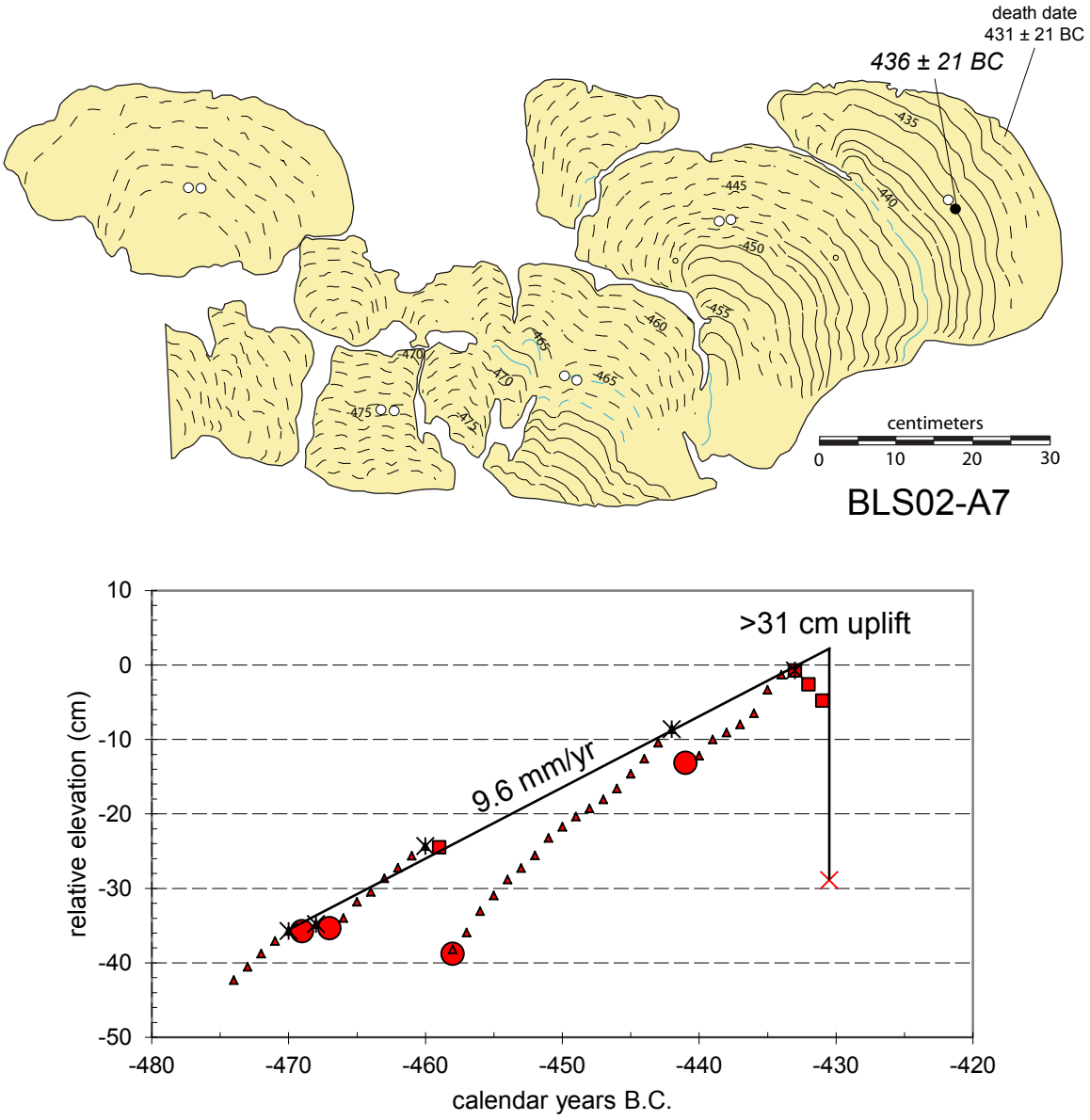

Figure 3.S4. Cross section and growth plot of BLS02-A7. Symbology as in Fig. 3.S1.

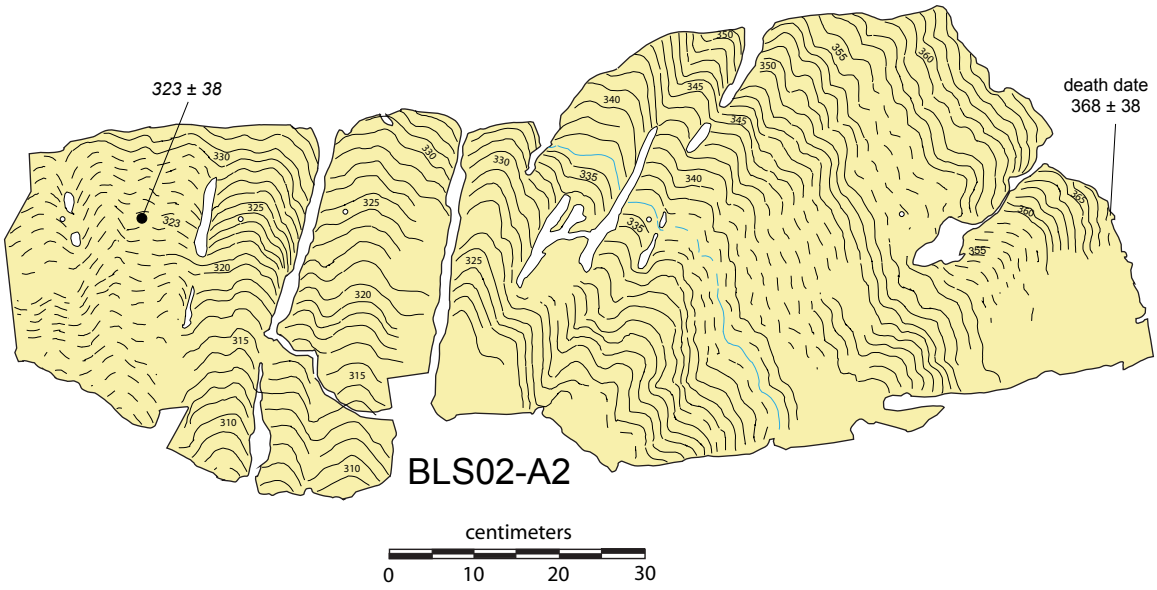

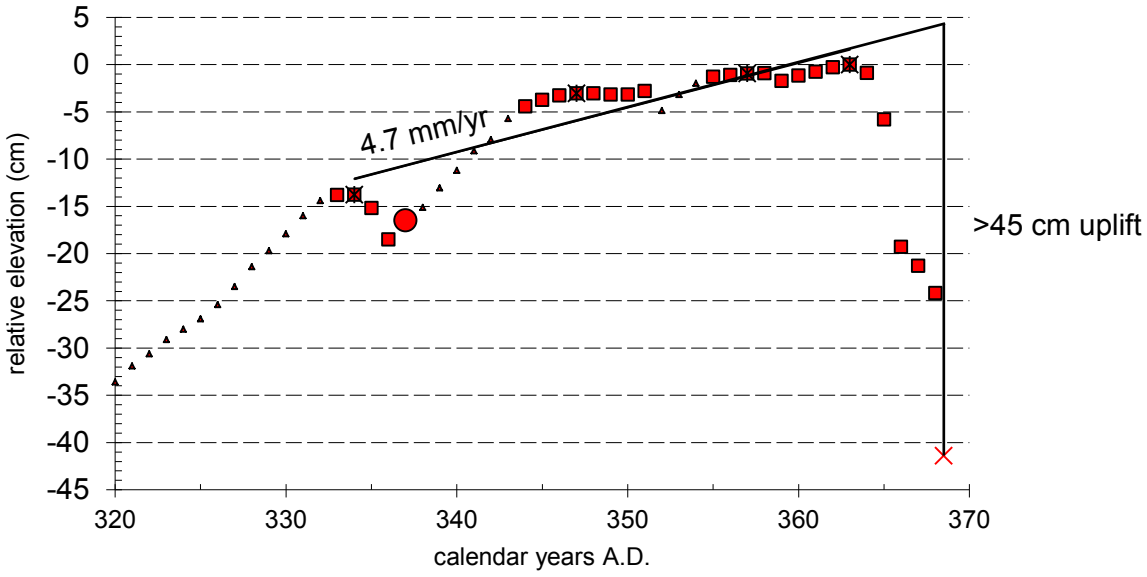

Figure 3.S5. Cross section and growth plot of BLS02-A2. Symbology as in Fig. 3.S1. Derived interseismic subsidence rate may be inaccurately low since only one climatic die-down is preserved in this record.

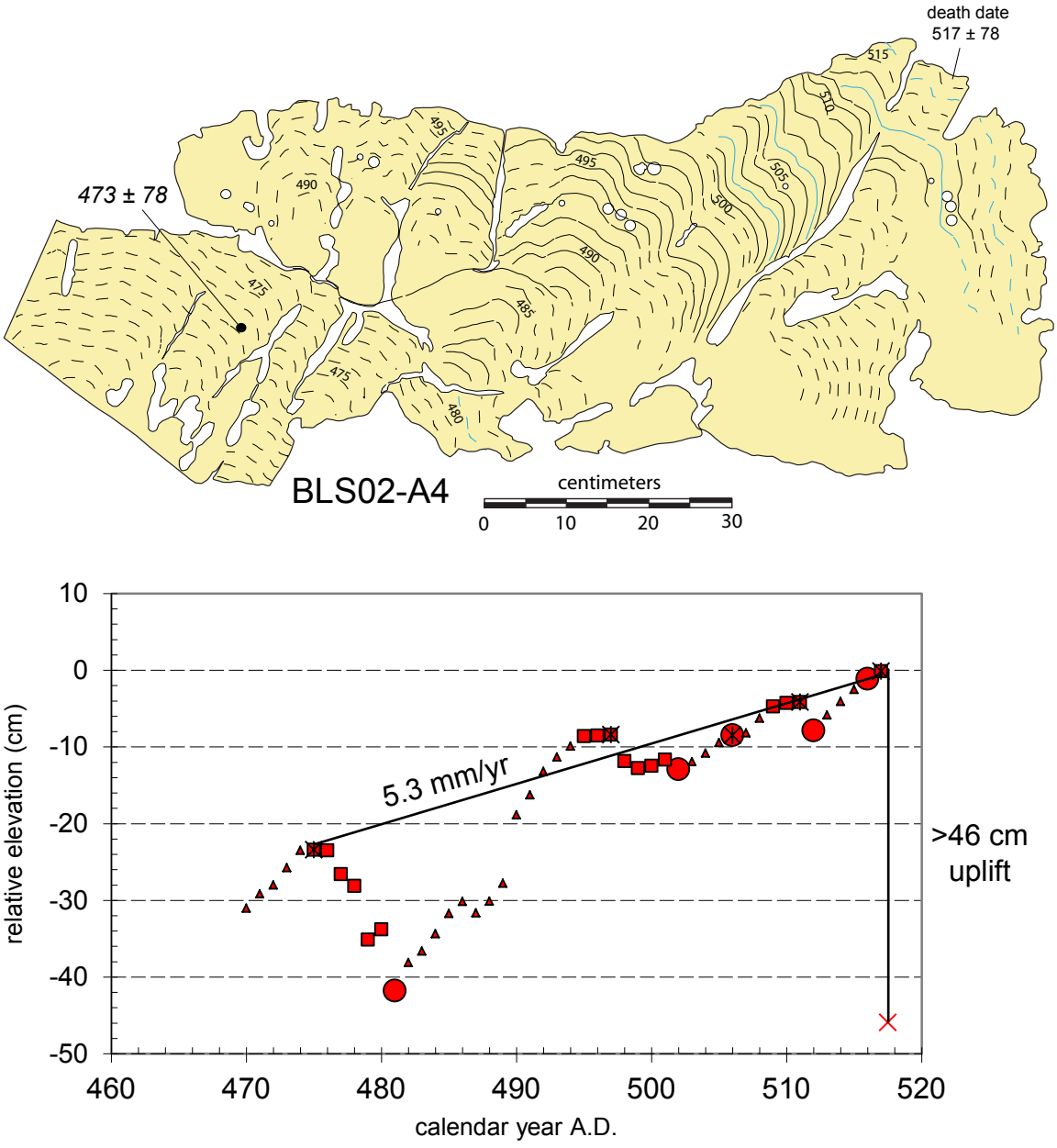

Figure 3.S6. Cross section and growth plot of BLS02-A4. Symbology as in Fig. 3.S1.

Table 3.S1. Uranium and thorium isotopic compositions and ^{230}Th ages of coral subsamples by MC-ICPMS with dates A.D.

Subsample	Weight	^{238}U	^{232}Th	δ^{234}U	[^{230}Th/^{238}U]	[^{230}Th/^{232}Th]	Age	Age	$\delta^{234}U_{initial}$	Calendar	Site
	g	ppb	ppt	measured[a]	activity[c]	ppm[d]	uncorrected	corrected [c,e]	corrected[b]	Year A.D.[f]	Name
PSR10-A3-1	0.1663	**2432.3 ± 2.3**	**4079.7 ± 9.8**	**146.1 ± 1.7**	**0.008112 ± 0.000080**	**79.85 ± 0.80**	**775.5 ± 7.7**	**713 ± 63**	**146.4 ± 1.7**	**1295 ± 63**	Pulau Pasir
PSR10-A3-3	0.0964	**2477.3 ± 5.7**	**1218.4 ± 7.6**	**147.9 ± 2.9**	**0.007636 ± 0.000068**	**256.3 ± 2.7**	**728.7 ± 6.8**	**710 ± 20**	**148.2 ± 2.9**	**1299 ± 20**	Pulau Pasir
PSR10-A3-core	0.1811	**2432.9 ± 2.0**	**3574 ± 12**	**144.2 ± 1.4**	**0.009228 ± 0.000096**	**103.7 ± 1.1**	**884.1 ± 9.2**	**829 ± 56**	**144.6 ± 1.4**	**1179 ± 56**	Pulau Pasir
PSR08-A1-1	0.0943	**2055.6 ± 1.6**	**2968.4 ± 8.7**	**145.7 ± 1.6**	**0.002437 ± 0.000072**	**27.86 ± 0.82**	**232.5 ± 6.8**	**178 ± 55**	**145.7 ± 1.6**	**1830 ± 55**	Pulau Pasir
PSR08-A2-5-1	0.1108	**2562.7 ± 3.2**	**4843 ± 11**	**146.8 ± 2.0**	**0.003544 ± 0.000084**	**30.96 ± 0.74**	**338.0 ± 8.0**	**267 ± 71**	**146.9 ± 2.0**		
PSR08-A2-5-2	0.1033	**2470.4 ± 2.7**	**4805 ± 12**	**147.0 ± 1.5**	**0.003527 ± 0.000097**	**29.94 ± 0.82**	**336.3 ± 9.2**	**263 ± 74**	**147.1 ± 1.5**		
PSR08-A2-5-3	0.0956	**2577.9 ± 3.7**	**4933 ± 12**	**147.2 ± 1.9**	**0.003525 ± 0.000074**	**30.42 ± 0.64**	**336.1 ± 7.1**	**264 ± 72**	**147.3 ± 1.9**		
							wt-averaged age	***265 ± 42***		**1744 ± 42**	Pulau Pasir
PSP08-A1-1	0.1310	**2503.0 ± 2.1**	**1095.9 ± 5.5**	**144.5 ± 1.6**	**0.003666 ± 0.000044**	**138.3 ± 1.8**	**641.5 ± 5.8**	**613 ± 29**	**144.7 ± 1.6**	**1395 ± 29**	Pasapuat

Table 3.S2. Uranium and thorium isotopic compositions and ^{230}Th ages of coral subsamples by MC-ICPMS with ages B.P. (before 1950 A.D.)

Subsample	Weight g	^{238}U ppb	^{232}Th ppt	δ^{234}U measured[a]	[^{230}Th/^{238}U] activity[c]	[^{230}Th/^{232}Th] ppm[d]	Age uncorrected	Age corrected [c,e]	$\delta^{234}U_{initial}$ corrected[b]	Age B.P.	Site Name
SMS10-A1-1	0.1027	**2398.6 ± 3.2**	**202.7 ± 6.8**	**147.0 ± 2.2**	**0.07102 ± 0.00016**	**13875 ± 465**	**6,970 ± 21**	**6,967 ± 21**	**149.9 ± 2.3**	**6906 ± 21**	Pulau Simasin
SRB02-A1	0.3948	**2721.0 ± 2.4**	**963.1 ± 2.2**	**140.9 ± 1.1**	**0.05275 ± 0.00013**	**2460.8 ± 7.8**	**5,164 ± 14**	**5,151 ± 19**	**143.0 ± 1.1**	**5098 ± 19**	Sarabua
SRB10-B4-1	0.1058	**2475.2 ± 3.2**	**1931 ± 10**	**145.4 ± 1.7**	**0.04876 ± 0.00021**	**1032.2 ± 6.9**	**4,746 ± 22**	**4,717 ± 37**	**147.4 ± 1.7**	**4657 ± 37**	Sarabua
SRB10-B2-1	0.1135	**2621.7 ± 9.4**	**2690 ± 11**	**147.3 ± 4.3**	**0.06531 ± 0.00033**	**1051.0 ± 5.7**	**6,393 ± 41**	**6,355 ± 56**	**150.0 ± 4.4**	**6295 ± 56**	Sarabua
SRB10-B1-1	0.1255	**2436.8 ± 8.2**	**2378 ± 11**	**148.6 ± 4.2**	**0.06729 ± 0.00035**	**1138.8 ± 6.9**	**6,584 ± 43**	**6,548 ± 57**	**151.4 ± 4.3**	**6488 ± 57**	Sarabua
MLK10-A1-1	0.1044	**2484.6 ± 9.2**	**2847 ± 12**	**145.0 ± 4.2**	**0.04222 ± 0.00023**	**608.5 ± 3.4**	**4,100 ± 27**	**4,057 ± 51**	**146.7 ± 4.2**	**3997 ± 51**	Malilimok
KMJ10-A1-1	0.1259	**2241.4 ± 5.2**	**40397 ± 263**	**148.7 ± 2.6**	**0.04349 ± 0.00072**	**39.84 ± 0.70**	**4,211 ± 72**	**3,535 ± 682**	**150.2 ± 2.6**	**3475 ± 682**	Pulau Karangmadjat
TRT10-A3-1	0.1163	**2562.6 ± 5.2**	**20408 ± 92**	**147.1 ± 2.3**	**0.02886 ± 0.00037**	**59.82 ± 0.81**	**2,781 ± 37**	**2,482 ± 301**	**148.1 ± 2.3**	**2422 ± 301**	Trait
TRT10-A2-1	0.1080	**2429.6 ± 6.0**	**20402 ± 94**	**145.6 ± 2.8**	**0.03085 ± 0.00037**	**60.65 ± 0.77**	**2,979 ± 37**	**2,664 ± 318**	**146.7 ± 2.8**	**2604 ± 318**	Trait
SKC08-D6	0.22386	**2571.0 ± 3.5**	**434.8 ± 3.2**	**146.7 ± 2.0**	**0.05277 ± 0.00011**	**5152 ± 38**	**5,140 ± 14**	**5,134 ± 16**	**148.9 ± 2.0**	**5076 ± 16**	Sikici
SKC08-D7	0.1945	**2571.5 ± 2.0**	**926.9 ± 3.9**	**144.4 ± 1.3**	**0.05727 ± 0.00013**	**2623 ± 13**	**5,600 ± 15**	**5,587 ± 20**	**146.7 ± 1.3**	**5529 ± 20**	Sikici
SKC08-D3-2-1	0.1055	**2314.2 ± 4.3**	**1063.2 ± 6.8**	**147.5 ± 2.4**	**0.06295 ± 0.00019**	**2262 ± 15**	**6,154 ± 23**	**6,137 ± 29**	**150.1 ± 2.5**		
SKC08-D3-2-2	0.1020	**2164.9 ± 2.4**	**909.1 ± 6.9**	**147.8 ± 1.6**	**0.06331 ± 0.00017**	**2489 ± 20**	**6,188 ± 19**	**6,173 ± 24**	**150.4 ± 1.6**		
							wt-averaged age	***6,157 ± 19***		**6098 ± 19**	Sikici
SKC08-D5	0.2846	**2202.6 ± 1.6**	**1224.5 ± 3.3**	**144.7 ± 1.4**	**0.06332 ± 0.00016**	**1880.5 ± 6.8**	**6,207 ± 18**	**6,186 ± 27**	**147.2 ± 1.4**	**6128 ± 27**	Sikici
SKC08-D4-2	0.1136	**2835.7 ± 4.8**	**85.3 ± 6.1**	**147.4 ± 2.0**	**0.06933 ± 0.00017**	**38050 ± 2734**	**6,798 ± 21**	**6,797 ± 21**	**150.2 ± 2.0**	**6738 ± 21**	Sikici
SGG03-A5	0.3900	**2601.3 ± 2.1**	**489.2 ± 1.9**	**147.7 ± 1.1**	**0.027767 ± 0.000087**	**2438 ± 12**	**2,673.1 ± 8.9**	**2,666 ± 11**	**148.8 ± 1.1**	**2612 ± 11**	Singingi
BSA03-A1	0.3670	**2316.4 ± 2.6**	**617.3 ± 2.1**	**144.8 ± 1.4**	**0.024009 ± 0.000086**	**1487.7 ± 7.2**	**2,313.6 ± 8.8**	**2,308.4 ± 9.1**	**145.7 ± 1.4**	**2254.4 ± 9.1**	Basua

Analytical errors are 2σ of the mean.

[a] $\delta^{234}U = ([^{234}U/^{238}U]_{activity} - 1) \times 1000$.

[b] $\delta^{234}U_{initial}$ corrected was calculated based on ^{230}Th age (T), i.e., $\delta^{234}U_{initial} = \delta^{234}U_{measured} X\ e^{\lambda 234 * T}$, and T is corrected age.

[c] $[^{230}Th/^{238}U]_{activity} = 1 - e^{-\lambda_{230} T} + (\delta^{234}U_{measured}/1000)[\lambda_{230}/(\lambda_{230} - \lambda_{234})](1 - e^{-(\lambda_{230} - \lambda_{234}) T})$, where T is the age.

Decay constants are 9.1577 x 10^{-6} yr^{-1} for ^{230}Th, 2.8263 x 10^{-6} yr^{-1} for ^{234}U (Cheng et al., 2000), and 1.55125 x 10^{-10} yr^{-1} for ^{238}U (Jaffey et al., 1971) .

[d] The degree of detrital ^{230}Th contamination is indicated by the [^{230}Th/^{232}Th] atomic ratio instead of the activity ratio.

[e] Age corrections were calculated using an estimated atomic ^{230}Th/^{232}Th ratio of 6.5 ± 6.5 ppm (Zachariasen et al., 1999).

[f] Calculated by subtracting the corrected sample age from the year of chemical analysis.

References

Cheng, H., R. L. Edwards, J. Hoff, C. D. Gallup, D. A. Richards, and Y. Asmerom (2000), The half-lives of uranium-234 and thorium-230, *Chemical Geology , 169,* 17-33.

Jaffey, A. H., K. F. Flynn, L. E. Glendenin, W. C. Bentley, and A. M. Essling (1971), Precision measurements of half-lives and specific activities of ^{235}U and ^{238}U, *Physical Review C , 4* , 1889-1906.

Zachariasen, J., K. Sieh, F. W. Taylor, R. L. Edwards, and W. S. Hantoro (1999), Submergence and uplift associated with the giant 1833 Sumatran subduction earthquake: Evidence from coral microatolls, *J. Geophys. Res. , 104* (B1), 895-919.

CHAPTER 4

OUTLINE OF THE 16TH–17TH-CENTURY SUPERCYCLE AND CONCLUSIONS

4.1 Microatolls from the 16th and 17th Centuries

In addition to the coral data covering the 14th, 18th–19th, and 20th centuries discussed in the previous chapters, we have also greatly expanded the dataset covering the rupture sequence that occurred in the late 16th to 17th centuries identified by *Sieh et al.* [2008]. Analysis of these data is not yet complete, but a picture has emerged of a rupture sequence distinctly different from the events of the 18th–19th centuries.

4.1.1 Site Locations

Eleven of our new microatoll collection sites have populations that date to the 16th–17th centuries: Sarabua and Muara Siberut on the east coast of Siberut; two sites on Pulau Panjang, a small island north of Sipora; North Pukarayat on the west coast of Sipora; Pasapuat on the north coast and Cimpungan on the east coast of North Pagai; Pulau Pecah Belah B, Pulau Kumbang, and Pulau Simungguk in the archipelago southeast of South Pagai; and a site on Sanding Island (Figure 4.1). Maps of each of these sites appear in Figures 4.2–4.12, except Simungguk which appears in Chapter 2. (Many of these sites also have populations of microatolls that died in 1797 and/or 1833, which were discussed in Chapter 2).

A notable common feature of several of these sites is a peaty mud layer which crops out beneath the beach, partially covering the field of fossil corals. Frequently, rotting

stumps of jungle trees are embedded in the peat. These peat layers are further confirmation of past coseismic uplifts which raised the coral platforms above high tide, transforming them into vegetated swamps where organic material could accumulate. Now, toward the end of the interseismic period, these peat layers have submerged into the intertidal zone, completing the cycle. We have never attempted to determine the age of these peats, but it seems likely that they accumulated in the 19th century after the uplifts in 1797 and 1833. Though at some sites they predominantly cover fields of 17th-century fossil corals, it seems unlikely that peat layers that accumulated in the 17th or early 18th centuries would have survived the submergence associated with the subsequent supercycle.

We have also reviewed and synthesized the microatoll records covering this time period presented by *Sieh et al.* [2008]. These come from Tabekat on northern Siberut, Pulau Masokut southeast of Siberut, the trio of Sikici sites on the east coast of Sipora, the two Simanganya sites on the north coast of North Pagai, Silabu on the west coast of North Pagai, and Bulasat and Saomang on the southwest side of South Pagai (Fig. 4.1). In combination with the new sites, we now have remarkably good coverage of all the Mentawai Islands during this time period.

4.1.2 Preliminary Interpretation

A notable feature of many of the microatolls from this time period is a conical hat shape, indicating a period of gradual uplift or several small uplifts closely spaced in time. Coral SMY02-A1 from Simanganya is the only previously published example with this

shape [*Sieh et al.*, 2008], but it is also a prominent feature of fossil microatoll populations at Pasapuat, Cimpungan, and Pecah Belah B (examples shown in Figure 4.13). The simplest interpretation, which is consistent with the radiometric ages, is that the period of uplift was contemporaneous at all of these sites. Consideration of all the radiometric ages suggests that the uplift started around 1590 and continued until at least 1630. Several other sites on Sipora and the Pagai Islands also have populations of microatolls that died or suffered large uplifts during the early part of this period (most notably Sikici), but do not exhibit the conical shape. Therefore, we infer that the uplift period included sudden, likely seismic events rather than gradual uplift. There appear to be at least three distinct events, in ~1597, ~1611, and ~1629.

The sequence of closely spaced uplifts was apparently limited to the southern Mentawais, as none of the microatolls from Siberut or northern Sipora exhibit the conical hat shape. All of the Siberut microatolls (as well as a few on Sipora) have ages consistent with death in ~1658, and numerous microatoll populations distributed between Sanding and northern Sipora have ages consistent with death in ~1703. These two later events seem more similar to the events of 1797 and 1833, completely killing the reefs at most of the sites where they manifest.

Given the radiometric ages, time intervals between uplift events, and allowance for erosion of the microatolls' outer surfaces, we are able to assign nearly all of the observed uplifts to one of these five dates (Table 4.1). A few microatolls at Sikici and Simanganya suggest an earlier uplift in ~1569, but the unperturbed growth of other nearby microatolls seems to contradict this hypothesis. The five-uplift scenario represents the smallest

number of events that can explain all of the data. In general, it is theoretically possible that uplifts with overlapping age uncertainties were not actually contemporaneous from one site to the next, but it is far more likely that a relatively small number of uplifts occurred, each affecting a large area. If an uplift happened at that time, it was clearly small and limited in geographic extent. Thanks to the combination of several particularly precise dates, the absolute age uncertainty of the entire scenario is quite small, about 10 years, and the relative timing of events is even more tightly constrained.

4.2 Four Differing Seismic Supercycles

Regardless of the accuracy of the details of the five-event scenario we propose, it is abundantly clear that the 16th–17th-century rupture sequence was more complex than the 1797/1833 doublet. There is no way to explain all of the data with only two events. Figure 4.14 is an updated version of the four-supercycles figure from *Sieh et al.* [2008], with ellipses indicating the approximate extents of the 16th- and 17th-century uplifts. The ~1703 event appears quite similar to the 1833 event. While the ~1658 event was similar to the 1797 event in the northwest, it apparently did not reach as far southeast and the overlap zone between uplift in ~1658 and ~1703 was limited to Sipora. The series of small-uplift events in the early 1600s provide a likely reason for this difference, as they primarily affected the Pagai Islands and can account for the southeastern half of the 1797 uplift area.

One of the most significant results of our study is the demonstration that each of the most recent four supercycle rupture sequences had unique features. While there is not

enough data from the 14th century to definitively state that there were only two events, there is no evidence for more than two. It is unclear whether there was any overlap between the uplift areas of the ~1350 and ~1380 events, and they certainly did not overlap on Sipora or North Pagai. While each of the three complete rupture sequences included a primary northwestern and a primary southeastern event, we can state with reasonable confidence that the zones of overlap differed in each case.

The 14th-century rupture sequence was preceded by a shallow rupture in ~1314 which produced substantial sudden subsidence on the southwest coast of South Pagai (see Chapter 3), likely a unique event over the past 700 years. The 2010 shallow rupture in the same vicinity confirms the propensity of the South Pagai area for shallow megathrust ruptures, but the 2010 event was not a repeat of 1314 as it produced little or no coseismic subsidence on the islands. The multiple closely spaced small uplifts during the early 1600s are similarly unique to that period; there are no other coral records from any other time period which have similar features.

So far, the modern rupture sequence does not closely resemble any of its three most recent predecessors. The termination of uplift in 2007 between South and North Pagai is reminiscent of the ~1350 event, but the scattering of multiple relatively small uplifts has a similar character to the events of the early 1600s. However, one caveat we must make is that the 2007–2008 rupture series violates our previous assumption that a single widespread uplift event is more likely than multiple local, non-contemporaneous uplifts over a short time period. If the 2007–2008 rupture series had occurred in the time before historical earthquake records, based on coral data we would almost certainly interpret all

four distinct uplift patches as a contemporaneous single event. Therefore, the ~1597 uplift (which covers approximately the same area as the combined modern uplifts) might actually have been an analogue of 2007–2008. Regardless, we can expect further uplift of the Pagai Islands and Sipora, and most certainly of Siberut, before the modern rupture sequence is complete.

All of our observations—the changes in interseismic coupling during a failure sequence, substantial zones of rupture overlap that vary significantly from one supercycle to the next, and fundamental differences in character between rupture sequences—support the conclusion that the frictional properties of the megathrust beneath the southern Mentawai Islands are quite heterogeneous. Fault models with heterogeneous frictional properties can reproduce the observed types of behavior [*Kaneko et al.*, 2010]. Calling to mind the pithy saying "nothing is certain but change," the only constant factor across the four supercycles is the variability of behavior. This characteristic presents a definite challenge for detailed earthquake and tsunami forecasting. However, having knowledge of the full range of potential behavior derived from a long paleoseismic record enables us to estimate worst-case and most likely scenarios, and is unquestionably a great advantage for disaster preparedness and resiliency planning.

References

Abram, N. J., M. K. Gagan, M. T. McCulloch, J. Chappell, and W. S. Hantoro (2003), Coral reef death during the 1997 Indian Ocean Dipole linked to Indonesian wildfires, *Science*, *301*, 952–955.

Kaneko, Y., J.-P. Avouac, and N. Lapusta (2010), Towards inferring earthquake patterns from geodetic observations of interseismic coupling, *Nature Geoscience*, *3*, 363–369.

Sieh, K., D. H. Natawidjaja, A. J. Meltzner, C.-C. Shen, H. Cheng, K.-S. Li, B. W. Suwargadi, J. Galetzka, B. Philibosian, and R. L. Edwards (2008), Earthquake supercycles inferred from sea-level changes recorded in the corals of west Sumatra, *Science*, *322*, 1674–1678.

Zachariasen, J. (1998), Paleoseismology and paleogeodesy of the Sumatran subduction zone: A study of vertical deformation using coral microatolls, Ph.D. thesis, 418 pp., Calif. Inst. of Technol., Pasadena, CA.

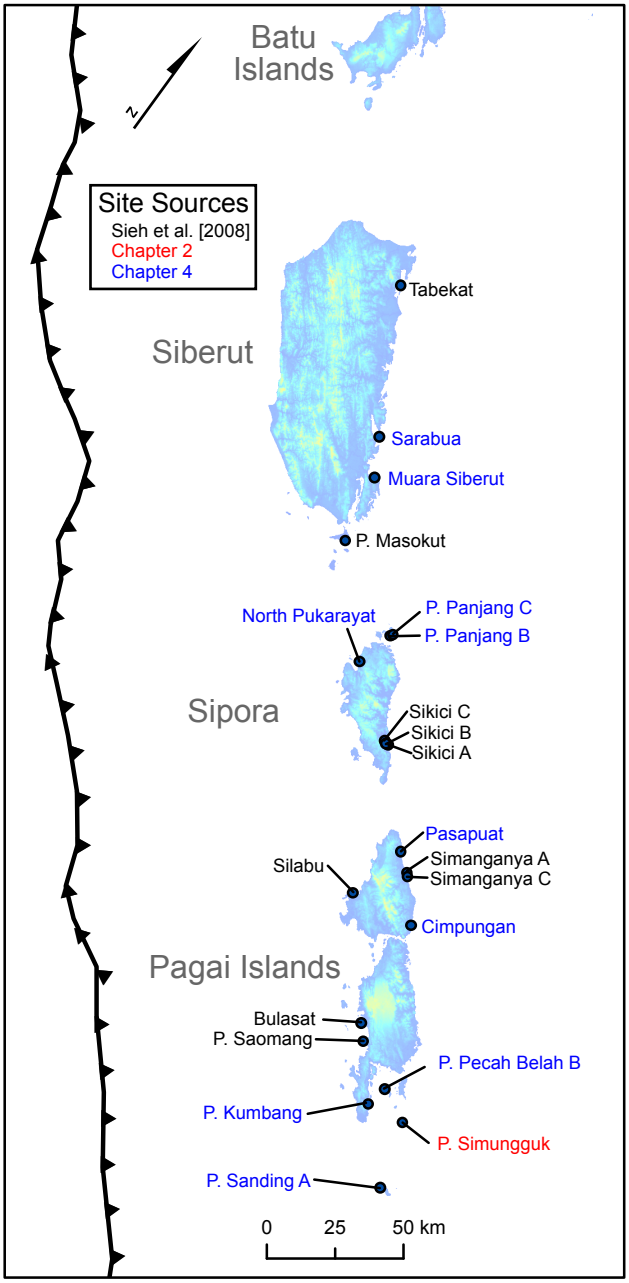

Figure 4.1. Index map of the Mentawai Islands showing sites with microatolls dating to the 16th–17th centuries.

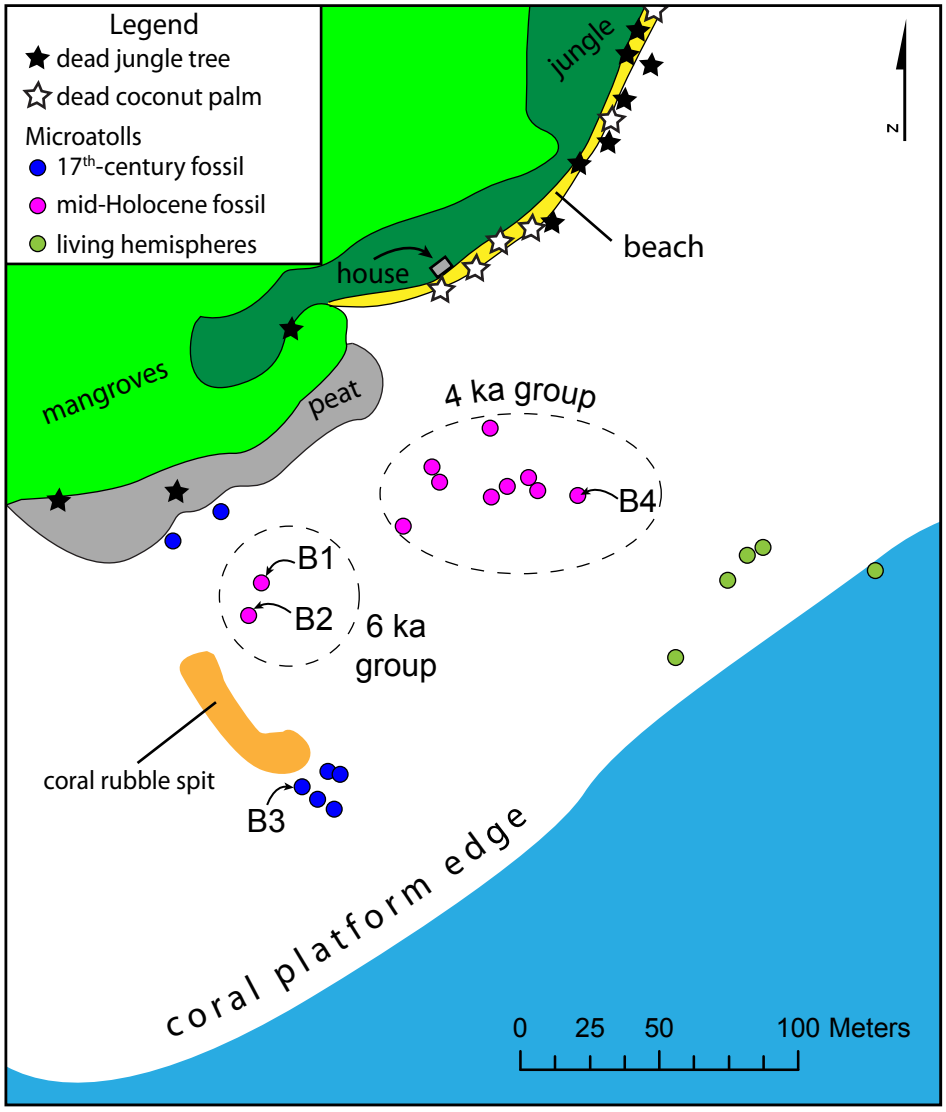

Figure 4.2. Map of Sarabua, a site on an islet in a large bay on the east coast of Siberut. Two populations of remarkably well-preserved mid-Holocene microatolls lie in the middle of the coral platform (dates discussed in Chapter 3). B3 comes from a population of *Goniastrea* microatolls that died in the 17th century. A peat layer and numerous dead trees along the beach are evidence of an ancient coseismic uplift and subsequent subsidence. Due to slow recovery from the extensive death of the reefs in this area during the catastrophic 1997–1998 IOD event and phytoplankton bloom [*Abram et al.* 2003], the living corals at this site in 2010 had not yet reached HLS and become microatolls.

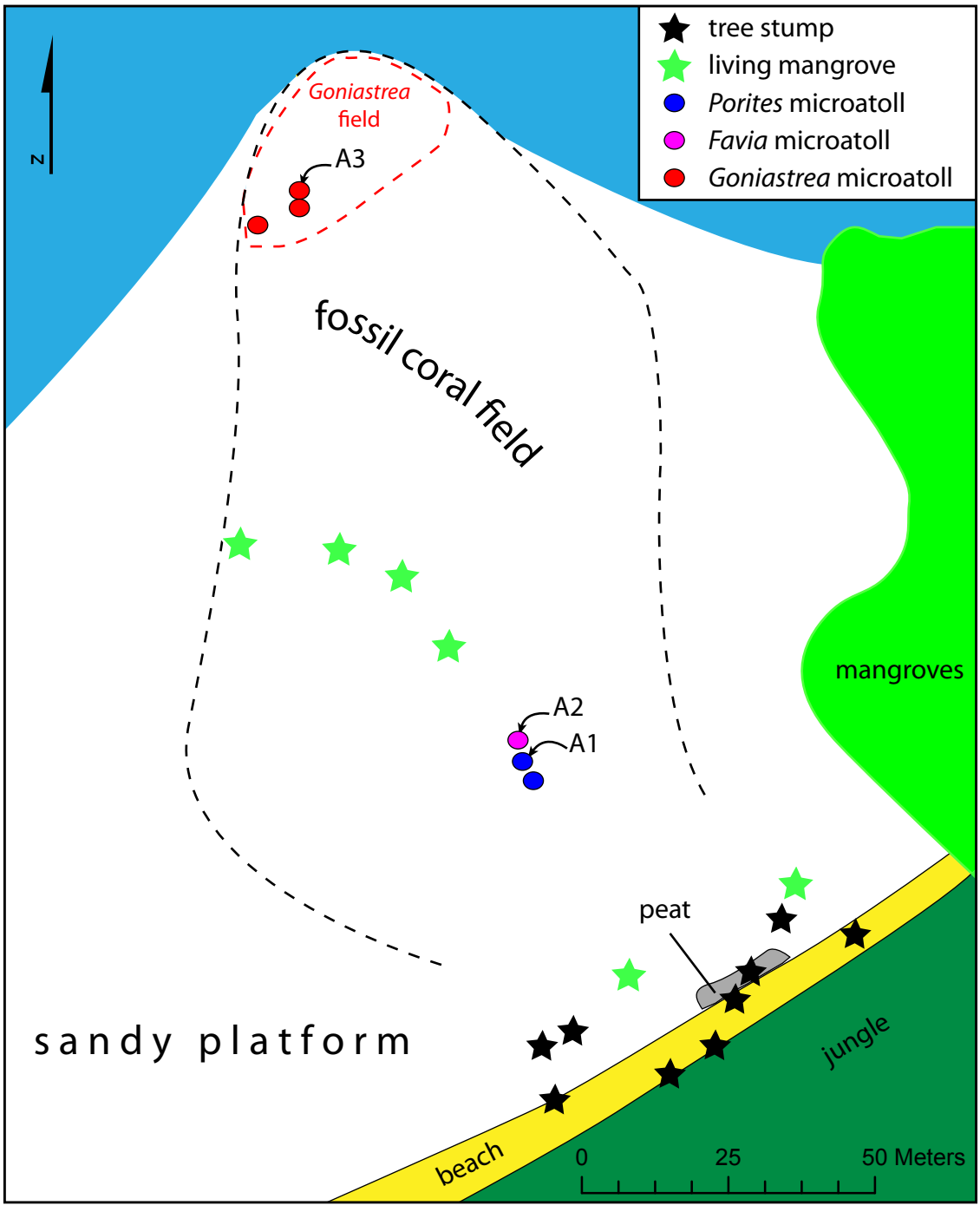

Figure 4.3. Map of Muara Siberut site on the east coast of Siberut. All the fossil corals at this site died in the 17th century. As at many other sites, remnants of a peat layer and stumps of jungle trees attest to a period when the coral platform was raised above the intertidal zone, and subsequent subsidence. A nearby stream outlet flooded this area with sand and prevented the growth of modern corals.

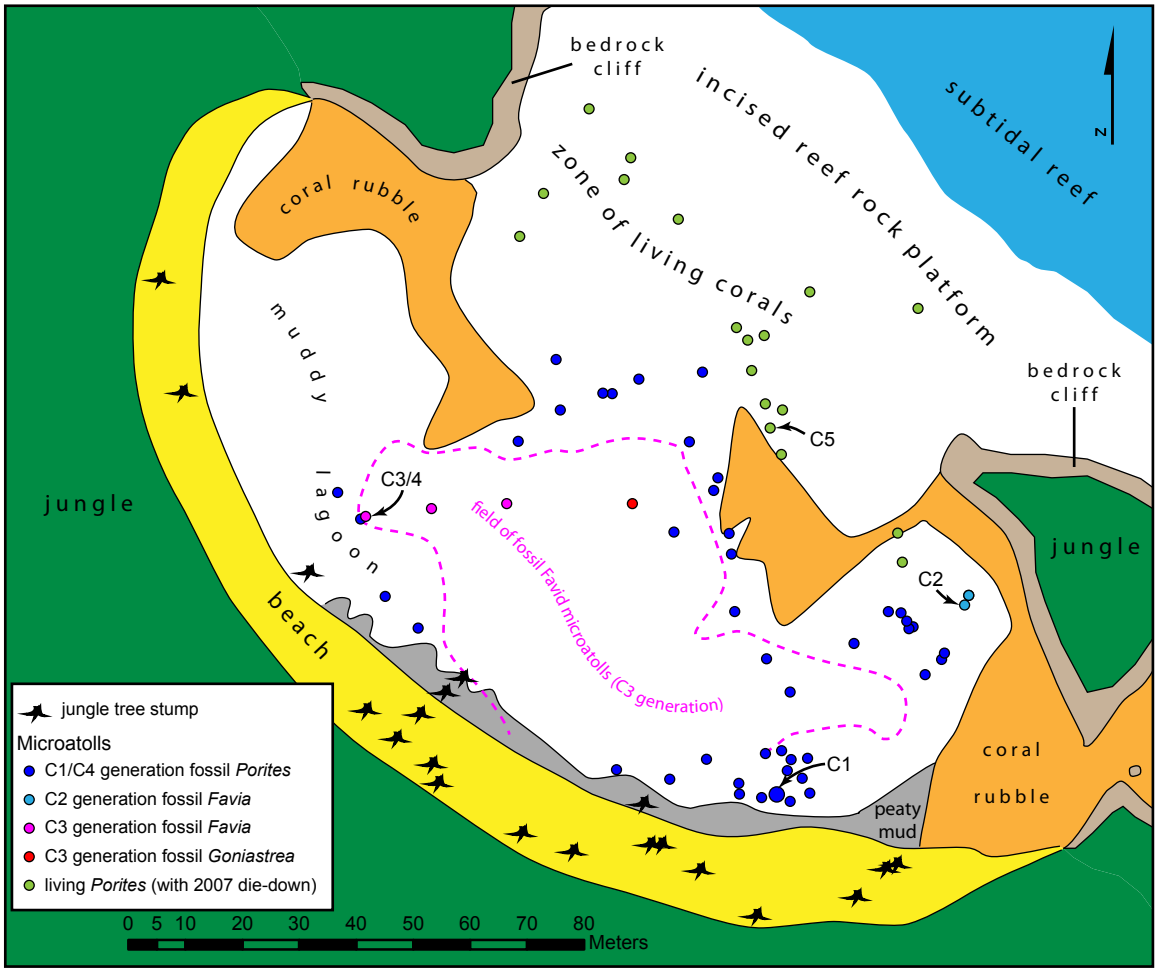

Figure 4.4. Map of Pulau Panjang site C, a bay on a small island north of Sipora. A peat layer and many tree stumps are evidence of an ancient coseismic uplift that raised the coral platform above the intertidal zone, and subsequent interseismic subsidence. The younger, higher generation of fossil Favid microatolls grew on top of the older, lower fossil *Porites* generation. The C3 generation died due to uplift during the 1797 earthquake (see Chapter 2). The C1/C4 and C2 generations died during the late 16th and mid-17th centuries, respectively.

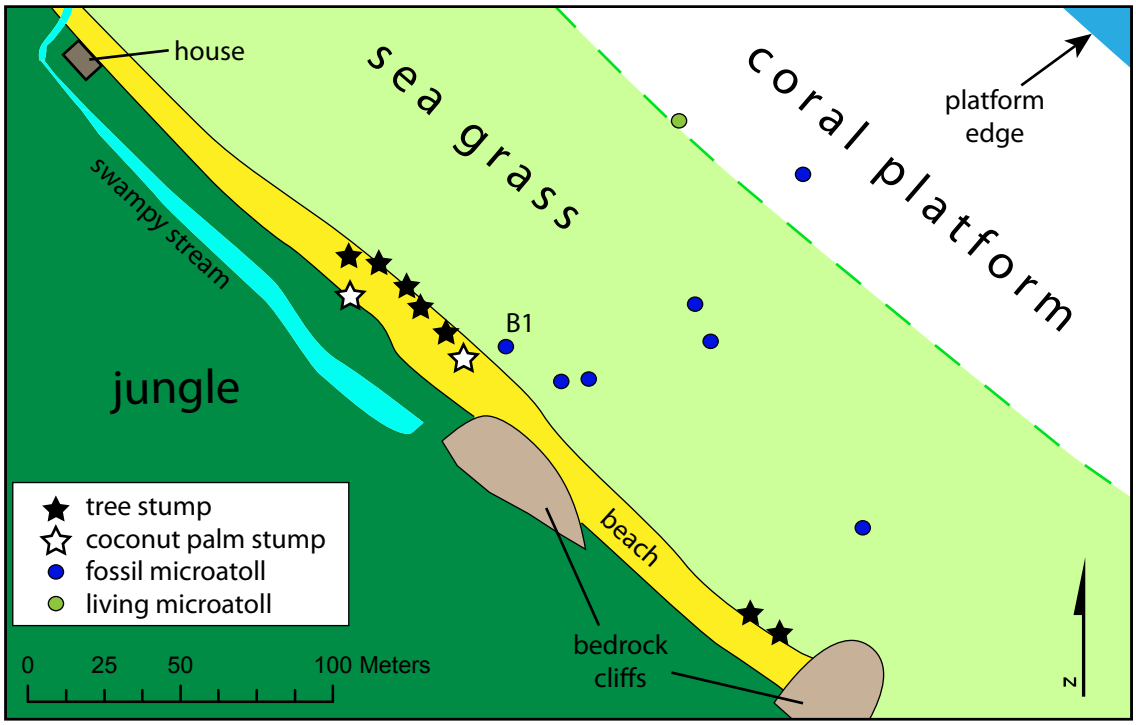

Figure 4.5. Map of Pulau Panjang site B, on a small island north of Sipora. Many tree stumps in the beach are evidence of recent interseismic subsidence. The single population of fossil corals at this site died in the late 16th century.

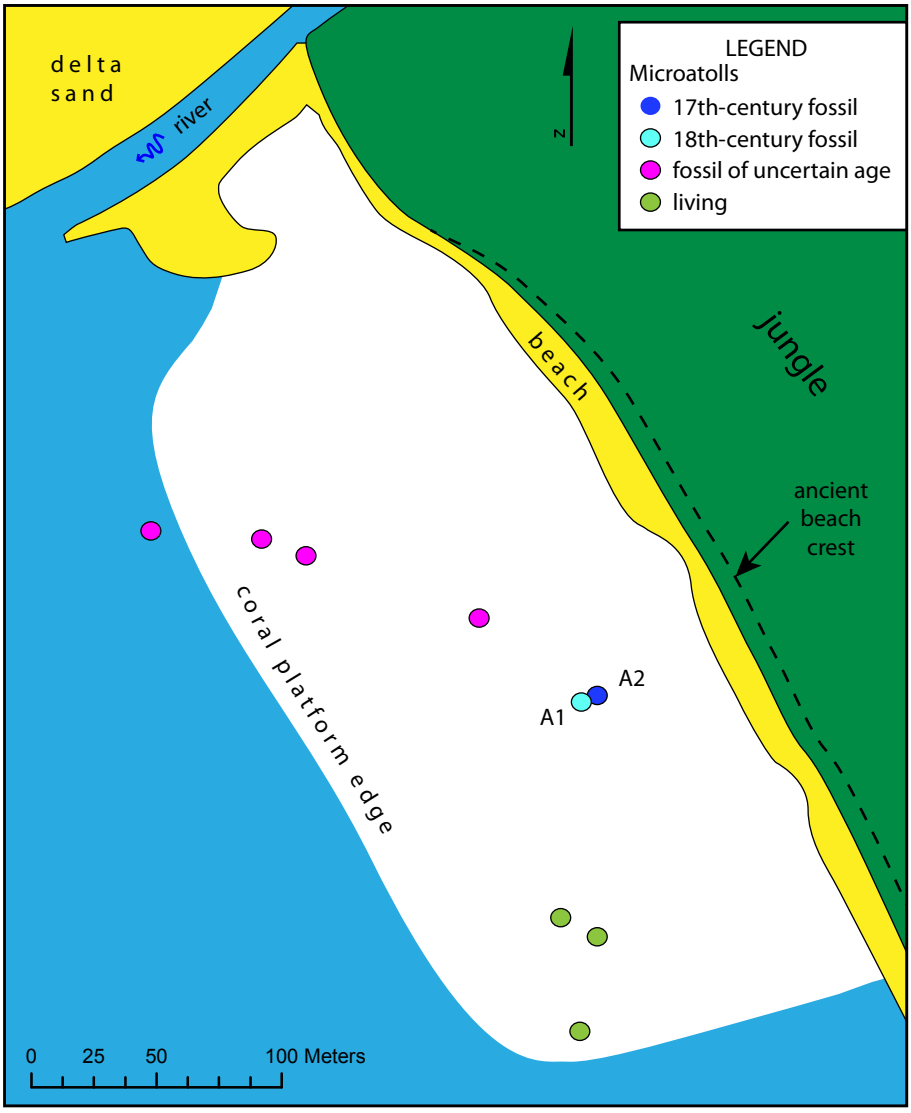

Figure 4.6. Map of North Pukarayat on the northwest coast of Sipora. Most fossil microatolls at this location were tilted and eroded, so it is unclear whether they were the same generation as A1 or A2. A2 died in the 18th century and was discussed in Chapter 2; A1 died in the 17th century and has a hat shape indicating two uplift events. An ancient beach crest likely corresponds to one of the two populations of fossil microatolls.

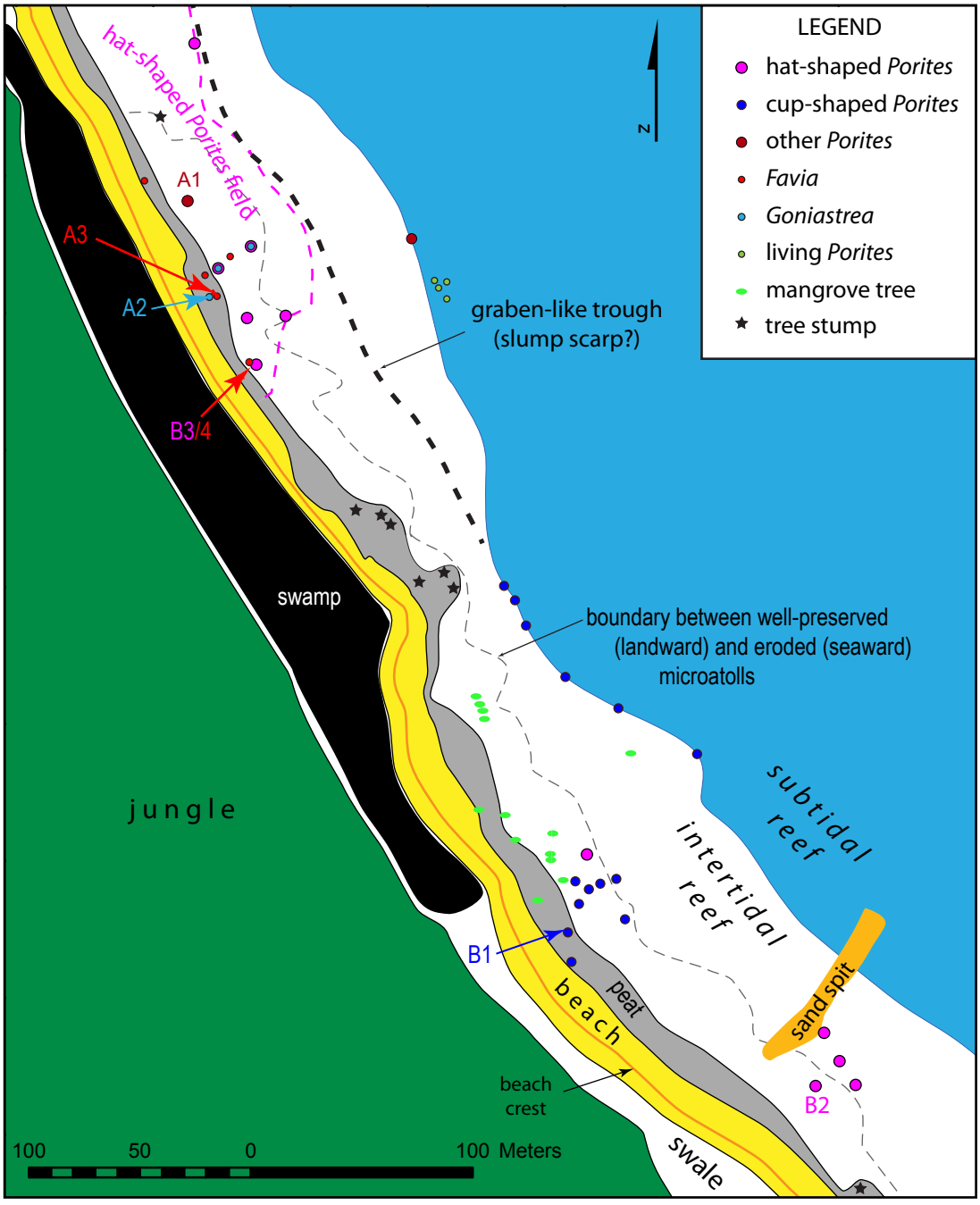

Figure 4.7. Map of Pasapuat on the northeast coast of North Pagai. A peat layer and embedded jungle tree stumps are evidence of a past coseismic uplift which raised the coral platform above the intertidal zone, and subsequent interseismic subsidence. The peat likely originally extended to the boundary between well-preserved and eroded microatolls, protecting the landward corals from erosion. Microatoll A1 and others of its generation died due to coseismic uplift in ~1390 (see Chapter 3). A2 and A3, which were directly covered by the peat, died due to uplift during the 1833 earthquake (see Chapter 2). All other microatolls died at different times during the 17th century.

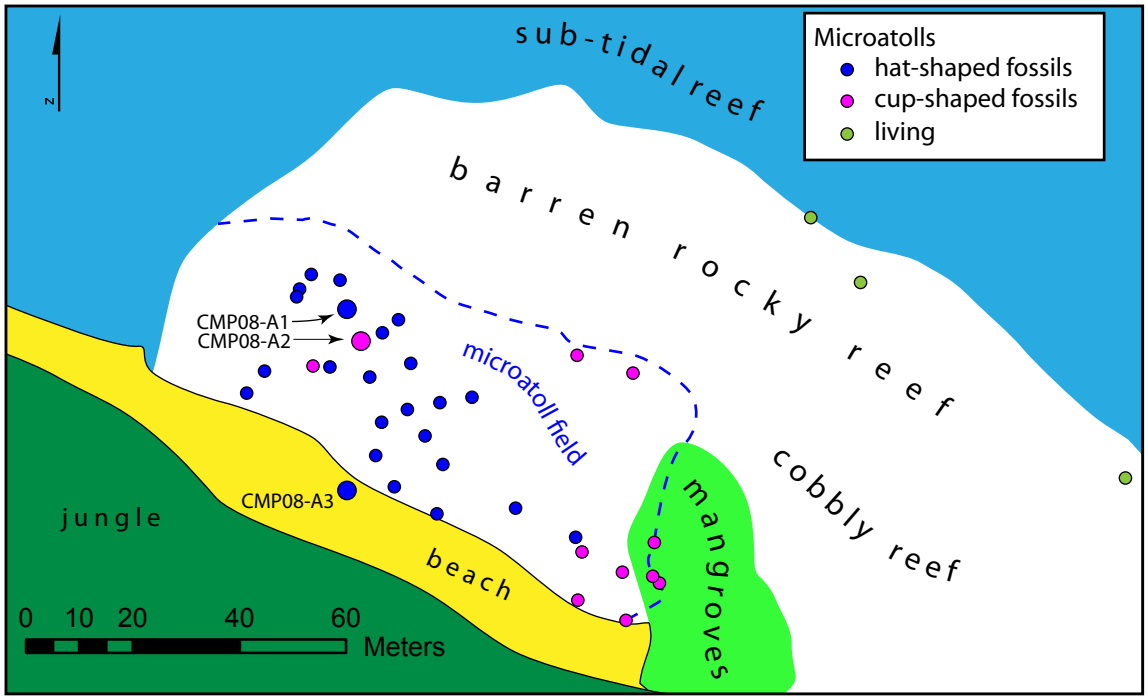

Figure 4.8. Map of Cimpungan site A on the east coast of North Pagai. The hat-shaped generation died during the early 17th century and the cup-shaped generation died in the early 18th century.

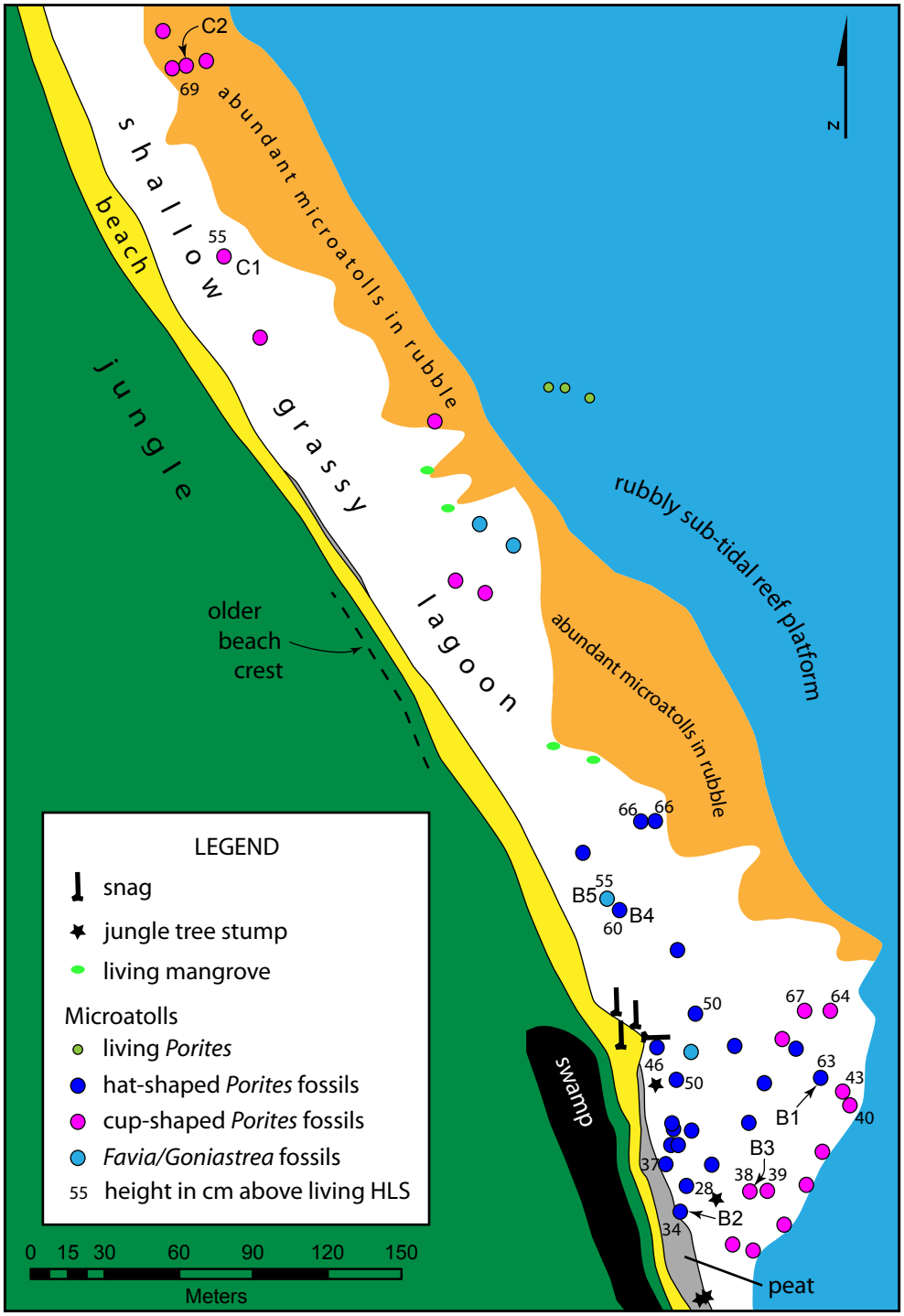

Figure 4.9. Map of Cimpungan sites B and C on the east coast of North Pagai. The peat eroding from beneath the beach likely accumulated after a major coseismic uplift, covering and preserving many microatolls. Jungle trees grew on the coral platform at that time, but have since drowned due to interseismic subsidence. Surveyed elevations of microatolls illustrate that many have settled into the muddy substrate, particularly toward the southern end of the microatoll field. An old beach crest may correspond to the population of fossil microatolls. All the microatolls collected here died during the 17th century.

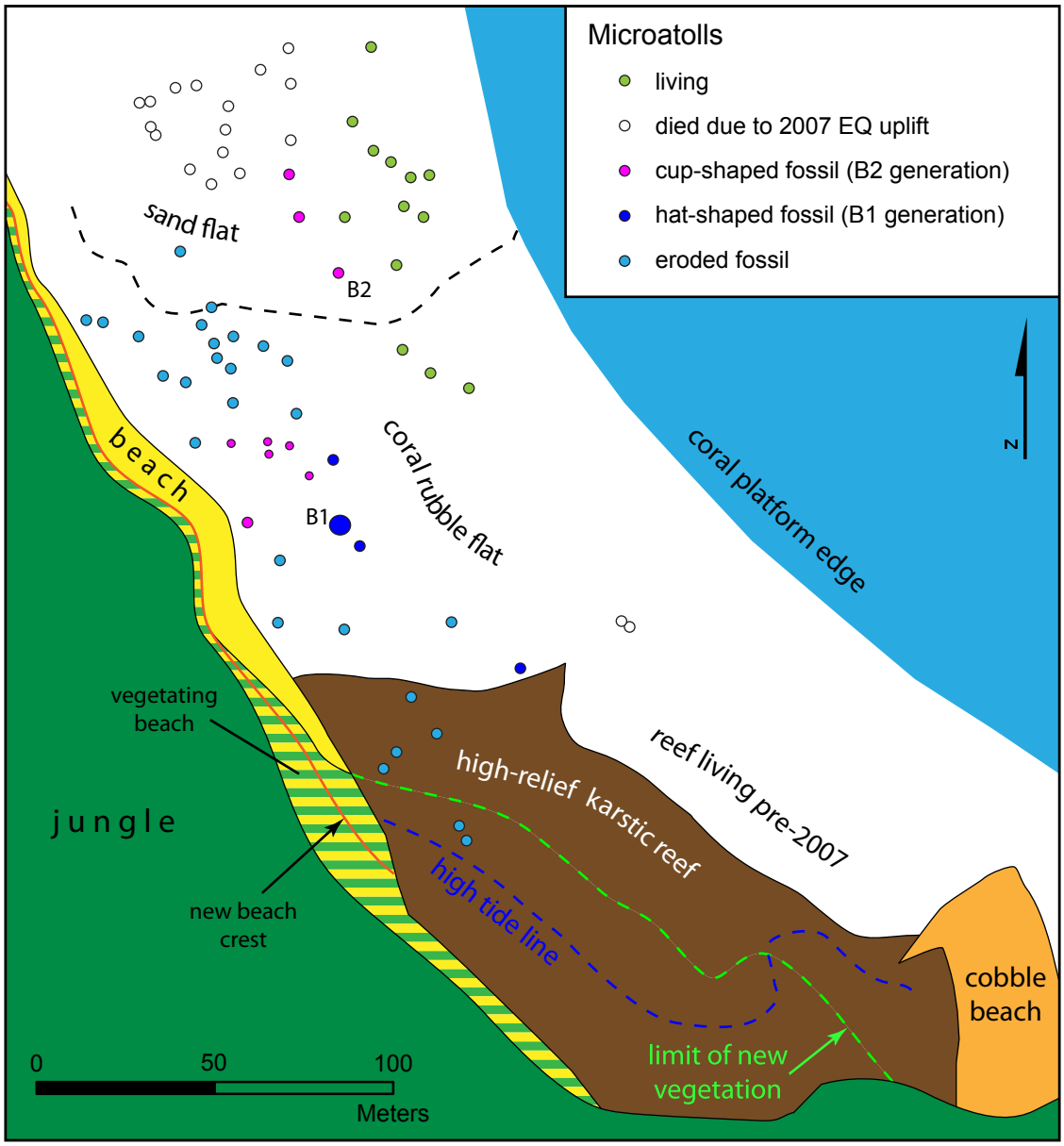

Figure 4.10. Map of Pecah Belah site B, on a small island in the South Pagai archipelago. Uplift during the 2007 earthquake (68 cm) killed much of the reef at this site and permitted vegetation to establish on the old beach and former intertidal zone. The younger cup-shaped generation of fossil microatolls (B2 group) died due to uplift during the 1833 earthquake (see Chapter 2). The B1 generation is the same group sampled by *Zachariasen* [1998] as P96L1, later mis-located by *Sieh et al.* [2008] on Taitanopo Island, which died at the beginning of the 18th century.

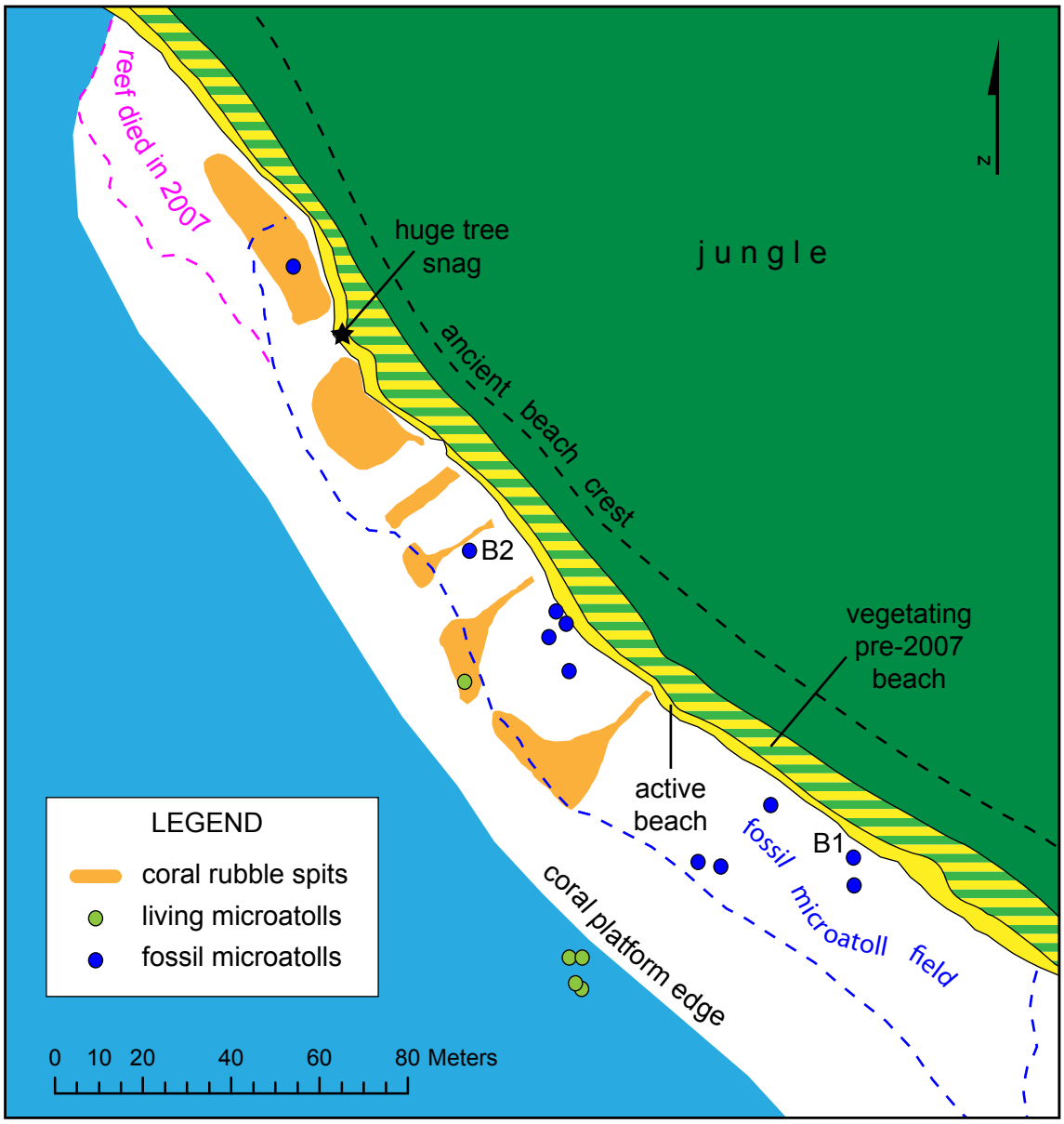

Figure 4.11. Map of Pulau Kumbang site, on a small islet in the South Pagai archipelago. Coseismic uplift in 2007 killed much of the living reef and permitted vegetation growth over most of the beach. A broad swath of cup-shaped fossil microatolls died (presumably also due to coseismic uplift) in about 1700. An ancient beach crest likely corresponds to this fossil population. This fossil population is the same group sampled by *Zachariasen* [1998] as P96M1, later mis-located by *Sieh et al.* [2008] on Siatanusa Island.

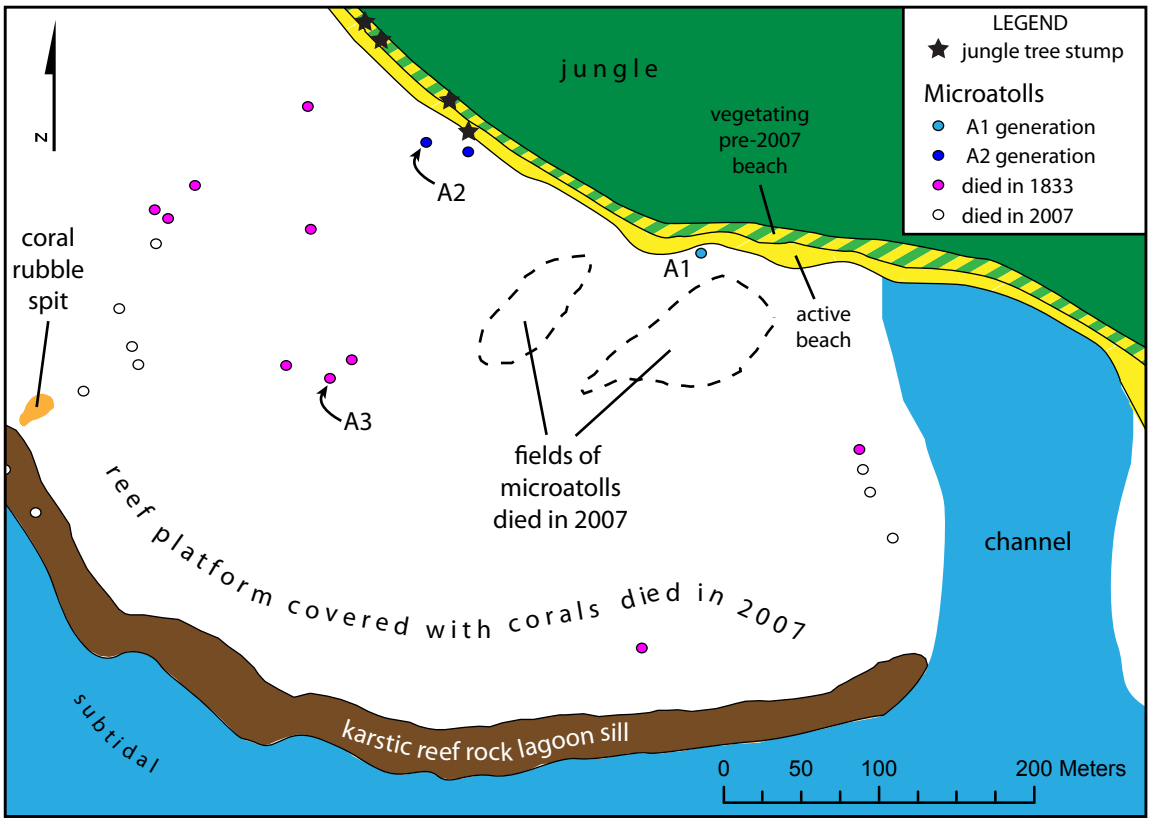

Figure 4.12. Map of the site on the south coast of Sanding Island. Here, the entire reef platform was killed due to ~1 meter of coseismic uplift in 2007. Stumps of jungle trees in the beach are evidence of interseismic subsidence prior to 2007; since the earthquake, that area has been re-vegetating. A population of fossil microatolls scattered over the middle of the reef platform died due to uplift in the 1833 earthquake (see Chapter 2). Other fossil microatolls close to the beach died in the 17th century.

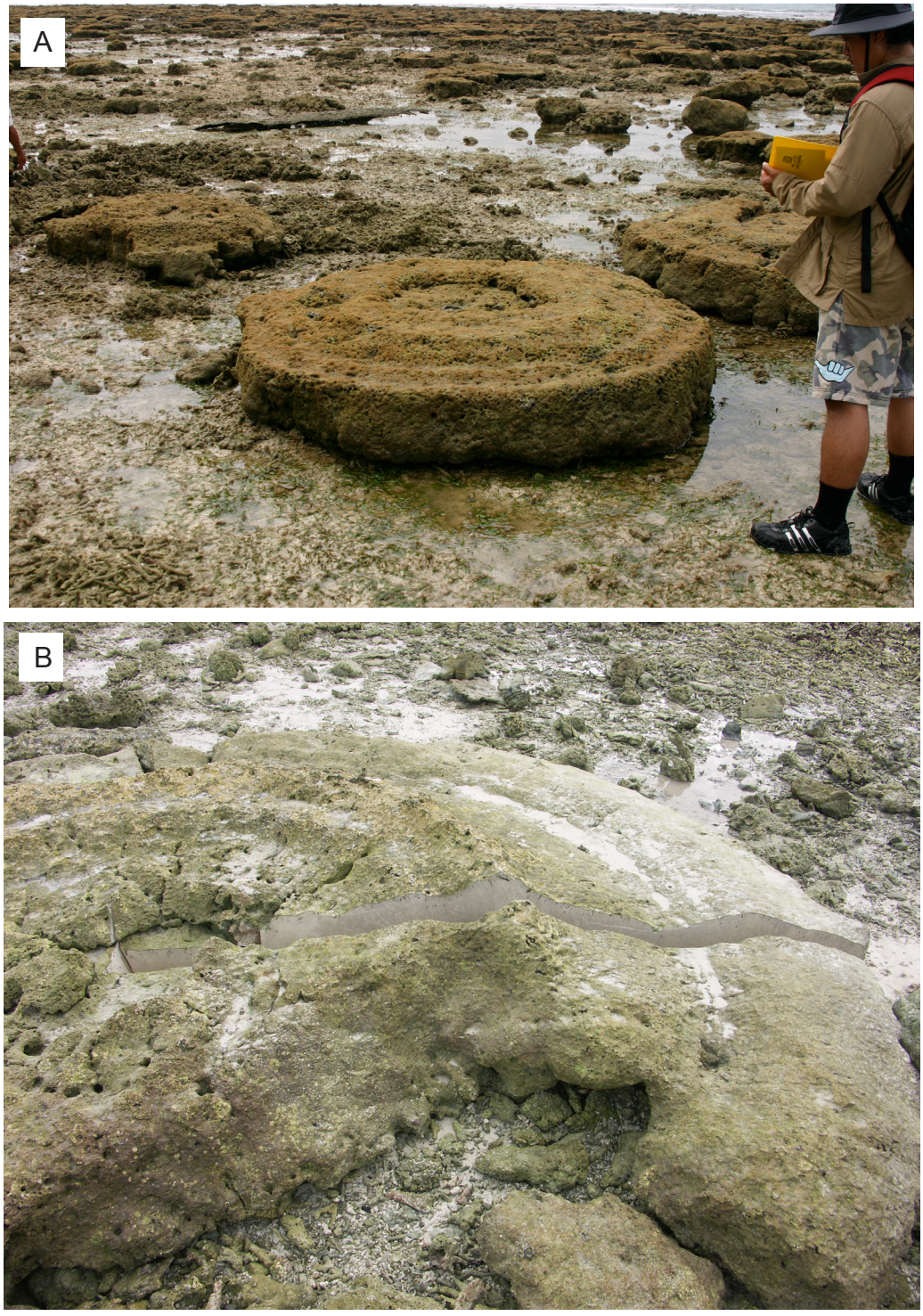

Figure 4.13. Microatolls with conical hat shapes indicating gradual uplift or several small uplifts closely spaced in time. A) A microatoll at Cimpungan, not one of those ultimately sampled but similar to CMP08-A1. B) Microatoll PCB08-B1 at Pecah Belah (2-meter radius). The inner parts of both microatolls are cup-shaped, indicating inter-seismic subsidence prior to the period of uplift.

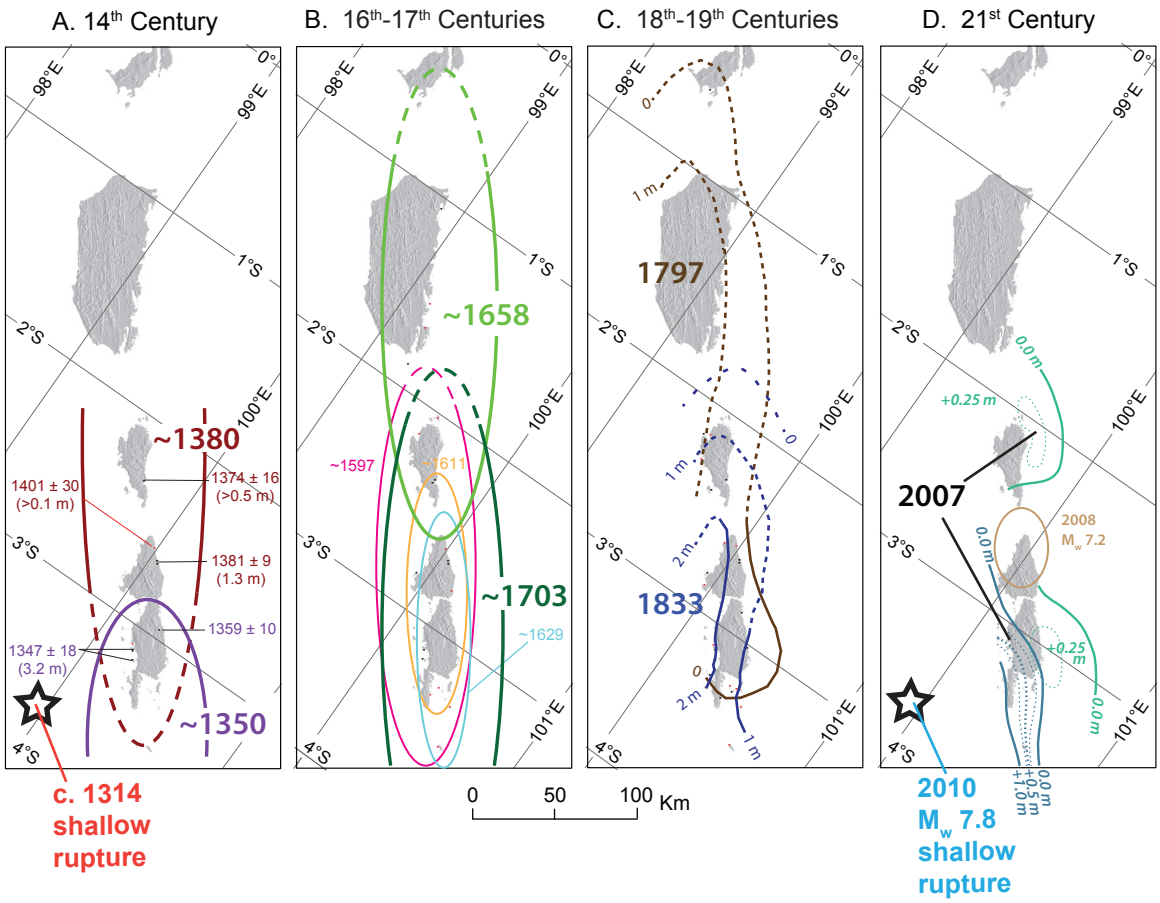

Figure 4.14. Comparison of the four most recent supercycle rupture sequences of the Mentawai segment, modified from *Sieh et al.* [2008]. Red dots show sites where we added new data and black dots show previously developed sites. Our only modifications to the 14th-century history are the addition of another microatoll death at Pasapuat which is consistent with the ~1380 event, and the shallow rupture that preceded the supercycle rupture sequence (see Chapter 3.) *Sieh et al.* [2008] proposed that the 16th–17th-century rupture sequence consisted of only two events; our expanded dataset suggests that there were at least three smaller events leading up to two larger events. Based on our analysis, the "~1685" event proposed by *Sieh et al.* was actually an averaged age of two separate events in ~1658 and ~1703, and the "~1606" event was actually a series of three smaller events that took place over three decades. This complex rupture sequence was clearly fundamentally different from the simple 1797/1833 doublet, appearing more similar in character to the 21st-century rupture sequence.

Table 4.1 Locations and Ages of Microatolls That Record Tectonic Uplifts In The 16th–17th Centuries

Latitude	Longitude	Full Name	Site Code	Microatoll	Youngest Band Date	1569	1597	1611	1629	1658	1703
-1.040	98.947	Tabekat	TBK	TBK02A1	1648 ± 26					x	
-1.498	99.187	Sarabua B	SRB	SRB10B3	1654 ± 5			-	-	x	
-1.606	99.234	Muara Siberut	MSB	MSB10A3	1653 ± 9			-	-	x	
-1.606	99.234	Muara Siberut	MSB	MSB10A1	1765 ± 164				-		
-1.606	99.234	Muara Siberut	MSB	MSB10A2	1636 ± 9			-	-		
-1.827	99.294	Masokut	MSK	MSK99A6	1668 ± 29					x	
-1.982	99.600	P. Panjang C	PJG-C	PJG12C4	1617 ± 43	-	x				
-1.982	99.600	P. Panjang C	PJG-C	PJG12C1	1599 ± 32	-	x				
-1.982	99.600	P. Panjang C	PJG-C	PJG12C2	1657 ± 6			-	-	x	
-1.987	99.602	P. Panjang B	PJG-B	PJG10B1	1573 ± 13	-	x?				
-2.123	99.565	North Pukarayat	NPK	NPK10A2	1645 ± 40					x?	x?
-2.274	99.784	Sikici C	SKC-C	SKC03C3	1589 ± 166	-	x				
-2.274	99.784	Sikici C	SKC-C	SKC03C2	1599 ± 108	-	x				
-2.274	99.784	Sikici C	SKC-C	SKC03C4	1579 ± 102		x				
-2.274	99.784	Sikici C	SKC-C	SKC03C5	1573 ± 51		x				
-2.274	99.784	Sikici C	SKC-C	SKC08C2	1591 ± 3		x				
-2.274	99.784	Sikici C	SKC-C	SKC08C5	1584 ± 5		x				
-2.286	99.785	Sikici B	SKC-B	SKC03B1_1	1631 ± 38	-	x		x		
-2.286	99.785	Sikici B	SKC-B	SKC03B1_3*	1662 ± 14		x			x	
-2.286	99.785	Sikici B	SKC-B	SKC03B2	1659 ± 21	-	x			x	
-2.289	99.802	Sikici A	SKC-A	SKC02A3	1542 ± 24	x?					
-2.289	99.802	Sikici A	SKC-A	SKC02A2	1523 ± 90		x				
-2.550	100.044	Pasapuat	PSP	PSP08B1	1695 ± 10						x
-2.550	100.044	Pasapuat	PSP	PSP08B2	1637 ± 22		x?	x?	x?		x?
-2.550	100.044	Pasapuat	PSP	PSP08B3	1647 ± 29	-	x	x	x		
-2.550	100.044	Pasapuat	PSP	PSP08B4	1634 ± 6	-	x	x	x		
-2.603	100.110	Simanganya C	SMY	SMY03C1	1564 ± 4	x					
-2.603	100.110	Simanganya C	SMY	SMY03C2	1536 ± 140	x					
-2.603	100.110	Simanganya C	SMY	SMY03C5	1572 ± 35		x				
-2.594	100.101	Simanganya A	SMY	NP00A2	1561 ± 7		x?				
-2.594	100.101	Simanganya A	SMY	SMY02A1	1607 ± 29	-	x	x			
-2.752	99.995	Silabu	SLB	SLB00A2*	1695 ± 8						x
-2.726	100.213	Cimpungan A	CMP	CMP08A3	1630 ± 23		x	x			
-2.726	100.213	Cimpungan A	CMP	CMP08A1	1622 ± 26		x	x			
-2.726	100.213	Cimpungan A	CMP	CMP08A2	1745 ± 44						x
-2.730	100.215	Cimpungan C	CMP	CMP08C1	1596 ± 13		x	x			
-2.730	100.215	Cimpungan C	CMP	CMP08C2	1626 ± 18		x	x			
-2.733	100.217	Cimpungan B	CMP	CMP08B1	1630 ± 10		x	x	x		
-2.733	100.217	Cimpungan B	CMP	CMP08B2	1619 ± 20		x	x			
-2.733	100.217	Cimpungan B	CMP	CMP08B3	1643 ± 59		x				
-2.733	100.217	Cimpungan B	CMP	CMP08B4	1624 ± 22		x	x			
-2.733	100.217	Cimpungan B	CMP	CMP08B5	1614 ± 5		x	x			
-3.083	100.268	Bulasat	BLS	BLS02A1	1604 ± 13	-	x				
-3.128	100.312	P. Saomang	SMG	SMG02A1	1721 ± 22					-	x
-3.213	100.460	P. Pecah Belah B	PCB	PCB08B1	1702 ± 6	-	x	x	x		x
-3.288	100.454	P. Kumbang B	KBG	KBG10B1	1692 ± 8						x
-3.288	100.454	P. Kumbang B	KBG	KBG10B2	1701 ± 61					-	x
-3.268	100.572	P. Simungguk	SGK	SGK10A3	1683 ± 5						x
-3.486	100.638	P. Sanding A	SDG	SDG10A2	1634 ± 3		x		x		
-3.486	100.638	P. Sanding A	SDG	SDG10A1	1699 ± 5				x		x

* Date represents youngest uplift event; coral colony survived the uplift but later died for apparently non-tectonic reasons.

x We interpret tectonic uplift occurred in this year, which is consistent with the radiometric ages.

x? We interpret tectonic uplift occurred in this year, but that interpretation implies incorrect radiometric ages and/or substantial erosion.

\- Coral record precludes significant tectonic uplift in this year.